Gene Therapy Approaches for Neurological Lysosomal Storage Diseases

by

Victoria Jane McCurdy

A dissertation submitted to the Graduate Faculty of
Auburn University
in partial fulfillment of the
requirements for the Degree of
Doctor of Philosophy

Auburn, Alabama
May 6, 2014

Keywords: gangliosidosis, gene therapy, lysosomal storage disease, neurological disease, feline model, adeno-associated virus

Approved by

Douglas R. Martin, Associate Professor, Anatomy, Physiology and Pharmacology
Eleanor M. Josephson, Associate Professor, Anatomy, Physiology and Pharmacology
Nancy R. Cox, Professor, Pathobiology
Bruce F. Smith, Professor, Pathobiology
Aime K. Johnson, Associate Professor, Clinical Sciences

Abstract

GM1 and GM2 gangliosidosis are lysosomal storage diseases caused by deficiency of enzymes required for ganglioside catabolism. Enzyme deficiencies cause neuronal accumulation of ganglioside resulting in progressive neurodegeneration and premature death. There is no cure for these fatal diseases. Feline GM1 and GM2 gangliosidosis models are close replicas of the human juvenile- and infantile- onset disease forms, respectively, and provide ideal large animal models to test therapies for translation to humans. Prior to the initiation of this research project evaluating adeno-associated virus (AAV) gene therapy, no experimental treatment had altered the course of the feline gangliosidoses.

Sixteen weeks after intracranial injection of AAV vectors in gangliosidosis cats, therapeutic enzyme activity was widely restored at near or above normal levels throughout the central and peripheral nervous system, and was also detected at lower levels in peripheral tissues. Restoration of enzyme activity resulted in substantial clearance of pathologic storage material and normalization of a secondary biomarker of lysosomal function. In long term treatment groups, mean survival of GM1 gangliosidosis cats treated before disease onset currently stands at >4.7 times that of untreated cats. The majority of treated cats remain alive and in good clinical condition, so mean survival continues to increase. Mean survival of GM2 gangliosidosis cats treated before disease onset was >4.3 times that of untreated. Enzyme activity was maintained throughout the current life span, but it was variable between subjects and between central nervous system regions, with several regions still demonstrating a substantial burden of storage

material. The significant increase in life span of treated GM2 gangliosidosis cats resulted in the emergence of previously subclinical peripheral disease symptoms that were the ultimate cause of death in seven out of nine cats. AAV-gene therapy also produced significant survival gains in GM2 gangliosidosis cats treated during the early symptomatic disease stage, which is when most human patients are diagnosed.

This research represents a significant advancement in the treatment of the feline gangliosidoses and supports the continued improvement and refinement of AAV gene therapy for translation to humans. Future studies should continue to investigate ways to maximize enzyme distribution throughout the central nervous system in order to further reduce storage material as well as investigate methods to treat peripheral disease pathology.

Acknowledgments

The author thanks her advisor Douglas R. Martin for providing the opportunity and guidance that made this enjoyable Ph.D. project possible. The author also thanks the other members of the graduate advisory committee, Nancy R. Cox, Bruce F. Smith, Eleanor M. Josephson, and Aime K. Johnson for their helpful advice and involvement. The author also greatly appreciates and thanks the following people: Heather L. Gray-Edwards and Allison M. Bradbury for their encouragement, support, and advice as well as for the provision of valuable MRI data and chapter 2 antibody titers, respectively; Misako Hwang for her ever helpful advice and willing assistance in the laboratory as well as for the provision of chapter 2 cellulose ion exchange chromatography data; Ashley N. Randle for her help and input with clinical rating scores and generation of neurological exam results; Nancy E. Morrison for her ever helpful assistance in the laboratory; Atoska S. Gentry for her kind assistance around the laboratory as well as for processing slides for histological analyses; and Brandon L. Brunson for chapters 1 and 2 histological analyses. The author also thanks the Auburn Cellular and Molecular Biosciences (CMB) Program who provided the opportunity and initial financial support to come to Auburn University to embark on a Ph.D. Finally, the author thanks Alan and Sheila Jones for their everyday love, support, and advice, and Jay McCurdy for his everyday love, support, and influence.

Table of Contents

List of Tables

Introduction

Chapter 1

Chapter 2

Chapter 3

Chapter 4

Appendix 1

Appendix 2

Appendix 3

List of Figures

Introduction

Chapter 1

Chapter 2

Chapter 3

Chapter 4

Appendix 1

Appendix 2

Appendix 3

List of Abbreviations

4MU	4-methylumbelliferone
AAV	Adeno-associated virus
Ab	Antibody
BBB	Blood brain barrier
βgal	β-galactosidase
CBA	Hybrid cytomegalovirus enhancer/chicken β-actin promoter
CNS	Central nervous system
CSF	Cerebrospinal fluid
DCN	Deep cerebellar nuclei
DRG	Dorsal root ganglia
EPS	Early post-symptomatic
ER	Endoplasmic reticulum
ERT	Enzyme replacement therapy
GA1	Asialo GM1 ganglioside
GA2	Asialo GM2 ganglioside
GM1	GM1 ganglioside (ganglioside mono sialic acid one)
GM2	GM2 ganglioside (ganglioside mono sialic acid two)
GM2A	GM2 activator protein gene
GM2AP	GM2 activator protein
GLB1	β-galactosidase gene

H&E	Hematoxylin and eosin
Hex	β-N-acetyl-hexosaminidase
HexA	Hexosaminidase A isozyme
HexB	Hexosaminidase B isozyme
HexS	Hexosaminidase S isozyme
HEXA	Hexosaminidase α-subunit gene
HEXB	Hexosaminidase β-subunit gene
HPTLC	High performance thin layer chromatography
HSCT	Hematopoietic stem cell transplantation
IC	Intracisternal
ICV	Intracerebroventricular
IT	Intrathecal
ITR	Inverted terminal repeat
IV	Intravenous
LOD	Limit of detection
LPS	Late post-symptomatic
LSD	Lysosomal storage disease
M6PR	Mannose 6 phosphate
MCB	Membranous cytoplasmic bodies
MRI	Magnetic resonance imaging
MPS	Mucopolysaccharidosis
MUG	4-methylumbelliferone-N-acetyl-β-D-glucosaminide
MUGS	4-methylumbelliferone-6-sulfa-2-Acetoamido-2-Deoxy-β-D-Glucopyranoside

Naphthol	naphthol AS-BI-N-acetyl-B-D-glucosaminide
NHP	Non-human primate
ORF	Open reading frame
PAS	Periodic Acid Schiff
PN	Peripheral nerve
PNS	Peripheral nervous system
rAAV	Recombinant AAV
SD	Sandhoff disease
SRT	Substrate reduction therapy
TSD	Tay-Sachs disease
vg	Vector genomes
WPRE	Woodchuck Hepatitis Virus posttranslational regulatory element
Xgal	5-bromo-4-chloro-3-indolyl-β-D-galactopyranoside

Introduction

Lysosomal Storage Diseases

The lysosome catabolizes marcomolecules to their constituent monomeric components. Lysosomal enzymes responsible for catabolism are primarily soluble acid hydrolases located in the lumen and often require a non-enzymic activator protein for function. Lysosomal storage diseases (LSDs) comprise a group of over 50 distinct inherited metabolic diseases, which collectively have an estimated frequency of 1 in 7000-8000 live births[1, 2]. LSDs are characterized by accumulation of un-degraded macromolecules in lysosomes. The majority of LSDs result from genetic deficiency of a lysosomal enzyme or it's activator protein, but a minority result from deficiency in the activation or trafficking of lysosomal enzymes[3]. Approximately 60% of LSDs are neuronopathic and are collectively a common cause of neurodegeneration in children. Non-neuronopathic LSDs are characterized by involvement of various visceral organs and tissues, but not the central nervous system (CNS). The gangliosidoses are neuronopathic LSDs and result from accumulation of ganglioside inside lysosomes: GM1 ganglioside (GM1) accumulation causes GM1 gangliosidosis and GM2 ganglioside (GM2) accumulation causes the GM2 gangliosidoses.

History of the gangliosidoses

The first clinical description of what is now known as GM2 gangliosidosis was in 1881 by the British ophthalmologist, Warren Tay, who described a cherry red-spot on the retina of a 1-year old child with psychomotor degeneration[4]. Further characterization came in 1896 when the

American neurologist, Bernhard Sachs, described distended cytoplasm in neurons from affected Jewish patients[5, 6]. In the 1930s the German biochemist, Ernst Klenk, identified the stored substrate in brain tissue of GM2 gangliosidosis patients as a sialic acid containing glycolipid, which was termed ganglioside due to a high concentration in ganglion cells[7]. The stored substrate was identified as GM2 in 1962 following isolation of the major storage product from the brain of an infantile GM2 gangliosidosis patient, and lysosomal Hexosaminidase (Hex) was suspected as the deficient enzyme[8]. Following the identification of different Hex isozymes in 1968, then the characterization of Hex isozyme subunit compositions in 1973, and the identification of a GM2 activator protein (GM2AP) in 1978, it is now known that GM2 gangliosidosis has three disease subtypes[9-11]. Tay-Sachs disease (TSD), Sandhoff disease (SD), and GM2AP deficiency result from defects in the Hex α-subunit, Hex β-subunit, and GM2AP, respectively. GM1 gangliosidosis was first described in 1959, but was not recognized as a distinct disease. Instead it was termed 'Tay-Sachs disease with visceral involvement'[12]. Between 1963 and 1965 biochemical analyses from several GM1 gangliosidosis patients revealed the disease to be a specific entity with GM1 as the stored substrate[13, 14]. β-galactosidase (βgal) was identified as the deficient enzyme in 1965[15].

Ganglioside Structure, Catabolism and Function

Gangliosides are one of four classes of glycosphingolipids, the major glycolipid in mammals. Gangliosides are most abundant in neurons and are primarily located in the outer leaflet of the plasma membrane, particularly in regions of nerve endings and dendrites. The highest ganglioside content is in brain gray matter. A small proportion of ganglioside is also present in endoplasmic reticulum (ER), mitochondria, and glial cells. A hydrophobic ceramide

backbone anchors the molecule to the membrane and is linked via a terminal hydroxyl group to a hydrophilic oligosaccharide chain with or without sialic acid residues (**Figure 1**)[16, 17].

Ceramide is formed at the cytosolic face of the ER and is transported to the Golgi apparatus. Ceramide glucosyltransferase transfers a glucose residue from UDP-glucose to ceramide on the cytosolic face of the Golgi to form glucosylceramide. Lactosyl ceramide and higher gangliosides are synthesized on the luminal side of the Golgi through the action of membrane bound glycosyltransferases, which catalyze the stepwise addition of monosaccharides to the growing glycan chain[16, 17].

Ganglioside catabolism takes place in the lysosome (**Figure 2**). Following endocytosis from the plasma membrane, gangliosides become components of the lysosomal membrane through vesicular flow. Acid hydrolases in the lysosol sequentially cleave sugar residues from the non-reducing end of gangliosides. Oligosaccharide chains of one to four residues are not accessible to acid hydrolases, so activator proteins are required to mediate interaction between the membrane bound substrate and water-soluble enzyme (**Figure 3)**[17].

The structural pattern of gangliosides changes with cell development, differentiation, and ontogenesis. Although the function of individual gangliosides is poorly understood, there is evidence they are important in cell differentiation, recognition, and adhesion as well as in the regulation of growth factor receptors, regulation of protein kinases, synaptic transmission, and cellular calcium homeostasis[18-20]. Additionally, exogenously added gangliosides can promote survival and repair of damaged neurons[21, 22]. Due to a high concentration at nerve endings and dendrites, gangliosides are also implicated in neuritogenesis. Specifically, GM1 promotes neurite outgrowth in a number of cell culture systems, and concentration of GM1 and GM2 correlates with ectopic dendrite growth in ganglioside storage diseases[19, 23].

Enzyme deficiency causing GM1 Gangliosidosis

Lysosomal β-gal (EC 3.2.1.23) hydrolyzes terminal β-1,3- or β-1,4-linked galactose residues from GM1, asialo GM1 (GA1), and numerous glycoconjugates[24]. Defective βgal causes GM1 gangliosidosis, which has an estimated prevalence of 1 in 244, 000-384,000 conceptions in the general population[1]. A higher frequency is reported in the Maltese Islands (1 in 3700[25]), the Gypsy population (1 in 10,000[26]), Southern Brazil (1 in 17,000[27, 28]), and Japan (high but unknown incidence of adult onset disease[29]).

The 2.4 kilobase βgal cDNA is composed of 16 exons encoded by *GLB1* on chromosome 3p21.33. βgal is synthesized as a 677 amino acid (84 kilodalton) precursor with a 23 amino acid N-terminal signal peptide. The signal peptide is cleaved off upon entry into the ER where the precursor is glycosylated with high-mannose oligosaccharides. In the Golgi, βgal is phosphorylated on mannose residues and binds the mannose-6-phosphate receptor (M6PR) for targeting to the lysosome. The βgal precursor is C-terminally processed in the endodomal/lysosomal compartment within two hours to a mature 64 kilodalton polypeptide. C-terminal processing and stability depend on the association of βgal with cathepsin A. The majority of lysosomal βgal exists in a 680 kilodalton complex containing four βgal monomers and eight cathepsin A protomers. In the absence of cathepsin A, precursor βgal is produced normally and is functionally identical to the mature form, but the half-life is reduced by one-tenth due to excessive intralysosomal degradation. A 1.27 megadalton ternary complex also exists, which additionally contains neuraminidase and N-acetylgalactosamine-6-sulfate-sulfatase. The two complexes are present in a 10:1 ratio in the lysosome[30]. βgal has a pH optimum of 4.5 to 4.75 and is activated by chloride ions. Hydrolytic activity against GM1 requires the presence of the saposin B activator protein or the GM2AP (**Figure 3**)[31].

At least 91 mutations resulting in GM1 gangliosidosis have been reported on *GLB1*. Mutation types include missense/nonsense, small deletions, small insertions, and splicing defects. Common mutations are found in certain ethnic groups, such as the R208C mutation in American infantile onset patients[32] and the I51T mutation in Japanese adult onset patients[29]. The latter mutation results in an enzyme that is not phosphorylated, so only a small amount of βgal reaches the lysosome.

Enzyme Deficiency Causing GM2 Gangliosidosis

Defective lysosomal β-N-acetylhexosaminidase (Hex) (EC 3.2.1.52) causes GM2 gangliosidosis. *HEXA* and *HEXB* encode the Hex α- and Hex β-subunit, respectively. The Hex subunits dimerize to form two major isozymes, HexA (αβ) and HexB (ββ), as well as a minor isozyme, HexS (αα). Hex removes terminal β-1,4-N-acetyl-glucosamine and N-acetyl-galactosamine residues from GM2, asialo GM2 (GA2), and numerous other glycoconjugates. The GM2AP is required for Hex activity to facilitate interaction between the lipid based substrate and water soluble hydrolase. HexA and HexB have overlapping substrate specificities, but only HexA is capable of hydrolyzing charged substrates, including GM2 (**Figure 3**). HexS is an unstable isoform present at very low levels. It is considered to have negligible catalytic activity towards most substrates, but may play a role in the degradation of glycosaminoglycans (**Figure 4**). GM2 gangliosidosis has three disease forms: 1) TSD results from *HEXA* mutations and is associated with deficient HexA, but normal HexB, 2) SD results from *HEXB* mutations and is associated with deficient HexA and HexB, and 3) GM2AP deficiency results from mutations in *GM2A*, causing the inability to form a GM2/GM2AP complex[11]. TSD and SD have an estimated prevalence of 1 in 201,000-244, 000 and 1 in 322, 600-384,000 conceptions,

respectively[1]. Higher frequencies have been reported in some ethnic groups, such as the Ashkenazi Jewish population, with a TSD carrier frequency of 1 in 3600[33]. However, most North American infantile onset TSD patients are now of non-Jewish ancestry due to successful carrier screening within the high risk population.

HEXA and *HEXB* are located on chromosomes 15q23-q24 and 5q13, respectively. Both genes are composed of 14 exons and the gene products exhibit 57% homology in amino acid sequence. The α-subunit is synthesized as a 529 amino acid pro-polypeptide (~68 kilodaltons) with a 23 amino acid signal sequence. The β-subunit is synthesized as a 556 amino acid pro-polypeptide (~68 kilodaltons) with a 43 amino acid signal sequence. **Figure 5** shows the post-translation modifications to Hex pro-polypeptides. Upon entry into the ER, the signal sequence is cleaved off and the pro-polypeptides are glycosylated on asparagine residues with high-mannose oligosaccharides. Dimerization of β-subunits to form HexB occurs rapidly in the ER. As HexB is the most stable isozyme, α-subunit monomers must accumulate for ~5 hours to provide a high enough concentration to force newly processed β-subunit monomers to form the less stable HexA. In the Golgi, Hex isozymes are phosphorylated at mannose residues and directed to the lysosome by association with the M6PR. Hex isozyme precursors undergo final proteolytic processing in the lysosome to generate an α-subunit of ~56.6 kilodaltons consisting of two polypeptides and a β-subunit of ~55.9 kilodaltons consisting of three polypeptides[33-35].

At least 123 *HEXA* mutations leading to TSD and 36 *HEXB* mutations leading to SD have been characterized. Mutation types include small insertions, small deletions, gross deletions, missense/nonsense, base substitutions, and base insertions causing incorrect splicing. Common mutations occur in certain ethnic groups. For example, the 1278ins4 mutation, which introduces a premature stop codon, accounts for up to 80% of mutations in Ashkenazi Jewish

infantile onset TSD patients[36]. A 16 kilobase deletion extending from the promoter region of *HEXB* in to intron five is common in French and French-Canadian SD patients, and it may account for up to one third of *HEXB* mutations[35].

Clinical Progression

Neuronal storage of ganglioside leads to progressive psychomotor degeneration. Infantile-, juvenile-, and adult-onset clinical disease forms are recognized and are characterized by the age of onset and progression of clinical symptoms, which are largely determined by the residual level of enzyme activity (**Figure 6**)[35, 37]. GM1 and GM2 gangliosidosis share many clinical features (**Table 1**). In the most common infantile-onset disease form, developmental arrest occurs between birth and 6 months old and progressive psychomotor deterioration ensues. Macular cherry red spots on the ocular fundus, seizures, increased startle response to sounds, and blindness are characteristic. Children become vegetative in late stage disease, and death typically occurs before age five. Additionally, dysmorphism, hepatosplenomegaly, and skeletal dysplasia (dystosis multiplex) are common features of infantile GM1 gangliosidosis. Peripheral tissue abnormalities are less commonly reported in GM2 gangliosidosis patients despite the storage of neutral substrates in peripheral tissues of SD patients. GM2AP deficiency has similar clinical characteristics to early onset TSD[35, 38]. Symptoms of juvenile-onset gangliosidosis are similar to those seen in infantile-onset patients, but progression is slower with death typically occurring at 10 to 15 years old.

Adult-onset gangliosidosis occurs from childhood to adulthood and clinical phenotype varies widely. Gait and speech disturbances, abnormal posture, progressive dystonia, extrapyramidal signs, and motor neuron disease (muscle wasting, weakness, and fasciculation)

are common symptoms. Additionally, mild intellectual impairment and skeletal abnormalities (flattening of vertebral bodies) are common symptoms in GM1 gangliosidosis patients[24, 29, 38, 39]. Psychosis is common in GM2 gangliosidosis patients, but intelligence is not impaired[35]. Mild peripheral and autonomic nervous system dysfunction has been reported in late-onset SD patients and less commonly in TSD patients. Symptoms include: decreased sympathetic skin responses[40], esophageal dysmotility[41], chronic diarrhea[42], urinary incontinence[43], loss of libido[41], cardiac dysrhythmia[41], decreased nerve conduction velocity[41, 43, 44], muscle denervation[41, 44, 45], and storage in myenteric plexus neurons[44, 45] as well as in tissues from appendix[45], muscle[44], and rectal submucosa[41].

Disease Pathology

Pathologically the gangliosidoses are characterized by ganglioside accumulation in brain gray matter. GM1 and GA1 accumulate to approximately 10 times normal in GM1 gangliosidosis patients and GM2 and GA2 accumulate to 100 to 300 times normal and 20 to 100 times normal, respectively, in GM2 gangliosidosis patients. Total ganglioside storage is similar in both diseases because GM1 comprises a greater proportion of total ganglioside in the normal brain. Substrate accumulation is also evident in peripheral tissues. GM1 accumulates to approximately 20 to 50 times normal in liver of GM1 gangliosidosis patients. Also, storage vacuoles and foamy histiocytes are apparent in other peripheral tissues due to accumulation of galactose containing oligosaccharides[24, 38]. Visceral tissues of TSD patients often show no pathologic signs. SD patients have GA2 accumulation in the liver as well as storage vacuoles and foamy histiocytes in other peripheral tissues due to accumulation of globoside and neutral substrates[35].

Computed tomography (CT) scans and magnetic resonance imaging (MRI) show diffuse atrophy of the CNS as well as myelin loss[24, 38, 46]. The neurodegeneration that characterizes gangliosidosis disease progression is likely a result of several mechanisms. Ganglioside accumulation causes neuronal hypertrophy with cytoplasmic vacuolation, loss of Nissl substance, and margination of nuclei. Neuronal and glial cytoplasmic inclusions consist of characteristic membranous cytoplasmic bodies (MCBs), which are composed of multiple concentric lamellae containing cholesterol, phospholipid and ganglioside (**Figure 7a**). Increased lysosomal storage may disrupt other catabolic processes, depriving the cell of precursors and leading to secondary dysfunction in other pathways. Also, there may be reduced entry of materials into swollen lysosomes, causing build-up elsewhere in the cell with disruptive consequences[23].

Soma-dendritic changes have been described in human[6, 35] and feline gangliosidosis diseases. In feline models, the development of meganeurites- massive swellings of the axon hillock region- are related to disease severity (**Figure 7b**). Some meganeurites show growth of ectopic dendrites with evidence of aberrant synapse formation, which could alter normal electrophysiology and neuronal connections. Ectopic dendrite growth appears to be correlated with GM2 storage and can also occur at the axon hillock in the absence of meganeurite formation[23, 47-52]. In an induced α-mannosidosis feline model, ectopic neutrites and their synaptic connections were not reversible even though other cellular changes were normalized following treatment[53].

Also apparent in feline models are axonal spheroids- swellings containing organelles- which develop distal to the axon hillock region and may affect action potential propagation (**Figure 7c**)[23, 51, 54-56]. Axonal spheroids may be caused by a block in retrograde transport due to disruption of the cell body, therefore depriving axons of important components. There is a

correlation between disease severity and the incidence of axonal spheroids in GABAergic neurons. GABAergic neurons, particularly Purkinje cells, likely have a high incidence of axonal spheroids because they have a high firing rate requiring fast turnover of axonal components. Loss of inhibitory circuits could promote the characteristic seizures in late stage disease. The block in axonal transport is also thought to contribute to myelin loss, as is loss of oligodendrocytes[57].

Increased neuronal apoptosis has been reported in human and mouse disease[58]. In mice, perturbation of calcium homeostasis causes an ER stress response as well as mitochondrial apoptotic signaling, which contribute to apoptosis[20, 59, 60]. In SD, mice neuroinflammation is high in areas of marked neuronal death[58, 61, 62]. It is hypothesized that macrophage/microglial cells initiate an inflammatory response as they engulf and destroy apoptotic neurons. However, the inability to degrade storage material results in a continued inflammatory response and further microglial expansion[62]. Other mechanisms thought to promote disease progression include activation of autophagy leading to mitochondrial dysfunction[63] and neuronal accumulation of synucleins[64]. Thus, several different mechanisms likely contribute to disease progression.

Feline Gangliosidosis Models

Knock out mouse models of GM1 gangliosidosis[65-67] and SD[68] share many similarities with the human diseases and are invaluable for the initial testing of therapies. However, feline models provide important advantages over mice for translational research. The cat brain is 75 times larger than the rodent brain and only 10 to 20 times smaller than a human child's brain, therefore providing a valid indication of enzyme distribution challenges that need to be overcome in a large, complex brain. Cats have a life span that allows long term measurements

and a body size that facilitates clinical manipulations and evaluations, surgical interventions, and frequent sampling of tissues and body fluids. Unlike mice, cats have a heterologous genetic background providing an indication of the variability in treatment outcome and immune responses that can be expected in humans[69]. The feline gangliosidoses are highly analogous to the human diseases, therefore providing an ideal large animal model to test therapeutic strategies.

Feline GM1 gangliosidosis was first described in Siamese cats[70] and in a domestic cat[71]. The Siamese model is maintained at Auburn University, but is now outbred and comprises a mixed breed colony. First described in 1971, the feline model is a close replica of human juvenile-onset GM1 gangliosidosis[70, 72]. The genetic mutation is G1448C causing an Arg483Pro substitution in exon 14 resulting in production of a mutant protein that does not reach the lysosome[73]. β-gal activity is <0.15-fold normal in the CNS, kidney, skin, and cultured fibroblasts. Initial reports described disease onset at 2 to 3 months old with tremors of the head and pelvic limbs followed by generalized dysmetria, severe balance disturbances, and spastic paraplegia, which defines the humane endpoint at 7 to 8 months old. Tissues show widespread neuronal degeneration characterized by varying degrees of swelling, cytoplasmic vacuolation, lack of Nissl substance, and margination of nuclei. Total ganglioside content is 2 to 3 times normal. GM1 ganglioside content is approximately 8 times normal and is stored in MCBs characteristic of the human disease. Gliosis and neuronophagia are evident in some areas of severe neuronal degeneration, but there is little neuronal loss. Peripherally, vacuolated macrophages and hepatocytes are evident, but cats do not display hepatosplenomegaly. Testes of pubescent cats are devoid of mature spermatozoa.

Feline GM2 gangliosidosis has been described in American shorthair domestic[74], Korat[75], Japanese domestic[76], and Burmese breeds[77]. The American domestic shorthair colony is

maintained at Auburn University. First described in 1977, it is a close replica of human infantile-onset SD[74, 78]. The genetic mutation is a 25 base pair inversion at the carboxyl terminus of exon 14 causing a translation stop codon 8 amino acids premature, which results in protein levels much lower than normal[79]. Less than 0.02-fold normal Hex activity is found in the CNS, liver, and fibroblasts of SD cats. Initial reports described the onset of head tremors at 4 to 10 weeks old, followed by ataxia and then paresis, which defines the humane endpoint at ~4.5 months old. Neurons throughout the CNS are distended, lack Nissl substance and contain MCBs characteristic of the human disease, with cerebellar Purkinje cells particularly affected. Total ganglioside content is 2 to 3 times normal and GM2 content is approximately 700 times normal. Unlike the human disease, there is little evidence of neuronal loss or gliosis. Peripherally, membrane bound storage vacuoles are present in visceral organs throughout the body.

Treatment Options

Although the first description of GM2 gangliosidosis was in 1881, the gangliosidoses as a group remain untreatable. Effective treatments will require the delivery of therapeutic enzyme to all cells with lysosomal enzyme deficiency. There are two observations that encourage the ongoing efforts to find an effective therapy. Firstly, a small proportion of lysosomal enzyme is secreted from the cell where it can be taken up by neighboring cells by the M6PR present in the plasma membrane[80-82]. Therefore, a small proportion of donor cells are able to restore lysosomal enzyme activity in a larger cell population (**Figure 9**). This cross-correction mechanism forms the basis of therapeutic approaches currently under investigation. Secondly, tissues of asymptomatic individuals heterozygous for gangliosidosis have as low as 0.11- to 0.20-fold

normal lysosomal enzyme activity, and adult onset patients can have activity at only 0.02- to 0.04-fold normal[83]. Therefore, very low level enzyme restoration may be therapeutic.

Enzyme replacement therapy (ERT)

ERT involves delivery of a functional enzyme via intravenous (IV) or cerebrospinal fluid (CSF) routes. ERT is approved for use to treat peripheral symptoms of six non-neuronopathic LSDs including Gaucher disease type I, Fabry disease, Mucopolysaccharidosis (MPS) types I, II and VI, and Pompe disease. ERT has also effected improved neurological function in a number of neuronopathic LSD animal models (reviewed in[84]), but not in gangliosidosis animals. Intracerebroventricular (ICV) administration of human HexA to SD mice only resulted in a 0.13-fold survival increase over untreated[85], and IV administration of human HexA to SD cats did not result in survival benefit. However, HexA activity in SD cats was at least 0.44 fold normal in all 11 peripheral tissues analyzed with subsequent reductions in GM2 and GL4 globoside. Treatment also resulted in up to 1.74-fold normal brain HexA activity, but there was no substantial decrease in brain ganglioside content, possibly because the enzyme was not taken up by neurons[86]. ERT requires regular infusions, and the high cost of products makes it prohibitively expensive for rare diseases such as the gangliosidoses.

Cell based therapies

Hematopoietic stem cell therapy (HSCT) from healthy donors has been tested in a number of neuronopathic LSDs, but therapeutic benefit has largely been limited to a small subset of late-onset patients. Transfused donor derived HSCs provide metabolically competent progeny cells, such as macrophages and microglia, which migrate to affected tissues and provide a source

of functional enzyme. Better outcome is expected following early transplantation as donor engraftment can take several months, during which time disease progresses. HSCT success has been most notable in patients with Hurler's syndrome and Globoid Cell Leukodystrophy. Outcome has been more variable in other LSDs with efficacy seen in some patients, but failure to improve symptoms despite engraftment in others[87-89].

HSCT showed moderate therapeutic efficacy in gangliosidosis mouse models[90-92], resulting in survival increases of up to ~2-fold over untreated. However, HSCT failed to benefit a GM1 gangliosidosis Portuguese Water dog[93], a SD cat[94], and infantile onset GM1[95] and GM2 gangliosidosis patients[96] transplanted before disease onset. The variable success of HSCT between different LSDs may depend on how efficiently leukocytes release a particular lysosomal enzyme. For example, brain microglia release more α-mannosidase versus Hex in culture[97]. It may also depend on the relative disruption of the blood brain barrier (BBB) between different LSDs, which would affect infiltration of HSC derived cells.

Transplantation of genetically modified HSCs proved successful in human patients with early onset Metachromatic Leukodystrophy (onset in the second year) transplanted pre-symptomatically[98]. Stable engraftment was demonstrated beginning 1 month after transplant, and therapeutic enzyme activity in CSF was comparable to healthy donors for up to 2 years. At 39 months old, patient one required a single aid to walk, but otherwise showed continuous motor development, normal IQ, and improvements in existing peripheral neuropathy. Patients two and three remained fully asymptomatic at 30 and 25 months old. The outcome is highly encouraging for the prospect of treating neurodegenerative LSDs.

Substrate reduction therapy (SRT)

SRT aims to decrease the amount of deficient enzyme substrate synthesized by cells. Two imino sugars, N-butyldeoxynojirimycin (NB-DNJ;Miglustat) and N-butyldeoxygalactonojirimycin (NB-DGJ), are competitive inhibitors of ceramide-specific glucosyltransferase (GlcT), the enzyme that catalyzes the first step in glycosphingolipid biosynthesis, and have demonstrated moderate therapeutic benefit in gangliosidosis mouse models, resulting in up to a 1.36-fold survival increase versus untreated[99-102]. Miglustat is in clinical use as an effective treatment for peripheral symptoms of non-neuronopathic Gaucher disease type I and Niemann-Pick type C, but has not proven effective to treat neuronopathic symptoms of Gaucher disease type III. Miglustat did not provide any measurable benefit for infantile-onset GM2 gangliosidosis patients[103]. Outcome was variable in juvenile onset GM2 gangliosidosis patients, with some continuing to show neurological deterioration[104, 105] and others demonstrating disease stabilization[106, 107]. However, stable periods are part of the natural disease course, so it is hard to assess treatment benefit in such a heterogeneous group with short follow up periods. In mouse models, SRT used in combination with cell therapy provided a synergistic therapeutic effect over the monotherapies[91, 108, 109].

Chaperone therapy

Pharmacological chaperones are small molecules that bind and stabilize the native folded conformation of mutant enzyme that retains partial catalytic function. Once inside the acidic lysosome, the enzyme substrate will displace the chaperone. However, mutations in gangliosidosis patients are heterogeneous and complex. It is estimated that only 30% of GM1 gangliosidosis patients have unstable, but catalytically active enzyme that would be a candidate

for chaperone therapy[110]. The galactose derivative, N-octyl-4-epi-β-valienamine (NOEV), has shown moderate efficacy in GM1 gangliosidosis mouse models resulting in up to a 1.3 fold survival increase versus untreated[110, 111]. Additionally, NOEV can increase βgal activity in fibroblasts from juvenile-onset patients as well as 30% of infantile-onset patients[111, 112]. N-nonyl-DGJ (NN-DGJ), a long alkyl-chain iminosugar derivative can also act as a chaperone in fibroblasts from GM1 gangliosidosis cats and human patients[113]. However, cell based studies may not be indicative of in vivo effect. Cell studies on human GM2 gangliosidosis fibroblasts showed that Pyrimethamine (PYR) could enhance HexA activity in some mutation types, but two subsequent phase I/II clinical trials did not report any notable success in late-onset patients[114 115, 116]. In one trial HexA activity did not approach the theoretical 0.1-fold normal level thought to be therapeutic, and the other trial was suspended due to the extent of side effects experienced by most patients[115].

Adeno-associated virus gene therapy

Gene therapy has the potential to provide a permanent source of deficient enzyme following cellular transduction. Adeno-associated virus (AAV) vectors have become the vectors of choice for gene delivery to the CNS due to their efficiency at transducing neurons leading to long term expression of therapeutic genes with no apparent toxicity and limited inflammation at the site of injection[117, 118]. AAV is a non-pathogenic, single stranded DNA virus belonging to the Dependovirus genus of the Parvoviridae family. The AAV life cycle consists of a latent phase and a lytic phase, which requires co-infection of adenovirus or herpes simplex virus for replication. The 4.7 kilobase AAV genome consists of two open reading frames (ORFs), flanked by two inverted terminal repeats (ITRs). The *rep* gene encodes proteins required for excision,

replication and integration, and the *cap* gene encodes proteins for capsid formation (**Figure 8a**). The ITRs are the only *cis* elements required for viral replication and packaging. Recombinant AAV gene therapy vectors are produced by replacing *rep* and *cap* with cDNA encoding a therapeutic transgene expression cassette. The recombinant genome is packaged into an AAV capsid by providing Rep and Cap proteins as well as adenovirus helper functions in *trans* (**Figure 8b**).

Following AAV attachment to cell surface receptors, the virus is endocytosed and subject to endosomal processing, which is an important step for viral nuclear transport. It is thought that AAV escapes from the late endosome prior to lysosomal maturation and traffics to the nucleus, but little is known about the process that controls nuclear translocation. Inside the nucleus, AAV uncoats prior to genome conversion from a single stranded DNA to a double stranded DNA intermediate capable of expressing proteins[119]. Through the action of Rep proteins, wild type AAV integrates in a site specific manner in chromosome 19[120]. As recombinant AAVs are devoid of viral ORFs, they lose capacity to integrate and persist primarily in episomal form[121 122, 123]. Random integration events occur at a frequency significantly lower than the generally accepted rate for spontaneous mutation in human genes[121]. Therefore, the risk of insertion mutagenesis is extremely low.

A unique AAV serotype is one that cannot be efficiently neutralized by serum generated against viruses of other known serotypes. AAV1 was discovered as a contaminant in simian Adenovirus stock in 1965[124]. The discovery of AAV2 followed in 1966, and AAV2 became the first serotype to be cloned into a bacterial plasmid in 1982[125]. AAV serotypes differ in their cellular tropism due to the composition of capsid proteins, which facilitate binding to cell surface receptors. AAV1 and AAVrh8 are the serotypes utilized in this dissertation research project. The

cellular receptor for AAV1 is N-linked sialic acid, and AAV1 has a natural tropism for CNS, heart, and skeletal muscle[126]. AAVrh8 was isolated from the rhesus monkey in 2004 by screening tissues for endogenous AAV sequences[127]. Its cellular receptors are unknown, but it has tropism for hepatocytes, muscle, and CNS, therefore displaying similar tropism to AAV1[128].

AAV gene therapy in LSD animal models

AAV intracranial gene therapy has been tested in many different LSD mouse models with varying success. It is hard to compare outcomes between different LSD models because there are many variables between studies which could affect the extent of therapeutic enzyme and vector distribution. Following injection of AAV vectors in the CNS, enzyme and vector are disseminated from injection sites by diffusion[129], axonal transport to interconnected areas (**Figure 9**)[130-133], and CSF flow[130, 134]. Therefore, reports of widespread distribution have followed injection of vectors into highly interconnected structures including the thalamus[135-137], deep cerebellar nuclei (DCN)[137-140], lateral ventricles[141], striatum[137, 140, 142-144], lumbar cistern[145, 146], and cisterna magna[141, 146, 147].

Different vector serotypes have different cellular tropisms depending on their capsid properties. As AAV2 was the first serotype to be cloned it was the predominant one used in early gene therapy studies. However, comparisons have since shown that serotypes differ in their CNS distribution capability, and that other serotypes can achieve more widespread CNS distribution than AAV2[137, 139, 148-150]. Different serotypes have different propensities to undergo either anterograde or retrograde axonal transport (**Figure 10**). For example, AAV2 favors anterograde axonal transport whereas AAV6 favors retrograde transport, which affects the distribution characteristics of each vector when injected in the striatum and thalamus[151]. Axonal transport of

vector/enzyme is affected by efficiency of uptake at the plasma membrane, so higher vector doses may promote axonal transport[152]. Vector purification method can impact transduction efficiency when comparing between different serotypes, and the choice of regulatory elements can affect therapeutic transgene expression[153]. For example, the hybrid cytomegalovirus enhancer/chicken β-actin (CBA) promoter was shown to promote stronger expression of green fluorescent protein (GFP) compared to the cytomegalovirus (CMV) promoter[154], and inclusion of the Woodchuck hepatitis virus posttranscriptional regulatory element (WPRE) increases transcript expression[145]. Following translation, the use of non-species specific cDNA can limit protein distribution due to immune responses against foreign sequences[141]. Therefore, there are many variables between different gene therapy studies that can determine outcome.

Due to mechanical injury, the intracranial injection procedure in naïve animals produces an innate local inflammatory response, which subsides over time. Following vector delivery, a neutralizing antibody (Ab) response to the AAV capsid is usually encountered, but does not correlate with CNS vector transduction efficiency, protein expression, or clinical outcome[141, 155, 156]. The presence of pre-existing serum Abs against AAV2, AAVrh8, and AAV9 was shown to reduce CNS vector transduction when the same serotype vector was administered in mice[137, 155] and non-human primates[147]. However, in other studies pre-existing Abs against AAV9 did not have a substantial effect on subsequent CNS AAV9 vector transduction in dogs[141] and non-human primates[146]. Therefore, the presence of pre-existing neutralizing Abs may or may not affect CNS vector transduction. Ab responses against the therapeutic transgene can have a detrimental effect on protein distribution if non species specific transgenes are used[141, 157], or if animals do not generate any natural protein (that is, negative for cross-reactive material, or CRM-)[158, 159].

AAV gene therapy has been highly successful in gangliosidosis mouse models. GM1 gangliosidosis mice treated neonatally with bilateral ICV injections of AAV1-mouse (m) βgal showed several-fold normal βgal activity throughout the brain, and normalization of GM1 storage at the 3-month pre-determined endpoint[160]. In a later study, all but one GM1 gangliosidosis mouse treated at 6 to 8 weeks old with bilateral injections of AAV2/1-mβgal in the thalamus and DCN survived until the 52-week experiment endpoint (untreated endpoint, 32 weeks old). βgal activity was restored to the presumed therapeutic level (>0.1-fold normal) throughout the brain and spinal cord, with near normalization of substrate storage in the brain, and 50% clearance in the spinal cord[135].

SD mice injected bilaterally in the striatum and DCN or hippocampus and DCN with AAV1-*HEXA* + AAV1-*HEXB* (1:1 vector formulation) survived to a median of 681 days and 609 days, respectively (untreated SD lifespan, 131 days). In both groups histochemical staining demonstrated widespread Hex activity and striking absence of storage material throughout the entire CNS[140], which was irrespective of treatment age[161]. However, clinical benefit decreased with increasing treatment age due to pathological changes that could not be reversed, such as demyelination and neuronal apoptosis[161]. Other studies have also demonstrated that clinical efficacy decreases with increasing treatment age[162, 163].

Whilst mouse models are invaluable for initial testing of therapeutic approaches, gene therapy must also be proven in large animal models with closer resemblance to human patients. Intracranial AAV gene therapy has been reported in the α-mannosidosis feline model[164] and MPS type I and III canine models[158, 165]. Vector delivery to these large animal brains has demonstrated extensive enzyme distribution and clearance of storage material, although there was often much inter animal variation. Although the previous studies in LSD animal models were not designed to

determine clinical efficacy, treated α-mannosidosis cats demonstrated reversal of clinical progression and displayed only mild neurological disease at the 18-week study endpoint (untreated lifespan, 18 weeks). Of two cats followed-up long term, one reached humane endpoint at 30 weeks old and the other was euthanized at the 52-week experimental endpoint, at which time there had been no deterioration in clinical status since the 18-week time-point[164].

AAV gene therapy in humans

Intracranial AAV gene therapy has so far been reported in human phase I and II trials for Parkinson's disease[166-168] and two neuronopathic LSDs: Canavan disease[169, 170] and Batten disease (Late Infantile Neuronal Ceroid Lipofuscinosis)[171]. There have been no adverse safety consequences from any of the trials that could be definitively attributed to the injection procedure or AAV vectors, indicating that the approach is safe for human application.

The initial stages of human clinical trials are concerned with safety, so patients are administered a dose per kilogram that is much lower than the effective dose in animals. Therefore, clinical efficacy cannot be concluded from early stage trials. In the phase I trial for Batten disease, AAV2 vectors were administered to six cortical locations in ten patients aged 3.4 to 10 years old (disease onset 2 to 4 years). Only a mild transient humoral immune response was reported in four of ten patients. One subject died of status epilepticus 49 days following vector administration. However, seizures are part of the natural disease progression and the subject had no signs of CNS inflammation, so it is likely that the seizures were not a result of vector administration. Clinical data from the 36-month follow-up period suggested that decline per year was slower compared to the untreated control group, but outcome was not significant.

The phase I trial for Canavan was designed to investigate long-term safety of AAV2 vector administration to six cortical locations in ten patients treated between 4 and 83 months old (disease onset 3 to 9 months old). Only a low level transient immune response was reported in three of ten patients, and no long term adverse events were reported in up to 10 years follow-up. Over a minimum follow-up period of 60 months, MRI detected decreased substrate storage, normalization of myelination in some areas, and reversal or stabilization of brain atrophy in some areas with regional and subject-specific variation. Significant clinical improvements occurred for some parameters, such as gross motor function; alertness; spasticity of the lower extremities; and seizure frequency, but not in visual tracking; motor skills; self-care; mobility; social function; and cognitive function. As expected, patients treated at an earlier age experienced the greatest magnitude of clinical improvement.

This dissertation research project describes the outcome of extensive preclinical gene therapy studies in GM1 gangliosidosis and SD cats. The long term goal is to optimize an AAV gene therapy approach that can be translated to human clinical trials. Results demonstrate the effective translation of intracranial gene therapy from gangliosidosis mice to gangliosidosis cats with an ~70-fold-scale-up in brain size, which is indicative of successful scale up to the larger human brain with minimal modification of approach.

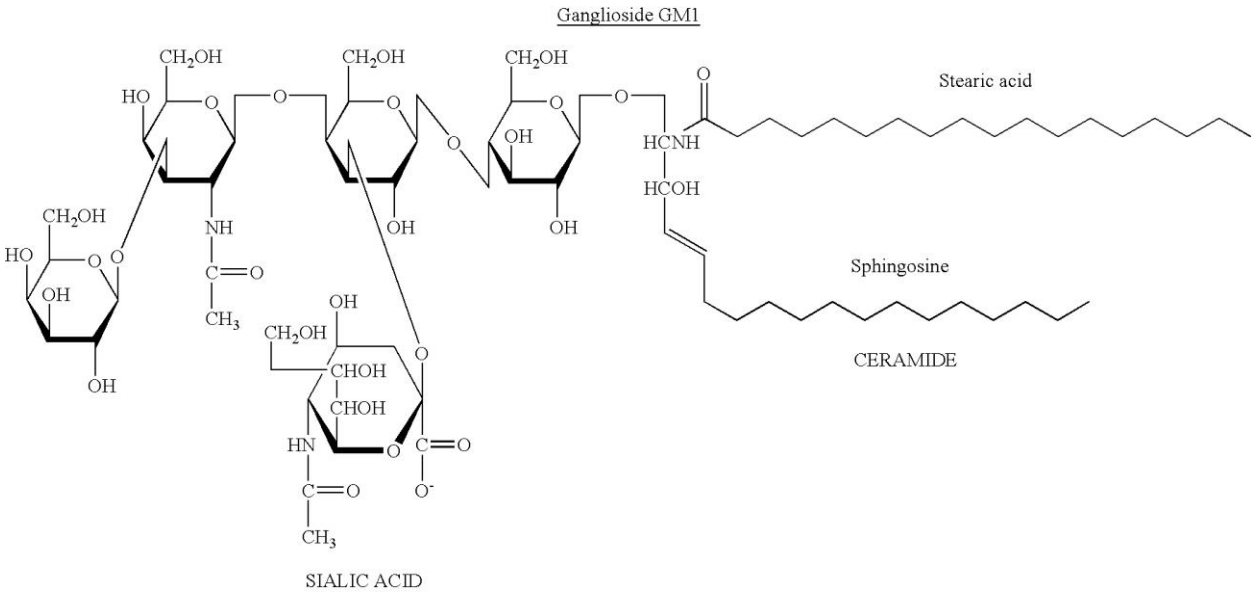

Figure 1. Structure of GM1 ganglioside. The hydrophobic ceramide backbone is the anchor portion of the molecule, and it consists of a sphingosine base linked via an amide linkage to a long chain fatty acid. Ceramide is linked via the terminal hydroxyl group to a hydrophilic oligosaccharide chain containing a sialic acid residue. GM1 is named as such because it contains a mono sialic acid and it is the first molecule in the mono sialic acid series. Cleavage of the terminal galactose residue by βgal yields GM2, the second molecule in the ganglioside mono sialic acid series.

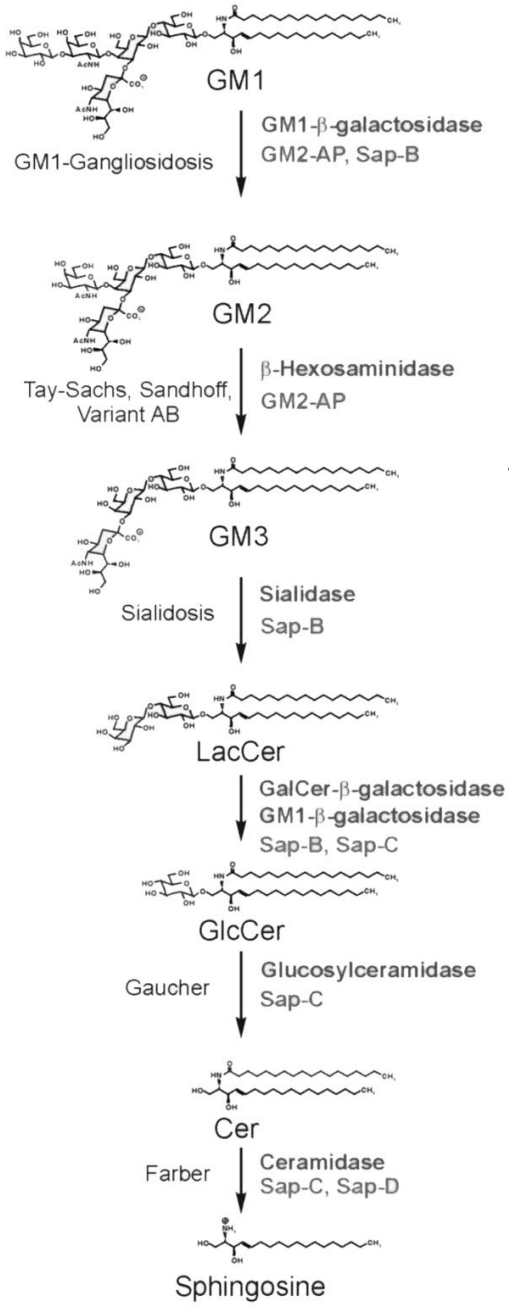

Figure 2. GM1 and GM2 ganglioside catabolic pathway. The ganglioside catabolic pathway takes place in the lysosome. Acid hydrolase enzymes and their activator proteins sequentially cleave monosaccharide residues and sialic acid from the non-reducing end of the molecule to leave the ceramide backbone. Ceramide is cleaved by ceramidase to sphingosine and fatty acid.

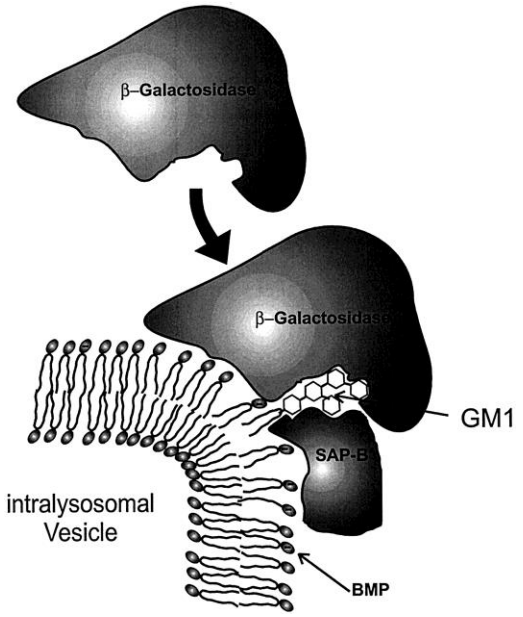

Figure 3[31]**.** Degradation of membrane bound GM1 ganglioside. The saposin B activator protein or GM2 activator protein is required for in vivo cleavage of GM1 by βgal. In the figure, βgal binds to the negatively charged BMP-containing membrane surface. Saposin B acts as a physiological detergent that facilitates the interaction between membrane bound substrate and water soluble hydrolase enzyme, likely by disrupting the membrane surface and lifting the GM1 side chain into the βgal active site. In a similar manner the GM2AP facilitates interaction between HexA and GM2.

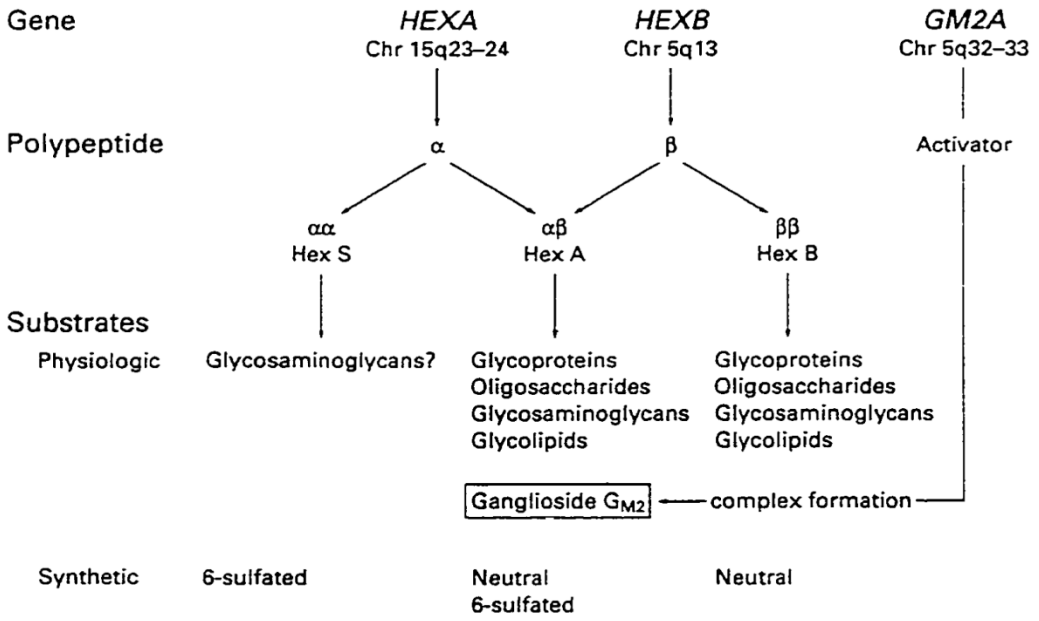

Figure 4[35]**.** Hexosaminidase isozyme subunit composition and substrate specificity. The Major Hex isozymes, HexA and HexB, have overlapping substrate specificities, but only HexA, with the aid of the GM2AP, is capable of GM2 degradation. HexS has negligible catalytic activity toward most Hex substrates, but may be important in the degradation of glycosaminoglycans as SD patients only show modest N-acetyl-galactosamine linked glycosaminoglycan storage despite the absence of the major Hex isozymes. HexA can cleave neutral or charged synthetic substrates, but HexB can only cleave neutral synthetic substrates. HexS can cleave charged synthetic substrates, but with a much lower specific activity then HexA.

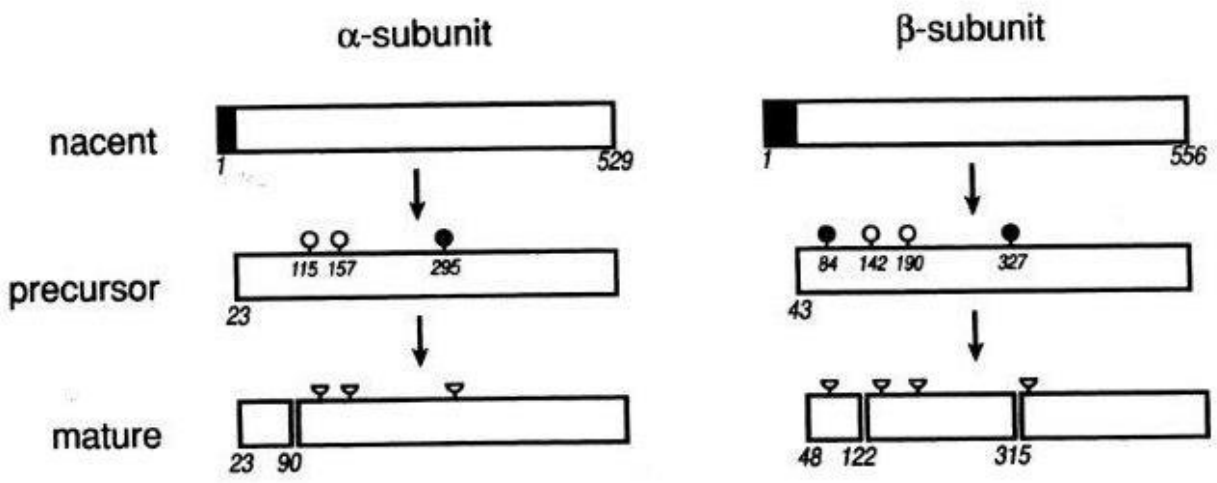

Figure 5[35]. Posttranslational processing of Hexosaminidase α- and β-subunits. Bars represent polypeptides, and filled bars represent signal sequences. Numbers below bars represent the amino acids of the termini. Numbers in bars represent asparagine residues modified by oligosaccharides. Circles represent oligosaccharides, and filled circles indicate preferred phosphorylation sites. The fragments of the mature subunits are held together by disulfide bonds (not shown). Half circles indicate oligosaccharide structures degraded in lysosomes without any effect on activity.

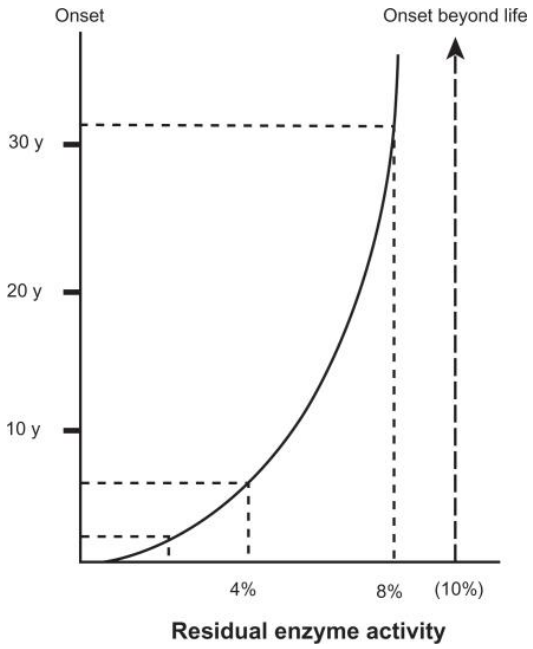

Figure 6. Correlation between residual β-gal activity and clinical disease onset. Residual enzyme activity is positively correlated with the age of clinical disease onset. At least 0.1-fold normal enzyme activity is necessary for normal catabolism of ganglioside. The age of onset in patients expressing enzyme activity above this level is theoretically beyond the human life span. This figure is based on enzyme assay results using cultured skin fibroblasts and the synthetic fluorogenic substrate 4-methylumbelliferyl β-galactopyranoside. Figure taken from: Chaperone therapy update: Fabry disease, GM1-gangliosidosis and Gaucher disease. *Brain and development*. (2013) 35: 517.

Table 1. Characteristic symptoms of the gangliosidoses

Characteristic	GM1 Gangliosidosis			GM2 Gangliosidosis		
	Infantile	Juvenile	Adult	Infantile	Juvenile	Adult
Onset	3-6 mo.	7 mo.- 3 yrs	3-30 yrs	3-6 mo.	2-6 yrs	Child- to adulthood
Age at death (years)	< 2	5-15	Variable course	< 5	5-15	Variable course
CNS involvement	Generalized	Generalized	Localized	Generalized	Generalized	Localized
Mental regression	+	+	+/-	+	+	+/-
Major motor system affected	Pyramidal	Pyramidal	Extrapyramidal[A]	Pyramidal	Pyramidal	Extrapyramidal
Cardiomyopathy[B]	+/-	+/-	+/-	NR	NR	-
Muscle atrophy	-	-	+/-	-	-	+/-
Ocular cherry red spots	+	+/-	-	+	+/-	+/-
Hepatosplenomegaly	+	+/-	-	-	-	-
Dysmorphism	+/-	+/-	-	-	-	-
Skeletal dysplasia	Generalized	Localized	Localized	-	-	-
Visual loss	+	+	-	+	+	-
Startle response to sound	+	+	-	+	+	-
Seizures	+	+	-	+	+	-
Macrocephaly	rarely	-	-	+	-	-
Glomerular epithelial ballooning	+	+	NR	-	-	-
Foam cells in marrow	+	+	+/-	-	-	-
Oligosaccharide storage	+	+	+	+ (SD)	+ (SD)	+ (SD)
Neuronal lipidosis	+	+	+	+	+	+ (Localized)
Visceral histiocytosis	+	+	+	mild (SD)	-/+ (SD)	-
Keratan sulfate storage	+	+	NR	-	-	-
Globoside storage	-	-	-	+ (SD)	+ (SD)	+ (SD)

[A]Pyramidal signs are also present in a minority of patients.

[B]Cardiomyopathy has been reported in all GM1 gangliosidosis disease forms.

Abbreviations: NR = not reported; SD = reported in Sandhoff disease patients; mo. = months

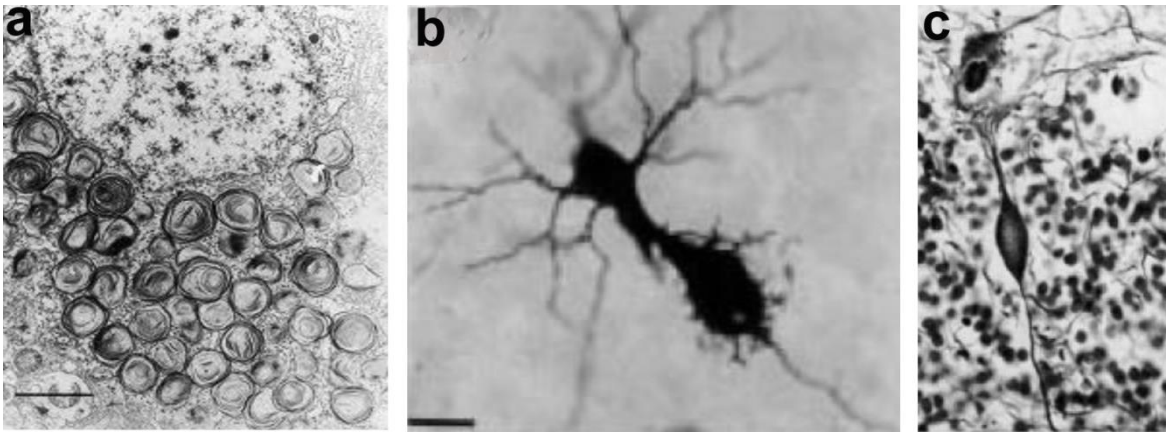

Figure 7[23, 35]**.** Characteristic pathological changes in gangliosidosis diseases. Images are from feline gangliosidosis models. (**a**) Storage material accumulates in MCBs composed of concentric lamellae. (**b**) Meganeurites are swellings of the axon hillock region that sometimes show growth of ectopic dendrites. (**c**) Axonal spheroids are swellings containing organelles, which develop distal to the axon hillock region and are likely caused by a block in retrograde transport.

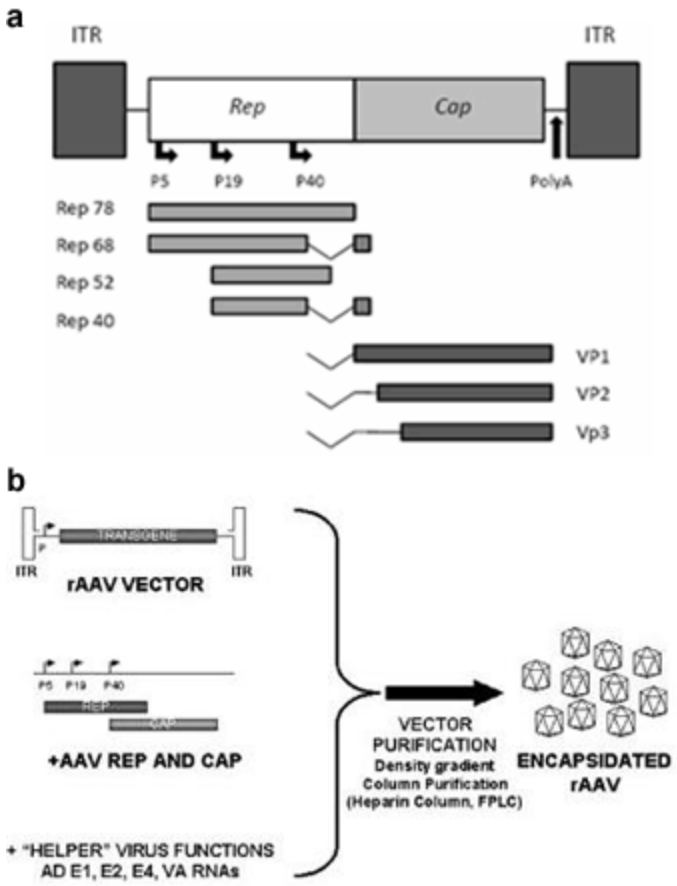

Figure 8[117]**.** AAV genome and production of recombinant AAV vectors. (**a**) The AAV genome consists of *rep*, encoding proteins for replication and packaging; *cap*, encoding proteins for capsid formation; and ITRs. Arrows indicate promoters for transcription of Rep and Cap genes. (**b**) For AAV gene therapy, *rep* and *cap* are replaced by a therapeutic transgene cassette. The viral ITRs are the only elements required in *cis* for replication and packaging of the rAAV genome. Rep and Cap genes are provided on a plasmid in *trans* along with adenovirus helper proteins.

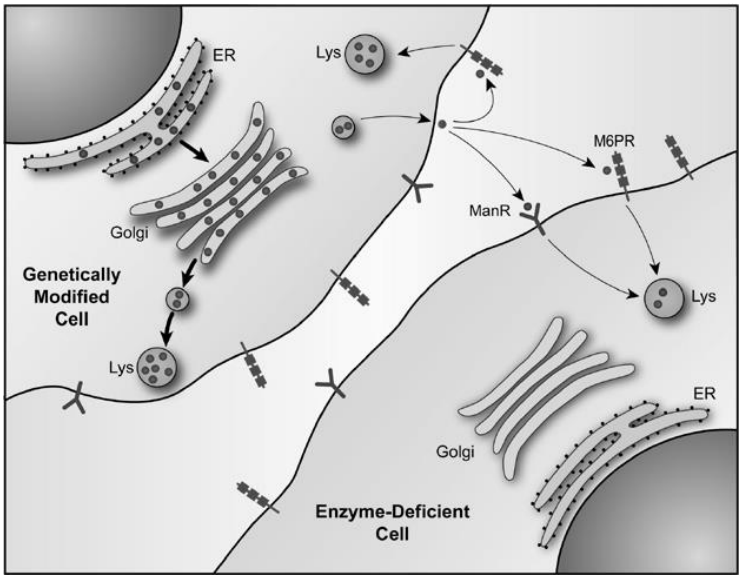

Figure 9. Lysosomal enzyme trafficking and cross-correction. In the Golgi, lysosomal enzymes bind the mannose 6-phosphate receptor (M6PR). The majority (heavy arrows) of the enzymes are trafficked to the mature lysosome (Lys), but a minority (fine arrows) are secreted from the cell. Extracellular phosphorylated or non-phosphorylated enzyme can bind the plasma membrane-localized M6PR or the mannose receptor (ManR), respectively, for lysosomal targeting. Expression of ManR is limited to fixed tissue macrophages. Figure taken from: Gene Therapy for Lysosomal Storage Diseases. *Molecular Therapy*. (2006) 13: 841.

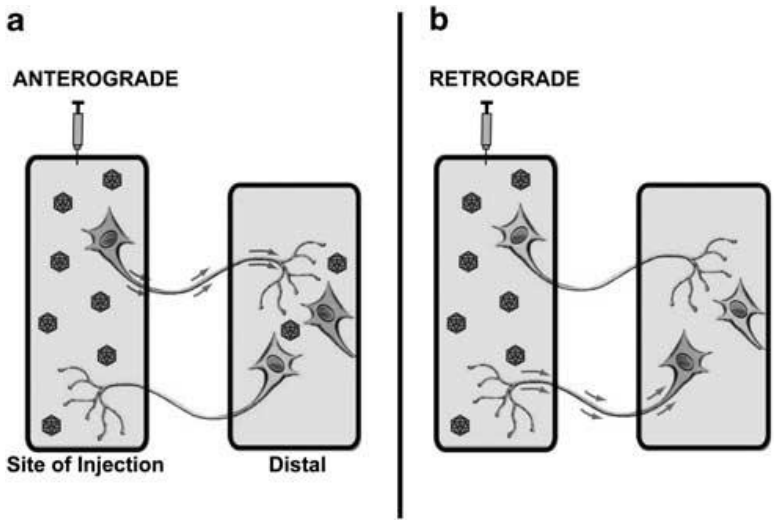

Figure 10[151]**.** Anterograde and retrograde transport after AAV injection. AAV vectors can be transported from the site of injection by anterograde and retrograde transport to connected regions. (**a**) Axonal anterograde transport requires the transport of viral particles via an axon projecting from the site of vector injection to a distal area with subsequent transduction of cells located within the brain region where the axon ends. (**b**) Retrograde transport of AAV vectors occurs when viral particles are taken up by axonal terminals in the injection site and are then transported back to the neuronal cell soma where they subsequently transduce the neuron.

Methods

Surgeries (chapters 1-4 and appendices 1-3)

General anesthesia was induced with ketamine (10 mg/kg) and dexmedetomidine (0.04 mg/kg) through an intravenous catheter and maintained using isoflurane (0.5 to 1.5%) in oxygen delivered through an endotracheal tube. For intracranial injections, cats were positioned sternally using a Horsley-Clark stereotaxic apparatus. Cats received injections of adeno-associated virus (AAV) vectors either 1) bilaterally in the thalamus and deep cerebellar nuclei (DCN), 2) bilaterally in the thalamus and the left lateral ventricle, or 3) intracisternally (IC). Craniotomy sites were made with a 20 gauge (G) needle at the following distances (in cm) from bony landmarks on the skull: thalamus (relative to bregma), anterior-posterior (AP) -0.7, mediolateral (ML) ±0.4, dorsoventral (DV) -1.6 (from meninges); DCN (relative to lambda), AP 0.0, ML ±0.4, DV -1.25 (from meninges); left lateral ventricle, caudo-thalamic notch located by magnetic resonance imaging (MRI) and ultrasound guidance through the bregma or median suture after a 1.5 cm incision of the scalp. Vector was delivered using a Hamilton syringe with a non-coring needle (22 to 25 G). A total of 70 µl was injected into each thalamus in 10 to 20 µl boluses, a total of 24 µl was injected into each DCN in a 10 µl and 14 µl bolus, and a total of 200 µl was injected into the left lateral ventricle at a rate of 15 µl/min. Injection rate was 2 µl/min and the needle was raised 0.15 cm between boluses. For IC injection, the atlanto-occipital joint was accessed with a 25G, 1.5 inch spinal needle then a 1 ml syringe was attached for injection of 200 µl of vector over approximately 2 minutes.

Tissue Preparation (chapters 1-4 and appendices 1-3)

For biochemical analysis, brains were divided into coronal blocks of 0.6 cm from the frontal pole through the cerebellum (chapter 1, **Figure 1A**). Coronal blocks from the right hemisphere were frozen in optimum cutting temperature medium and used for the following analyses: lysosomal enzyme distribution by histochemical staining, lysosomal enzyme specific activity by 4-methylumbelliferone (4MU) enzyme assays (performed in duplicate for each block), AAV vector distribution by SYBR Green quantitative PCR (performed in triplicate for each block), and sialic acid storage by periodic acid Schiff staining. Coronal blocks from the left hemisphere were halved to 0.3 cm and fixed in 10% formalin for routine hematoxylin and eosin (H&E) staining, or stored at -80 °C for analysis of lipid storage by high performance thin layer chromatography (HPTLC) or resorcinol based assay (performed in duplicate).

AAV vector design and preparation for GM1 cats (chapter 1 and appendix 1)

The feline β-galactosidase (βgal) cDNA sequence has the GenBank accession number AF006749. AAV vectors were produced as previously described by triple transfection of 293T cells with vector plasmid (derived from the plasmid pAAV-CBA-EGFP-W by replacing enhanced green fluorescent protein (EGFP) with the cDNA for feline βgal)[73], a mini adenovirus helper plasmid pFΔ6, and AAVrh8 helper plasmid pAR8, or AAV1 helper plasmid pXR1[149]. The inverted terminal repeats (ITRs) in the vectors are derived from AAV2. Transgene expression is controlled by a hybrid cytomegalovirus enhancer/chicken β-actin promoter (CBA). All vectors carry the Woodchuck hepatitis virus posttranslational regulatory element (WPRE).

AAV vector design and preparation for GM2 cats (chapters 2-4 and appendices 2-3)

The feline hexosaminidase (Hex) α- and β- subunit cDNA sequences have GenBank accession numbers JF899596 and JF899597, respectively. AAV vectors were produced as previously described by triple transfection of 293T cells with vector plasmid (derived from the plasmid pAAV-CBA-MGB-W by replacing MGB with cDNA for feline *HEXA* or feline *HEXB*[157]), a mini adenovirus helper plasmid pFΔ6, and AAVrh8 helper plasmid pAR8[149]. The ITRs in the vectors are derived from AAV2. Transgene expression is controlled by CBA, and vectors carry the WPRE element.

Determination of lysosomal enzyme activity (chapters 1-4 and appendices 1-3)

For brain and spinal cord tissue extraction, several frozen sections (50 μm) were cut from each coronal block (**Chapter 1, Figure 1A**). For peripheral nervous system (PNS) and visceral tissue extraction, a sample was taken from tissue stored at -80 °C. Tissue was homogenized manually in 50 mM citrate phosphate buffer, pH 4.4 (50 mM citric acid, 50 mM Na_2HPO_4, 10 mM NaCl) containing 0.1% TritonX 100 and 0.05% bovine serum albumin (BSA), followed by two freeze-thaw cycles and centrifugation at 15,700 g for 5 minutes at 4 °C. Cerebrospinal fluid (CSF) samples were analyzed directly from -80 °C. The activity of βgal, Hex A, total Hex and α-mannosidase activity were measured as previously described using synthetic 4MU fluorogenic substrates[157, 172], but for βgal we measured 10 μl of sample for brain and 30 μl for spinal cord. βgal, 4-MU-β-D-galactopyranoside, pH 3.8; HexA, 1mM 4-MU-6-sulfa-2-Acetoamido-2-Deoxy-β-D-Glucopyranoside (MUGS), pH 4.2; total Hex, 1mM 4-MU-N-acetyl-β-D-glucosaminide (MUG); α-mannosidase, 2 mM 4-MU-α-D-manopyranoside, pH 4.2. Total Hex activity in 8 mm punch biopsy samples was measured as previously described using 40 μl of

sample supernatant and 20 µl of MUG substrate[108]. Specific activity was expressed as nmol 4MU/mg/hr after normalization to protein concentration by the Lowry method.

Histochemical staining for Hex activity (chapters 2-4 and appendices 2-3)

Frozen sections at 40 µM were thawed and fixed for 15 minutes in the presence of 0.1% glutaraldehyde in 4% paraformaldehyde in 0.1M phosphate buffer, pH 7.25. Sections were washed in phosphate buffered saline and then in citrate phosphate buffer (50 mM $Na_2HPO_4.7H_2O$, 50 mM citric acid monohydrate), pH 4.5. Tissue sections were then incubated for 3 hours at 4 °C in citrate phosphate buffer, pH 4.5 containing 0.20 mM naphthol AS-BI-N-acetyl-B-D-glucosaminide (naphthol) followed by a 2 hour incubation at room temperature in citrate phosphate buffer, pH 5.2, containing 0.25mM naphthol in the presence of 4% hexazotized pararosalinine (containing 4% pararosaniline hydrochloride and 4% $NaNO_2$) as previously described[173]. Sections were washed in ddH_2O, dehydrated and mounted.

Histochemical staining for βgal activity (chapter 1 and appendix 1)

Frozen sections at 40 µM were thawed and fixed in 0.5% glutaraldehyde in citrate phosphate buffer (50 mM $Na_2HPO_4.7H_2O$, 50 mM citric acid monohydrate, 10 mM NaCl), pH 4.2 (brain) or pH 5.2 (spinal cord) for 10 minutes followed by washes in citrate phosphate buffer. Tissue sections were then incubated at 37 °C overnight in citrate phosphate buffer, pH 4.2 (brain) or pH 5.2 (spinal cord) containing 20 mM $K_4Fe(CN)_6$, 20 mM $K_3Fe(CN)_6$, 2 mM $MgCl_2$,0.02% IGEPAL, 0.01% deoxycholic acid and 2 mg/ml 5-bromo-4-chloro-3-indolyl-β-D-galactopyranoside (Xgal). The next day, sections were washed, dehydrated and mounted.

Periodic Acid Schiff (PAS) staining for ganglioside storage material (chapters 1, 3, and 4)

Storage material was assessed qualitatively with PAS staining, which detects the oligosaccharide side chain of ganglioside. Frozen sections (20 μM) were washed in phosphate buffered saline (PBS), fixed for 7 minutes with 3.7% paraformaldehyde in 95% ethanol/5% ddH_2O (pH 7.4), washed again with PBS, incubated for 3 minutes in 0.5% periodic acid, washed in double distilled H_2O and incubated in Schiff reagent for 45 seconds (brain) or 60 seconds (spinal cord).

Lipid extraction and sialic acid quantification (Chapters 1 and 4)

Punch biopsies of 8 mm diameter were taken from representative areas of the brain and spinal cord and lyophilized overnight. The next day, 10-25 mg of dry weight sample was rehydrated in 0.5 ml of water and total lipids extracted in 5 ml of chloroform: methanol (1:1 by volume). Samples were stirred at room temperature for at least 4.5 hours and centrifuged at 850 g for 20 minutes. Supernatant was collected and the pellet extracted again in 2 ml of chloroform: methanol for 15 minutes before another centrifugation. Supernatants for each sample were combined to measure sialic acid by the method of Svennerholm[174] with modification from Miettinen[175]. A 0.25 ml aliquot was evaporated, re-dissolved in 0.5 ml of H_2O, dissolved in 0.5 ml of resorcinol reagent (5 ml of distilled H_2O, 40 ml of HCl, 0.125 ml of 0.1M copper sulfate, 5 ml of 2% resorcinol stock in distilled H_2O), and boiled for 15 minutes. After cooling for 10 minutes, 1 ml of butyl acetate:butanol solution (85:15 v/v) was added and each sample was mixed vigorously. The upper phase was removed and read at 580 nm using a Shimadzu UV 160U spectrophotometer. Sialic acid concentration was expressed as nmol/mg.

Lipid extraction and sialic acid quantification (chapter 2 and appendix 2)

Samples were homogenized in water and lyophilized overnight. Lipid isolation and purification has been detailed previously[102]. Briefly, dried tissue was rehydrated in 0.5 ml of H_2O and lipids were extracted in chloroform ($CHCl_3$):methanol (MeOH) (1:1 v/v). Neutral and acidic lipids/gangliosides were separated using ion exchange chromatography on a DEAE-Sephadex column as previously described. Neutral lipids and cholesterol were eluted with ($CHCl_3$:CH_3OH:dH_2O, 30:60:8 v/v/v) and acidic lipids and gangliosides were eluted with $CHCl_3$:CH_3OH:0.8 M CH3COONa (30:60:8 v/v/v). Acidic lipids and gangliosides were dried by rotary evaporation, separated by Folch partitioning, base treated and desalted. Total ganglioside content was quantified before and after desalting using a resorcinol assay. Neutral lipids were dried by rotary evaporation and re-suspended in CHCl3:CH3OH (2:1 v/v). To further purify GA2, an aliquot was evaporated under a stream of nitrogen, treated with 1 N of NaOH and Folch partitioned.

High performance thin layer chromatography (HPTLC) (chapter 2 and appendix 2)

All lipids were analyzed qualitatively by HPTLC as detailed previously[102]. To enhance precision, oleoyl alcohol was added as an internal standard to the neutral and acidic lipid standards and samples. Lipids were spotted on 10 x 20 cm Silica gel HPTLC plates using a Camag Linomat V semi-automatic TLC spotter. Purified lipid standards were purchased from Matreya or were a gift from Dr. Robert Yu (Medical College of Georgia, Augusta, GA). Each lane was spotted with: 1.5 μg of sialic acid for gangliosides, 70 μg of dry weight for neutral lipids and 200 μg of dry weight for acidic lipids and GA2. Ganglioside and GA2 HPTLC plates were developed in a single ascending run for 90 minutes with $CHCL_3$: CH_3OH: dH_2O (55:45:10

v/v/v for gangliosides; $CHCL_3$:CH_3OH:dH_2O 65:35:8 v/v/v for GA2) containing 0.02% $CaCl_2$ (aq). Plates were sprayed with resorcinol-HCl reagent and heated at 95 °C face down for 10 minutes and face up for 1 minute to visualize gangliosides, or face up for 5 minutes to visualize GA2. Neutral and acidic lipid HPTLC plates were developed to a height of 4.5 or 6 cm, respectively, in $CHCL_3$:CH_3OH:CH_3COOH:$CHOOH$:dH_2O (35:15:6:2:1 v/v/v/v/v). Plates were dried and developed to the top in C_6H_{14}:$C_6H_{14}O$:CH_3COOH (65:35:2 v/v/v). Bands were visualized by charring with 3% cupric acetate in 8% phosphoric acid solution for 7 minutes.

Quantification of individual lipids (chapter 2 and appendix 2)

The percent distribution and density of individual bands was determined as previously described[108]. Total brain ganglioside distribution was normalized to 100% and the percentage distribution values were used to calculate sialic acid concentration of GM2 (μg/100 mg dry weight). Density values of neutral lipids, acidic lipids and GA2 were fit to a standard curve and used to calculate individual concentrations.

Serum antibody titers (chapter 2)

100 ng of AAV vector was coated onto enzyme linked immunosorbent assay (ELISA) plates and incubated overnight at 4 °C. Plates were washed then blocked with 5% non-fat powdered milk in phosphate-buffered saline for 90 minutes at room temperature. Next, 100 μl of two-fold serial dilutions of feline serum samples were added. Goat anti-feline IgG:HRP (1:20,000) was used for color development with tetramethylbenzidine.

DEAE cellulose anion exchange chromatography (chapter 2)

Several frozen sections (50 µm) were cut from the coronal block containing the thalamus. Frozen brain tissue was extracted as previously described[23] in a 10 nmol/l sodium phosphate buffer (pH 6.0) containing 0.1% Triton-X 100. Supernatant was applied to a diethylaminoethyl (DEAE) cellulose column and 0.5 ml each of fractions 1 to 26 were collected as previously described[23] by washing the column with buffer (above) containing sodium chloride at increasing concentrations ranging from 0 to 400 mmol/l.

Quantitative PCR for vector genomes (chapters 1-4 and appendices 1-3)

Vector was measured by quantitative PCR using SYBR®Green-based reactions with primers specific for WPRE in the vector (forward 5'-AGTTGTGGCCCGTTGTCA-3'; reverse 5'-GAGGGGGAAAGCGAAAGT-3'). Samples were incubated for 2 minutes at 50 °C, 10 minutes at 95 °C, and then amplified for 40 cycles of 95 °C for 30 seconds, 62 °C for 30 seconds, and 72 °C for 45 seconds. Genomic DNA samples (20 ng for spinal cord, 50 ng for brain and 25-250 ng for peripheral tissue) were measured in triplicate on a BioRad CFX96 Real-Time System and compared to a standard curve generated from a plasmid containing WPRE (1×10^8 to 1×10^0 copies). The assay limit of detection (LOD) above background was 20 AAV copies/reaction. Background amplification was determined on DNA from untreated normal and untreated GM1 gangliosidosis or SD cats.

Magnetic resonance imaging (MRI) (chapters 1, 3 and 4)

Data were acquired on a 3T MAGNETOM Verio scanner with an eight channel phased array wrist coil. Whole-brain anatomical images were acquired with 3D MP RAGE (three-

dimensional magnetization-prepared rapid gradient echo) with 0.4 mm isotropic resolution and repetition time (TR)/ echo time (TE) of 1900/3.3 ms, followed by whole-brain multi slice 2D axial T2 TSE (turbo-spin echo) images with TR/TE of 4630/107 ms, turbo factor of 9 and a resolution of $0.3\times0.3\times1$ mm^3. MRI data were analyzed with eFilm 3.2 software.

Clinical rating scores (chapters 1-4)

Cats were assigned a clinical rating score (CRS) using two separate, independent readouts: (1) neurological exams performed by a veterinarian at two to four week intervals and (2) video footage at approximately 1 month intervals, which was retrospectively analyzed by the author.

Statistical Analysis

Data are expressed as means ± standard deviation throughout the text and figures. Statistics were performed with SAS 9.2 software, and $P \leq 0.05$ was considered significant for all tests. The Wilcoxon signed rank test was used for pairwise comparisons of lysosomal enzyme activity, AAV vector distribution, and sialic acid levels. One-sided testing is reported throughout the text and figures to determine directional significance (that is, significantly higher or lower values), which would often not be realized using two-sided testing because of low animal numbers when using a feline model. The logrank test was used for survival comparison between groups. No data were excluded from analysis and, because outliers are hard to determine with small sample sizes, no data points in the study were defined as outliers.

Chapter 1: Sustained normalization of neurological disease after intracranial gene therapy in a feline model of GM1 gangliosidosis

Published as: Sustained Normalization of Neurological Disease After Intracranial Gene Therapy in a Feline Model. In: *Science Translational Medicine*. Volume 6, Issue 231 (2014).

Abstract

Progressive debilitating neurological defects characterize feline GM1 gangliosidosis, a lysosomal storage disease caused by deficiency of lysosomal β-galactosidase. No effective therapy exists for affected children, who often die before age 5 years. An adeno-associated viral vector carrying the therapeutic gene was injected bilaterally into two brain targets (thalamus and deep cerebellar nuclei) of a feline model of GM1 gangliosidosis. Gene therapy normalized β-galactosidase activity and storage throughout the brain and spinal cord. The mean survival of 12 treated GM1 gangliosidosis animals was >38 months compared to 8 months for untreated animals. Seven of the eight treated animals remaining alive demonstrated normalization of disease, with abrogation of many symptoms including gait deficits and disequilibrium. Sustained correction of the GM1 gangliosidosis disease phenotype after limited intracranial targeting by gene therapy in a large animal model suggests that this approach may be useful for treating the human version of this lysosomal storage disorder.

Introduction

GM1 gangliosidosis is an autosomal recessive lysosomal storage disease (LSD) caused by deficiency of β-galactosidase (βgal, EC 3.2.1.23), the enzyme that hydrolyzes terminal galactose residues from numerous molecules. βgal deficiency leads to neuronal storage of GM1 ganglioside and its asialo derivative (GA1), resulting in progressive neurodegeneration and death death[15, 24]. Three clinical forms exist and are thought to result from differing levels of residual enzyme activity[37]. Infantile- and juvenile-onset forms are fatal by ages 5 and 15 years, respectively, whereas the adult-onset phenotype varies considerably, with some patients living into the sixth decade[24]. No effective therapy exists for GM1 gangliosidosis.

Because βgal deficiency affects the central nervous system (CNS) globally, successful treatment strategies must target widespread areas of the brain and spinal cord. Whereas the circulatory system provides global access to the CNS for select molecules, lysosomal enzymes are excluded by the blood-brain barrier (BBB), making the task of enzyme replacement challenging. Therapeutic challenges posed by the BBB may be overcome by several key characteristics of lysosomal enzymes. First, even low concentrations of enzyme may be therapeutic, with activity in adult-onset LSD patients and clinically normal carriers reported at 2 to 4% and 11% of homozygous normal, respectively[83]. Also, diseased cells are able to endocytose and use normal lysosomal enzymes, so a locus of treated cells may "cross-correct" a broad sphere of untreated neighboring tissue[80, 81]. Finally, lysosomal enzymes are distributed in the CNS by multiple mechanisms such as diffusion[129], axonal transport[130-132] and cerebrospinal fluid (CSF) flow[132, 140, 141, 146, 160], which also apply to gene therapy vectors.

Recently, adeno-associated viral (AAV) vectors have achieved widespread CNS distribution of lysosomal enzymes after injection into highly interconnected brain structures such as the ventral tegmental area, striatum, thalamus, and deep cerebellar nuclei (DCN)[131, 135, 139, 140,

[142]. Most GM1 gangliosidosis mice treated by AAV injection of the thalamus and deep cerebellar nuclei survived for 52 weeks (the experimental endpoint) compared to a median survival of 38 weeks in untreated animals. βgal activity was restored to a presumed therapeutic level (>10% wildtype mice) throughout the CNS, with normalization of substrate storage in the brain and a 50% reduction of substrate storage in the spinal cord[135]. Because the mouse brain is 1000 times smaller than that of a human infant, we tested AAV-based gene therapy in a feline model of GM1 gangliosidosis.

First described in 1971, naturally occurring feline GM1 gangliosidosis is an accurate model of the human juvenile-onset disease in terms of enzymatic deficiency (<10% normal βgal activity), storage levels, and CNS and peripheral organ pathology[46, 70, 72, 176]. Clinical disease progression is remarkably stereotypical, with affected cats reaching a humane endpoint at 8.0 (± 0.6) months. The naturally occurring feline mutation is analogous to a well-characterized human mutation that generates normal amounts of enzymatically defective βgal protein (that is, positive for cross-reactive material, or CRM+)[73, 177-179]. The feline brain is ~20 times smaller than an infant's brain and provides a good approximation of enzyme and vector distribution challenges that need to be overcome for human gene therapy. Here, GM1 gangliosidosis cats were treated by intracranial injection of AAV vectors encoding feline βgal. Short- and long-term assessments of therapeutic effect included clinical and MRI-based analyses accompanied by postmortem assays to evaluate normalization of biochemical defects.

Results

Treatment groups

Twenty three GM1 gangliosidosis cats were treated before the average age of clinical disease onset by bilateral injection of the thalamus and deep cerebellar nuclei with AAV vectors expressing feline βgal from a hybrid cytomegalovirus enhancer/chicken β-actin (CBA) promoter [serotype AAV1 (n = 8) or AAVrh8 (n = 15)]. Cats were treated with either a traditional serotype already in human use (AAV1) or a new serotype that has shown promise in mouse experiments (AAVrh8). Outcomes were assessed at 16 weeks after injection (short term, n = 7) or at the humane endpoint (long term, n = 16), defined by the inability to stand on two consecutive days. **Table 1** summarizes the study design.

Widespread distribution of βgal and AAV

Sixteen weeks after a single surgery lasting ~90 minutes, βgal activity exceeded normal (homozygous for the wildtype allele) concentrations throughout the brain and spinal cord of GM1 gangliosidosis cats (**Figure 1A-C**). Activity was highest at the injection sites (**Figure 1B**) and decreased with distance from the thalamus and deep cerebellar nuclei, yet βgal staining was normal or above normal in most brain regions. Specific activity measured with a synthetic fluorogenic substrate ranged from 1.1- to 4.1-fold that of normal across all coronal brain blocks for cats treated with AAVrh8 (**Table 2**). In AAV1-treated cats, βgal brain activity ranged from 1.4- to 4.2-fold that of normal, and there was no statistical difference in βgal concentrations when compared to the AAVrh8 cohort ($P \geq 0.22$ for each block; **Table 2** and **Figure S1**).

βgal activity in the spinal cord at 16 weeks after injection also was near- or above-normal, with no statistical difference between the two AAV vectors ($P \geq 0.22$ for each block;

Table 2). When measured in seven coronal blocks from the cervical, thoracic and lumbar spinal cord, βgal activity ranged from 1.6- to 4.8-fold that of normal in the AAVrh8 cohort and from 0.9- to 4.2-fold that of normal in the AAV1 cohort (**Figure 1C**, **Figure S1**, and **Table 2**). Residual βgal activity in untreated GM1 gangliosidosis cats ranged from 0.0- to 0.1-fold and 0.0- to 0.04-fold that of normal in the brain and spinal cord, respectively. Both vector cohorts demonstrated statistically significant increases in βgal activity versus untreated animals ($P \leq$ 0.026 for each block). Vector genomes (vg) were detected in all brain and spinal cord blocks, demonstrating widespread dissemination from the injection sites, although vector levels did not always correlate with βgal activity (**Table 3**).

CSF βgal activity was 28-fold that of normal in the AAVrh8 cohort and 42-fold that of normal in the AAV1 cohort, which was significantly higher than in untreated GM1 gangliosidosis cats (P = 0.026 for each cohort; **Table 2**). Additionally, βgal activity and vector genomes were present in the liver of both AAV-treated cohorts demonstrating dissemination of enzyme and vector to peripheral tissues after intraparenchymal brain injection (**Tables 2 and 3**). Liver βgal activity measured 0.38- and 0.24-fold that of normal in the AAVrh8 and AAV1 cohort, respectively, which was significantly higher than in untreated GM1 gangliosidosis cats (AAVrh8, P = 0.015; AAV1, P = 0.026).

Clearance of storage material

As glycosphingolipids with complex oligosaccharide side chains containing one or more sialic acid residues[16], gangliosides can be detected colorimetrically by a variety of methods. To evaluate the clearance of stored substrate by vector-generated βgal, we performed periodic acid Schiff (PAS) staining in the CNS in GM1 gangliosidosis cats 16 weeks after treatment. Storage

levels were substantially normalized throughout most of the brain and spinal cord, but clearance was incomplete in focal areas of the temporal lobe and cervical spinal cord (**Figure 2A**) that corresponded with sites of minimal βgal activity in **Figure 1**.

When quantitative sialic acid assays were performed on 15 samples throughout the CNS (**Figure 2B, C**), concentrations in untreated GM1 gangliosidosis cats were significantly higher than that of normal in the cerebrum (2.5- to 3.9-fold normal; $P \leq 0.015$), cerebellum (1.8- to 1.9-fold normal; $P \leq 0.015$) and spinal cord (1.9- to 2.5-fold normal; $P \leq 0.015$). Treatment with AAV1 or AAVrh8 significantly reduced storage in all CNS samples ($P \leq 0.026$), with the exception of the caudal cerebellum from AAV1-treated cats, for which samples from only two animals were available (**Figure 2B, C**, block h, $P = 0.053$). Although reduced by gene therapy, storage remained above normal in 4 of 15 samples including the temporal lobe (sample d3 in **Figure 2B**), rostral and middle cerebellum (samples f and g1 in **Figure 2B**), and cervical spinal cord (sample K in **Figure 2B**). In one sample from the frontal pole of AAVrh8-treated cats, sialic acid was reduced to 0.83-fold of normal (sample a in **Figure 2B**; $P = 0.033$).

Normalized activity of other lysosomal enzymes

In βgal deficiency, the activity of other lysosomal enzymes is above normal[70, 180]. For example, lysosomal β-N-acetylhexosaminidase (EC 3.2.1.52) activity was elevated up to 3.7-fold that of normal in the CNS and 2.0-fold that of normal in the liver of untreated GM1 gangliosidosis cats ($P \leq 0.015$ for each CNS block and for liver; **Figure 3**). Treatment for 16 weeks with either AAV serotype reduced hexosaminidase activity significantly in the brain ($P \leq 0.026$ for each block), spinal cord ($P \leq 0.026$ for each block) and liver ($P \leq 0.026$), demonstrating normalization of a secondary lysosomal biomarker after gene therapy (**Figure 3**).

Long-term clinical benefit of AAV treatment

Long term clinical benefit in GM1 gangliosidosis cats was assessed after treatment with AAV1 (n = 5) or AAVrh8 (n = 7) serotypes. As shown in **Table 1**, animals were treated with 3×10^{12} to 4×10^{12} vector genomes (vg) ("full dose," n = 9) or 1.2×10^{13} vg when AAV1 titers made this "high dose" possible (n = 3). Statistically significant increases in survival have been achieved for both the AAV1 ($P = 0.0004$) and AAVrh8 ($P < 0.0001$) cohorts (**Figure 4A**). Currently, the mean survival of treated GM1 gangliosidosis cats is >4.7 times that of untreated cats: 39.1 (± 10.1) months for the AAV1 cohort and 37.7 (± 12.4) months for the AAVrh8 cohort. Eight of 12 treated cats remain alive, most with subtle or no disease signs. The oldest cats from each vector cohort remain alive and well at 52.8 (AAV1) and 50.5 (AAVrh8) months, or >6.3 times the life span of untreated cats. Of the four cats no longer living, two had normal gait at 29.0 months (9-1515) and 47.9 months (8-1397) but were euthanized because of abnormal recovery from anesthesia.

Disease onset in treated cats was delayed versus untreated GM1 gangliosidosis controls, whose stereotypical disease progression began at 4.1 (± 0.6) months of age with fine tremors of the head and tail. Clinical symptoms in untreated animals progressed to generalized muscle weakness, wide-based stance, ataxia, carpal hyperextension (in 80% of cats), instability with occasional falling, loss of ambulation, and finally the inability to stand, which defined the humane endpoint at 8.0 (± 0.6) months. Of 12 treated GM1 gangliosidosis cats, disease onset is yet to be determined in four animals ranging from 34.6 to 44.9 months of age. Also, three cats whose disease onset occurred at 10.2, 36.6 and 37.0 months currently have only mild disease at 44.8, 50.5 and 52.8 months, respectively (8-1435, 8-1364 and 9-1356).

Quality of life for treated GM1 gangliosidosis cats has improved markedly, as measured by a clinical rating scale that reflects an animal's departure from normal function (**Figure 4B, C**). Clinical rating scores decrease from 10 (normal function) to 1 (lateral recumbency) as animals become more debilitated by gait defects and balance disturbances/instability. Currently, minimal disease progression has been documented for five of seven animals in the AAVrh8 cohort (**Figure 4B, C**) and four of five animals in the AAV1 cohort (**Figure S2**), whose composite clinical rating scores at 40 months of age were 9.5 (± 0.6) and 9.7 (± 0.6), respectively. Whereas untreated GM1 gangliosidosis cats have severe dysequilibrium and gait defects by 7 months of age, most treated GM1 gangliosidosis cats remain overtly normal or have only subtle gait abnormalities. No difference in therapeutic benefit is discernible between the AAV1 and AAVrh8 cohorts.

In 3 of 12 AAV-treated cats, therapeutic response was clearly positive but less marked. One cat that was symptomatic at the time of surgery (8-1626) has moderately progressive disease at 29.4 months of age, although current symptom acquisition has been delayed about threefold. Two animals had disease onset at 6.1 (8-1378) and 4.6 (9-1545) months of age, ultimately reaching humane endpoint at 17.5 and 25.3 months, respectively. Conclusions regarding why 3 of 12 treated animals responded less robustly than others await tissue analysis from more cats in the long term cohort. However, diminished enzyme activity is a reasonable hypothesis because both cats that reached the humane endpoint (8-1378 and 9-1545) had low βgal concentrations in the spinal cord (≤0.4-fold normal and ≤0.14-fold that of samples from the 16 week time point). In contrast, two cats that had normal gait at 29.0 and 47.9 months of age (9-1515 and 8-1397, respectively) had above-normal βgal activity in the spinal cord that was comparable to the 16 week cohort (**Figure 5**). βgal activity in CSF was above normal (2.5 to 63.1 fold) in all cats from

the long term cohort, perhaps explaining why there was no correlation between CSF activity and clinical outcome/life span (**Figure 5**).

Half of all treated cats in the long term cohort (6 of 12) experienced seizure activity, well-controlled by medication, with a mean onset of 20.1 (± 7.4) months (Table 1). Common symptoms included blank stares, salivation, and facial twitches, but progression to undirected running and tonic-clonic seizures did occur in some animals. In at least three of six animals, seizures were demonstrably inducible by sounds such as running water. No seizures occurred in GM1 gangliosidosis cats treated for only 16 weeks (n = 7). Seizures are a known feature of late-stage feline GM1 gangliosidosis[46, 72], although no untreated GM1 gangliosidosis cats in the current study had seizures because they occur well beyond the humane endpoint used.

Normalization of MRI brain architecture

On T2-weighted MRI, cortical white matter is hypointense to (that is, darker than) gray matter in normal cats but is hyperintense to (that is, lighter than) gray matter in untreated GM1 gangliosidosis cats with moderate to severe disease. Also, the deep cerebellar nuclei area is hypointense to cerebellar gray matter in normal cats but becomes isointense with disease progression in untreated GM1 gangliosidosis cats. Therefore, MRI provides an easily discernible, non-invasive biomarker of disease progression (**Figure 6**). In AAV-treated GM1 gangliosidosis cats, hypointensity of white matter to gray matter is substantially normalized in the cortex to at least 32 months of age (cat 8-1364), or more than five times longer than in untreated cats. Additionally, hypointensity of the deep cerebellar nuclei area to surrounding gray matter is largely preserved after AAV treatment. Overall brain architecture of treated GM1 gangliosidosis cats is normal, although slight widening of sulci is appreciated in some animals.

To date, the only abnormality associated with AAV treatment is an irregularly-shaped locus of T2 hyperintensity in the thalamus of 5 of 11 cats evaluated (**Figure 6**). In previous studies of gene therapy in feline GM2 gangliosidosis (Sandhoff disease), similar hyperintense loci were thought to be associated with eosinophilic, botryoid neurons in hematoxylin and eosin sections from the dorsal thalamic nuclei[157]. In treated GM1 gangliosidosis cats in the current study, fine eosinophilic granules were found in scattered cortical and hippocampal neurons dorsal to the injection site (**Figure S3**), but not in thalamic regions corresponding to T2 hyperintensities. The underlying cause of hyperintense thalamic loci remains to be defined. Detected in AAV-treated cats by 6 months of age, T2 hyperintensities were not present in untreated cats at any age, including the humane endpoint of ~8 months. No histological or MRI anomalies were found in three normal cats injected with saline and followed for >18 months.

Dose response

When GM1 gangliosidosis cats were treated with one-tenth of the full AAVrh8 dose, mean survival was 17.1 (± 3.6) months, significantly lower than the full dose cohort ($P = 0.0046$, **Figure 4A**). Of four cats treated with the one-tenth dose, two reached the humane endpoint at 14.2 and 19.1 months of age, one was euthanized at 13.9 months due to chronic weight loss and lethargy, and one was euthanized at 21.2 months because of dysphagia, also reported in juvenile-onset GM1 gangliosidosis patients[181]. Nevertheless, the mean survival of the one-tenth dose cohort was 2.1 times greater than that of the untreated GM1 gangliosidosis cats ($P = 0.0012$). βgal activity and vector copies for the one-tenth dose cohort are detailed in **Tables 2 and 3**. Liver βgal activity of only 0.17-fold that of normal was sufficient to fully normalize hexosaminidase activity ($P = 0.015$ versus untreated GM1 gangliosidosis cats; **Figure S4**).

Restoration of breeding function

In >40 years of study, no female GM1 gangliosidosis cat has become pregnant and no GM1 gangliosidosis male has been fertile. After AAV injection, two treated males bred two treated females and four untreated carrier females, producing a total of nine litters (27 kittens). Treated GM1 gangliosidosis cats bred successfully from 9.8 to at least 28.6 months of age. Fertility onset for carrier or normal colony cats is ~7 months. GM1 × GM1 matings produced litters composed entirely of GM1 gangliosidosis kittens, which had stereotypical disease progression and life span. In agreement with previous reports[182, 183], vector was detected only transiently in gonads and no evidence of germ line gene transmission was found in treated cats or their offspring (**Table S1**).

Discussion

As a group, LSD prevalence is ~1 in 7,700 live births[1], similar to that of cystic fibrosis or hemophilia. Like most lysosomal diseases, GM1 gangliosidosis is neurodegenerative and fatal, with only palliative measures currently available to patients. Promising results have been achieved with intracranial AAV injections in rodent models of gangliosidosis. Treated GM2 gangliosidosis mice demonstrate near normalization of life span, representing a more than fivefold survival increase versus untreated GM2 gangliosidosis mice[140]. Also encouraging are data from large animal models of neurodegenerative lysosomal diseases. In dogs with mucopolysaccharidosis I or IIIb, intracranial gene therapy with AAV vectors improved storage and histological lesions throughout most of the brain, although no clinical or survival benefit was demonstrated[158, 165]. Cats with α-mannosidosis treated by intracranial injections of an AAV1 vector through 14 burr holes had only mild neurological disease at the untreated humane

endpoint of 18 weeks, with restoration of α-mannosidase activity to ~4% normal in the brain. Because of the study design, improved survival benefit was not achieved, although one of two treated cats followed long term had only mild disease when euthanized at 56 weeks of age[164].

The current report documents above-normal βgal activity throughout the GM1 gangliosidosis cat brain and spinal cord after intracranial injections of AAV vectors carrying the therapeutic gene through only four burr holes in a surgery lasting ~90 minutes. The successful translation of a treatment approach from GM1 gangliosidosis mice to GM1 gangliosidosis cats, with an approximate 70-fold scale-up of brain size suggests that this approach may be beneficial in human patients. Although the human brain is ~20 times larger than the cat brain, the thalamus and deep cerebellar nuclei also are proportionally larger, allowing an equivalent AAV dose per kilogram of brain weight. In 12 treated animals followed long term, mean life span was extended greater than 4.7-fold and continues to increase because most of the treated cats are disease-free or have only subtle symptoms at present. Quality of life improved profoundly, with only 2 of 12 treated animals having progressed to the most debilitating symptoms such as dysequilibrium and severe ataxia. Clinical outcomes were similar for the two vector serotypes tested: AAV1, currently in human clinical trials[184-187] or approved for human use[188, 189] and AAVrh8, a new serotype[190] that showed promise in a related feline model[157].

Little toxicity was apparent from the vector. The eosinophilic granules in brain neurons of treated GM1 gangliosidosis animals may represent a less extreme version of the large, botryoid hypereosinophilic inclusions previously reported in Sandhoff and normal cats treated with AAVrh8 vectors that overexpressed feline hexosaminidase, often at >50 times normal[157]. In our treated GM1 gangliosidosis cats, typical βgal expression is less than or equal to fourfold normal, so it is possible that fine eosinophilic granules represent inclusions with mildly over-

expressed βgal. Additionally, there was limited toxicity from the injection procedure. A thalamic hemorrhage documented by MRI in one animal (8-1435) caused ataxia, head tilt and cortical blindness that resolved after 1 week of treatment with mannitol and steroids. Now >44 months of age, 8-1435 has only slight hind limb gait deficits and is the first fertile male in the 40-year history of the research colony.

Although about half of AAV-treated GM1 gangliosidosis cats had hyperintense thalamic loci on T2-weighted images, no histopathological or clinical correlates were identified. In related ongoing studies, similar loci were found in the thalamus of four of six normal cats treated with AAVrh8 vectors expressing feline hexosaminidase, none of which had seizures in >18 months of follow-up. Because no seizure activity was observed in three of five treated GM1 cats with T2 anomalies, a causal relationship between hyperintense thalamic loci and seizures is unlikely. Known to occur in late-stage GM1 gangliosidosis disease in both humans[181, 191, 192] and cats[46, 72], seizures in treated animals may result from progressive disease in the temporal lobe, one of the few brain regions with incomplete restoration of βgal activity (**Figure 1B**) and only partial normalization of storage (**Figure 2A, C**). Seizures in treated GM1 gangliosidosis cats often resemble temporal lobe epilepsy, with short duration, initial motionless stare, impaired awareness, involuntary motor behaviors, and salivation[193-195]. Improved treatment and abrogation of seizure activity may be achieved by adding injection sites that target areas of suboptimal therapeutic response.

Above-normal βgal activity in the spinal cord after injection of the brain parenchyma was among the surprising findings of this study, even with injection targets (thalamus and deep cerebellar nuclei)[135, 139] chosen for a high degree of interconnectivity with other CNS structures. βgal activity and vector genomes were detected throughout the spinal cord, up to 14 cm from the

deep cerebellar nuclei injection site at the time of surgery. We hypothesize that a portion of vector transport to the spinal cord occurred through CSF, known to be an effective medium for AAV transfection of the CNS[140, 141]. For our thalamic injections, the needle transects the lateral ventricle, which may provide a path of least resistance for vector backflow through the needle tract. Similarly for cerebellar injections, vector may travel into the subarachnoid space dorsal to the cerebellum. Varying degrees of vector leakage into the CSF because of slight differences in needle placement or anatomy may explain the reduced βgal activity in the spinal cord of cats that responded less robustly to treatment.

Vector likely gained access to peripheral organs via blood vessels disrupted during the injection procedure and via CSF, which ultimately is reabsorbed into the circulatory system[196]. To date, there have been no apparent peripheral disease symptoms in AAV-treated GM1 gangliosidosis animals. It is likely that residual βgal activity (~5% normal) in GM1 gangliosidosis cats delays development of clinical peripheral disease, but the increased βgal activity in peripheral tissues of AAV-treated GM1 gangliosidosis cats also may contribute to therapeutic success. Normalized liver activity of lysosomal hexosaminidase in all AAV-treated groups indicates that even partial restoration of liver βgal activity is beneficial (**Figure S4**).

Although it was not possible to blind investigators to the treatment status of cats in the present study, clinical rating scores were assigned independently by two investigators to attempt to limit bias. Survival and MRI data provided objective clinical measures, and biochemical analyses from the deceased long term cats supported their clinical scores. The promising therapeutic results in this study after intraparenchymal injections through only four needle tracts, with little evidence of toxicity, support the initiation of AAV-based clinical trials for GM1 gangliosidosis in human patients. Although deep cerebellar nuclei injection was effective in

restoring enzyme activity to the cerebellum, a similar strategy in human patients must weigh the benefit of direct cerebellar treatment versus the risk of hemorrhage in the posterior fossa. Safety studies in non-human primates will assess potential vector and procedural toxicity in human patients. Should the risk of deep cerebellar nuclei injection be considered too great, CSF-mediated approaches to treating the cerebellum may be incorporated, such as those deemed successful in mice and dogs[141, 160]. When predicting outcomes in human patients it must be considered that GM1 gangliosidosis cats in this study were treated pre-symptomatically, whereas most human patients are diagnosed after disease onset, so gene therapy may be less efficacious when administered later in the disease course. Nevertheless, as evidence for the benefits of AAV gene therapy continues to build in animal models, addition of future clinical trials to those already under way for human LSDs[170, 171] will determine whether this therapeutic potential is realized for GM1 gangliosidosis and for other LSDs.

Table 1. Treatment groups and current clinical status of AAV-treated GM1 gangliosidosis cats

Duration[A]	Serotype	Dose[B]	Cat	Gender	Tx age (mos.)	Endpoint or current age (mos.)	Clinical description	± Seizures*
Long term	AAV1	High	9-1356	F	1.9	52.8	Mild hind limb weakness, carpal hyperextension	+
			8-1483	F	1.9	41.4	Normal	+
			8-1485	F	2.0	41.2	Normal	-
		Full	9-1545	F	2.3	25.3	Deceased	-
			8-1551	F	2.1	34.6	Normal	+
	AAVrh8	Full	8-1364	M	1.6	50.5	Mild hind limb weakness	-
			8-1378	M	1.3	17.5	Deceased	-
			8-1397	F	1.7	47.9	Deceased[#]	+
			9-1424	F	2.9	44.9	Normal	-
			8-1435	M	2.8	44.8	Mild hind limb weakness	+
			9-1515	M	1.9	29.0	Deceased[#]	-
			8-1626	M	3.0	29.4	Weakness of carpi and limbs (hind/fore), pelvic ataxia, tremors	+
		Tenth	8-1574	M	1.8	21.2	Deceased	+
			8-1578	F	1.8	13.9	Deceased	-
			8-1576	F	1.8	14.2	Deceased	-
			9-1620	F	2.3	19.1	Deceased	-
Short term (16 weeks)	AAV1	Full	9-1553	F	2.3	N/A	Normal	-
			9-1555	F	2.3	N/A	Normal	-
			8-1617	M	2.5	N/A	Normal	-
	AAVrh8	Full	9-1494	M	1.9	N/A	Normal	-
			9-1502	M	1.8	N/A	Normal	-
			8-1525	F	1.9	N/A	Normal	-
			8-1526	F	1.9	N/A	Normal	-

[A] Cats in the long term cohort were euthanized at clinical humane endpoint. Short term cats were euthanized 16 weeks after injection. Cats received bilateral injections of the thalamus and deep cerebellar nuclei.

[B] Doses: High, 1.2×10^{13} vg; Full, 3×10^{12} to 4×10^{12} vg; one-tenth dose, 3×10^{11} vg.

*Animal developed seizures that were well controlled by medication. The mean age of seizure onset was 20.1 ± 7.4 months. #Cat 8-1397 had normal gait at 47.9 months of age but did not recover from an anesthetic procedure and was euthanized. Cat 9-1515 was clinically normal at 29.0 months of age but did not recover properly from anesthesia for MRI and was euthanized.

Abbreviations: Tx = treatment; mos. = months; N/A = not applicable.

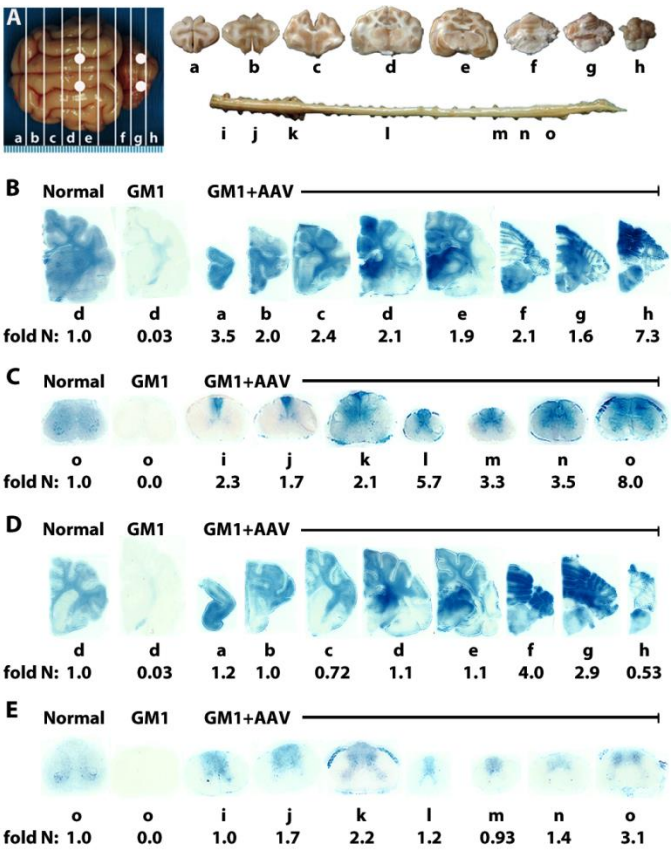

Figure 1. Therapeutic enzyme distribution in the CNS of GM1 gangliosidosis cats after AAVrh8 treatment. GM1 gangliosidosis cats were injected bilaterally in the thalamus and deep cerebellar nuclei with AAVrh8-CBA-βgal-WPRE (3×10^{12} to 3×10^{12} vector genomes total). (**A**) Injection sites (white circles) and 0.6 cm coronal blocks of the brain (a-h) and spinal cord (i-o) collected at necropsy. Blocks were halved and analyzed for sialic acid concentration (left) or for enzyme activity (right). Lysosomal βgal activity (blue) detected with Xgal at acidic pH was visualized throughout the brain (**B**) and spinal cord (**C**) of a representative, treated short term cat (GM1 + AAV; 8-1526). Lysosomal βgal activity was visualized throughout the brain (**D**) and spinal cord (**E**) of a treated long term cat (GM1 + AAV; 9-1515) at 29 months old. Corresponding βgal activity is shown below each block as fold increase over concentrations in untreated normal healthy cats (fold N). Similar distribution occurred with AAV1 (**Figure S1**). Representative

control sections are shown from untreated normal healthy cats along with untreated GM1 gangliosidosis cats, which express ≤0.10-fold normal βgal activity in brain blocks a-h (B,d) and ≤0.04-fold normal βgal activity in spinal cord blocks i-o (C, o). The ranges of specific activities for normal control blocks were: brain, 12.5 (a) - 42.1 (e); spinal cord, 3.2 (l) - 8.8 (k) nmol 4MU/mg/hr.

Table 2. βgal activity in brain, spinal cord, CSF, and liver of AAV-treated and untreated GM1 gangliosidosis cats

Region	Block	Fold-normal βgal specific activity, mean (s.d)					
		Short term, full dose[A] AAVrh8[*]	Short term, full dose[B] AAV1[*]	Long term, tenth dose[C] AAVrh8	Long term, full dose[D] AAVrh8	Long term, full dose[E] AAV1	GM1 no tx
Cerebrum	A	**2.7** (0.85)	**4.1** (4.4)	**0.48** (0.24)	**0.96** (0.37)	**0.48**	**0.00** (0.00)
	B	**1.8** (0.62)	**2.3** (2.4)	**0.42** (0.11)	**0.71** (0.30)	**0.42**	**0.00** (0.00)
	C	**1.7** (0.56)	**2.2** (2.0)	**0.63** (0.57)	**0.56** (0.17)	**0.61**	**0.01** (0.01)
	D	**1.7** (0.70)	**2.6** (1.1)	**0.62** (0.40)	**0.78** (0.27)	**1.2**	**0.02** (0.07)
	E	**1.1** (0.56)	**1.4** (1.1)	**0.33** (0.16)	**0.78** (0.35)	**0.82**	**0.05** (0.02)
Cerebellum	F	**1.5** (1.2)	**3.0** (1.2)	**0.55** (0.90)	**2.9** (1.5)	**0.40**	**0.10** (0.04)
	G	**2.2** (1.8)	**4.2** (2.1)	**0.33** (0.23)	**2.5** (0.96)	**0.33**	**0.04** (0.02)
	H	**4.1** (2.6)	**1.7** (1.1)	**0.27** (0.34)	**1.4** (1.6)	**0.30**	**0.04** (0.03)
Spinal cord	I	**2.0** (1.5)	**1.0** (0.38)	**0.00** (0.00)	**0.74** (0.65)	**0.07**	**0.00** (0.00)
	J	**1.6** (1.4)	**0.85** (0.60)	**0.03** (0.06)	**1.2** (0.93)	**0.04**	**0.00** (0.00)
	K	**1.9** (1.0)	**0.89** (0.28)	**0.05** (0.08)	**1.5** (1.1)	**0.10**	**0.03** (0.05)
	L	**3.2** (2.5)	**1.0** (0.46)	**0.07** (0.09)	**0.93** (0.62)	**0.00**	**0.03** (0.06)
	M	**2.1** (1.4)	**2.2** (1.9)	**0.07** (0.13)	**0.75** (0.68)	**0.05**	**0.00** (0.00)
	N	**2.3** (1.1)	**1.8** (1.5)	**0.09** (0.15)	**1.3** (0.98)	**0.05**	**0.04** (0.07)
	O	**4.8** (3.1)	**4.2** (3.2)	**0.38** (0.61)	**6.6** (8.5)	**0.17**	**0.01** (0.02)
CSF	N/A	**28** (20)	**42** (28)	**2.7** (1.3)	**32** (42)	**8.3**	**0.03** (0.08)
Liver	N/A	**0.38** (0.25)	**0.24** (0.16)	**0.17** (0.11)	**0.20** (0.19)	**0.08**	**0.05** (0.01)

[*] βgal activity was not significantly different between AAVrh8 (n = 4) and AAV1 (n = 3) cohorts at the 16 week time point (**a-h** and **i-o**, $P \geq 0.22$ for each block; **CSF**, $P = 0.19$; **liver**, $P = 0.43$).

[A] n = 4; βgal specific activity was significantly higher than that of untreated GM1 gangliosidosis cats (n = 4) in **a-h** and **i-o** ($P \leq 0.015$ for each block), **CSF** ($P = 0.026$, n = 3, no sample available for 8-1526), and **liver** ($P = 0.015$).

[B] n = 3; βgal specific activity was significantly higher than that of untreated GM1 gangliosidosis cats (n = 4) in **a-h** and **i-o** ($P \leq 0.026$ for each block), **CSF** ($P = 0.026$), and **liver** ($P = 0.026$).

[C] n = 4; βgal specific activity was significantly higher than that of untreated GM1 gangliosidosis cats (n = 4) in **a-e**, **g**, and **h** ($P \leq 0.021$ for each block), **CSF** ($P = 0.015$), and **liver** ($P = 0.015$), but not in **f** ($P = 0.15$) or **i-o** ($P \geq 0.20$ for each block).

[D] n = 3; βgal specific activity was significantly higher than that of untreated GM1 gangliosidosis cats (n = 4) in **a-h**, **j-l**, and **n-o** ($P \leq 0.025$ for each block), as well in **CSF** ($P = 0.025$), but not in blocks **i** and **m** ($P = 0.061$), or **liver** ($P = 0.054$).

[E] Not enough subjects currently available for statistical analysis.

Abbreviations: no tx = no treatment; N/A = not applicable; CSF = cerebrospinal fluid

Table 3. Vector copy number in brain, spinal cord, and liver of AAV-treated GM1 gangliosidosis cats

Region	Block	Vector copy number per µg genomic DNA, mean (s.d)				
		Short term full dose AAVrh8[A, B]	Short term full dose AAV1[A]	Long term tenth dose AAVrh8[C]	Long term full dose AAVrh8[B]	Long term full dose AAV1
Cerebrum	A	**14,000** (12,000)	**28,000** (14,000)	**630** (110)	**6,900** (3,500)	**6,000**
	B	**8,700** (6,900)	**15,000** (7,500)	**630** (520)	**4,800** (4,800)	**1,600**
	C	**11,000** (6,700)	**14,000** (9,400)	**380** (180)	**5,500** (6,900)	**1,700**
	D	**60,000** (55,000)	**100,000** (130,000)	**6,500** (5,700)	**7,400** (1,700)	**1,900**
	E	**40,000** (35,000)	**15,000** (8,700)	**6,400** (11,000)	**27,000** (24,000)	**13,000**
Cerebellum	F	**4,400** (1,800)	**16,000** (9,500)	**6,700** (13,000)	**59,000** (91,000)	**4,600**
	G	**89,000** (170,000)	**75,000** (11,000)	**570** (510)	**140,000** (230,000)	**550**
	H	**170,000** (170,000)	**26,000** (24,000)	**20,000** (39,000)	**9,000** (13,000)	**950**
Spinal cord	I	**4,500** (2,200)	**76,000** (80,000)	**170** (180)	**3,700** (2,100)	**15,000**
	J	**4,800** (1,300)	**57,000** (37,000)	**540** (820)	**2,300** (2,800)	**10,000**
	K	**4,600** (3,000)	**65,000** (58,000)	**140** (200)	**3,600** (2,100)	**3,100**
	L	**1,600** (1,300)	**54,000** (41,000)	**69** (110)	**2,300** (800)	**13,000**
	M	**2,700** (1,900)	**60,000** (31,000)	**210** (260)	**3,000** (2,900)	**8,700**
	N	**4,200** (1,800)	**68,000** (49,000)	**130** (170)	**3,100** (2,000)	**8,800**
	O	**3,500** (2,900)	**60,000** (67,000)	**290** (430)	**1,900** (1,100)	**4,200**
Liver	N/A	**230,000** (230,000)	**23,000** (14,000)	**13,000** (16,000)	**9,700** (8,200)	**18,000**

[A] Vector copy number was not significantly different between AAVrh8 (n = 4) and AAV1 (n = 3) cohorts at the 16 week time point, probably because of high standard deviations between cats (**a-h** and **i-o**, $P \geq 0.052$ for each block; **liver**, $P = 0.19$).

[B] Vector copy number was not significantly different between the short term (n = 4) and long term (n = 3) full dose AAVrh8 cohorts in **a-h** and **i-o** ($P \geq 0.056$ for all blocks), but was significantly lower in the **liver** of the long term cohort versus the short term cohort ($P = 0.026$).

[C] n = 4; vector copy number was significantly lower than in the long term full dose AAVrh8 cohort (n = 3) in **a-c**, **g**, **i**, and **l-o** ($P \leq 0.026$ for each block).

Block lettering corresponds to **Figure 1A**. Abbreviations: N/A = not applicable.

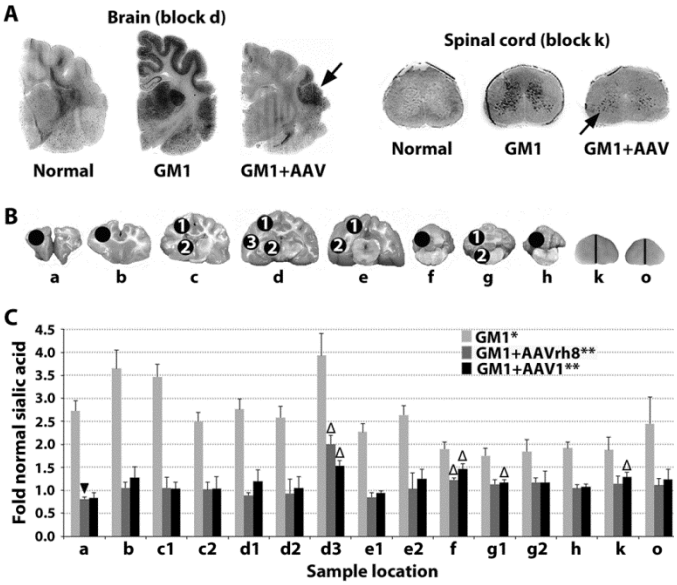

Figure 2. Storage in the CNS of GM1 gangliosidosis cats 16 weeks after treatment. (**A**) Storage in untreated GM1 gangliosidosis cats was visualized by dark PAS staining in the gray matter and thalamus. In treated brains, residual ganglioside storage was present in focal areas (black arrows) of the temporal lobe [block d in (B)] and cervical spinal cord [block k in (B)]. (**B**) Sample sites for sialic acid quantitation (circles) in brain (a-h) and spinal cord (k and o correspond to **Figure 1A**; half of each block was used). (**C**) Sialic acid concentrations were measured in untreated GM1 gangliosidosis cats (n = 4) and after treatment with AAVrh8 (n = 4) or AAV1 (n = 3) for comparison to normal healthy cats (n = 4). *, Concentration in all samples from untreated GM1 gangliosidosis cats was significantly higher than in normal cats ($P \leq 0.015$ for each block); **, concentration in all samples from treated GM1 gangliosidosis cats was significantly lower than in untreated GM1 gangliosidosis cats ($P \leq 0.026$ for each block) except AAV1 block h, because only two samples were available ($P = 0.053$); Δ, samples from treated GM1 gangliosidosis cats in which concentration was significantly higher than in normal cats ($P \leq 0.035$); ▼, a sample from treated GM1 gangliosidosis cats in which concentration was significantly lower than in normal cats ($P = 0.033$). The Wilcoxon signed rank test was used for statistical comparisons.

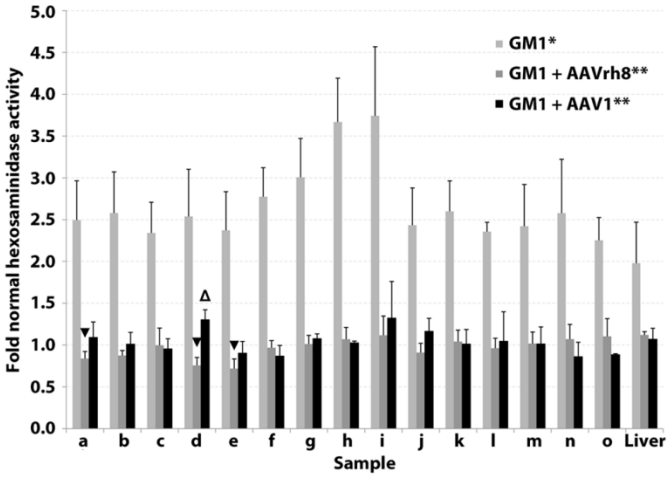

Figure 3. Normalization of lysosomal hexosaminidase activity in the CNS and liver of GM1 gangliosidosis cats 16 weeks after treatment. GM1 gangliosidosis cats were injected bilaterally in the thalamus and deep cerebellar nuclei with 3×10^{12} to 4×10^{12} vector genomes of AAVrh8 (n = 4, dark gray bars) or AAV1 (n = 3, black bars). Tissues were collected 16 weeks after treatment and hexosaminidase activity compared to untreated GM1 gangliosidosis cats (n = 4, light gray bars) and normal healthy cats (n = 4) in the brain (a-h), spinal cord (i-o), and liver. Lettering of brain and spinal cord blocks corresponds to **Figure 1A**. *, Activity in all samples from untreated GM1 gangliosidosis cats was significantly higher than in normal cats ($P \leq 0.015$ for each sample). **, Activity in all samples from treated GM1 gangliosidosis cats was significantly lower than in untreated GM1 gangliosidosis cats ($P \leq 0.026$ for each sample). Δ, a sample from treated cats that had significantly higher activity than in normal cats ($P = 0.026$); ▼, samples from treated cats that had significantly lower activity than in normal cats ($P \leq 0.030$). The Wilcoxon signed rank test was used for statistical comparisons.

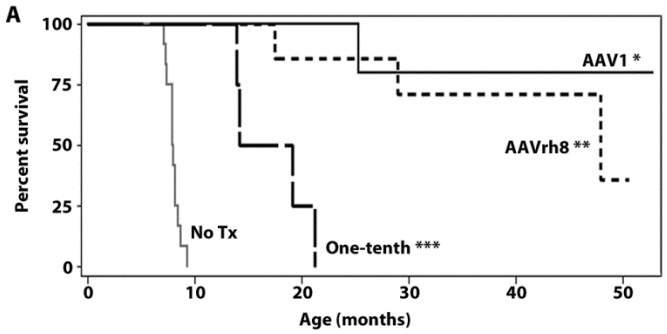

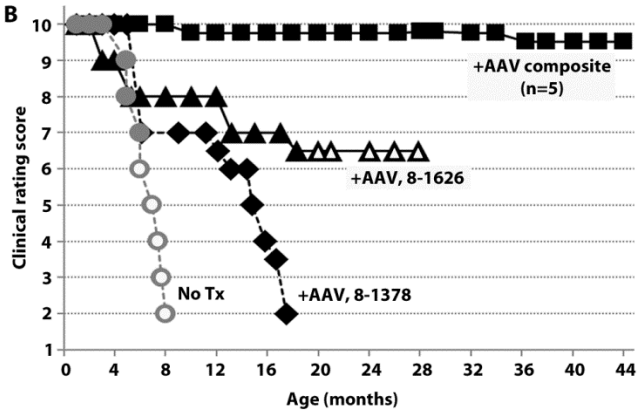

C

Score[#]	Clinical status	Age (mos.)
10	Normal	<4.1 ± 0.6
9 ↔ 8	Muscle weakness ↔ Wide stance	4.9 ± 0.7 ↔ 4.9 ± 0.5
7 ↔ 6	Carpal hyperextension ↔ Ataxia	6.0 ± 1.3 ↔ 6.0 ± 0.6
5	Instability with occasional falling	6.9 ± 0.4
4	Limited walking	7.4 ± 0.7
3	Standing but not walking	7.7 ± 0.7
2	Cannot stand on 2 consecutive days	8.0 ± 0.6
1	Lateral recumbency	> 8.0

[#] ↔ indicates that the symptoms are acquired at similar ages; higher score is assigned for 1 of the 2 symptoms, lower score assigned for both symptoms

Figure 4. Survival and clinical progression of AAV-treated GM1 gangliosidosis cats. (**A**) Kaplan-Meier survival curves for untreated GM1 gangliosidosis cats [No treatment (No Tx), n = 12] and GM1 gangliosidosis cats treated long term with gene therapy, which have significantly increased survival compared to untreated animals using the logrank test: **P* = 0.0004, AAV1 (n = 5); ***P* < 0.0001, AAVrh8 (n = 7); ****P* = 0.0012, one-tenth dose AAVrh8 group (n = 4). Survival of AAVrh8 treated cats was significantly higher for full dose versus one-tenth dose (*P* = 0.0046). (**B**) Full dose AAVrh8-treated cats were scored on a scale based on disease progression in untreated GM1 gangliosidosis cats (No Tx). A composite of five cats that responded robustly

to treatment is shown (+AAV composite), whereas two cats that responded less favorably are depicted separately (8-1626 and 8-1378). Solid lines signify living cats; dashed lines represent deceased cats. Open symbols denote whole-body tremors, which occurred in all untreated cats but only one treated animal. (**C**) Age of symptom onset is shown for untreated GM1 gangliosidosis cats (mean ± SD, n = 12). The scale is based on gait defects, which ultimately defined the humane endpoint, with initial deficits appearing at 4.9 months. However, disease onset begins at 4.1 months with fine head and tail tremors that progress to whole-body tremors at 6.2 months. For clarity, only whole-body tremors are depicted in (B).

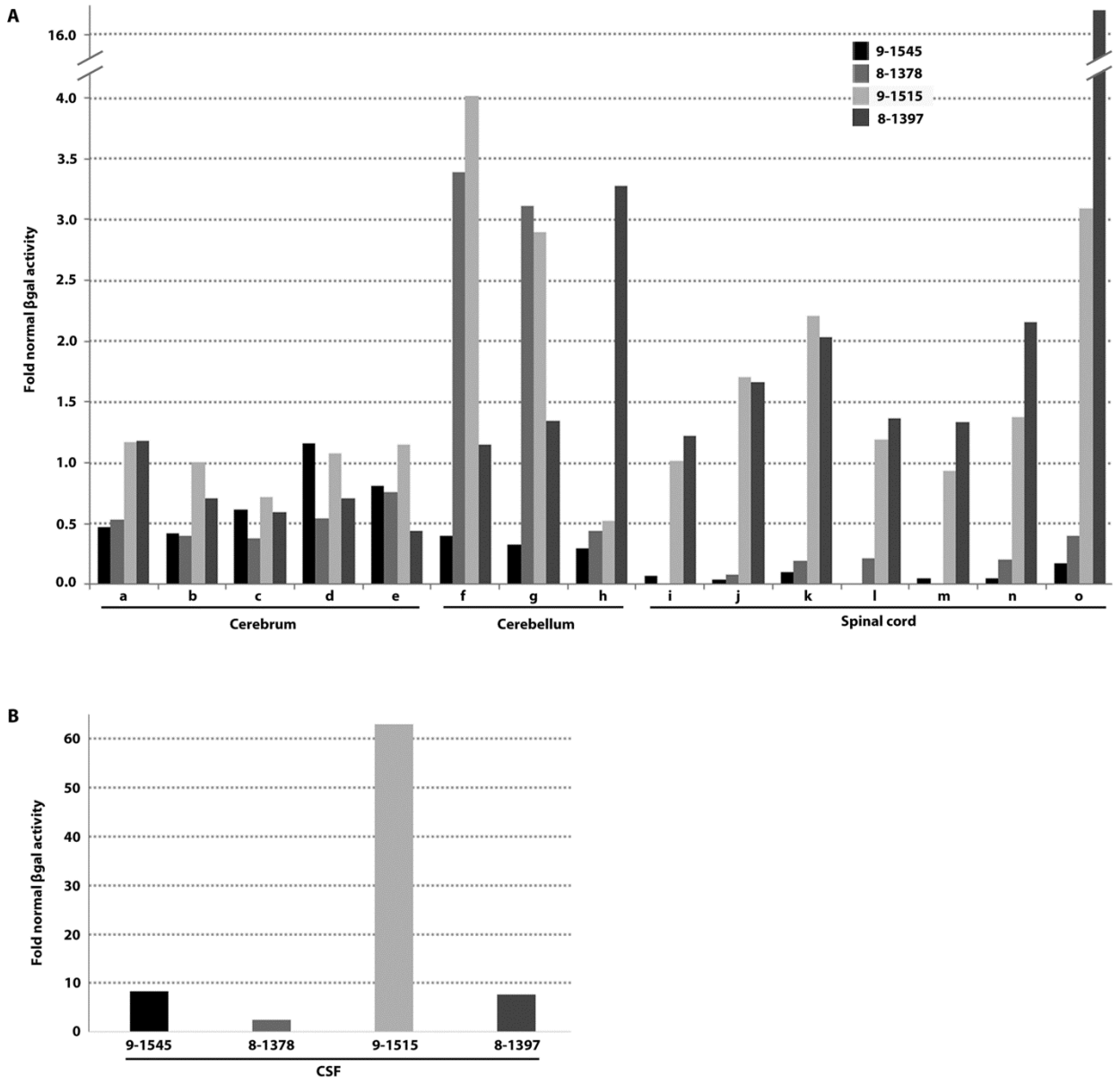

Figure 5. βgal activity in the CNS and CSF of GM1 gangliosidosis cats treated long term. Cats were treated with the full dose of AAV1 (9-1545) or AAVrh8 (8-1378, 9-1515 and 8-1397). (**A**) Animals whose disease progressed to the humane endpoint (8-1378 and 9-1545) had substantially lower activity in the spinal cord than cats with normal gait that were euthanized due to abnormal recovery from anesthesia (9-1515 and 8-1397). Reduced βgal activity cannot be attributed solely to a generalized decrease in expression over time, since the highest activities

were found in animals that lived the longest (9-1515, 29.0 months; 8-1397, 47.9 months). Lettering of brain and spinal cord blocks correspond to **Figure 1A**. 9-1545, black bars; 8-1378, medium gray bars; 9-1515, light gray bars; 8-1397, dark gray bars. (**B**) βgal activities in CSF were variable and there was no correlation between activity level and clinical therapeutic effect. However, it may not be possible to assess the correlative value of βgal activity in CSF since all cats had above-normal levels.

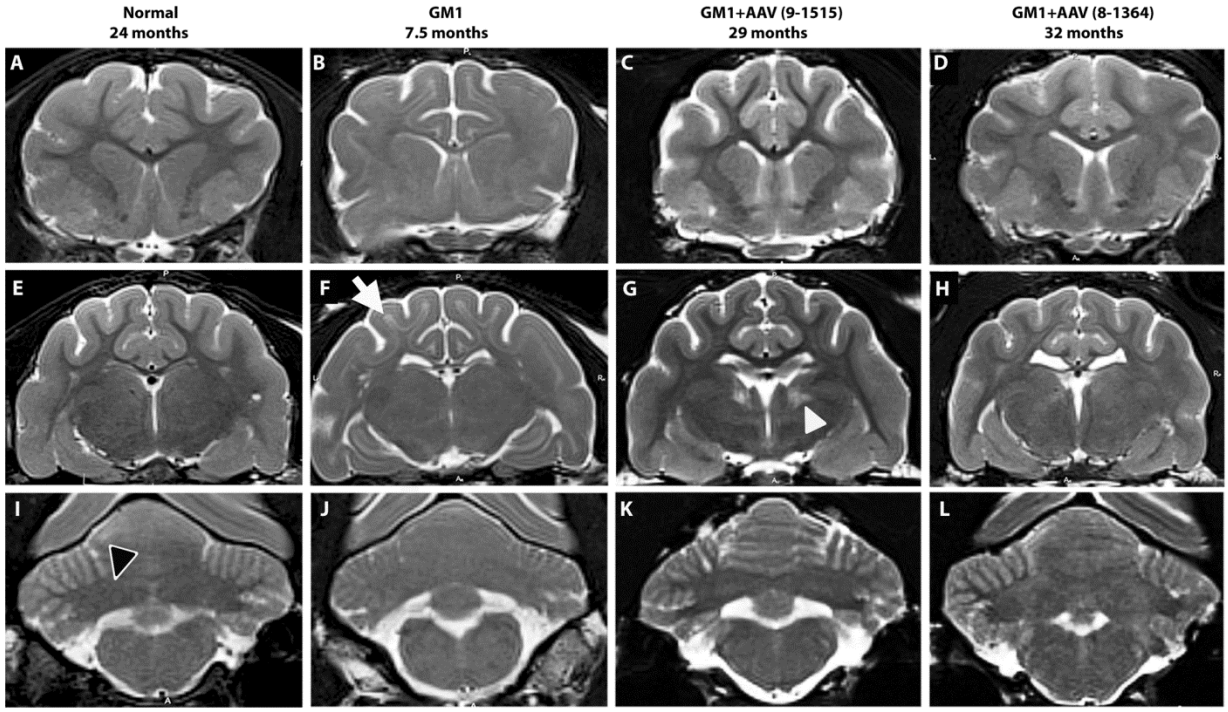

Figure 6. MRI evaluation of GM1 gangliosidosis cats. T2-weighted MRI images (3T) were taken at the level of the caudate nucleus (**A-D**), thalamus (**E-H**) and deep cerebellar nuclei (**I-L**). Cortical white matter is hypointense to (that is, darker than) gray matter in normal healthy cats, but hyperintense to (that is, lighter than) gray matter in untreated GM1 gangliosidosis cats [white arrow in (F)]. Also, the deep cerebellar nuclei area is hypointense to surrounding gray matter in normal healthy cats [outlined black arrowhead in (I)], but becomes isointense with disease progression in untreated GM1 gangliosidosis cats. In AAV-treated GM1 gangliosidosis cats (GM1+AAV), hypointensity of cortical white to gray matter and deep cerebellar nuclei area to cerebellar gray matter was largely preserved, indicating reduced myelin loss after treatment. Both AAV-treated cats were clinically normal at the time of imaging. In 5 of 11 treated cats tested, a locus of hyperintensity was noted in the thalamus [white arrowhead in (G)], although no clinical or histopathological correlates have been identified to date. Ages in months are shown for each cat. MRI images were acquired by Heather L. Gray-Edwards.

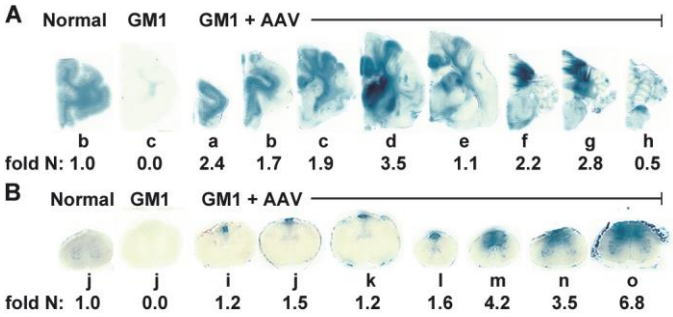

Figure S1. βgal distribution in the CNS of GM1 gangliosidosis cats 16 weeks after AAV1 treatment. GM1 gangliosidosis cats were injected bilaterally in the thalamus and deep cerebellar nuclei with AAV1-CBA-βgal-WPRE (3×10^{12} to 4×10^{12} vector genomes total) and tissues were collected 16 weeks later. Block lettering corresponds to **Figure 1A**. Blocks were halved and analyzed for sialic acid concentration (left) or for enzyme activity (right). Lysosomal βgal activity (blue) detected with Xgal at acidic pH was visualized throughout the brain (**A**) and spinal cord (**B**) of a representative, treated GM1 gangliosidosis cat (GM1+AAV; 9-1553). Corresponding βgal activity is shown below each block as fold normal level (fold N). Representative control sections are shown from untreated normal cats along with untreated GM1 gangliosidosis cats, which express ≤0.10-fold normal βgal activity in the brain and ≤0.04-fold normal βgal activity in the spinal cord. The ranges of specific activities for normal control blocks were: brain, 13 (a) - 42 (e); spinal cord, 3.2 (l) - 8.8 (k) nmol 4MU/mg/hr.

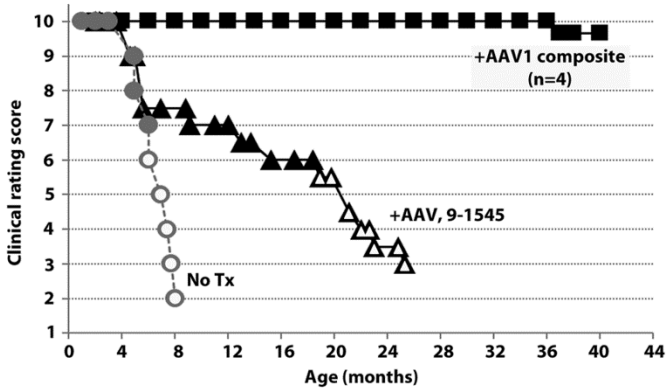

Figure S2. Clinical progression of AAV1-treated GM1 gangliosidosis cats. AAV1-treated cats were scored on the clinical scale shown in **Figure 4C**. A composite of four cats that responded robustly to treatment is shown (+AAV composite), while one cat that responded less favorably is depicted separately (9-1545). Solid lines signify living cats; dashed lines represent deceased cats. Open symbols denote whole-body tremors, which occurred in all untreated cats but only one treated animal.

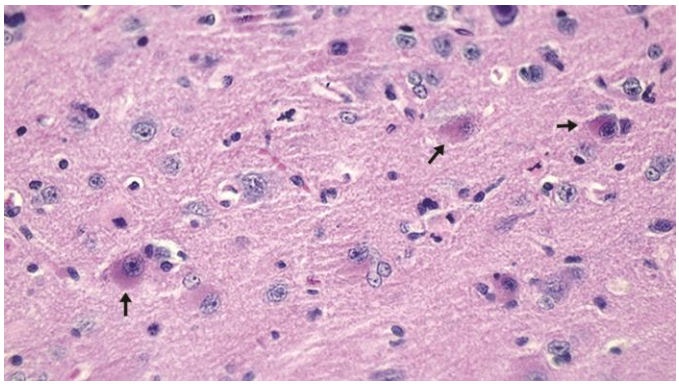

Figure S3. Hypereosinophilic neurons in the cortex of an AAV-treated GM1 gangliosidosis cat. Cat 9-1515 was treated with the full dose of AAVrh8. Fine eosinophilic granules (arrows) were found in scattered cortical and hippocampal neurons dorsal to the injection site. Histological analysis was provided by Brandon L. Brunson.

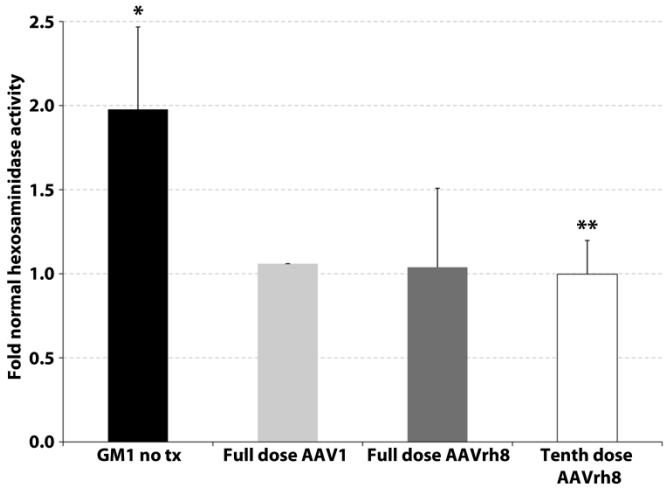

Figure S4. Hexosaminidase activity in the liver of GM1 gangliosidosis cats treated long term. Cats were treated with the full dose of AAV1 (n = 1) or AAVrh8 (n = 3), or with a one-tenth dose of AAVrh8 (n = 4). Liver was collected at humane endpoint and analyzed for hexosaminidase activity. * = activity was significantly higher in untreated GM1 gangliosidosis cats (n = 4) versus normal cats (n = 4) (P = 0.015); **, activity was significantly lower than in untreated GM1 gangliosidosis cats (P = 0.015). Hex activity in the full dose AAVrh8 group was not significantly different from that of untreated GM1 gangliosidosis cats (P = 0.056). Insufficient cats were available in the full dose AAV1 group for statistical analysis.

Table S1. Vector copy number and βgal activity in AAV-treated GM1 gangliosidosis cats and their offspring

Cohort	Number & gender	Tissue	Number of positive samples	Vector copy number/μg DNA	βgal activity (fold normal, range)[E]
6 weeks[A]	3F	Gonad	3/3	630-2,800	0.00-0.03
16 weeks[A]	4F, 3M	Gonad	0/7	<LOD	0.00-0.05
Long term[B] full dose	2M, 2F	Gonad	0/4	<LOD	0.03-0.05
Long term[B] tenth dose	1M, 3F	Gonad	0/4	<LOD	0.02-0.06
Untreated offspring of AAV-treated GM1 cats[C]	3M, 2F	Gonad	0/5	<LOD	0.00-0.06
		Brain[D]	0/5	<LOD	0.00-0.07
		Spinal cord[D]	0/5	<LOD	0.00
GM1 no tx	3M, 5F	Gonad	0/8	< LOD	0.00-0.05

[A] Time interval between treatment and analysis; 6 week cohort was treated with AAVrh8; 16 week cohort was treated with AAV1 (n = 3) or AAVrh8 (n = 4).

[B] Long term cohorts were analyzed at humane endpoint. See **Table 1** for ages.

[C] GM1 x GM1 offspring were untreated. Four offspring reached humane endpoint between 7.1 and 8.4 months old and the fifth was euthanized at 3.4 months for an early time point analysis.

[D] Included all coronal blocks from the brain (a-h) and spinal cord (i-o) in **Figure 1A**.

[E] βgal specific activity for normal cats in nmol 4MU/mg/hr was: Testes, 350 (n = 1, 18.7 months) and 383 ± 31 (n = 2, ~6 months); ovary, 177 ± 10 (n = 2, ~6 months); brain minimum, 12.5 (block a), maximum, 42.1 (block e); spinal cord minimum, 3.2 (block l), maximum, 8.8 (block k).

Abbreviations: no tx, no treatment; M = male; F = female

Chapter 2: Widespread correction of central nervous system disease following intracranial gene therapy in a feline model of Sandhoff disease

Abstract

Sandhoff disease (SD) is caused by deficiency of N-acetyl-β-hexosaminidase (Hex) resulting in pathologic accumulation of GM2 ganglioside in lysosomes of the central nervous system (CNS) and progressive neurodegeneration. There is currently no treatment for SD, which often results in death by age 5 years. Adeno-associated virus (AAV) gene therapy achieved global CNS Hex restoration and widespread normalization of storage in the SD mouse model. Using a similar treatment approach, we sought to translate the outcome in mice to the feline SD model as an important step toward human clinical trials. Sixteen weeks after four intracranial injections of AAVrh8 vectors, Hex activity was restored to above normal levels throughout the entire CNS and in cerebrospinal fluid, despite a humoral immune response to the vector. In accordance with significant normalization of a secondary lysosomal biomarker, CNS ganglioside storage was substantially improved, but not completely cleared. At the study endpoint, 5-month old AAV-treated SD cats had clearly preserved neurologic function and gait compared to untreated animals (humane endpoint, 4.4 ± 0.6 months) demonstrating clinical benefit from AAV-treatment. Translation of widespread biochemical disease correction from the mouse to feline SD model provides optimism for treatment of the larger human CNS with minimal modification of approach.

Introduction

The GM2 gangliosidoses are recessively inherited lysosomal storage diseases (LSDs) caused by impaired degradation of GM2 ganglioside (GM2) resulting in progressive neurodegeneration and early death. These disorders result from deficiency of either N-acetyl-β-hexosaminidase (Hex) (EC 3.2.1.52) or the non-catalytic GM2 activator protein (GM2AP). Hex hydrolyzes terminal N-acetyl-galactosamine or N-acetyl-glucosamine residues from numerous glycoconjugates. The two major Hex isozymes, HexA (αβ) and HexB (ββ), have overlapping substrate specificities, but only HexA is capable of substantial GM2 catabolism in humans. A minor isozyme, HexS (αα), is unstable and has little catalytic activity in the CNS. Genetic deficiency of *HEXA* encoding the Hex α-subunit, *HEXB* encoding the Hex β-subunit, or *GM2A* encoding the GM2AP causes Tay-Sachs disease (TSD), Sandhoff disease (SD), and GM2AP deficiency, respectively. All of the gangliosidosis variants are clinically similar, despite additional accumulation of neutral substrates in SD patients[35].

The GM2 gangliosidoses have a spectrum of clinical forms characterized by the age of disease onset and progression of clinical symptoms, which are largely determined by the residual level of Hex activity[83]. The infantile-onset form is most common, resulting from negligible HexA activity that leads to death by age 5 years[35]. There is currently no effective treatment for the GM2 gangliosidoses although several approaches have been tested without success in human patients including substrate reduction therapy[103-105], chemical chaperone therapy[115, 116], and bone marrow transplantation[96].

HexA deficiency affects the CNS globally, so successful treatment strategies must target widespread areas of the brain and spinal cord. Adeno-associated virus (AAV) intracranial gene therapy has the potential to generate a permanent source of Hex in the CNS. The ability of vector

transduced cells to secrete a proportion of lysosomal enzyme and "cross-correct" diseased cells[80, 81] means that only a fraction of the brain would need to be transduced by AAV vectors. In addition to local diffusion, AAV vector and enzyme are distributed by axonal transport[130, 132] and CSF flow[132, 141] to regions widely dispersed from the injection site.

AAV gene therapy has proven effective in several animal models of LSDs[141, 159, 163, 164, 197] including SD mice[140, 142] and SD cats[157]. First described in 1977, naturally occurring feline SD provides an unparalleled opportunity to test gene therapy in a large animal model highly analogous to human infantile-onset SD in terms of enzymatic deficiency (≤0.02-fold normal Hex activity), neuropathology, and clinical disease progression[74, 78, 79]. Up to a 2.3-fold mean increase in life span was previously reported for SD cats treated with bilateral thalamic injections of AAVrh8 vectors encoding feline Hex. Hex activity was restored to 0.83- to 5.5-fold that of normal throughout the forebrain, but activity was limited in the cerebellum of some subjects[157]. Studies in the related GM1 gangliosidosis (GM1) feline model[198] and in SD mice[140] demonstrated that bilateral injections of AAV vectors in the striatum or thalamus *and* deep cerebellar nuclei (DCN) is an effective method to globally restore CNS lysosomal enzyme activity resulting in significant clearance of pathological storage material and increase in life span. Here, the extent of biochemical disease correction following thalamus and DCN directed gene therapy was evaluated in the feline SD model.

Results

Widespread enzyme and vector distribution

Three SD cats (11-762, 7-770 and 7-774) were injected bilaterally in the thalamus and DCN with monocistronic AAVrh8 vectors encoding feline Hex α- and Hex β-subunits (1:1 ratio,

4.4×10^{12} vector genomes total). Histochemical staining with a substrate cleaved specifically by Hex showed widespread brain Hex distribution for AAV-treated SD cats 16 weeks after injection (**Figure 1a, b**). Hex staining was most intense at the parenchymal injection sites (blocks E and G in **Figure 1b**). Spinal cord Hex distribution was also widespread and was most intense in lumbar block O. In cat 7-770 (shown in **Figure 1c**), Hex staining was highest in the dorsal funiculus, but also extended into the gray matter of all spinal cord blocks. In cats 11-762 and 7-774, Hex staining was not as well distributed in the gray matter of cervical spinal cord blocks I-K (**Figure S1**). Hex activity in untreated SD cats was not detectable by histochemical staining.

Hex activity was measured quantitatively with the synthetic fluorogenic substrates 4-methylumbelliferone-6-sulfa-2-Acetoamido-2-Deoxy-β-D-Glucopyranoside (MUGS) and 4-methylumbelliferone-N-acetyl-β-D-glucosaminide (MUG). MUGS binds to the same positively charged pocket in the α-subunit that binds GM2 ganglioside and is HexA specific in humans and HexA preferred in cats. MUG is hydrolyzed by the Hex α- or β- active site and is a measure of total Hex activity. Residual Hex activity against MUGS in untreated SD cats was ≤0.01-fold that of normal in the brain and ≤0.02-fold that of normal in the spinal cord. In AAV-treated SD cats, mean HexA activity was significantly higher than in untreated SD cats and normal cats (homozygous for the wildtype allele) in all brain (2.7- to 45-fold normal) and spinal cord (4.2- to 14-fold normal) blocks (**Table 1)**. Results were similar with MUG substrate. A fold normal MUGS:MUG ratio of 0.91 to 1.3 demonstrated that HexA and HexB isozymes formed in a relatively normal ratio (**Table 1)**. Ion exchange chromatography was also used to calculate the relative production of each isozyme and demonstrated that the HexA:HexB ratio was comparable between AAV-treated cats and normal cats (**Figure 2**).

Lysosomal enzyme gains access to and may be distributed via CSF and perivascular flow following intraparenchymal injection in mice[140] and cats[198]. Hex activity in CSF of AAV-treated SD cats ranged from 4.9- to 15-fold that of normal indicating that CSF transport may have been an effective mode of dissemination. Additionally, enzyme was detected in pituitary and sciatic nerve demonstrating transport to the neuroendocrine and peripheral nervous system following intraparenchymal injection (**Table 1)**. AAV vector was detected by quantitative PCR in all blocks from AAV-treated SD cats indicating widespread dissemination from injection sites (**Table S1**).

Humoral antibody response to the AAV vector

A humoral antibody (Ab) response to the AAV vector may result from vector entering the cervical lymph node via CSF transport or vector leakage into the vasculature as blood vessels are traversed during intraparenchymal injection[118, 199]. Serum Ab titers to the AAVrh8 capsid were undetectable in SD cats before treatment. After treatment, titers were 1:65,536 in 7-774 and 7-770 at 16 weeks after injection. Cat 11-762 had a lower Ab response, which peaked 6 weeks after injection at 1:4,096 (**Figure 3**). Histological analysis showed no evidence of a cell mediated response to the vector. The only abnormalities detected were 1) rare multifocal expansion of leptomeninges by accumulation of lymphocytes and fibroblasts, and 2) scattered, moderately swollen cerebral cortical neurons and Purkinje cells, which both contained copious amounts of foamy, cytoplasmic storage vacuoles (**Figure S2**). Both abnormalities were more diffusely present in untreated SD cats and are likely disease related.

Substantial normalization of storage material

Total ganglioside sialic acid accumulates to several fold that of normal in the brain of SD cats, and GM2 accounts for 67% of total gangliosides compared to undetectable concentrations in normal cats. Asialo GM2 (GA2) is also elevated in the SD cat brain, but is undetectable in normal cats[74, 200]. Samples from cortex (block C), thalamus (block D), cerebellum (block G), and cervical intumescence (CI, block K in **Figure 1a**) were analyzed for gangliosides and other lipids by HPTLC (**Figure 4a-e**). In untreated SD cats, Hex activity was negligible, and total sialic acid accumulated significantly to 1.9- to 4.0-fold normal (**Figure 5a,b**). In AAV-treated SD cats, mean sialic acid concentration was decreased in all samples, but remained significantly higher than in normal cats in cortex C, thalamus, and CI (**Figure 5b**). GM2 and GA2 were absent in samples from normal cats with the exception of sample K in which trace amounts were detected. In untreated SD cats, GM2 and GA2 concentrations were significantly higher than that of normal (**Figure 5c,d**). In AAV-treated SD cats there was significant reduction of GM2 and GA2 in the brain (GM2, 89-99%; GA2, 91-100%) and CI (GM2, 72%; GA2, 73%), although mean storage of GM2 and/or GA2 remained significantly higher than in normal cats in cortex C, cerebellum G, and CI (**Figure 5c, d**). Storage material was also analyzed in frontal cortex (block B), striatum (block C), rostral cerebellum (block F), and lumbar intumescence (LI, block O in **Figure 1a**). Total sialic acid, GM2, and GA2 were substantially normalized in all AAV-treated versus untreated SD cats, but significance could not be determined for all samples because of low control numbers (normal, n = 2; untreated SD, n = 2 to 4) (**Figure S3 and Table S2**).

Demyelination occurs with disease progression[201], resulting in a decrease of myelin-enriched cerebrosides and sulfatides[200]. In the brain of untreated SD cats, cerebroside and sulfatide concentrations were significantly reduced to 0.29- to 0.54-fold that of normal and 0.26-

to 0.56-fold that of normal, respectively, suggesting substantial demyelination (**Figure S4a, b**). Surprisingly, brains of AAV-treated SD cats showed no significant improvement in cerebroside and sulfatide concentration versus untreated SD cats (**Figure S4a, b**), although variability among samples was unusually high. In the CI, there was no significant difference in cerebroside and sulfatide concentrations between normal and untreated SD cats suggesting that spinal cord demyelination is less pronounced compared to brain demyelination.

Partial normalization of a secondary lysosomal biomarker

In lysosomal storage diseases, activity of non-mutant lysosomal hydrolases is often elevated[143]. In untreated SD cats, α-mannosidase activity was significantly elevated up to 8.4-fold that of normal in the brain and 11-fold that of normal in the spinal cord. Intraparenchymal treatment for 16 weeks with AAV-*fHEXA* and AAV-*fHEXB* significantly reduced α-mannosidase activity in all CNS blocks compared to untreated SD cats. However, activity remained significantly higher than in normal in most spinal cord blocks revealing incomplete spinal cord restoration of this secondary lysosomal biomarker despite restoration of HexA activity to several fold that of normal. Mannosidase activity was not normalized in pituitary tissue, which had only a small increase in Hex activity (**Figure 6 and Table 1**).

Delayed clinical disease progression

Disease onset in AAV-treated SD cats was delayed up to the 16 week post-treatment experimental endpoint versus untreated SD cats whose stereotypical disease progression began at 1.3 ± 0.2 months old with fine tremors of the head and tail. Clinical symptoms in untreated animals progressed according to the clinical rating scale in **Figure 7a**, which reflects an animal's

departure from normal function. Cats reached the inability to stand on two consecutive days at 4.4 ± 0.6 months old, which defined the humane endpoint. When scored on the same clinical rating scale, the composite score of AAV-treated SD cats was 7.7 at the pre-determined study endpoint of ~5 months old. In contrast, untreated SD cats reached a score of 3 (humane endpoint) by 4.4 months old (**Fig. 7b**). AAV-treated cats developed generalized hind limb muscle weakness at the same age as untreated cats (~2 months old), but subsequently, disease progression in treated cats was stabilized. At the study endpoint, 11-762 had a wide based stance and 7-770 and 7-774 displayed mild ataxia. Whilst subtle tremors were present in all three AAV-treated cats, none developed overt whole body tremors, which are evident in untreated SD cats by 2.4 months old and become progressively debilitating.

Discussion

The GM2 gangliosidoses belong to a group of over 40 LSDs with a combined incidence of 1 in 7700 live births[1]. There is currently no effective treatment for human GM2 gangliosidoses, with palliative measures being the current standard of care. Enzyme replacement therapy (ERT)[85, 202], substrate reduction therapy[91, 108, 203], and stem cell transplantation[91, 92, 108, 109] have shown moderate success in mouse models of gangliosidoses, but similar efficacy in larger animals has not been achieved[86,93]. Dramatic therapeutic effect using AAV-mediated gene therapy was reported in the mouse model of SD[140, 142], prompting our evaluation of this approach in cats as an intermediate step toward human application. Initial studies to test AAV gene therapy in the feline SD model utilized bilateral thalamic injections of AAV vectors and resulted in the first report of unequivocal therapeutic effect in a non-rodent gangliosidosis model[157]. Superior CNS enzyme distribution and clinical therapeutic benefit was since demonstrated in

GM1 gangliosidosis cats by delivering thalamus *and* DCN injections[198]. Here, the thalamus and DCN treatment approach was tested in SD cats and, as in the feline GM1 gangliosidosis model[198], restoration of enzymatic activity was demonstrated globally throughout the brain and spinal cord, with accompanying decreases in storage material. Similar approaches involving multiple parenchymal injections have been effective in correcting CNS disease in other LSD models, including Niemann Pick type A mice[197], Batten disease mice[163], Mucopolysaccharidosis (MPS) I or IIIb dogs[165], and α-mannisidosis cats[164].

Therapeutic Hex was effective against its native substrates as evidenced by reduction of sialic acid in all samples and near normalization of GM2 and GA2 storage in brain samples. However, GM2 and GA2 are absent or found in only trace amounts in normal cats ≥5 months old, so storage in AAV-treated SD cats was not completely cleared despite several fold normal Hex activity. Similarly, in SD mice and GM1 gangliosidosis mice, a therapeutic level of enzyme restoration resulted in greatly diminished, but not fully normalized ganglioside storage in some areas. As hypothesized in the mouse studies, residual biochemical storage in SD cats could be because of uneven therapeutic enzyme distribution within the sample with supranormal Hex activity in some cells skewing measurements of total activity[140, 142]. This scenario is particularly likely in the CI of two of three treated cats, which had intense Hex staining in the dorsal funiculus but patchy activity in gray matter, leading to the highest residual ganglioside storage of all samples tested (**Figure S1**). The cat with superior CI Hex distribution (7-770, **Figure 1c**) also had the lowest level of CI GM2 storage (**Figure 4e**). The CI was similarly more resistant than other samples to clearance of storage material in GM1 gangliosidosis cats[198] and MPS I dogs treated intravenously with a low dose of recombinant therapeutic enzyme[204]. Mice with a similar LSD (MPS IIIA) showed incomplete clearance of glycosaminoglycans (GAGs) in the brain at 4

months, but GAG content was normalized at 10 to 12 months[141]. Therefore, a sustained period of enzyme expression may be necessary to completely clear storage material.

In LSDs, elevation of non-deficient lysosomal enzyme activity may be due to impaired degradation and turnover of acid hydrolases or increased synthesis of acid hydrolases in storage distended cells as lysosomal hydrolases are a target of the transcription factor TFEB, which translocates to the nucleus under conditions of lysosomal stress[205]. Normalization of α-mannosidase throughout the brain of AAV-treated SD cats correlated with restoration of Hex activity and reduction of storage material. In accordance with the higher residual ganglioside storage in the CI versus the brain of AAV-treated SD cats, there was significant reduction but not normalization of spinal cord α-mannosidase activity, likely due to uneven Hex distribution as already discussed.

With above normal Hex restoration and significant reduction of storage material in the brain, it was surprising that there was no significant preservation of myelin enriched-lipids. Studies in SD mice determined that myelin deficiencies cannot be restored following therapy[161], and that myelin deficiencies are apparent before clinical disease onset[206]. Therefore, it is possible that demyelination was already present at the 1-month treatment age and was not restored. However, findings must be interpreted with caution. There was substantial variation for acidic and neutral lipids. Longer-term studies with larger numbers of treated animals will be helpful in understanding myelin abnormalities in treated animals.

Serum Ab titers to the AAVrh8 vector varied considerably between subjects at 6 and 16 weeks after injection. Importantly, Hex distribution was widespread and activity was above normal despite a substantial serum Ab response to the vector. Whilst asymmetrical distribution of Abs across the blood brain barrier may have played a role[141], it is also likely that very low

levels of pre-existing antibodies to the novel AAVrh8 capsid allowed the vector to transduce cells effectively before a humoral immune response was generated. In one study in non-human primates, the presence of pre-existing serum Abs blocked subsequent CNS transduction following AAV administration[147]. In other studies, the presence of preexisting serum Ab titers resulted in a small attenuation of CNS vector transduction in dogs[141] and non-human primates[146]. However, transduction of peripheral tissues was blocked[141]. Therefore, the presence of pre-existing Abs could have implications for SD cats if vector re-administration or treatment of peripheral disease manifestations ever becomes necessary.

Hex activity reached supranormal levels similar to those previously reported in clinically normal AAV-treated heterozygote cats[157]. In transgenic mice and AAV-treated heterozygote cats, massive overexpression of lysosomal enzyme was clinically benign and did not affect life span even though very high enzyme levels were present in lysosomes[157, 207]. However, toxicity due to overexpression of GFP and Tau in the substantia nigra of mice has been reported[154]. Therefore toxicity due to overexpression may be protein, cell type and/or species dependent, so caution must be applied when translating approaches from cats to other species, including humans.

Clinical benefit was demonstrated in all AAV-treated SD cats. At the study endpoint subjects displayed only mild disease symptoms and were otherwise active and in excellent physical health. Long term studies are currently underway to more thoroughly evaluate the clinical therapeutic benefit of thalamus and DCN directed gene therapy. The ability to achieve near global CNS distribution of therapeutic enzyme from only four injection sites in a second feline LSD model is encouraging for the further development of treatments for these devastating, untreatable neurologic diseases.

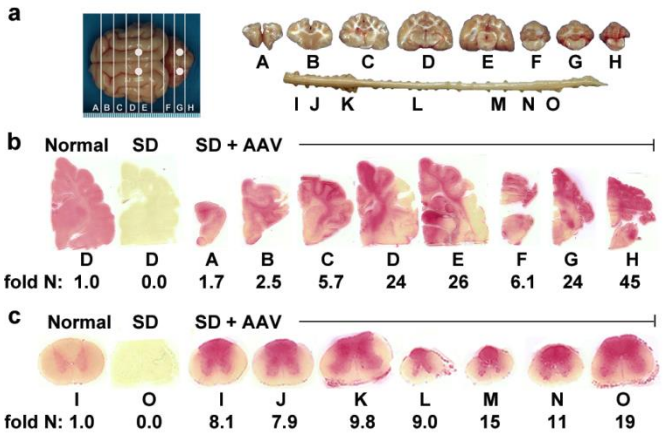

Figure 1. Therapeutic enzyme distribution in the CNS of Sandhoff disease (SD) cats 16 weeks after AAV treatment. SD cats were treated with thalamus and deep cerebellar nuclei injections of AAV-*fHEXA* and AAV-*fHEXB* (4.4 x 10^{12} vector genomes total , 1:1 vector ratio), and tissues were collected 16 weeks after treatment. (**a**) Injection sites (white circles) and 0.6 cm coronal blocks of the brain (A-H) and spinal cord (I-O) collected at necropsy. Blocks were halved and analyzed for storage material (left) or for enzyme activity (right). Lysosomal Hex activity (red) detected with a naphthol-based substrate at acidic pH was visualized throughout the brain (**b**) and spinal cord (**c**) of a representative, AAV-treated SD cat (SD + AAV; 7-770). Corresponding Hex activity against MUGS substrate is shown below each block as fold normal level (fold N). Representative control sections are shown from untreated normal cats along with untreated SD cats, which express ≤0.02-fold normal HexA activity in the brain and spinal cord. The ranges of specific activities for normal control blocks were: brain, 30 (F) – 51 (D); spinal cord, 8.3 (M) – 17 (K) nmol 4MU/mg/hr. Abbreviations: AAV = adeno associated virus; 4MU = 4-methylumbelliferone; MUGS = 4-MU-6-sulfa-2-Acetoamido-2-Deoxy-β-D-glucopyranoside; Hex = hexosaminidase

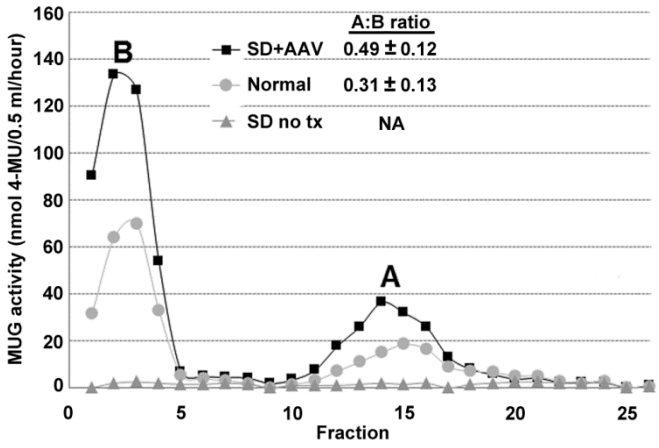

Figure 2. Ratio of Hex isozymes separated by DEAE cellulose ion exchange chromatography. Fractions of 0.5 ml eluates from block E were collected using a 0 to 400 mmol/l NaCl gradient and Hex activity was measured using MUG substrate. The activity of each isozyme was calculated by summing activities from fractions 1 to 8 (B) or 10 to 20 (A), and ratios of A:B were calculated for AAV-treated SD cats (n = 3, black squares), normal cats (n = 4, gray circles), and untreated SD cats (n = 1 gray triangles). A representative AAV-treated cat (7-770) is shown along with a representative normal cat and untreated SD cat. The A:B ratio was not significantly different between AAV-treated cats and normal cats (P = 0.14). Hex activity was not detected in untreated SD cats. HexS was not detected, but generally elutes after fraction 20. Peak heights depict enzyme activity, not specific activity, and therefore can only be used to compare relative isozyme levels (not absolute levels) between cats. Abbreviations: DEAE= diethylaminoethyl; tx = treatment; NA = not applicable; MUG = 4-MU-N-acetyl-β-D-glucosaminide; SD = Sandhoff disease. DEAE cellulose ion exchange chromatography was performed by Misako Hwang.

Table 1. Hex activity in the brain, spinal cord, CSF, sciatic nerve, and pituitary of AAV-treated and untreated Sandhoff disease (SD) cats

		Fold normal Hex activity[A,B,C]					**Fold normal MUGS:MUG ratio**
		SD + AAV				**SD no tx**	**SD + AAV**
Region	Block	11-762	7-770	7-774	Mean, (s.d)	Mean, (s.d)	Mean, (s.d)
Cerebrum	A	4.1	1.7	2.5	**2.8** (1.2)	**0.0** (0.0)	**1.2** (0.06)
	B	3.2	2.5	2.3	**2.7** (0.47)	**0.0** (0.0)	**1.2** (0.07)
	C	4.1	5.7	3.6	**4.5** (1.1)	**0.0** (0.0)	**1.2** (0.10)
	D	7.1	24	31	**21** (12)	**0.0** (0.0)	**1.2** (0.13)
	E	88	26	21	**45** (37)	**0.0** (0.0)	**1.0** (0.10)
Cerebellum	F	4.7	6.1	10	**6.9** (2.7)	**0.0** (0.0)	**1.2** (0.12)
	G	22	24	60	**35** (21)	**0.01** (0.01)	**1.0** (0.15)
	H	32	45	3.5	**27** (21)	**0.0** (0.0)	**1.3** (0.24)
Spinal cord	I	4.9	8.1	2.0	**5.0** (3.1)	**0.0** (0.0)	**1.1** (0.12)
	J	2.5	7.9	2.3	**4.2** (3.2)	**0.0** (0.0)	**1.1** (0.14)
	K	4.3	9.8	2.3	**5.5** (3.9)	**0.0** (0.01)	**1.1** (0.07)
	L	9.7	9.0	4.0	**7.6** (3.1)	**0.02** (0.03)	**0.91** (0.50)
	M	7.0	15	4.8	**8.9** (5.4)	**0.02** (0.04)	**1.1** (0.16)
	N	7.2	11	3.9	**7.4** (3.6)	**0.01** (0.02)	**1.1** (0.08)
	O	17	19	4.7	**14** (7.7)	**0.01** (0.01)	**1.1** (0.11)
CSF	N/A	15	4.9	8.5	**9.5** (5.1)	**0.03** (0.04)	-
Sciatic N.	N/A	4.8	4.9	2.1	**3.9** (1.6)	**0.02** (0.01)	**1.1** (0.02)
Pituitary	N/A	0.12	0.09	0.14	**0.12** (0.03)	**0.03** (0.01)	**1.5** (0.14)

[A] MUGS values are shown with the exception of CSF for which only MUG was measured due to limited sample volume.

[B] HexA activity against the α-subunit preferred substrate (MUGS) was significantly higher in AAV-treated SD cats (n = 3) than in untreated SD cats (n = 5) in **A-H** ($P \leq 0.013$ for each block), **I-O** ($P \leq 0.016$ for each block), **sciatic nerve** ($P = 0.018$), and **pituitary** ($P = 0.018$). Total Hex specific activity against the β-subunit specific substrate (MUG) was significantly higher in AAV-treated SD cats than in untreated SD cats in **A-H** ($P \leq 0.018$ for each block), **I-O** ($P \leq 0.013$ for each block), **CSF** ($P = 0.025$), **sciatic nerve** ($P = 0.018$), and **pituitary** ($P = 0.018$).

[C] HexA specific activity against the α-subunit preferred substrate (MUGS) was significantly higher in AAV-treated SD cats (n = 3) than in normal cats (n = 4) in **A-H** and **I-O** ($P \leq 0.026$ for each block), as well as in **sciatic nerve** ($P = 0.018$), but was significantly lower than in normal cats in **pituitary** ($P = 0.026$). Total Hex specific activity against the β-subunit specific substrate (MUG) was significantly higher in AAV-treated SD cats than in normal cats in **A-H** ($P \leq 0.026$ for each block), **J-O** ($P \leq 0.026$ for each block), **CSF** ($P = 0.026$), and **sciatic nerve** ($P = 0.018$), but not in block **I** ($P = 0.056$), and was significantly lower than in normal cats in **pituitary** ($P = 0.026$).

Abbreviations: no tx = no treatment; N/A = not applicable; Sciatic N. = sciatic nerve; CSF = cerebrospinal fluid, SD = Sandhoff disease; AAV = adeno associated virus; Hex = hexosaminidase; MUG = 4-MU-N-acetyl-β-D-glucosaminide; MUGS = 4-MU-6-sulfa-2-Acetoamido-2-Deoxy-β-D-glucopyranoside

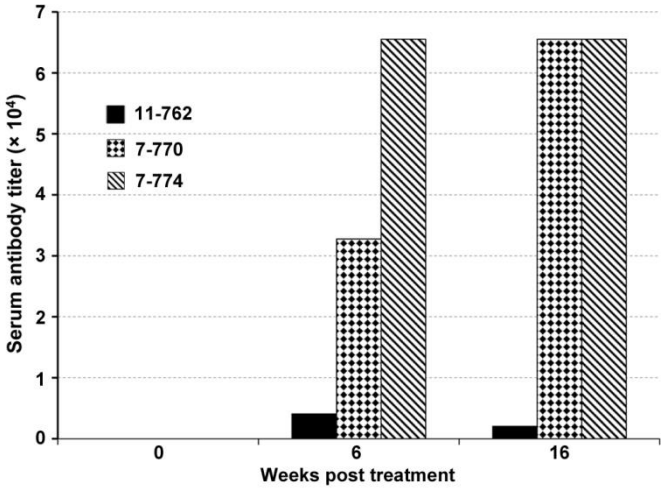

Figure 3. Serum antibody titers to the AAVrh8 vectors in AAV-treated Sandhoff disease (SD) cats. Serum antibody titers to the AAVrh8 vectors were measured in SD cats before treatment and 6 and 16 weeks after injection of AAV-*fHEXA* and AAV-*fHEXB* in the thalamus and deep cerebellar nuclei (4.4 x 10^{12} vector genomes total, 1:1 vector ratio). Bars: black = 11-762; checkered = 7-770; diagonal stripes = 7-774. Enzyme linked immunosorbent assays (ELISA) were performed by Allison M. Bradbury.

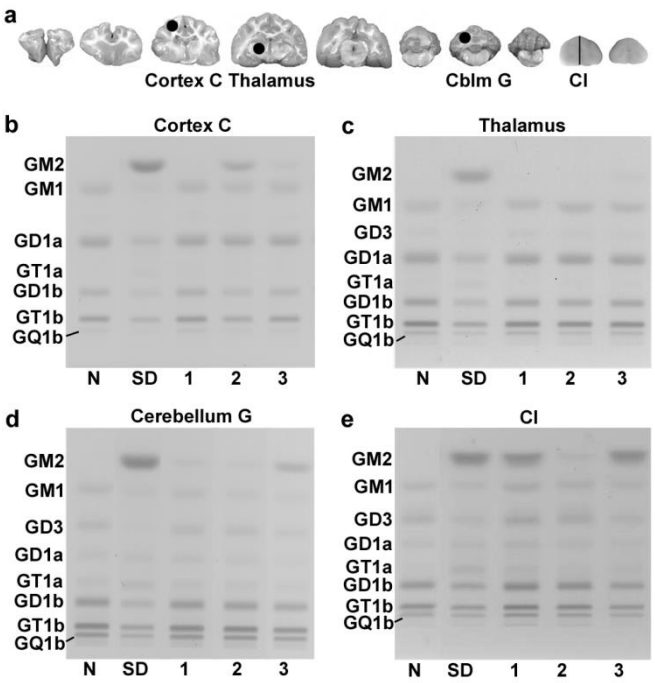

Figure 4. HPTLC of glycosphingolipids in the CNS of Sandhoff disease (SD) cats 16 weeks after treatment. SD cats were treated with thalamus and deep cerebellar nuclei injections of AAV-*fHEXA* and AAV-*fHEXB* (4.4 x 10^{12} vector genomes total, 1:1 vector ratio). Tissues were collected 16 weeks after treatment and ganglioside distribution was compared to that of normal cats and untreated SD cats. (**a**) Locations of the 8 mm punch biopsy samples from representative CNS locations. The qualitative distribution of gangliosides on chromatograms was visualized in the (**b**) cortex block C, (**c**) thalamus block D, (**d**) cerebellum block G, and (**e**) cervical intumescence (CI, block K in **Figure 1a**; half of the block was used). The amount of gangliosides spotted per lane was equivalent to 1.5 μg sialic acid. N, representative normal cat; SD, representative untreated SD cat; 1, cat 7-774; 2, cat 7-770; 3, cat 11-762. Abbreviations: Cblm = cerebellum; CNS = central nervous system; HPTLC = high performance thin layer chromatography. HPTLC plates were provided by Julian R. Arthur.

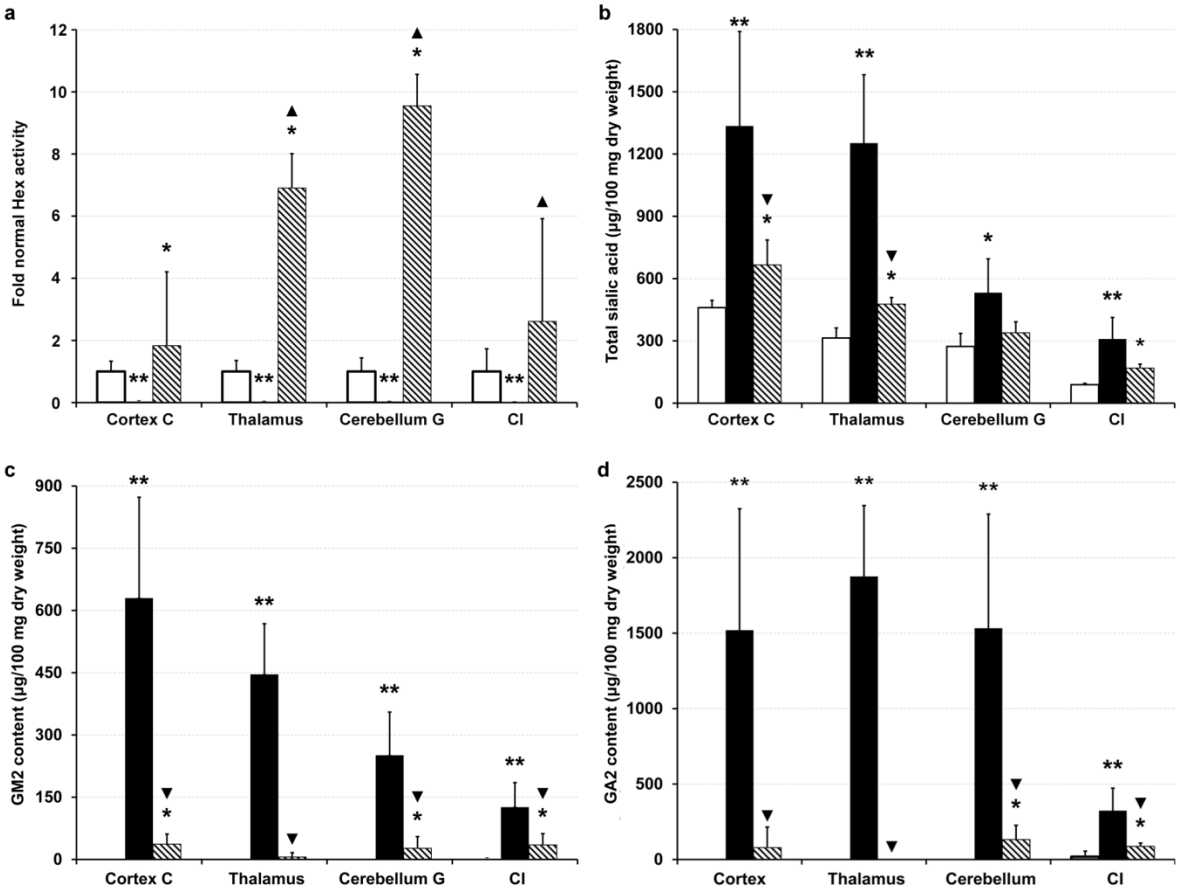

Figure 5. Quantification of therapeutic enzyme activity and storage material in the CNS of Sandhoff disease (SD) cats 16 weeks after treatment. SD cats were treated with thalamus and deep cerebellar nuclei injections of AAV-*fHEXA* and AAV-*fHEXB* (4.4 x 10^{12} vector genomes total, 1:1 vector ratio). Tissues from AAV-treated SD cats (n = 3, striped bars) were collected 16 weeks after treatment and Hex activity and substrate storage were quantified in 8 mm punch biopsy samples (shown in **Figure 4a**) for comparison to that of normal cats (n = 4, white bars) and untreated SD cats (n = 6, black bars). (**a**) Hex activity quantified against MUG substrate. (**b**) Sialic acid concentration quantified using a resorcinol based assay. (**c**) GM2 concentration quantified by densitometric scanning of ganglioside HPTLC plates (shown in **Figure 4**). (**d**) GA2 concentration quantified by densitometric scanning of asialo HPTLC plates. **, Concentration was significantly higher/lower than in normal cats ($P \leq 0.0071$); *, concentration

was significantly higher/lower than in normal cats ($P \leq 0.049$); ▼, concentration was significantly lower than in untreated SD cats ($P \leq 0.026$); ▲, concentration was significantly higher than in untreated SD cats ($P \leq 0.014$). Error bars represent standard deviation. Abbreviations: CI = cervical intumescence; HPTLC = high performance thin layer chromatography; Hex = hexosaminidase; MUG = 4-MU-N-acetyl-β-D-glucosaminide. HPTLC was performed by Julian R. Arthur and Hannah E. Rockwell.

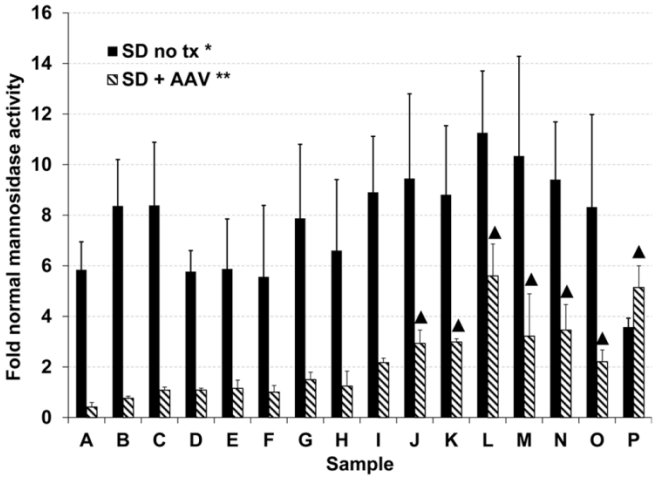

Figure 6. Lysosomal α-mannosidase activity in the CNS and pituitary of Sandhoff disease (SD) cats 16 weeks after treatment. SD cats were treated with thalamus and deep cerebellar nuclei injections of AAV-*fHEXA* and AAV-*fHEXB* (4.4 x 10^{12} vector genomes total, 1:1 vector ratio). Tissues from AAV-treated cats (n = 3, striped bars) were collected 16 weeks after treatment and lysosomal α-mannosidase activity was compared to that of untreated SD cats (n = 5, black bars) and normal cats (n = 4) in the brain (A-H), spinal cord (I-O), and pituitary. CNS sample lettering corresponds to **Figure 1a**; sample P = pituitary. *, Activity in all samples from untreated SD cats was significantly higher than in normal cats (A-H, $P \leq 0.015$ for each block; I-O, $P = 0.01$ for each block; pituitary, $P = 0.01$); **, activity in all CNS samples from AAV-treated SD cats was significantly lower than in untreated SD cats (A-H, $P = 0.018$ for each block; I-O, $P \leq 0.037$ for each block), except that activity in pituitary remained significantly higher than in untreated SD cats ($P = 0.018$); ▲, samples from AAV-treated SD cats that had significantly higher activity than in normal cats ($P = 0.026$). Error bars represent standard deviation. Abbreviations: AAV = adeno associated virus; tx = treatment

a

Score	Clinical Status*	Age (Months)
10	Normal	< 1.3 ± 0.2
9	Hind limb muscle weakness	2.1 ± 0.0
8	Wide stance	2.2 ± 0.3
7	Ataxia	2.5 ± 0.1
6	Instability with occasional falling	2.9 ± 0.4
5	Limited walking	3.5 ± 0.5
4	Standing but not walking	3.9 ± 0.5
3	Cannot stand on 2 consecutive days	4.4 ± 0.6
2	Lateral recumbency	> 4.4
1	Uncontrollable neurological symptoms	> 4.4

*Onset of mild tremors begins at 1.3 ± 0.2 months old; Onset of overt whole body tremors begins at 2.4 ± 0.1 months old.

b

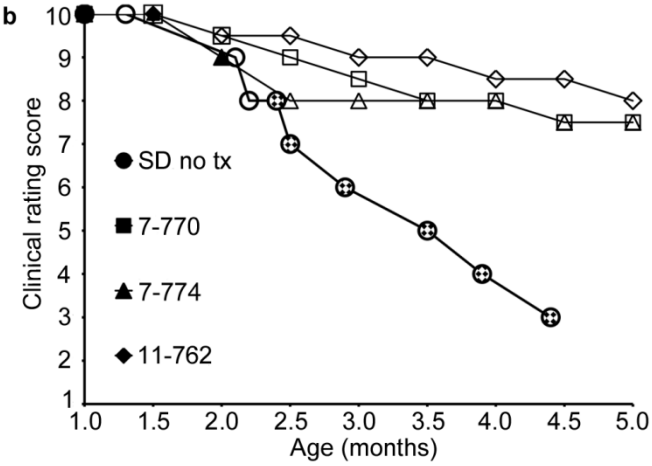

Figure 7. Clinical progression of AAV-treated and untreated Sandhoff disease (SD) cats. SD cats were treated with thalamus and deep cerebellar nuclei injections of AAV-*fHEXA* and AAV-*fHEXB* (4.4 x 10^{12} vector genomes total, 1:1 vector ratio). Treated and untreated SD cats were followed for 16 weeks after treatment using a scale based on disease progression in untreated SD cats. (**a**) Age of symptom onset is shown for untreated SD cats (mean ± s.d, n = 14). The scale is based on gait defects, which ultimately define humane endpoint, with initial deficits at 2.1 months old. However, disease onset begins at 1.3 months with subtle tremors of the head/tail that progress to overt whole-body tremors at 2.4 months. (**b**) Clinical rating scores for each individual AAV-treated SD cat and a composite for untreated SD cats (SD no tx, n = 14). Filled symbols

denote the absence of tremors, open symbols denote the presence of subtle tremors, and checkered symbols denote the presence of overt whole body tremors, which were absent in all treated cats. Abbreviations: tx = treatment

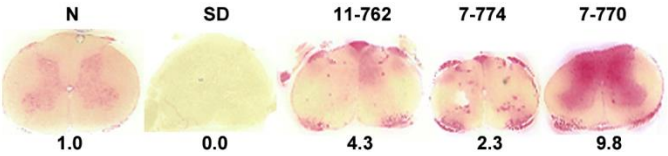

Figure S1. Therapeutic enzyme distribution in the cervical spinal cord of Sandhoff disease (SD) cats 16 weeks after AAV-treatment. SD cats were treated with thalamus and deep cerebellar nuclei injections of AAV-*fHEXA* and AAV-*fHEXB* (4.4×10^{12} vector genomes total , 1:1 vector ratio) and tissues were collected 16 weeks after treatment. Lysosomal Hex activity (red) detected with a naphthol-based substrate is shown for the cervical intumescence (block K) of AAV-treated SD cats. Corresponding HexA activity against MUGS substrate is shown below each block as fold normal level. Representative control sections for block K are shown from untreated normal cats (N) and untreated SD cats (SD), which express 0.00 ± 0.01-fold normal HexA activity in block K. Specific activity for the normal control block was 17 ± 3.8 nmol 4MU/mg/hr. Abbreviations: MUGS = 4-MU-6-sulfa-2-Acetoamido-2-Deoxy-β-D-glucopyranoside

Table S1. Vector copy number in brain, spinal cord, sciatic nerve, and pituitary of AAV-treated Sandhoff disease (SD) cats

Region	Block	Vector copy number per μg genomic DNA			
		7-762	7-770	7-774	Mean, (s.d)
Cerebrum	A	12,000	7,300	27,000	**15,000** (10,000)
	B	7,600	6,500	11,000	**8400** (2,300)
	C	17,000	12,000	9,900	**13,000** (3,600)
	D	35,000	36,000	54,000	**42,000** (11,000)
	E	79,000	25,000	36,000	**47,000** (29,000)
Cerebellum	F	1,900	6,300	5,200	**4,500** (2,300)
	G	71,000	4,900	67,000	**48,000** (37,000)
	H	Nd	8,000	nd	-
Spinal cord	I	2,100	1,300	3,900	**2,400** (1,300)
	J	3,600	950	6,800	**3,800** (2,900)
	K	2,700	1,500	4,500	**2,900** (1,500)
	L	4,500	3,200	6,000	**4,600** (1,400)
	M	2,200	1,200	2,900	**2,100** (850)
	N	2,600	850	2,600	**2,000** (1,000)
	O	2,600	2,100	3,500	**2,700** (710)
Sciatic nerve	-	7,400	1,900	2,700	**4,000** (3,000)
Pituitary	-	1,125	2,800	600	**1,500** (1,100)

Central nervous system block lettering corresponds to **Figure 1a**.

Abbreviations: nd = not determined as no sample was available for qPCR analysis.

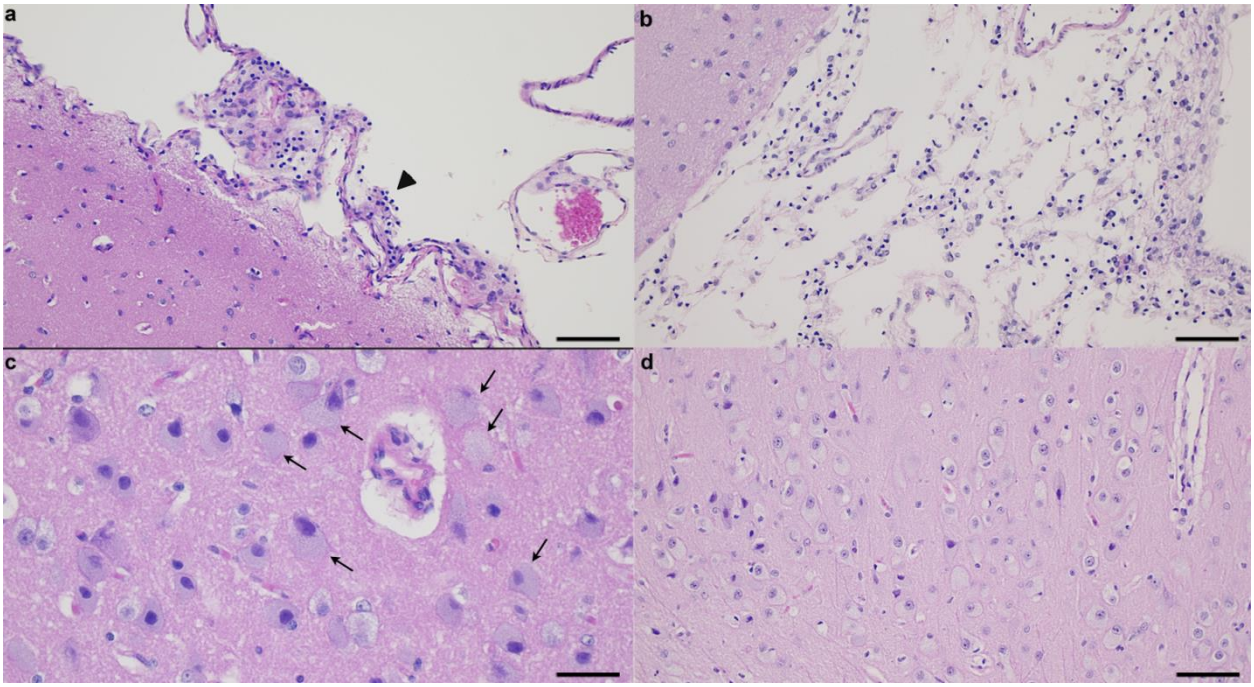

Figure S2. Histological abnormalities in the CNS of AAV-treated and untreated Sandhoff disease (SD) cats. SD cats were treated with thalamus and deep cerebellar nuclei injections of AAV-*fHEXA* and AAV-*fHEXB* (4.4×10^{12} vector genomes total , 1:1 vector ratio). Tissues were collected 16 weeks after treatment and analyzed for histological abnormalities. (**a**) Shown is a representative region from cat 7-770, block D. Rarely, the leptomeninges are multifocally expanded by small accumulations of lymphocytes and fibroblasts (black arrow head). Bar = 50 µM. (**b**) The abnormality was more diffusely seen in untreated SD cats. Bar = 50 µM. (**c**) Shown is a representative region from cat 7-770, block E. Mildly swollen neurons with copious, foamy, cytoplasmic vacuoles, which occasionally displace the neuronal nucleus peripherally (black arrows), were seen in discrete locations of deeper cortical laminae and scattered throughout cortical gray matter. Bar = 12.5 µM. (**d**) In untreated SD cats, markedly swollen neurons with copious cytoplasmic vacuoles and a peripherally displaced nucleus were apparent throughout all cerebral cortical lamina and scattered throughout the remaining cerebral gray matter. Bar = 50 µM. Histological analyses were provided by Brandon L. Brunson.

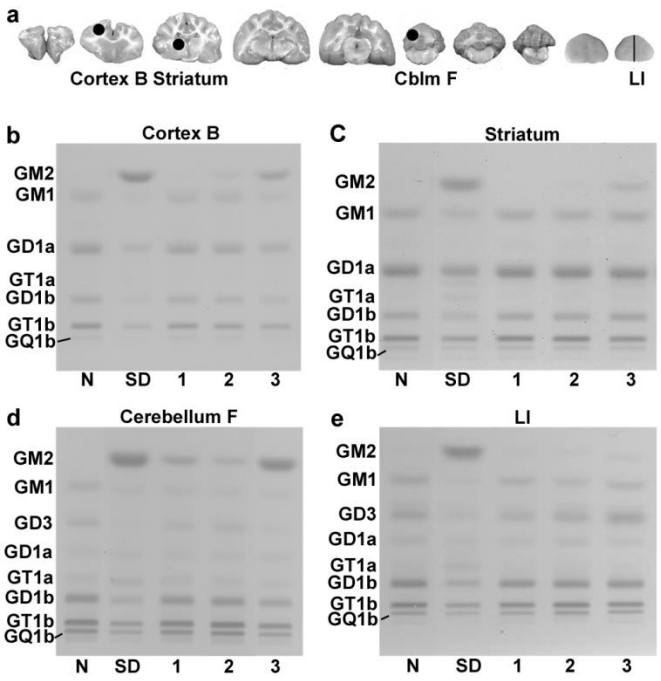

Figure S3. HPTLC of glycosphingolipids in the CNS of Sandhoff disease (SD) cats 16 weeks after treatment. SD cats were treated with thalamus and deep cerebellar nuclei injections of AAV-*fHEXA* and AAV-*fHEXB* (4.4 x 10^{12} vector genomes total, 1:1 vector ratio). Tissues were collected 16 weeks after treatment and ganglioside distribution was compared to that of normal cats and untreated SD cats. (**a**) Locations of the 8 mm punch biopsy samples from representative CNS locations. The qualitative distribution of gangliosides on chromatograms was visualized in the (**b**) cortex block B, (**c**) striatum block C, (**d**) cerebellum block F, and (**e**) lumbar intumescence (LI, block O in **Figure 1a**; half of the block was used). The amount of gangliosides spotted per lane was equivalent to 1.5 μg sialic acid. N, representative normal cat; SD, representative untreated SD cat; 1, cat 7-774; 2, cat 7-770; 3, cat 11-762. Abbreviations: Cblm = cerebellum; CNS = central nervous system. HPTLC plates were provided by Julian R. Arthur.

Table S2. Quantification of storage material in the CNS of Sandhoff disease (SD) cats 16 weeks after treatment

Sample[A]	Tx group	N value	Total sialic acid	GM2	GA2
			(μg/100 mg dry weight, mean (s.d.))		
Cortex B	Normal no tx	2	**550** (130)	**0.0** (0.0)	**0.0** (0.0)
	SD no tx	4	**1,200** (620)	**570** (310)	**1,200** (330)
	SD + AAV	3	**550** (54)*	**61** (73)*	**120** (200)*
Striatum	N no tx	2	**380** (40)	**0.0** (0.0)	**0.0** (0.0)
	SD no tx	3	**1,100** (270)	**440** (100)	**1,200** (410)
	SD + AAV	3	**470** (70)**	**14** (17)**	**4.0** (4.6)**
Cerebellum F	Normal no tx	2	**430** (28)	**0.0** (0.0)	**0.0** (0.0)
	SD no tx	2	**930** (14)	**510** (24)	**1,800** (40)
	SD + AAV	3	**490** (120)	**95** (85)	**340** (270)
LI	Normal no tx	2	**140** (13)	**1.5** (2.1)	**1.5** (2.1)
	SD no tx	4	**470** (160)	**240** (120)	**490** (150)
	SD + AAV	3	**140** (14)*	**4.0** (0.0)*	**2.0** (1.7)*

[A] Concentration of storage material was quantified in 8 mm punch biopsy samples shown in **Figure S3a** for comparison to normal cats and untreated SD cats.

*, Concentration was significantly lower than in untreated SD cats, $P \leq 0.026$; **, concentration was significantly lower than in untreated SDS cats, $P = 0.040$.

Abbreviations: Tx = treatment; LI = lumbar intumescence

HPTLC analysis was performed by Julian R. Arthur and Hannah E. Rockwell

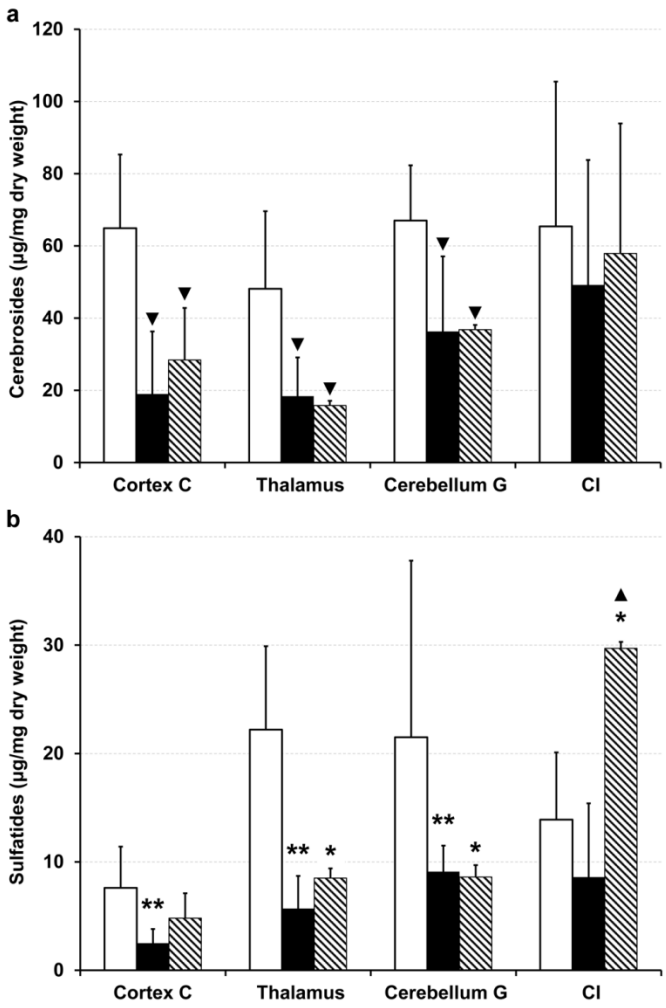

Figure S4. Quantification of myelin enriched lipids in the CNS of Sandhoff disease (SD) cats 16 weeks after treatment. SD cats were treated with thalamus and deep cerebellar nuclei injections of AAV-*fHEXA* and AAV-*fHEXB* (4.4 x 10^{12} vector genomes total, 1:1 vector ratio). Tissues from AAV-treated SD cats (n = 3, striped bars) were collected 16 weeks after treatment and myelin enriched lipid concentrations were quantified in 8 mm punch biopsy samples (shown in **Figure 4a**) for comparison to that of normal cats (n = 4, white bars) and untreated SD cats (n = 6, black bars). (**a**) Cerebroside concentration was quantified by densitometric scanning of neutral lipid HPTLC plates. (**b**) Sulfatide concentration was quantified by densitometric scanning of acidic HPTLC plates. Error bars represent standard deviation. **, Concentration was

significantly higher/lower than in normal cats ($p \leq 0.0091$); *, concentration was significantly higher/lower than in normal cats ($p \leq 0.036$); ▲, concentration was significantly higher than in untreated SD cats ($p \leq 0.014$). Abbreviations: CI = cervical intumescence; HPTLC = high performance thin layer chromatography. HPTLC alanysis was performed by Julian R. Arthur and Hannah E. Rockwell.

Chapter 3: Dramatic phenotypic improvement after adeno-associated virus gene therapy in a feline model of Sandhoff disease

Abstract

The GM2 gangliosidoses, Tay-Sachs disease and Sandhoff disease (SD), are fatal neurodegenerative lysosomal storage diseases, respectively caused by defects in the α- or β-subunit of lysosomal β-hexosaminidase (Hex), the enzyme that cleaves the terminal residue from GM2 ganglioside. This study reports the greatest survival gains yet achieved in the feline SD model. Following injection of adeno-associated virus (AAV) vectors into four brain locations in SD cats, lifespan gains of 2.0- to 8.1-fold over untreated were achieved. Widespread enzyme and vector distribution were demonstrated throughout the nervous system for up to 35.7 months, but distribution was variable between animals. Clearance of pathologic storage material correlated with Hex distribution. Significant therapeutic benefit was also demonstrated with a ten-fold lower vector dose. The unprecedented lifespan gains were accompanied by the emergence of previously subclinical peripheral disease symptoms, which limited life span before the attainment of neurological endpoint in most animals. Results support the ongoing development of AAV gene therapy for the GM2 gangliosidoses, but future approaches must also address enzyme restoration to peripheral tissues of SD cats.

Introduction

The GM2 gangliosidoses are recessively inherited lysosomal storage diseases (LSDs) resulting from impaired degradation of GM2 ganglioside (GM2) and related glycoconjugates. *HEXA* and *HEXB* encode the β-N-acetyl-hexosaminidase (Hex, EC 3.2.1.52) α- and β-subunit, respectively, which dimerize to form two major isozymes, HexA (αβ) and HexB (ββ), and a minor isozyme HexS (αα), which has negligible catalytic activity in humans. The major isozymes have overlapping substrate specificities, but only HexA can degrade charged substrates including GM2 in humans. Defects in *HEXA* and *HEXB* cause Tay-Sachs disease (TSD) and Sandhoff disease (SD), respectively, which both have HexA deficiency resulting in neuronal accumulation of GM2. In SD, the additional absence of HexB results in accumulation of neutral glycoconjugates in visceral tissues, although clinical peripheral symptoms remain subtle. *GM2AP* encodes the non-catalytic GM2 activator protein (GM2AP), also required for GM2 ganglioside degradation. Defects in *GM2AP* cause a third rare form of GM2 gangliosidosis, which is clinically similar to TSD.

GM2 gangliosidosis has a spectrum of clinical disease forms characterized by the age of disease onset and progression of clinical symptoms. The most common infantile-onset form results from negligible HexA activity resulting in rapid neurodegeneration and death in early infancy. The juvenile- and adult-onset disease forms are associated with low-level residual HexA activity. Juvenile-onset disease typically begins after 1-year of age and has a slower rate of disease progression compared to the infantile-onset form. Adult-onset disease characteristically begins later in life, and common symptoms include spinocerebellar disease, extrapyramidal signs, lower motor neuron disease, and psychosis, but intellect is usually affected little.

There is currently no effective treatment for the GM2 gangliosidoses. As HexA deficiency globally affects the central nervous system (CNS), successful treatment strategies

must target widespread areas of the brain and spinal cord. The ability of enzyme-competent cells to secrete lysosomal enzyme and "cross-correct" diseased cells[80, 81] means that only a fraction of the brain need be transduced by gene therapy vectors. Also, enzyme and vector may be further distributed by axonal transport [130-132] and cerebrospinal fluid (CSF) flow [132, 140, 141] to regions widely dispersed from the injection site. Adeno-associated virus (AAV) intracranial gene therapy has proven highly effective in SD murine[140, 142] and feline models (chapter 2) as well as the related GM1 gangliosidosis feline model[198]. SD mice injected bilaterally in the striatum and deep cerebellar nuclei (DCN) with monocistronic AAV vectors encoding Hex α- and Hex β-subunits showed widely distributed CNS Hex activity and striking absence of storage material, which increased lifespan to a median of 681 days (untreated SD lifespan, 131 days) [140].

First described in 1977, naturally occurring feline SD provides an ideal opportunity to test gene therapy in a large animal model with close similarity to the human infantile-onset disease in terms of enzymatic deficiency (≤0.02-fold normal Hex activity), neuropathology, and clinical disease progression. The naturally occurring feline *HEXB* mutation results in β-subunit protein levels that are much lower than normal (but still positive for cross-reactive material, or CRM+). Up to a 1.8-fold survival increase over untreated was previously reported for SD cats treated with bilateral thalamic injections of monocistronic AAVrh8 vectors expressing feline HexA and HexB cDNAs. It was subsequently demonstrated that global enzyme restoration resulting from bilateral delivery of AAV vectors to the forebrain *and* DCN could be translated from the mouse CNS to the larger feline CNS without the need for additional injection targets (chapter 2). This report describes the outcome of a 3-year study to investigate the long term therapeutic outcome of thalamus and DCN AAV gene therapy in SD cats.

Results

Study Design

Nineteen SD cats were treated at 0.9 to 1.3 months old, prior to disease onset (1.3 ± 0.2 months), with bilateral injections of the thalamus and DCN and were euthanized at humane endpoint. The study design consisted of four treatment groups, which are summarized in **Table 1**. Cats were given one of three vector genome (vg) doses: "full," 4.0×10^{12} to 4.4×10^{12} vg; "low," 2.2×10^{12} vg; or "one-tenth," 4.4×10^{11} vg. Previous studies in cultured fibroblasts showed that maximum HexA production requires co-expression of *HEXA* and *HEXB*[208-210]. Therefore, nine SD cats were treated with monocistronic AAVrh8 vectors expressing feline Hex α- and Hex β-subunit cDNAs in a 1:1 vector formulation (full dose α+β group). To investigate a dose response to treatment, six SD cats were treated with a ten-fold lower dose (one-tenth dose α+β group). To confirm that maximum therapeutic efficacy requires co-expression of both Hex subunits, two cats were treated with a full dose of AAV-*fHEXB* only (full dose β only group). An additional two cats were treated with a low dose of AAV-*fHEXB* only (low dose β only group) to determine if over-expression of the β-subunit limits HexA (αβ) production due to the preference of β-subunits to form the more stable HexB (ββ). Animals were euthanized at humane endpoint, defined by the inability to stand on two consecutive days. Controls were age-matched untreated normal cats (n = 4 to 6) and untreated SD cats (n = 5 for biochemical analysis; n = 14 for clinical analysis).

HexA distribution in the nervous system of SD cats treated with AAV-fHEXA and AAV-fHEXB

Naphthol staining specific to the Hex β-subunit showed widespread Hex distribution in the CNS of the full dose α+β group up to 35.7 months old demonstrating maintenance of activity

throughout the current life span (**Figure 1b, c**). However, Hex was often not evenly distributed within blocks, and the extent of distribution correlated with survival outcome, particularly in the cerebrum and cervical spinal cord (contrast the naphthol staining in **Figure 1b, c** and **Figure 4d** from 7-763 and 11-732, respectively, with **Figure 4b** from 7-816). Hex was most apparent in the dorsal funiculus throughout the spinal cord, but activity also penetrated the gray matter of thoracolumbar spinal cord blocks (M-O). In cervical spinal cord blocks (I-K) the four longest surviving cats demonstrated superior distribution to gray matter compared with the remaining cats. In the one-tenth dose group, Hex activity was present throughout the brain, but the extent of distribution also varied between animals (**Figure 1d**). In the spinal cord there was absence of any discernible activity in three of six cats. In the other three of six cats, Hex activity was well distributed in the lumbar spinal cord, but was restricted to the dorsal funiculus in cervical blocks I-K (**Figure 1e**).

HexA activity was measured quantitatively in nervous system tissues using the α-subunit preferred MUGS substrate (**Table 2**). In the full dose cohort, HexA activity was significantly higher than in untreated SD cats and normal cats throughout the brain (2.1- to 23-fold normal) and spinal cord (2.2- to 19-fold normal) as well as in dorsal root ganglia (cervical, 20-fold normal; lumbar, 36-fold normal), and peripheral nerve (PN) (3.4-fold normal). The fold normal HexA:total Hex ratio was 1.2 to 1.4 in CNS blocks indicating that Hex isozymes formed in a relatively normal ratio (**Figure 2**). The ratio was slightly higher in peripheral nervous system (PNS) samples.

In the one-tenth dose cohort, HexA activity ranged from 1.1- to 28-fold normal in the brain, which was significantly higher than in untreated SD cats, but significantly lower than in the full dose cohort in blocks D and F. Spinal cord HexA activity in the one-tenth dose cohort

ranged from 0.15- to 1.2-fold normal and was significantly lower than in the full dose cohort in most blocks. Spinal cord HexA activity only reached significance versus untreated SD cats in blocks M-O. HexA activity was 20-fold normal in the lumbar dorsal root ganglia (DRG), but was significantly lower than in the full dose cohort in the cervical DRG and PN (**Table 2**).

As survival of the full dose α+β group varied greatly, the group was separated into a medium survival cohort (n = 5, survival ≥15.3 months) and a long-survival cohort (n = 4, survival ≤ 18.9 months) for further HexA activity comparison. Both cohorts expressed significantly higher HexA than untreated SD cats in all samples. Although at near or above normal levels, HexA activity in the medium survival cohort was significantly lower versus the long survival cohort in brain blocks B and C as well as in spinal cord blocks J, K and N (**Figure 3a**).

HexA distribution to peripheral tissues

During intraparenchymal injection of AAV vectors, enzyme and vector may gain access to peripheral circulation via the CSF and bloodstream (discussed in chapters 1 and 2) as ventricles and blood vessels are traversed during the procedure. In the full dose and one-tenth dose cohorts, HexA activity in liver tissue was 0.49- and 0.23-fold normal, respectively, which was significantly higher than in untreated SD cats. Mean activity was also higher in muscle, but it did not reach significance versus untreated SD cats in either the full dose or one-tenth dose group (**Table 2**). When the medium and long survival cohorts were analyzed separately, HexA activity in the long survival cohort was significantly higher than in untreated SD cats in liver as well as muscle and was not significantly different to that of normal cats in either tissue.

Therefore, the long survival cohort demonstrated superior peripheral HexA distribution (**Figure 3**).

HexA distribution in SD cats treated with AAV-HEXB

In β only groups, Hex staining with naphthol was present throughout the brain, but showed restricted distribution in the cervical spinal cord (not shown) that was similar to the full dose α+β medium survival cohort and the one-tenth dose α+β cohort. HexA activity against MUGS substrate was below that of normal in most blocks from β only cats with the exception of blocks corresponding to injection sites and lumbar spinal cord block O. Statistical significance could not be determined versus normal cats due to low animal numbers. However, HexA activity was significantly higher than in untreated SD cats in all brain blocks, all full dose spinal cord blocks, and low dose spinal cord blocks J-O. HexA activity was significantly lower in the full dose β only group versus the full dose α+β group in most blocks except G and I (**Table 2**). The HexA:total Hex ratio for the full dose β only group was 0.09 to 0.4 indicating that HexB was the predominant isozyme produced (**Figure 2**).

AAV vector distribution

AAV vector demonstrated widespread dissemination from injection sites. The presence of vector genomes in the CNS correlated with enzyme expression, although vector copies were not always proportional to enzyme activity. Vector copies were significantly lower in the one-tenth dose α+β cohort versus the full dose α+β cohort in the rostral cerebrum as well as in all spinal cord blocks (**Table 3**).

Clearance of pathologic storage material

Total sialic acid accumulates to 2- to 4-fold normal in the brain of SD cats (chapter 2). Periodic acid Schiff (PAS) staining detects the oligosaccharide side chain of ganglioside. Staining intensity is darker in the gray matter of untreated SD cats versus normal cats. In AAV-treated cats, PAS staining appeared normalized in areas corresponding to Hex activity, but dark, dense staining was apparent in areas lacking Hex activity, indicating substantial accumulation of storage material (**Figure 4**).

Survival benefit

Compared to untreated SD cats, which reach humane endpoint at 4.4 ± 0.6 months old (n = 14), survival of AAV-treated SD cats was significantly increased (**Figure 5a**) for the full dose α+β group (19.1 ± 8.6 months, $P < 0.0001$) and one-tenth dose α+β group (15.1 ± 1.7, $P = 0.0002$), with no significant difference between groups ($P = 0.0811$). Survival of β only groups was also significantly increased compared to untreated SD cats for the full dose (20.1 ± 0.1 months, $P = 0.0189$) and low dose (17.2 ±0.4 months, $P = 0.0189$) cohorts. There was no significant survival difference between the full dose α+β and full dose β-only groups ($P = 0.9205$).

Delayed CNS disease progression

Clinical disease progression in SD cats became apparent at 1.3 ± 0.2 months old with subtle tremors of the head and tail. Symptoms progressed according to the clinical rating scale in **Figure 5b** and humane endpoint, defined by the inability to stand on two consecutive days, was reached at 4.4 ± 0.6 months old. Disease progression was delayed in all AAV-treated SD groups

(**Figure 5c-e**). Treated cats commonly progressed to ataxia by 3 to 6 months old, but then showed a protracted period of clinical stabilization with gradual progression of ataxia to loss of ambulation. Disease stabilization may have been largely due to the complete absence of overt whole body tremors in all groups, which become highly debilitating to untreated SD cats. The full-dose α+β group varied greatly in response to therapy with a survival range of 9.8 to 35.7 months. Consistent subtle tremors occurred in four of nine cats with a mean onset of 17.6 ± 11.9 months old. The one-tenth dose group also varied in response to therapy with a survival range of 7.5 to 16.9 months. The group progressed to ataxia at a significantly earlier age than the full dose group (full dose, 5.5 ± 0.9 months old; one-tenth dose 3.8 ± 1.0 months old; $P = 0.0039$), and developed consistent subtle tremors at a significantly earlier age (1.8 ± 0.6 months old; $P = 0.0068$). Cats in both β only cohorts developed consistent subtle tremors, but the full dose of AAV-*HEXB* was more effective than the low dose at delaying tremor onset (full-dose, 12.3 ± 4.9 months old; low-dose, 4.8 ± 3.1 months old).

Emergence of peripheral disease manifestations

SD cats are deficient in Hex activity in all tissues, but relentless CNS deterioration causes death before peripheral disease manifestations appear. The significant life span extension of AAV-treated SD cats resulted in appearance of previously subclinical peripheral organ disease (**Table 4**). Peripheral dysfunction was the hypothesized cause of death prior to attainment of neurological endpoint (score of 3 in **Figure 5b**) in seven of nine full dose α+β cats and five of six one-tenth dose α+β cats (**Table 5**). Two cats from each group reached premature neurologic endpoint due to patellar luxation, which compromised the use of the hind legs. Patellar luxation did not occur in any normal cats. It is thought to result from weakened muscles around the joint

and it is therefore attributed to peripheral disease causes. All β only treated cats progressed to humane endpoint according to the clinical rating scale in **Figure 5b,** although they were not spared of peripheral disease involvement (**Table 4**).

MRI analysis

Disease progression in SD cats[201] and humans[211, 212] is characterized by progressive demyelination upon MRI. In normal cats, cortical white matter is hypointense to (darker than) cortical gray matter and the area of the DCN is hypointense to (lighter than) the surrounding cerebellar gray matter. In untreated SD cats, cortical white matter and the area of the DCN were hyperintense to (lighter than) surrounding gray matter by 4 months old (**Figure 6**). Additionally, deepened sulci indicated brain atrophy. Brain architecture was substantially normalized in cat 7-773 at 24 months old (>6 times longer than in untreated SD cats). Hypointensity of the white to gray matter was largely preserved in the cerebral cortex and striatum, but isointensity of white to gray matter was seen in the thalamus. Hypointensity of the DCN area to surrounding gray matter appeared preserved. Widening of sulci was appreciated, but was not as severe as in untreated SD cats.

Discussion

SD is a progressive, terminal neurologic LSD for which only palliative care is available. AAV gene therapy has proven the most successful experimental treatment to date in murine[140, 142] and feline SD models[157] (chapter 2) as well as in the closely related feline GM1 gangliosidosis model[198]. In these studies, forebrain and DCN vector delivery resulted in widespread enzyme distribution and the greatest survival benefits yet reported. Injection of AAV

vectors in the thalamus and DCN of SD cats resulted in near global CNS enzyme distribution and substantial clearance of ganglioside storage material at 16 weeks after injection (chapter 2). This study documented the long term therapeutic outcome in SD cats treated with the same protocol.

Hex activity and AAV vector genomes were distributed throughout the CNS, PNS, and peripheral tissues for up to 35.7 months, which is in accordance with other studies reporting stable AAV expression in the brain of non-human primates (NHPs) for up to 8 years[213]. In SD cats long term Hex expression resulted in delayed clinical disease progression and significant life span extension for all treatment groups. Although thalamus and DCN directed gene therapy was able to widely disseminate enzyme in the CNS of some SD cats, distribution in the majority falls short of being global at endpoint. The extent of Hex distribution correlated with clinical outcome, with the medium survival cohort showing more restricted distribution compared to the long survival cohort.

Sixteen weeks following treatment of SD cats with AAV-vectors, storage material was substantially normalized in all areas sampled (chapter 2). Although quantitative analysis of storage material was not performed in this study, PAS staining showed ganglioside clearance in Hex expressing areas, but dense accumulation of storage in areas lacking Hex activity. Therefore, disease pathology is likely corrected or controlled in areas with sufficient Hex activity, but continues to progress in Hex deficient areas. In the GM1 gangliosidosis feline model treated by the same injection procedure, half of the subjects experienced seizure episodes attributed to lack of disease correction in the temporal lobe[198]. Likewise, Hex activity was deficient in the temporal lobe of most AAV-treated SD cats, but only 4 of 19 experienced seizure episodes. CNS enzyme distribution must be further enhanced if storage material is to be more widely eliminated. This may be achieved by adding additional deposits of vector to target brain

sites less consistently corrected, such as the rostral cerebral cortex (**Figure 3a**) and temporal lobe region (**Figures 1 and 4**). Alternatively, co-administration of mannitol with AAV injection was shown to increase CNS distribution in mice and NHPs, as was the provision of sorbitol in the vehicle solution[214, 215]. Such practices may enhance enzyme distribution from the current targets and would be less invasive than adding additional vector deposits.

In accordance with previous findings in SD cats treated for 16 weeks (chapter 2), Hex activity was well restored in the lumbar spinal cord, possibly via transport of enzyme and/or vector in CSF, which pools in the lumbar region. However, enzyme delivery to the cervical spinal cord gray matter was inconsistent and correlated with clinical outcome in the full dose α+β group. Short term studies in SD cats revealed that thalamus and intracerebroventricular (ICV) injections of AAV vector provided more effective enzyme distribution to the cervical spinal cord, resulting in superior clearance of storage material compared to thalamus and DCN vector delivery (appendix 2). Thalamus and ICV injections also resulted in above normal cerebellar Hex activity, so direct ICV vector delivery could be utilized as an additional or alternative injection site to the DCN. Additionally, vector serotypes that may have greater affinity for motor neurons could be tested, such as AAV9. Intracisternal (IC) delivery of AAV9 resulted in robust transduction of spinal motor neurons in pigs, and intravenous (IV) delivery of AAV9 resulted in up to 39% transduction of cervical spinal cord motor neurons in neonatal cats[216-218].

Substantial correction of nervous system disease resulted in delayed clinical progression and longer life span, which allowed the emergence of previously subclinical peripheral organ manifestations. Hex activity was present in liver and muscle and, importantly, correlated with survival outcome in the full dose cohort. Enzyme gains access to peripheral circulation via

leakage of vector into blood vessels and CSF during the injection procedure. The incidence of peripheral problems, particularly heart abnormalities and gastrointestinal dysfunction, indicates that Hex activity in peripheral organs was insufficient to support normal function. Several AAV mediated approaches are being investigated for their ability to achieve widespread peripheral biodistribution of therapeutic enzyme and offer the prospect of a one-time treatment. IC injection of AAV9 vector in mucopolysaccharidosis (MPS) IIIA mice resulted in near normalization of storage in all peripheral tissues analyzed. However, both IC and ICV injection of AAV9-GFP in dogs provided high vector transduction of liver, but minimal transduction of other somatic tissues[141]. Likewise, IV delivery of AAV9 in mice and NHPs shows organ dependent transduction efficiency with high level transduction of liver and muscle, but often much lower transduction of other tissues[215]. Therefore, it seems unlikely that current AAV gene therapy methods will be able to provide sufficient peripheral Hex activity for all organs.

Enzyme replacement therapy (ERT) is currently available for six LSDs, but not all peripheral manifestations respond well, such as bone in type I Gaucher disease and heart and kidney in Fabry disease[219]. In a previous study in SD cats, ERT with human HexA demonstrated the ability to achieve at least 0.44-fold normal HexA activity in all 11 tissues analyzed with subsequent reductions in GM2 and GL4 globoside[86]. Hematopoietic stem cell (HSC) transplantation is another treatment that has successfully ablated peripheral disease symptoms in some LSDs and also has the ability to enhance CNS enzyme activity[89, 219]. Furthermore, the developing protocol of ex vivo vector transduction of autologous HSCs prior to infusion may enhance HSC delivery of therapeutic enzyme and eliminates the risk of graft versus host disease[98]. Therefore, several methods of restoring peripheral enzyme activity could be tested in combination with intracranial gene therapy.

On a scale defined by gait defects it is hard to separate out clinical demise due to nervous system deficiencies from clinical demise due to peripheral tissue deficiencies. For example, the inability to support weight on hind limbs could result from both defective functioning of CNS nerve pathways as well as muscle denervation or severe muscle weakness caused by insufficient muscle HexA restoration. Additionally, spinal cord compression, documented in several AAV-treated SD cats at necropsy[157], is caused by bony or soft tissue abnormalities, but could affect neurological pathways. In order for further survival benefits to be realized in SD cats, methods to improve CNS enzyme distribution and peripheral distribution must be investigated in concert.

Studies in rodent LSD models showed a dose response to treatment with regard to enzyme activity, clearance of pathologic storage material, and survival[141, 145, 197]. In this study enzyme activity was significantly lower in the rostral cerebellum, spinal cord, and peripheral nerve of the one-tenth dose group, which could account for the earlier onset of subtle tremors and ataxia. However, there was no significant difference in survival outcome between the full and one-tenth dose groups as survival of the majority of subjects was ultimately affected by peripheral disease manifestations. It is encouraging that minimal enzyme restoration in the spinal cord can be therapeutic. However, when peripheral organ disease is more effectively treated, we expect that limited spinal cord correction will limit survival of the one-tenth dose group on a scale defined by gait defects.

If provision of only AAV-*HEXB* were efficacious it would enable double the copy number of deficient subunit to be delivered. However, studies using cell culture and rodent models of TSD demonstrated that maximum HexA expression requires provision of both Hex subunits[208-210]. As expected, HexA activity was substantially lower in the full dose β only group versus the full dose α+β group. However, lower activity did not translate to a difference in the

age of disease onset or life span. In fact, all low dose and full dose β only cats lived longer than five of nine α+β cats, and the two full dose β only cats lived longer than seven of nine full dose α+β cats. Our results indicate that low level HexA restoration may be sufficient for degradation of GM2, which supports the finding that as little as 0.11-fold normal fibroblast lysosomal enzyme activity is compatible with symptom free existence in humans. Alternatively, the feline β-subunit may have limited activity towards GM2. Regardless, all β only cats progressed through the clinical rating scale to reach neurological endpoint in contrast to several α+β cats that ultimately reached endpoint due to peripheral disease. Once peripheral treatment is addressed, we expect that survival of α+β cats will surpass survival of β only cats.

This is the second report of significant long term biochemical and clinical therapeutic benefit following AAV gene therapy in a large animal neuronopathic LSD model[198]. Results support the continued development of gene therapy approaches for these devastating, untreatable diseases. The outcome is particularly encouraging for the prospect of treating later-onset disease forms that have less severe peripheral involvement as well as neuronopathic LSDs that lack severe peripheral manifestations, such as TSD. If further therapeutic gains are to be achieved in the feline SD model, treatment of previously subclinical peripheral disease must be investigated in concert with ways to further enhance CNS distribution.

Table 1. Treatment groups and survival for long term AAV-treated Sandhoff disease cats

Vectors[A]	Dose cohort[B]	Cat	Gender	Tx age (mo.)	Survival (mo.)	Average survival (mo.) mean (s.d)
AAV-*HEXB* only	Full	11-798	M	1.1	20.0	20.1 (0.1)
		11-799	M	1.1	20.1	
	Low	11-844	M	1.0	16.9	17.2 (0.4)
		11-878	F	1.2	17.5	
AAV-*HEXA* + AAV-*HEXB*	Full	7-714	F	1.2	14.5	19.1 (8.6)
		7-826	M	0.9	12.7	
		7-857	M	1.0	9.8	
		7-748	F	1.1	18.9	
		7-746	M	0.9	21.5	
		7-816	M	1.0	15.5	
		11-732	F	1.3	29.9	
		7-763	F	0.9	35.7	
		7-821	M	1.0	13.3	
	One-tenth	7-773	F	1.2	16.9	13.1 (3.2)
		7-787	F	1.0	15.3	
		11-778	F	0.9	13.0	
		11-789	M	1.1	13.0	
		11-793	F	1.1	13.1	
		11-777	M	0.9	7.5	

[A] Cats received bilateral thalamus and DCN injections of AAV-*fHEXA* + AAV-*fHEXB* (1:1 ratio) or AAV-*HEXB* only.

[B] Doses: low, 2.2×10^{12} vector genomes (vg) total; one-tenth, 4.4×10^{11} vg total; full, 4.4×10^{12} vg total.

Abbreviations: mo = months; Tx = treatment

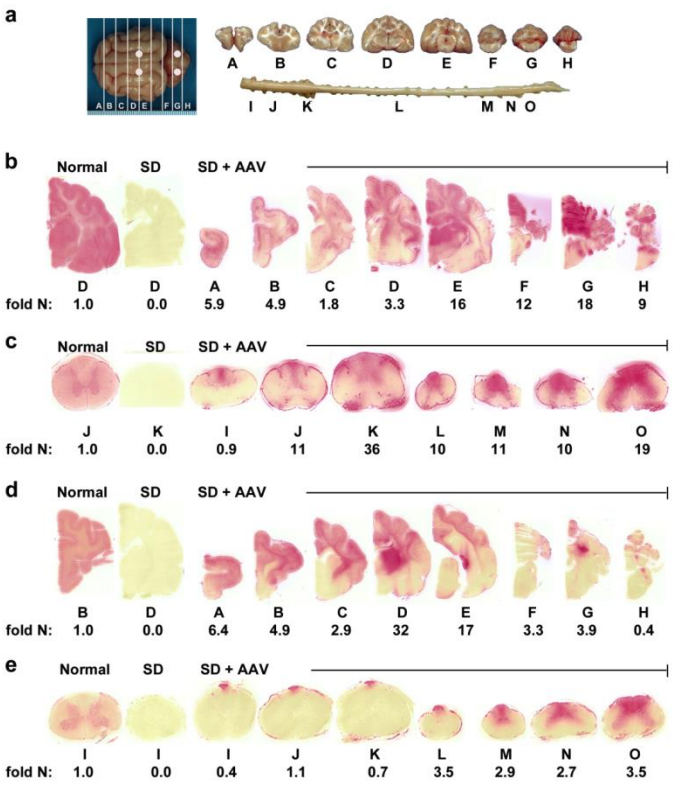

Figure 1. Therapeutic enzyme distribution in the CNS of long term AAV-treated Sandhoff disease (SD) cats. SD cats were treated with the full dose or one-tenth dose of AAV-*fHEXA*+AAV-*fHEXB* and tissues were collected at endpoint. (**a**) Injection sites (white circles) and 0.6 cm coronal blocks of the brain (A-H) and spinal cord (I-O) collected at necropsy. Lysosomal Hex activity (red) detected with naphthol at acidic pH was visualized throughout the brain (**b**) and spinal cord (**c**) of full dose α+β AAV-treated 7-763 (SD + AAV) at 35.7 months old. Lysosomal Hex activity was visualized throughout the brain (**d**) and spinal cord (**e**) of one-tenth dose α+β AAV-treated 7-773 (SD + AAV) at 16.9 months old. Corresponding HexA activity against MUGS substrate is shown below each block as fold normal level (fold N). Representative control sections are shown from normal cats along with untreated SD cats, which express ≤0.02 fold normal HexA activity in the brain and spinal cord. The ranges of specific

activities for normal control blocks were: brain, 28 (H) – 60 (D); spinal cord, 6.5 (L) – 18 (K) nmol 4MU/mg/hr.

Table 2. HexA activity in the nervous system and periphery of long term AAV-treated Sandhoff disease (SD) cats

Region	Block	Fold normal HexA activity (mean, s.d.)			
		Full dose (α+β) n = 9	1/10 dose (α+β) n = 6	Full dose (β only) n = 2	Low dose[A] (β only) n = 2
CNS					
Cerebrum	A	**2.6** (2.2) [*]	**2.2** (2.1) [*]	**0.54** (0.09) [*♦]	**0.44** (0.05) [*]
	B	**2.1** (1.7) [*]	**1.5** (1.7) [*]	**0.40** (0.07) [*♦]	**0.25** (0.05) [*]
	C	**2.4** (1.9) [*]	**1.1** (0.93) [*]	**0.33** (0.02) [*♦]	**0.23** (0.03) [*]
	D	**9.3** (4.7) [*▲]	**6.7** (13) [*♦]	**1.69** (0.82) [*♦]	**0.56** (0.43) [*]
	E	**15** (10) [*▲]	**28** (22) [*]	**0.76** (0.10) [*♦]	**2.34** (2.91) [*]
Cerebellum	F	**5.2** (3.2) [*▲]	**1.2** (1.0) [*♦]	**0.45** (0.18) [*♦]	**0.27** (0.05) [*]
	G	**20** (18) [*▲]	**19** (29) [*]	**8.65** (7.48) [*]	**1.73** (1.88) [*]
	H	**23** (22) [*▲]	**26** (54) [*]	**0.39** (0.07) [*♦]	**3.26** (1.75) [*]
Spinal cord	I	**2.2** (1.8) [*]	**0.15** (0.20) [▼♦]	**0.31** (0.38) [*]	**0.0** (0.00)
	J	**4.0** (3.2) [*▲]	**0.29** (0.45) [♦]	**0.25** (0.04) [*♦]	**0.10** (0.10) [*]
	K	**14** (15) [*▲]	**0.18** (0.30) [▼]	**0.45** (0.16) [*♦]	**0.21** (0.26) [*]
	L	**5.2** (4.4) [*▲]	**0.92** (1.4) [♦]	**0.27** (0.01) [*♦]	**0.29** (0.13) [*]
	M	**8.6** (9.5) [*▲]	**0.77** (1.1) [*♦]	**0.58** (0.23) [*♦]	**0.65** (0.04) [*]
	N	**8.4** (6.4) [*▲]	**1.2** (1.6) [*♦]	**0.65** (0.12) [*♦]	**0.65** (0.33) [*]
	O	**19** (20) [*▲]	**1.2** (1.3) [*♦]	**1.02** (0.35) [*♦]	**0.90** (0.54) [*]
PNS	-				
Cervical DRG	-	**20** (13) [*▲]	**0.05** (0.06) [▼♦]	**0.71** (0.85) [*♦]	**0.09** (0.06) [*▼]
Lumbar DRG	-	**36** (6.7) [*▲]	**20** (22)	**3.7** (4.7) [*♦]	**6.2** (1.5) [*▲]
PN	-	**3.4** (2.5) [*▲]	**0.46** (0.47) [*♦▼]	**0.40** (0.19) [*▼♦]	**0.31** (0.06) [▼]
Periphery	-				
Liver	-	**0.49** (0.48)[*▼]	**0.23** (0.12) [*▼]	**0.15** (0.08) [▼*]	**0.09** (0.03) [▼*]
Muscle	-	**0.27** (0.34) [▼]	**0.08** (0.16) [▼]	**0.00** (0.00) [▼]	**0.02** (0.03) [▼]

[*] HexA activity was significantly higher than in untreated SD cats (n = 5): **full dose α+β** (**A-O**, $P \leq 0.0031$ for each block; **C DRG**, $P = 0.0021$; **L DRG**, $P = 0.0022$; PN, $P = 0.0016$; **liver**, $P = 0.012$); **one-tenth dose** (**A-H**, $P \leq 0.0057$; **M-O**, $P \leq 0.034$; **PN**, $P = 0.04$; **liver**, $P = 0.0036$); **full dose β-only** (**A-O**, $P \leq 0.0353$; **C DRG**, $P = 0.039$; **L DRG**, $P = 0.041$; **PN**, $P = 0.035$;

liver, $P = 0.034$); **low dose β-only** (**A-H**, **J-O**, $P \leq 0.0276$; **C DRG**, $P = 0.039$; **L DRG**, $P = 0.041$; **PN**, $P = 0.035$; **liver**, $P = 0.034$).

▲ HexA activity was significantly higher than in normal cats (n = 6, full dose α+β; n = 4 for other groups): **full dose α+β** (**D-H**, $P = 0.0009$; **J-O**, $P \leq 0.0258$; **C DRG**, $P = 0.0017$; **L DRG**, $P = 0.0022$; **PN**, $P = 0.0017$); **low dose B only** (**L DRG**, $P = 0.041$).

▼ HexA activity was significantly lower than that of normal: **full dose α+β** (**liver**, $P = 0.012$; **muscle**, $P = 0.008$); **one-tenth dose** (**I** and **J**, $P = 0.0065$; **C DRG**, $P = 0.0041$; **PN**, $P = 0.0498$; **liver**, $P = 0.004$; **muscle**, $P = 0.0034$); **full dose β only** (**PN**, $P = 0.041$; **liver**, $P = 0.041$; **muscle**, $P = 0.039$); **low dose β only** (**C DRG**, $P = 0.041$; **PN**, $P = 0.041$; **liver**, $P = 0.041$; **muscle**, $P = 0.041$).

♦ HexA activity was significantly lower than in **full dose α+β** AAV-treated cats: **one-tenth dose** (**D**, **F**, **I-J**, **L-O**, $P \leq 0.0259$; **PN**, $P = 0.0009$; **C DRG**, $P = 0.0021$); **full dose β-only** (**A-F**, **H**, **J-O**, $P \leq 0.0385$; **PN**, $P = 0.023$; **C DRG**, $P = 0.045$; **L DRG**, $P = 0.025$).

[A] Statistical comparisons were not made between the full dose α+β group and the low dose β-only group.

Mean fold normal HexA activity in untreated SD cats was: **A-H**, 0.0 to 0.01; **I-O**, 0.0 to 0.02; **C DRG**, 0.02 ± 0.01; **L DRG**, 0.02 ± 0.01; **PN**, 0.02 ± 0.01; **liver**, 0.02 ± 0.00; **muscle**, 0.02 ± 0.02).

Abbreviations: DRG = dorsal root ganglia; PN = peripheral nerve; CNS = central nervous system; PNS = peripheral nervous system

Allison M. Bradbury contributed to Hex activity data for peripheral nerve, liver, and muscle.

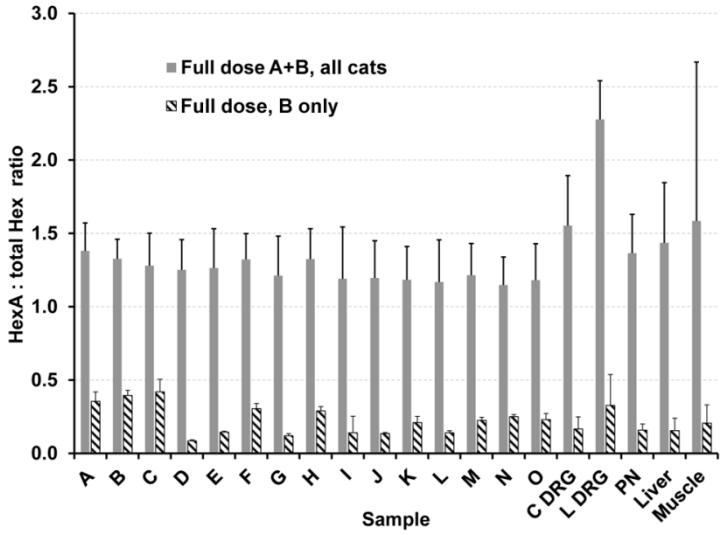

Figure 2. HexA:total Hex ratio in the nervous system, liver, and muscle of long term AAV-treated Sandhoff disease (SD) cats. SD cats were treated with the full dose of AAV-*fHEXA* + AAV-*fHEXB* or the full dose of AAV-*fHEXB* only. Tissues were analyzed for HexA activity against MUGS substrate and total Hex activity against MUG substrate. CNS block lettering corresponds to **Figure 1a**. Allison M. Bradbury contributed to Hex activity data for peripheral nerve, liver, and muscle.

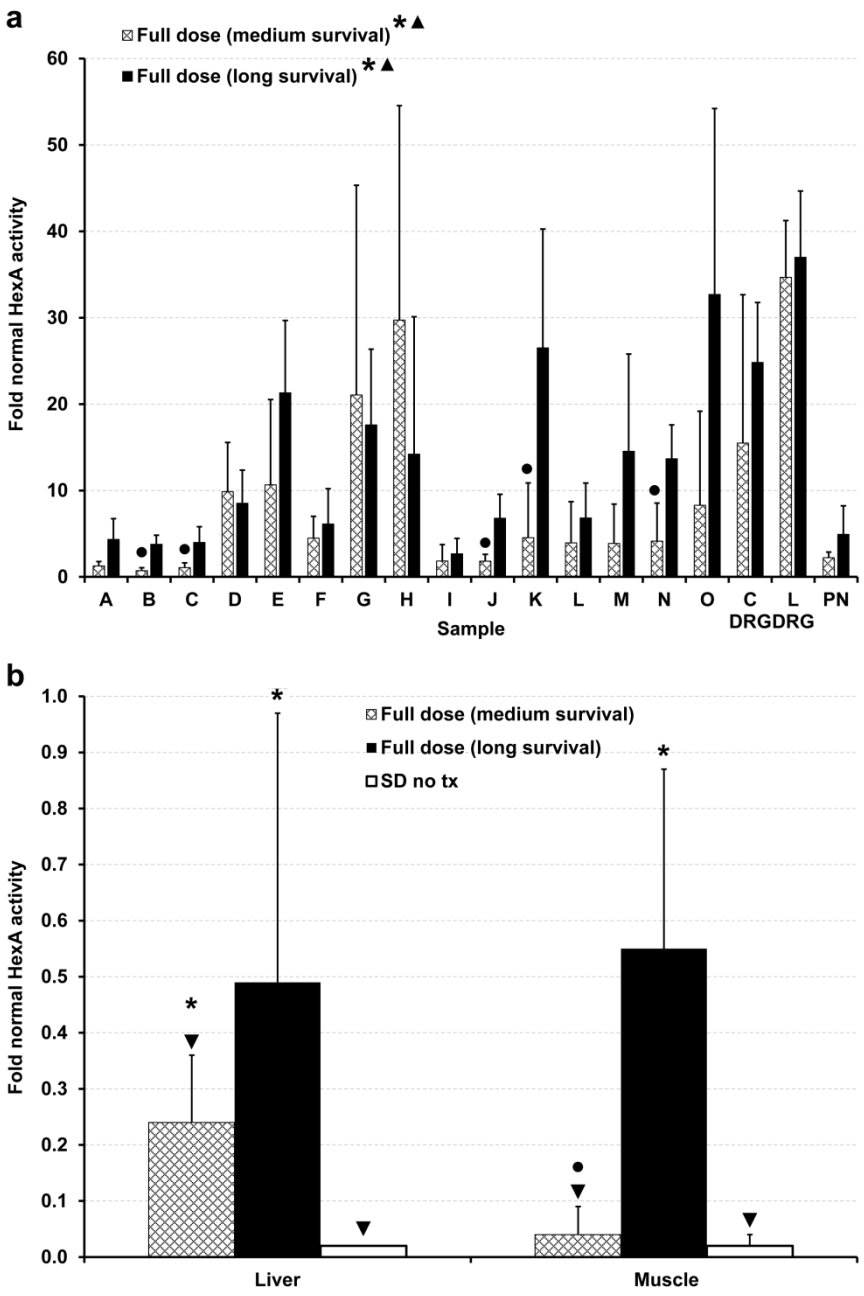

Figure 3. HexA activity in the nervous system and periphery of Sandhoff disease (SD) cats treated with the full dose of AAV-*fHEXA* + AAV-*fHEXB*. Cats were assigned to either a medium survival cohort (n = 5) or a long survival cohort (n = 4), and HexA activity against MUGS substrate was compared to that of normal cats (n = 6) and untreated SD cats (n =5). (**a**) CNS block lettering corresponds to **Figure 1a.** *, HexA activity was significantly higher than in

untreated SD cats: medium and long survival (**A-O**, $P \leq 0.0105$ for all blocks; **C DRG**, $P \leq 0.0097$; **L DRG**; $P \leq 0.01$; **PN**, $P \leq 0.0090$); ▲, HexA activity in blocks **D-H** ($P = 0.0071$), **K-O** ($P \leq 0.041$), **L DRG** ($P = 0.01$), and **PN** ($P = 0.0061$) from the medium survival cohort was significantly higher than in normal cats, and HexA activity in blocks **A-H** ($P \leq 0.044$), **J-O** ($P \leq 0.0071$), **C DRG** ($P = 0.01$), **L DRG** ($P = 0.01$), and **PN** ($P = 0.01$) from the long survival cohort was significantly higher than in normal cats; ●, HexA activity was significantly lower versus that of the long survival cohort ($P \leq 0.019$). See **Table 2** for HexA activity ranges in untreated SD cats. **(b)** HexA activity in the periphery of untreated SD cats (white bars), long survival cats (black bars), and medium survival cats (criss cross bars). *, HexA activity was significantly higher than in untreated SD cats: **liver** (medium survival, $P = 0.0055$; long survival, $P = 0.0087$); **muscle** (long survival, $P = 0.0096$); ▼, HexA activity was significantly lower than in normal cats: **liver** (medium survival, $P = 0.0061$; SD no tx, $P = 0.0055$); **muscle** (medium survival, $P = 0.0056$; SD no tx, $P = 0.0058$); ●, HexA activity was significantly lower in the medium versus the long survival cohort ($P = 0.0090$). Allison M. Bradbury contributed to Hex activity data for peripheral nerve, liver, and muscle.

Table 3. Vector copy number in the brain and spinal cord of long term AAV-treated Sandhoff disease (SD) cats

Region	Block	Vector copy number per μg genomic DNA (mean, s.d.)			
		Full dose (α+β) n = 8	One-tenth dose (α+β) n = 6	Full dose (β only) n = 2	Low dose (β only) n = 2
CNS					
Cerebrum	A	**14,000** (13,000)	**3,400** (2,200)♦	**3,900** (350)	**5,200** (5,100)
	B	**7,100** (4,900)	**2,000** (1,800)♦	**1700** (1,100)♦	**3,800** (1,400)
	C	**8,200** (3,200)	**1,600** (1,000)♦	**1,900** (1,000)♦	**2,600** (160)
	D	**21,000** (16,000)	**4,600** (4,900)♦	**23,000** (17,000)	**14,000** (1,7000)
	E	**42,000** (31,000)	**17,000** (13,000)	**4,800** (2,400)	**14,000** (17,000)
Cerebellum	F	**7,000**(4,900)	**6,000** (7,600)	**2,400** (2,200)	**3,700** (3,000)
	G	**31,000** (41,000)	**13,000** (22,000)	**76,000** (93,000)	**5,800** (6,000)
	H	**23,000** (48,000)	**29,000** (66,000)	**2,200** (1,900)♦	**28,000** (27,000)
Spinal cord	I	**9,200** (17,000)	**440** (340)♦	**1,100** (440)♦	**490** (53)
	J	**10,000** (9,500)	**800** (610)♦	**3,200** (690)♦	**1,400** (690)
	K	**5,400** (3,400)	**410** (250)♦	**1,100** (1,100)♦	**1,000** (120)
	L	**11,000** (16,000)	**1,600** (2,600)♦	**5,400** (6,500)	**600** (71)
	M	**8,500** (11,000)	**1,200** (1,500)♦	**2,500** (2,800)	**610** (490)
	N	**7,300** (5,900)	**1,300** (1,300)♦	**2,300** (2,300)♦	**630** (140)
	O	**11,000** (11,000)	**830** (600)♦	**1,100** (640)♦	**1,100** (990)

♦ Vector copy number was significantly lower than in the full dose α+β group: **one-tenth dose** (**A-H**, $P \leq 0.012$; **I-O**, $P \leq 0.0085$); **full dose β only**: (**B**, **C**, **G**, **I-K**, **N** and **O**, $P \leq 0.045$). Block lettering corresponds to **Figure 1a**.

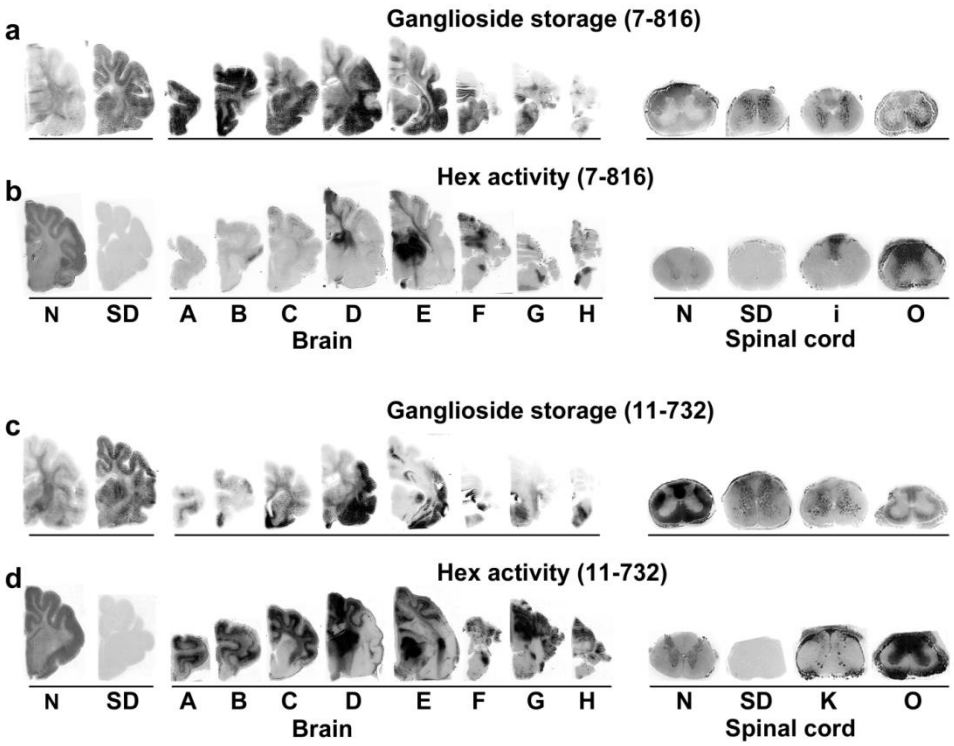

Figure 4. Correlation between Hex distribution and clearance of ganglioside storage material in the brain and spinal cord of long term AAV-treated Sandhoff disease (SD) cats. SD cats were treated with the full dose of AAV-*fHEXA* and AAV-*fHEXB* and tissues were collected at necropsy. Block lettering corresponds to **Figure 1a**. (**a, c**) Ganglioside storage is visualized by dark PAS staining in brain and spinal cord gray matter. In normal cats, myelin lipids in white matter also often stain darker than gray matter. (**b, d**). Hex activity is visualized by dark naphthol staining (the usually red colored stain has been converted to black and white). Shown are brain and spinal cord of a representative cat from the (**a, b**) medium survival cohort and (**c, d**) long survival cohort. Areas of Hex activity correlate with clearance of ganglioside storage material.

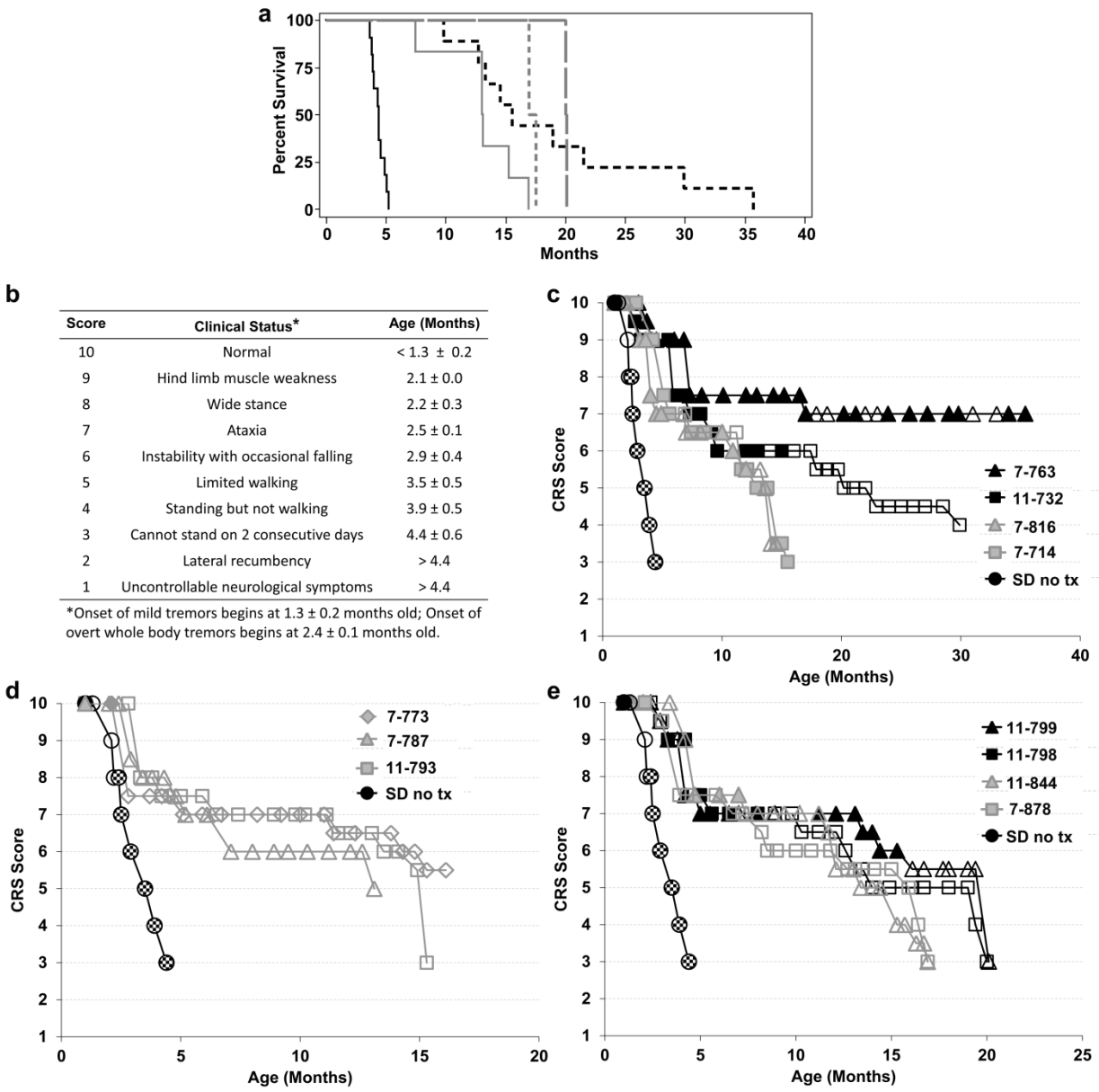

Figure 5. Survival and clinical progression of long term AAV-treated Sandhoff disease (SD) cats. (**a**) Kaplan-Meier survival curves for untreated SD cats (solid black line, n = 14) and SD cats treated long term, which have significantly increased survival compared to that of untreated SD cats: **full dose α+β**, $P = 0.0004$ (dashed black line, n = 9); **one-tenth dose α+β**, $P < 0.0001$ (solid grey line, n = 6); **full dose β only**, $P = 0.0012$ (long dashed grey line, n = 2); **low dose β only**, $P = 0.019$ (short dashed grey line, n = 2). Survival of full dose α+β cohort was not significantly different to that of the one-tenth dose α+β cohort ($P = 0.0046$). (**b**) Age of symptom

onset is shown for untreated SD cats (mean ± s.d, n = 14). The scale is based on gait defects, which ultimately define humane endpoint, with initial deficits at 2.1 months old. However, disease onset begins at 1.3 months old with subtle tremors of the head/tail that progress to overt whole-body tremors at 2.4 months old. (**c-e**) Composite clinical rating score over time is shown for untreated SD cats (black circles) and representative cats from the (**c**) full dose α+β group: black symbols = long survival cohort; grey symbols = medium survival cohort (**d**) one-tenth dose cohort, and (**e**) β only groups: black symbols = full dose cohort; gray symbols = low dose cohort. Neurological humane endpoint is reached at a score of 3. Closed symbols denote the absence of tremors; open symbols denote the presence of subtle tremors, and checkered symbols denote the presence of overt whole body tremors, which were absent in all treated cats. Abbreviations: no tx = no treatment; CRS = clinical rating score.

Table 4. Peripheral disease symptoms and seizure episodes reported in AAV-treated Sandhoff disease (SD) cats, untreated SD cats, and normal cats

Symptom	Symptom incidence (number of cats (percentage of cats)) and age of symptom onset (mean, s.d.)						
	Full dose long survival (n = 4)	Full dose medium survival (n = 5)	Tenth dose (n = 6)	β only (all cats) (n = 4)	Total AAV-treated (n = 19)	SD no tx (n = 14)	Normal no tx (n = 7)
Heart abnormality[A]	4/4 (100) 22 ± 2.2	3/5 (60) 9.0 ± 4.8	1/6 (17) 12	2/4 (50) 8.3 ± 12.1	10/19 (53)	2/14 (14) 3.1 ± 1.5	-
GI dysfunction[B]	4/4 (100) 24 ± 8.1	1/5 (20) 10	3/6 (50) 14 ± 3.3	4/4 (100) 13 ± 6.5	12/19 (63)	1/14 (7.1) 3.2	1/7 (14) 26.2
Bladder dysfunction[C]	2/4 (50) 22 ± 1.3	1/5 (20) 14	-	3/4 (75) 17 ± 0.2	6/19 (32)	-	-
Oral mass	2/4 (50) 12 ± 0.1	4/5 (80) 9.3 ± 2.9	2/6 (33) 12 ± 4.2	1/4 (25) 8.7	9/19 (47)	-	-
Spinal cord structural abnormality[D]	3/4 (75) PM	1/5 (20) PM	1/6 (17) PM	2/4 (50) 12 ± 0.1	7/19 (37)	-	-
Respiratory[E] distress	1/4 (25) 19	1/5 (20) 7.7	2/6 (33) 1.9	-	4/19 (21)	-	-
Respiratory infection	1/4 (25) 2.9	1/5 (20) 6.5	1/6 (17) 5.9	-	3/19 (16)	1/14 (7.1) 1.8	-
Horner's signs	1/4 (25) 8.0	1/5 (20) 11	-	-	2/19 (11)	-	-
Cystic kidney	-	-	1/6 (17) PM	-	1/19 (5.2)	-	-
Sudden death	2/4 (50) 20 ± 1.8	2/5 (40) 14 ± 0.8	-	-	4/19 (21)	-	-
Elbow contraction	-	1/5 (20) 12	-	-	1/19 (5.2)	-	-
Patellar luxation	-	3/5 (60) 8.2 ± 0.5	2/6 (33) 7.8 ± 0.4	-	5/19 (26)	-	-
Anisocoria	1/4 (25) 21	1/5 (20) 11	-	2/4 (50) 15 ± 3.0	4/19 (21)	-	-
Recurrent ocular/nasal discharge[F]	-	3/5 (60) 3.8 ± 2.4	3/6 (50) 1.8 ± 0.9	1/4 (25) 3.3	7/19 (37)	6/14 (43) 1.3 ± 0.67	-
Seizures	-	1/5 (20) 15	-	3/4 (75) 12 ± 3.6	4/19 (21)	-	-

[A] Includes one or more of the following diagnosed by radiographs, echocardiogram, histopathology evaluation, holter monitor, or visual evaluation at necropsy: enlarged heart; fluid around the heart; shrunken and hypereosinophilic Purkinje cells; pronounced vacuolar change in the heart valve; excess moderator bands; myxomatus degeneration; heart murmur; atrial valve thickening; myocardial degeneration; abnormality associated with papillary muscle in left ventricle; tricupsid insufficiency; bradycardia.

[B] Includes one or more of the following: gas distended stomach or small intestines, often requiring decompression; loss of serosal detail; delayed eosophageal or stomach motility; stomach erosion; gagging when eating or difficulty swallowing; mass in abdomen with distended loop of jejunum; severe weight loss requiring hand feeding; enlarged intestinal tract.

[C] Small bladder or large bladder upon palpation.

[D] Refers to one or more of the following: thickened cortical vertebral bodies; spinal canal stenosis; lordosis; enlarged costochondral junctions; trabecular pattern to vertebrae; bony lysis.

[E] Refers to one or more of the following: evidence of lung pathology on X-ray; open mouth breathing; raspy breathing; severe upper respiratory noise; increased upper respiratory effort.

[F] Recurrent means that the condition was reported on more than one occasion.

Abbreviations: GI = gastrointestinal; PM = diagnosed postmortem; dash = absence of symptom

Table 5. Cause of death for AAV-treated Sandhoff disease (SD) cats

Group	Cat	CRS at endpoint[A]	Cause of death
Full dose α+β	7-763	7	Peripheral organ disease (ileus)
	11-732	3	Neurologic endpoint
	7-748	7	Unknown, died unexpectedly
	7-746	5	Unknown, died unexpectedly
	7-816	3	Neurologic endpoint
	7-714	3	Neurologic endpoint but died unexpectedly prior to euthanasia
	7-821	6	Unknown, died unexpectedly
	7-826	3	Patellar luxation
	7-957	3	Patellar luxation
Tenth dose α+β	7-787	3	Cat was very ill in and out of ICU*
	7-773	5	Gastric perforation
	11-778	5	Respiratory distress
	11-793	5	Weight loss likely secondary to GI dysfunction
	11-798	3	Patellar luxation
	11-777	3	Patellar luxation
Full dose β only	11-999	3	Neurologic endpoint
	11-998	3	Neurologic endpoint
Low dose β only	11-844	3	Neurologic endpoint
	7-878	3	Neurologic endpoint

[A] CRS score corresponds to **Figure 5b**.

* May have promoted the weakness that eventually led to humane endpoint defined by the inability to stand.

Aabbreviations: CRS = clinical rating score; GI = gastrointestinal; ICU = intensive care unit

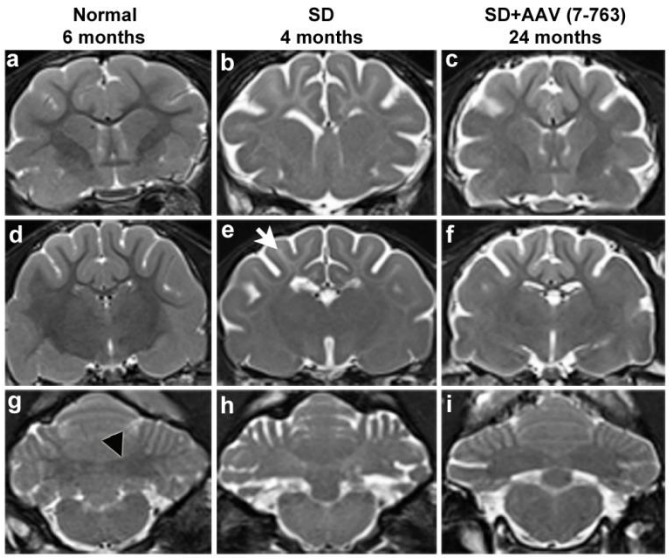

Figure 6. MRI evaluation of Sandhoff disease (SD) cats treated with AAV long term. T2-weighted MR images (3T) were taken at the level of the caudate nucleus (**a-c**), thalamus (**d-f**), and DCN (**g-i**). Cortical white matter is hypointense to (darker than) gray matter in normal cats but hyperintense to (lighter than) gray matter in untreated SD cats [white arrow in (e)]. Also, the DCN area is hypointense to surrounding gray matter in normal cats [outlined black arrowhead in (g)], but becomes hyperintense with disease progression in untreated SD cats. In AAV-treated cat 7-763, hypointensity of cortical white to gray matter and DCN area to cerebellar gray matter was largely preserved, indicating reduced myelin loss after treatment. At the time of imaging cat 7-763 was at a clinical rating score of 7 according to the scale in **Figure 4b**. Ages are shown for each cat. There were no appreciable differences between a normal cat brain at 6 months and older ages. MRI images were acquired by Heather L. Gray-Edwards.

Chapter 4: Significant therapeutic benefit after post-symptomatic intracranial gene therapy in a feline model of Sandhoff disease

Abstract

Sandhoff disease (SD) is an autosomal recessive lysosomal storage disease caused by defects in the β-subunit of β-N-acetylhexosaminidase (Hex), the enzyme that catabolizes GM2 ganglioside (GM2). Hex deficiency causes neuronal storage of GM2 and related glycoconjugates, resulting in progressive neurodegeneration and death, often in infancy. No effective treatment exists for human patients. Adeno-associated virus (AAV) gene therapy led to improved clinical outcome and survival of SD cats treated before disease onset was increased up to 8.1-fold over untreated. As most human patients are not diagnosed until disease symptoms become evident, it is imperative to test AAV gene therapy in post-symptomatic SD cats to provide a more realistic indication of therapeutic gains that can be expected in humans. Here, AAVrh8 vectors injected bilaterally into the thalamus and deep cerebellar nuclei of post-symptomatic SD cats resulted in widespread central nervous system enzyme distribution, although a substantial burden of storage material remained. Nevertheless, cats treated in the early symptomatic phase showed delayed disease progression and a 2.6-fold mean survival increase versus untreated SD cats. Treatment was less effective when administered later in the disease course, although therapeutic benefit may still be achieved in some animals. Results are encouraging for the treatment of human patients who are usually diagnosed after clinical disease onset and provide support for the ongoing development AAV gene therapy for human SD.

Introduction

The GM2 gangliosidoses are recessively inherited lysosomal storage diseases (LSDs) characterized by neuronal accumulation of GM2 ganglioside (GM2), progressive neurodegereration, and early death. Lysosomal β-N-acetylhexosaminidase (Hex, EC 3.2.1.52) cleaves the terminal residue from GM2 ganglioside and related glycoconjugates with terminal N-acetylgalactosamine or N-acetylglucosamine residues. Catabolism requires the concerted action of three gene products: the Hex α-subunit, Hex β-subunit, and the GM2 activator protein (GM2AP). Deficiencies in the gene products result in Tay-Sachs disease (TSD), Sandhoff disease (SD), and GM2AP deficiency, respectively. The two major Hex isozymes, HexA (αβ) and HexB (ββ), have overlapping substrate specificities, but only HexA can cleave charged substrates, such as GM2. A third isoform, HexS (αα), is unstable and has no appreciable catalytic activity in normal humans[35].

GM2 gangliosidosis occurs as three clinical disease forms distinguished by the age of symptom onset and progression of clinical symptoms, which is largely determined by the residual level of Hex activity[83]. The most common infantile-onset form is characterized by relentless neurodegeneration and premature death, often by age 3 to 5 years. Juvenile- and adult-onset disease forms progress slower and have a more heterogeneous clinical course. Typical symptoms of adult-onset disease include extrapyramidal signs, spinocerebellar disease, lower motor neuron disease, and psychosis, but intellect is usually preserved. TSD and SD are clinically similar, despite the additional accumulation of neutral substrates in peripheral tissues of SD patients because of combined HexA and HexB deficiency[35].

Several treatment approaches have been tested in humans, such as bone marrow transplantation[96], substrate reduction therapy[103-106], and chemical chaperone therapy[115, 116], but

there remains no effective treatment. As Hex deficiency globally affects the CNS, treatment strategies must target widespread areas of the brain and spinal cord. Adeno-associated virus (AAV) gene therapy has the potential to generate a permanent source of Hex in the CNS. Following transduction, a proportion of lysosomal enzyme can be secreted and cross-correct neighboring cells[80, 116]. In addition to local diffusion[129], enzyme is more widely distributed by axonal transport[130-132] and cerebrospinal fluid (CSF) flow[140, 141].

First described in 1977, the feline SD model (β-subunit deficient) is highly analogous to the human infantile-onset disease form and provides an ideal large animal model to test therapies for translation to humans. A naturally occurring mutation results in <0.02-fold normal CNS Hex activity, 700-fold normal brain GM2 storage, and progressive neurodegeneration, with death at 4.4 months old[74, 78, 79]. AAV gene therapy in pre-symptomatic SD murine and feline models demonstrated widespread CNS Hex distribution resulting in significant gains in clinical function and life span[140, 142] (chapter 3). Although the outcome is encouraging, the average delay from symptom onset to diagnosis for GM2 gangliosidosis humans is currently ~6.7 to 9.6 months[220, 221]. Therefore, most patients are in the symptomatic disease stage at the time of diagnosis, which would preclude pre-symptomatic gene therapy. Studies in SD mice demonstrated that enzyme restoration and clearance of storage material were independent of treatment age. However, clinical outcome declined with increasing treatment age, likely due to irreversible pathological changes, such as demyelination and neuronal apoptosis[161]. This study tested post-symptomatic AAV gene therapy in the feline SD model, with a size, complexity, longevity, and naturally occurring disease that more closely resemble humans. Results will be important to inform inclusion criteria for patients in future clinical trials.

Results

Treatment groups

Seven SD cats were treated after the average age of clinical disease onset with bilateral thalamus and DCN injections of monocistronic AAVrh8 vectors encoding feline Hex α- and Hex β-subunits (1:1 ratio, 4.4 x 10^{12} to 4.6 x 10^{12} vector genomes total). Vectors were the same as those that proved successful in a previous study in pre-symptomatic SD cats (chapter 3). Treatment groups are detailed in **Table 1**. Stereotypical disease progression in untreated SD cats (n = 14) begins at 1.3 ± 0.2 months old with fine tremors of the head and tail. Symptoms progress according to the clinical rating scale in **Figure 1a** until cats cannot stand on two consecutive days, which defines the humane endpoint at 4.4 (± 0.6) months old. Four SD cats were treated at the stage of subtle tremors but no gait defects (1.6 to 1.8 months old, early post-symptomatic (EPS) group), and three SD cats were treated at the stage of overt whole body tremors and ataxia, with or without instability (2.1 to 2.7 months old, late post-symptomatic (LPS) group). Controls included untreated SD cats (n = 5 for lysosomal enzyme analysis, n = 4 for storage analysis, and n = 14 for clinical analysis), and age matched normal cats (homozygous for the wildtype allele) for the EPS and LPS cohorts (for each cohort, n = 5 for enzyme analysis, n = 4 for storage analysis, and n = 7 for clinical analysis).

Clinical and survival outcome

AAV-treated SD cats were scored on a clinical rating scale that reflects stereotypical disease progression in untreated cats (**Figure 1a**). Disease progression was delayed for all cats in the EPS cohort, which demonstrated a 2.4 to 4.3-fold survival increase over untreated SD cats (mean survival, 15.4 ± 3.7 months, P = 0.0010, **Figure 1b**). Treated cats eventually lost the

ability to stand due to hind limb weakness, but debilitating whole body tremors characteristic of untreated SD cats did not develop (**Figure 1c**). In accordance with improved clinical performance, the EPS cohort also showed delayed acquisition of deficits on common neurological tests compared to untreated SD cats (**Figure 2**).

Survival of the LPS cohort was not significantly different versus untreated SD cats (6.6 ± 4.2 months, $P = 0.28$, **Figure 1b**), and it was significantly shorter than survival of the EPS cohort ($P = 0.048$). Two LPS cats (7-801 and 7-866) continued to develop clinical symptoms at the stereotypical age, including progressively worsening debilitating whole body tremors, and reached humane endpoint at 4.0 and 4.4 months old, respectively. Disease progression in cat 11-994 stabilized ~1 month after surgery despite the continued presence of whole body tremors, and cat 11-994 lived to 11.4 months old, or 2.6 times longer than untreated SD cats (**Figure 1d**). Therefore, mean survival was not significantly improved in LPS treated cats, but treatment can be beneficial in some individuals. Acquisition of neurological deficits on common tests was not delayed in the LPS cohort versus untreated SD cats (**Figure 2**).

On T2 weighted MRI, white matter is hypointense to (darker than) gray matter in the cortex and cerebellum of normal cats, but becomes hyperintense to (lighter than) gray matter by 4 months of age in untreated SD cats (**Figure 3**). Cat 11-994 at 11.5 months old showed some preservation of white matter intensity in the cortex, but the white matter area of the DCN was hyperintense to the surrounding cerebellar gray matter. Brain atrophy in cat 11-994 was comparable to the 4-month old untreated SD cat in terms of widening of cerebral sulci, cerebellar fissures, and ventricles. As cat 11-994 was treated in the LPS disease stage, it is likely that she had already experienced substantial brain atrophy and cerebellar demyelination before treatment.

Although disease progression in untreated cats is defined by neurological deterioration, Hex deficiency also affects peripheral tissues. In SD mice[140] and pre-symptomatic SD cats (chapter 3) treated with AAV-gene therapy, improved neurological outcome allowed the emergence of peripheral disease problems that were subclinical in untreated SD cats. SD cats treated post-symptomatically also developed peripheral disease symptoms (**Table S1**). However, peripheral disease did not limit survival of any subjects in this study as all cats reached their neurological humane endpoint (score of 3 in **Figure 1a**).

Therapeutic enzyme distribution

Postmortem histochemical naphthol staining specific to the Hex β-subunit showed Hex activity in all brain blocks of both cohorts, but distribution varied between animals, and activity was not uniformly distributed within blocks (**Figure 4**). In both cohorts, the extent of Hex distribution correlated with survival. Staining was most intense at the thalamus and DCN injection sites in the EPS cohort (block D and G in **Figure 4b, d**). In the LPS cohort, staining was also intense at the thalamus injection site, but a focal area of high activity was not as apparent at the cerebellar injection site (block G in **Figure 2b**). In both cohorts, Hex activity in the cervical spinal cord (blocks I-K) was restricted to the dorsal funiculus, with minimal activity detected in gray matter. In the thoracolumbar spinal cord (blocks M-O), staining was detected in the dorsal gray matter and also extended into the ventral gray matter (**Figure 2c, e**).

Hex activity was measured quantitatively with the synthetic Hex α-subunit preferred substrate, MUGS. Residual HexA activity against MUGS in untreated SD cats was ≤0.01-fold normal in the brain and ≤0.02-fold normal in the spinal cord. In both AAV-treated cohorts, mean HexA activity was significantly higher than in untreated SD cats in all brain (EPS, 2.8- to 22-fold

normal; LPS, 1.4- to 9.9-fold normal) and spinal cord (EPS, 0.83- to 4.7-fold normal; LPS, 0.34- to 2.8-fold normal) blocks (**Table 2**). HexA activity was significantly lower in the LPS cohort versus the EPS cohort in spinal cord blocks M and O, although mean activity for these blocks was above normal for both cohorts. AAV vector was detected by quantitative PCR in all CNS blocks from AAV-treated SD cats indicating widespread dissemination from injection sites (**Table S2**). In accordance with the lower HexA activity, vector copy number was significantly lower in blocks M-O of the LPS group versus the EPS group.

During intraparenchymal injection, vector may leak into and be distributed by cerebrospinal fluid (CSF) and the vasculature[137, 140]. Hex activity in CSF of the EPS and LPS cohorts was 2.3- and 2.7-fold normal, respectively, indicating that CSF transport may have contributed to enzyme dissemination (**Table 2**). HexA activity was also detected at near or above normal levels in dorsal root ganglia (DRG) and sciatic nerve of both cohorts (**Table 2**). In visceral tissues, mean HexA activity was significantly higher than in untreated SD cats in the heart of both cohorts and in the liver of the EPS, but not the LPS cohort. HexA activity was not significantly higher than that of untreated SD cats in muscle. Vector copies were also detected in liver and heart tissue of both groups indicating that a portion of HexA activity was due to vector transduction (**Table S2**). Vector was additionally detected in sciatic nerve and muscle of some LPS treated cats, but not EPS treated cats, possibly due to vector loss over time in longer surviving animals.

Clearance of storage material

Total ganglioside sialic acid accumulates to several fold normal in the brain of SD cats[74, 200]. As glycosphingolipids with complex oligosaccharide side chains containing one or more

sialic acid residues[16], gangliosides can be detected colorimetrically by periodic acid Schiff (PAS) staining. To evaluate the clearance of stored ganglioside by AAV vector generated Hex, PAS staining was performed on blocks A-O. Storage levels were normalized in areas corresponding to Hex restoration, but ganglioside accumulation was apparent in areas that lacked Hex activity (**Figure 5**).

When quantitative sialic acid assays were performed on 15 samples throughout the CNS (**Figure 5b, c**), concentrations in untreated SD cats were significantly higher than in normal cats in the cerebrum (2.6- to 4.9-fold normal), brainstem and cerebellum (2.0- to 3.8-fold normal), and spinal cord (3.2- to 3.8-fold normal). In the EPS and LPS AAV-treated cohorts, sialic acid concentration remained significantly higher than that of normal in 11 and 13 of 15 samples tested, respectively. In the LPS group, storage was significantly lower than in untreated SD cats in five of nine forebrain samples (A to E), the middle and caudal cerebellum (G and H), and the lumbar spinal cord (O). In the EPS group, sialic acid concentration was significantly lower than in untreated SD cats in all cerebellum and brainstem samples (F to H) as well as in the lumbar spinal cord (O), and storage was significantly higher than in untreated SD cats in the temporal lobe (D3). Unlike in the LPS cohort, storage in the EPS cohort was not significantly lower than in untreated SD cats in forebrain samples (A-H), likely because the longer survival of EPS treated cats allowed more storage to accumulate over time.

Cat 11-831 in the EPS group and cat 11-994 in the LPS group experienced seizure activity, well controlled by medication, with onset at 7.8 and 8.4 months old, respectively (**Table S1**). Seizures are a feature of late stage feline SD[46], but no untreated SD cats in the present study had seizures as they occur beyond the humane endpoint used. As previously reported (chapters 1 and 3), seizure activity may be related to lack of disease correction in the temporal lobe, which

was deficient in enzyme activity in both cats (**Figure 4b, d**) and contained a significant concentration storage material.

Activity of a secondary lysosomal biomarker

In LSDs, activity of non-mutant lysosomal hydrolases is often elevated[143]. In untreated SD cats, α-mannosidase activity was significantly elevated up to 8.4-fold normal in the brain, 11-fold normal in the spinal cord, and 4-fold normal in the liver. In AAV-treated EPS and LPS SD cats, α-mannosidase activity was significantly reduced in most CNS blocks compared to that of untreated SD cats (**Figure 6**). However, α-mannosidase activity remained significantly higher than in normal cats in most brain (EPS, 1.7- to 3.6-fold normal; LPS, 2.1- to 4.4-fold normal) and spinal cord (EPS, 3.8- to 8.4-fold normal; LPS, 3.7- to 6.9-fold normal) blocks, as well as in liver, indicating partial, but far from complete, normalization of this secondary lysosomal biomarker.

Discussion

The GM2 gangliosidoses, TSD and SD, are progressive, fatal, neurodegenerative lysosomal storage diseases with no effective treatment. To date AAV-mediated gene therapy has proven the most successful experimental treatment approach in SD murine[140, 142, 161] and feline models[157] (chapters 2 and 3) as well as in the closely related GM1 gangliosidosis feline model[198]. Delivery of therapeutic AAV-vectors to the forebrain and DCN of pre-symptomatic gangliosidosis mice and cats resulted in widespread CNS enzyme distribution as well as dissemination to some peripheral tissues. Life span was near-normalized in treated SD mice[140],

and up to 8.1-fold survival increases were demonstrated in treated versus untreated SD cats (chapter 3).

These unprecedented survival gains occurred in animals that were treated before clinical disease onset, which does not accurately reflect the clinical status at diagnosis for most human patients who will be the eventual recipients of therapy. Prenatal screening for GM2 gangliosidosis is only routinely performed in high risk populations, such as those with Jewish ancestry[222], so most human patients are not diagnosed until after the appearance of clinical symptoms[220, 221]. Currently, average definitive diagnosis of infantile TSD and SD occurs 7.3 and 9.3 months after symptom onset, respectively, which is in the early symptomatic disease stage. By this age, most patients have elevated noise sensitivity, and patients at the early end of the range may already display other neurological signs, such as loss of sitting, hypotonia, loss of head movement, spasticity, and diminished eyesight[220]. Therefore, it is important to determine clinical benefit from AAV gene therapy in SD cats treated after disease onset.

Studies in SD mice, as well as other LSD animal models, determined that clinical therapeutic benefit decreases with increasing treatment age[161-163, 165], and that a therapeutic window exists for treatment beyond which vector administration provides no clinical benefit[161]. Here, we translated the thalamus and DCN treatment approach from pre-symptomatic to post-symptomatic SD cats. In a previous SD mouse study, vector was administered at progressively older ages, but SD mice were not clinically symptomatic at any treatment time point. At the oldest time point tested (1 week before average symptom onset), no clinical benefit was achieved[161]. In contrast, all SD cats were treated after the age of clinical disease onset and clinical benefit was demonstrated in five of seven cats. This highlights the importance of using large animal models that more closely resemble human disease to inform preclinical studies.

All SD cats treated in the EPS disease stage demonstrated significant survival gains. Although average survival was lower than cats in a previous study treated pre-symptomatically (chapter 3) (mean survival, EPS group 15.4 months; pre-symptomatic group 19.1 months), two of four EPS treated cats survived longer than five of nine pre-symptomatic treated cats, so there was survival overlap between groups. This study was not able to definitively conclude a point beyond which treatment is ineffective as one cat in the LPS cohort demonstrated survival benefit that overlapped with the EPS cohort. However, treatment did not result in survival benefit for the other two of three LPS cats even though cat 7-866 was only treated 0.3 months later than the longest living EPS cat (11-831). This demonstrates that there may be a narrow window of time during which pathological disease progresses beyond a critical point that is not amenable to therapy. Although feline SD progression is stereotypical, some variation is associated with the disease course as evidenced by the attainment of humane endpoint between 3.8 to 5.2 months old in untreated cats (**Figure 1b**). At the time of treatment, the pathological disease progression of cat 11-944 was likely still within the critical threshold amenable to therapy.

While disease is still amenable to therapy, clinical outcome likely depends on the ability of vector to distribute sufficient therapeutic enzyme. Previous studies showed that enzyme and vector biodistribution are not affected by pathologic disease status at the time of treatment, which suggests that preexisting storage material does not affect enzyme dissemination from affected neurons[161, 163]. Here, enzyme distribution was variable between subjects in both the EPS and LPS cohorts, as previously reported in cats treated pre-symptomatically (chapter 3). Distribution was only significantly lower in the LPS versus EPS cohort in the thoracolumbar spinal cord, although activity was above normal, so it is unlikely to have influenced outcome. Variation in enzyme distribution likely occurred due to slight differences in anatomy between

cats as well as variation in the precise site of injection within the thalamus and DCN. For example, the thalamic injection site was in block D or E depending on the animal, and the DCN injection site was in block F, G or H.

Clearance of pathologic storage material was shown to be reversible in mice and not dependent on treatment age[134, 161, 163]. Here, areas positive for Hex activity also showed clearance of ganglioside storage upon PAS staining. However, Hex deficient areas showed dark, dense accumulations of storage material. Therefore, remaining storage was likely related to insufficient Hex activity in those areas. Quantitative measurement of sialic acid revealed substantial storage material remaining in most samples from both cohorts with the exception of the middle cerebellum and lumbar spinal cord for which both groups showed significantly normalized storage. The significant storage burden correlated with the incomplete restoration of lysosomal α-mannosidase activity. Sixteen weeks after AAV treatment of pre-symptomatic SD cats, storage material was substantially normalized in all areas sampled (chapter 2). However, when analyzed at humane endpoint, storage material had likewise accumulated over time in cells that likely remained Hex deficient (chapter 3). As the longest surviving cats in each cohort demonstrated the most widespread enzyme distribution, it is important to investigate ways to further enhance enzyme distribution as discussed in chapter 3.

In pre-symptomatic AAV-treated SD cats, partial correction of CNS disease allowed longer life span with the emergence of previously subclinical peripheral disease symptoms (chapter 3). Here, cats in the EPS cohort also suffered peripheral disease symptoms due to their longer survival. There was significant Hex correction in liver tissue of EPS treated cats, and low but significant Hex correction in heart tissue of EPS treated cats. Therefore, whilst some enzyme/vector was transported to the periphery, future studies must more effectively address

treatment of peripheral organs, as discussed in chapter 3. After peripheral gene therapy in Pompe disease mice, muscle was refractory to vector transduction in old mice compared to young mice, but liver and heart were not[223]. Here, mean peripheral tissue HexA activity was lower in LPS treated cats versus EPS treated cats, but values did not reach significance.

In LSD mouse models, clinical disease is stabilized, but not improved, following AAV-treatment. Lack of improvement is due to progressive development of irreversible pathologic changes, such as myelin abnormalities, persistence of ubiquitinated inclusions, and neuronal loss[161-163]. Ectopic dendrite formation also occurs in feline gangliosidosis models[23], and was refractory to therapy in an induced α-mannosidosis feline model[53]. Therefore, improving enzyme distribution and clearance of storage material in the CNS and periphery is important if further survival gains are to be achieved in EPS treated SD cats, but development of irreversible pathologic changes may still limit the degree of functional rescue in LPS treated SD cats.

In an α-mannosidosis feline model, AAV1 gene therapy in post-symptomatic cats resulted in reversal of clinical disease and improvements in myelination[164]. As demonstrated in SD mice, clinical disease stabilized in post-symptomatic AAV-treated SD cats, but did not improve, so the capacity for clinical improvement is likely disease specific rather than species specific. At humane endpoint, myelination in cat 11-994 was better in the cortex compared to untreated SD cats. Because cat 11-994 did not show reversal of clinical symptoms following treatment, it is likely that cortical myelination was preserved after treatment not that myelination was improved.

The current study in post-symptomatic SD cats demonstrates that AAV-gene therapy is therapeutic when administered during the EPS disease stage. Therapy may also provide disease stabilization when administered during the LPS disease stage. However, during the LPS stage it

should be considered whether the degree of expected functional improvement is sufficient to warrant intervention given that there is no evidence of disease reversal in treated SD cats. Results are highly encouraging for the prospects of treating human patients who are usually diagnosed during the early symptomatic disease stage[220]. If gene therapy, or any other treatment approach, becomes translated to the clinic then rapid diagnosis following symptom onset would be needed if patients are to be treated during the most beneficial early symptomatic stage. Also encouraging is the prospect of treatment for juvenile- and adult-onset disease forms; disease progression following diagnosis is slower, so there is a larger window of opportunity to treat late onset patients during the early symptomatic stage.

Table 1. Treatment groups for post-symptomatic AAV-treated Sandhoff disease (SD) cats

Treatment group	Cat	Gender	Tx age (mo.)	CRS score at tx[A]	Age at endpoint (mo.)	Survival (mo.) (mean, s.d.)
Late post-symptomatic	11-994	F	2.2	7.5**	11.5	6.6 (4.2)
	7-866	M	2.1	7.5**	4.4	
	7-801	F	2.7	6.5**	4.0	
Early post-symptomatic	7-877	F	1.6	10*	10.6	15.4 (3.7)
	11-869	F	1.6	10*	14.3	
	11-868	M	1.6	10*	17.7	
	11-831	M	1.8	10*	18.9	

[A] CRS score relates to **Figure 1a**.

* Mild tremors.

** Overt whole body tremors.

Abbreviations: CRS = clinical rating score; tx = treatment; mo = months

a

Score	Clinical Status*	Age (Months)
10	Normal	< 1.3 ± 0.2
9	Hind limb muscle weakness	2.1 ± 0.0
8	Wide stance	2.2 ± 0.4
7	Ataxia	2.5 ± 0.3
6	Instability with occasional falling	2.9 ± 0.5
5	Limited walking	3.5 ± 0.5
4	Standing but not walking	3.9 ± 0.5
3	Cannot stand on 2 consecutive days	4.4 ± 0.6
2	Lateral recumbency	> 4.4
1	Uncontrollable neurological symptoms	> 4.4

*Onset of mild tremors begins at 1.3 ± 0.2 months old; Onset of overt whole body tremors begins at 2.4 ± 0.1 months old.

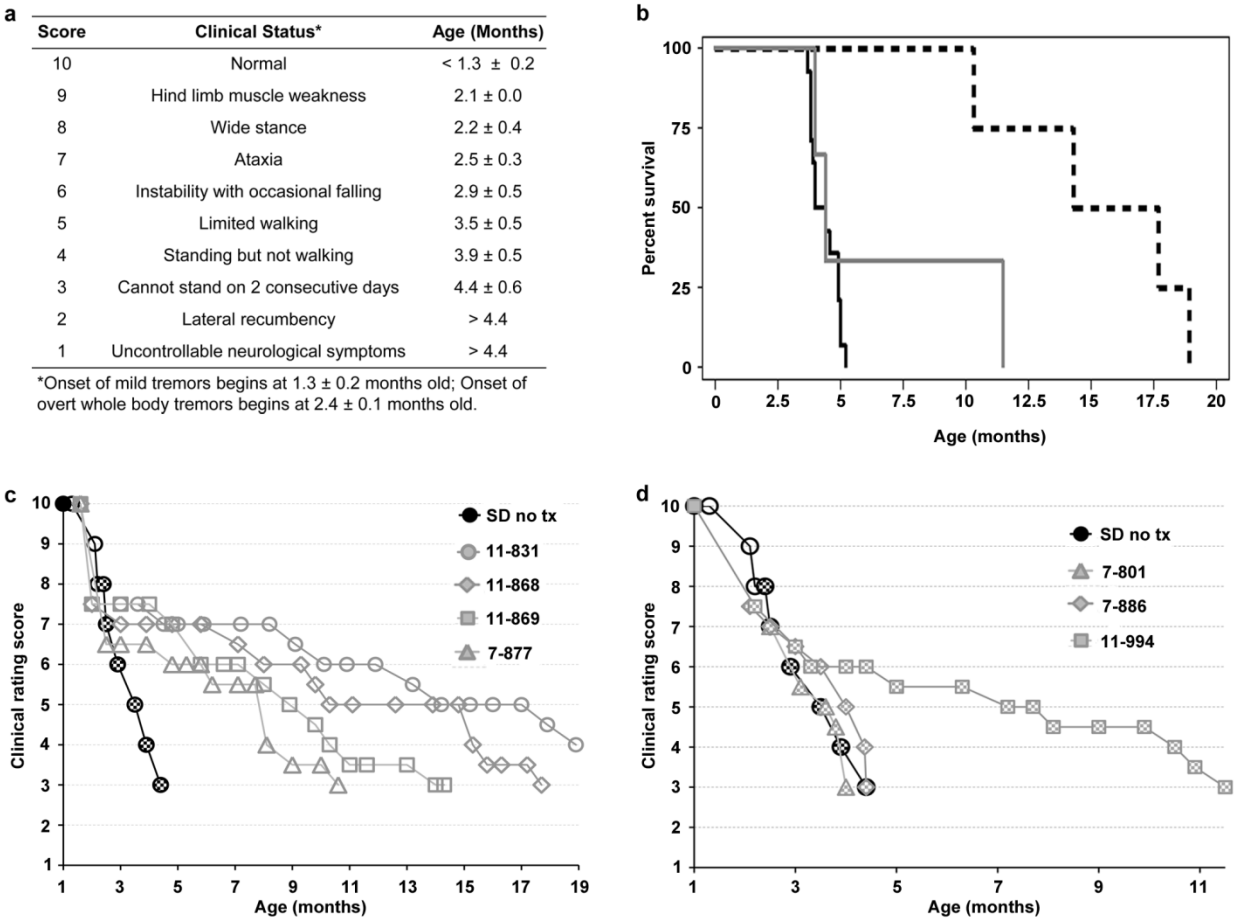

Figure 1. Survival and clinical progression of post-symptomatic AAV-treated Sandhoff disease (SD) cats and untreated SD cats. (**a**) Age of symptom onset is shown for untreated SD cats (mean ± s.d, n = 14). The scale is based on gait defects, which ultimately define humane endpoint, with initial deficits at 2.1 months old. However, disease onset begins at 1.3 months with subtle tremors of the head/tail that progress to overt whole-body tremors at 2.4 months. Neurologic humane endpoint is reached at a score of 3. (**b**) Kaplan-Meier survival curves for untreated SD cats (solid black line, n = 14) and SD cats treated post-symptomatically. Survival of the EPS cohort was significantly increased versus untreated SD cats (P = 0.0010, dashed black line, n = 4) and versus the LPS cohort (P = 0.048). Survival of the LPS cohort is not significantly increased versus untreated SD cats (P < 0.28, solid grey line, n = 3). (**c, d**) Composite clinical

scores are shown for untreated SD cats (n = 14), whereas EPS (**c**) and LPS (**d**) treated cats are depicted separately. Closed symbols denote the absence of tremors; open symbols denote the presence of subtle tremors, and checkered symbols denote the presence of overt whole body tremors, which were absent in all EPS treated cats but present in all LPS treated cats.

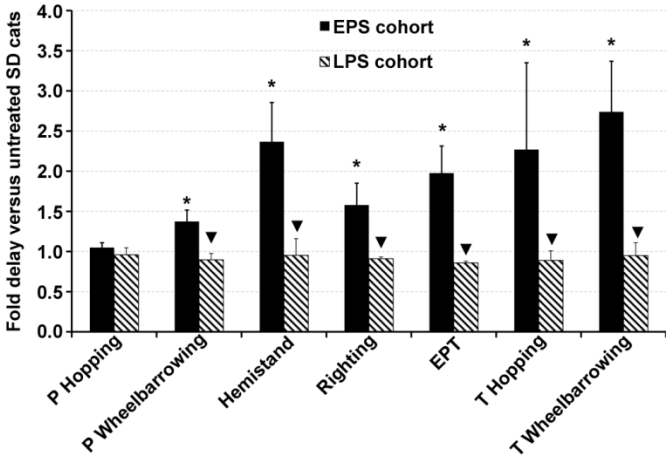

Figure 2. Neurological exam performance of post-symptomatic AAV-treated Sandhoff disease (SD) cats versus untreated SD cats. Cats were given a neurological examination twice monthly and deficits were recorded. * Onset of deficit was significantly delayed compared to untreated SD cats ($P \leq 0.011$); ▼, onset of deficit was significantly earlier compared to the EPS cohort ($P \leq 0.026$). Abbreviations: P = pelvic limb; T = thoracic limb, LPS = late post-symptomatic; EPS = early post-symptomatic.

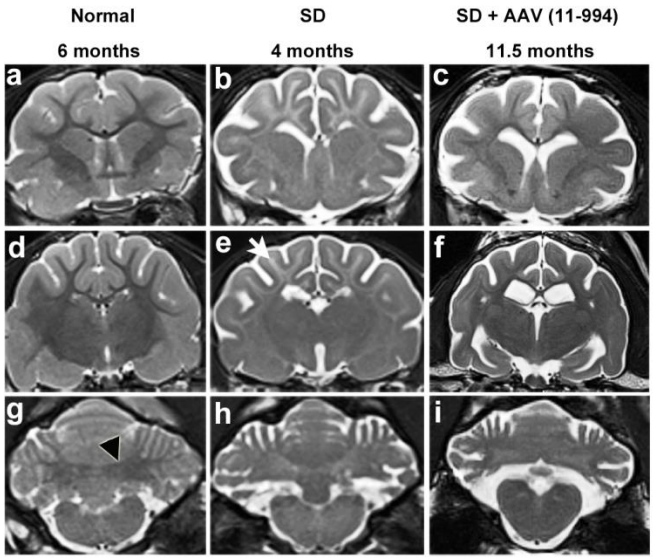

Figure 3. MRI evaluation of a late post-symptomatic AAV-treated Sandhoff disease (SD) cat and untreated controls. T2-weighted MR images (3T) were taken at the level of the caudate nucleus (**a-c**), thalamus (**d-f**) and DCN (**g-i**). Cortical white matter is hypointense to (darker than) gray matter in normal cats but hyperintense to (lighter than) gray matter in untreated SD cats [white arrow in (e)]. Also, the DCN area is hypointense to surrounding gray matter in normal cats [outlined black arrowhead in (g)], but becomes hyperintense with disease progression in untreated SD cats. In LPS AAV-treated cat 11-994 at humane endpoint, hypointensity of cortical white to gray matter is improved compared to untreated, but is not normal. However, the DCN area has turned hyperintense to gray matter, similar to the intensity in untreated SD cats. At the time of imaging cat 11-994 was on a clinical rating score of 3 (**Figure 1a**). There were no appreciable differences between a normal cat brain at 6 months old and at older ages. Brain atrophy (enlarged sulci and ventricles) in cat 11-994 at 11.5 months old was comparable to the untreated SD cat at 4 months old. MRI images were acquired by Heather L. Gray-Edwards.

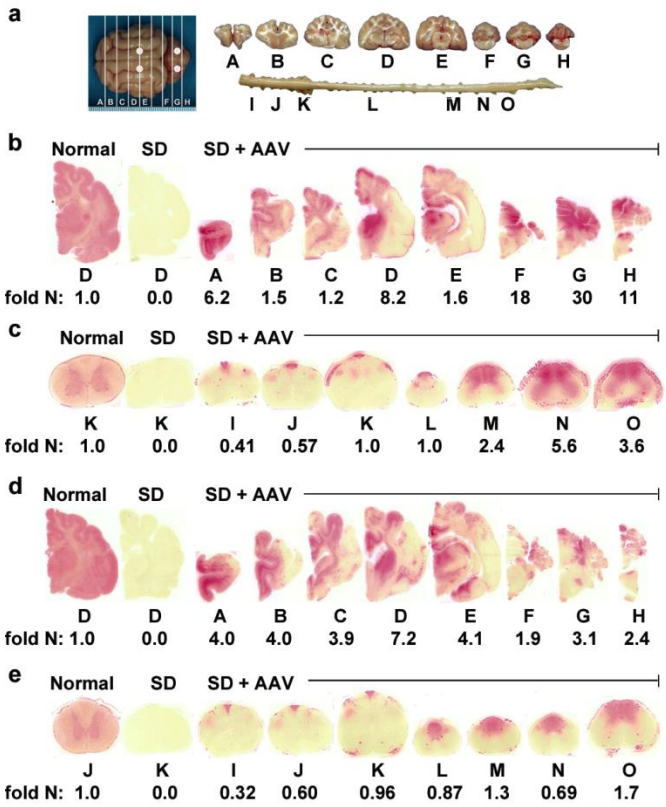

Figure 4. Therapeutic enzyme distribution in the CNS of post-symptomatic AAV-treated Sandhoff disease (SD) cats. Tissues from post-symptomatic AAV-treated SD cats were collected at humane endpoint. (**a**) Injection sites (white circles) and 0.6 cm coronal blocks of the brain (A-H) and spinal cord (I-O) collected at necropsy. Blocks were halved and the right half was assayed for enzyme activity. Lysosomal Hex activity (red) detected with naphthol at acidic pH was visualized throughout the brain (**b**) and spinal cord (**c**) of early post-symptomatic AAV-treated SD cat 11-831 (SD + AAV) at 18.9 months old. Lysosomal Hex activity was visualized throughout the brain (**d**) and spinal cord (**e**) of late post-symptomatic AAV-treated SD cat 11-994 (SD + AAV) at 11.5 months old. Corresponding HexA activity against MUGS substrate is shown below each block as fold normal level (fold N). Representative control sections are shown from untreated normal cats along with untreated SD cats, which express ≤0.02-fold normal HexA activity in the brain and spinal cord. The ranges of specific activities for normal control

blocks were: early post-symptomatic (brain, 29 (F) – 60 (D); spinal cord, 6.3 (L) – 16 (K and O) nmol 4MU/mg/hr); late post-symptomatic (brain, 30 (F) – 53 (D); spinal cord, 7.9 (L) – 17 (K).

Table 2. Hex activity in the nervous system, CSF, liver, muscle, and heart of AAV-treated and untreated Sandhoff disease (SD) cats

		Fold normal Hex activity[A] (mean, s.d.)		
		Treatment group		
Region	Block	EPS[B]	LPS[C]	SD no tx[D]
CNS and PNS				
Cerebrum	A	**2.8** (2.5)	**1.7** (2.0)	**0.00** (0.0)
	B	**1.1** (0.48)	**1.6** (2.1)	**0.00** (0.0)
	C	**2.0** (2.2)	**1.5** (2.1)	**0.00** (0.0)
	D	**6.5** (4.0)*	**2.9** (3.7)	**0.00** (0.0)
	E	**2.8** (2.4)*	**9.9** (5.4)*	**0.00** (0.0)
Cerebellum	F	**9.0** (8.4)*	**1.4** (1.1)	**0.00** (0.0)
	G	**22** (15)	**1.4** (1.4)	**0.00** (0.01)
	H	**12** (9.4)*	**3.6** (3.8)	**0.00** (0.0)
Spinal cord	I	**0.83** (0.38)	**0.34** (0.12)*	**0.00** (0.0)
	J	**0.92** (0.28)	**0.54** (0.10)*	**0.00** (0.0)
	K	**1.2** (0.33)	**0.68** (0.27)	**0.00** (0.01)
	L	**1.8** (0.55)	**0.89** (0.25)	**0.02** (0.03)
	M	**2.6** (0.73)*	**1.4** (0.31)▼	**0.02** (0.04)
	N	**4.7** (2.5)*	**1.8** (1.0)*	**0.01** (0.02)
	O	**3.9** (0.36)*	**2.8** (0.99)*▼	**0.01** (0.01)
CSF	-	**2.3** (1.3)	**2.7** (2.0)	**0.03** (0.04)
Cervical DRG	-	**8.2** (9.0)	**1.9** (1.3)	**0.02** (0.01)
Lumbar DRG	-	**33** (24)	**43**[E]	**0.02** (0.01)
Sciatic nerve	-	**2.2** (1.3)	**0.76** (0.40)	**0.02** (0.01)
Periphery	-			
Liver	-	**0.45** (0.56)	**0.13** (0.02)	**0.02** (0.00)
Muscle	-	**0.09** (0.12)	**0.02** (0.02)	**0.02** (0.00)
Heart	-	**0.05** (0.04)	**0.04** (0.00)	**0.00** (0.00)

[A] Hex activity against α-subunit preferred substrate (MUGS) is shown with the exception of CSF for which Hex activity against the β-subunit specific substrate (MUG) is shown due to limited sample volume for analysis.

[B] n = 4, Hex activity was significantly higher than in untreated SD cats (n = 5) in **A-H** ($P \leq 0.017$ for each block), **I-O** ($P \leq 0.018$ for each block), **CSF** ($P = 0.01$); **C DRG** ($P = 0.0097$), **L DRG** ($P = 0.01$), **sciatic nerve** ($P = 0.0097$), **liver** ($P = 0.033$), and **heart** ($P = 0.0090$).

[C] n = 3, Hex activity was significantly higher than in untreated SD cats (n = 5) in **A-H** ($P \leq 0.026$ for each block), **I-O** ($P \leq 0.033$ for each block), **CSF** ($P = 0.041$, n = 2, no sample available for cat 11-994), **C DRG** ($P = 0.093$), **sciatic nerve** ($P = 0.018$), and **heart** ($P = 0.016$).

[D] Hex activity was significantly lower in untreated SD cats (n = 5) than in normal cats (n = 5) in **A-O** ($P \leq 0.0097$ for each block), **C DRG** ($P = 0.0060$), **L DRG** ($P = 0.0061$), **sciatic nerve** ($P = 0.0060$), **liver** ($P = 0.0061$), **muscle** ($P = 0.0060$), and **heart** ($P = 0.0056$).

[E] Only one cat available for analysis (11-994).

*Hex activity was significantly higher/lower than in normal cats (n = 5) ($P \leq 0.037$); ▼, Hex activity was significantly lower than in the EPS cohort ($P = 0.026$).

Abbreviations: no tx = no treatment; DRG = dorsal root ganglia; CSF = cerebrospinal fluid; CNS = central nervous system; PNS = peripheral nervous system; EPS = early posy-symptomatic; LPS = late post-symptomatic

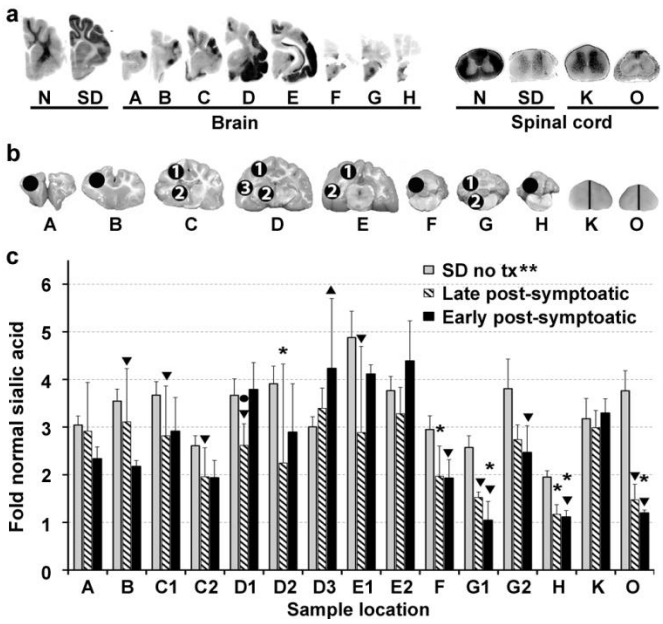

Figure 5. Storage in the CNS of post-symptomatic AAV-treated Sandhoff disease (SD) cats and untreated SD cats. (**a**) Shown is cat 11-831. Storage in untreated SD cats is visualized by dark PAS staining in gray matter. In treated brains, ganglioside storage was present in Hex deficient areas (see corresponding naphthol staining for 11-831 in **Figure 4b, c**), such as the temporal lobe (blocks d and e) and cervical spinal cord (block k). (**b**) Sample sites for sialic acid quantitation (circles) in brain (A-H) and spinal cord (K and O correspond to **Figure 4a**; half of each block was used). (**c**) Sialic acid concentration was measured in untreated SD cats (n = 4) and in the EPS (n = 4) and LPS (n = 3) treated cohorts for comparison to normal cats (n = 4 for each cohort). **, Concentration in all samples from untreated SD cats was significantly higher than in normal cats (P = 0.015 for each block); *, samples from treated cats that did not have a significantly higher concentration than in normal cats (samples without this symbol had a significantly higher concentration than in normal cats, $P \leq 0.030$ for each block); ▼, samples from treated cats that had a significantly lower concentration than in untreated SD cats ($P \leq 0.030$); ▲, a sample from treated cats that had a significantly higher concentration than in untreated SD cats (P = 0.015); ●, a sample that had a significantly lower concentration in the

LPS cohort versus the EPS cohort (P = 0.037). Abbreviations: EPS = early post-symptomatic; LPS = late post-symptomatic; tx = treatment.

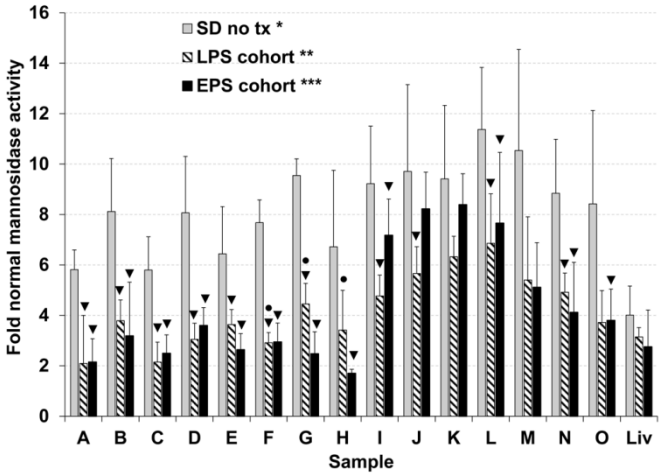

Figure 6. Lysosomal α-mannosidase activity in the CNS and liver of Sandhoff disease (SD) cats treated after disease onset. Cats from the EPS (n = 4, black bars) and LPS (n = 3, striped bars) cohorts were euthanized at humane endpoint and lysosomal α-mannosidase activity was compared to untreated SD cats (n = 5, gray bars) and normal cats (n = 5) in the brain (A-H), spinal cord (I-O), and liver (Liv). CNS sample lettering corresponds to **Figure 4a**. *, Activity in all samples from untreated SD cats was significantly higher than in normal cats (**A-H**, **I-O**, and **liver,** $P = 0.0061$ for each block); **, activity in samples **B-F**, **H**, **I-O,** and **liver** from the LPS cohort was significantly higher than in normal cats ($P \leq 0.037$ for each block); ***, activity in all CNS samples from the EPS cohort was significantly higher than in normal cats ($P \leq 0.019$ for each block), but liver activity was not significantly higher than in normal cats; ▼, samples from AAV-treated SD cats that had significantly lower activity than in untreated SD cats ($P \leq 0.037$); ●, samples that had significantly higher activity in the LPS cohort versus the EPS cohort ($P \leq 0.040$).

Table S1. Peripheral disease symptoms and seizure activity in post-symptomatic AAV-treated Sandhoff disease (SD) cats and untreated controls

	Incidence of symptom (number of cats (percent)) and age of symptom onset (mean, s.d.)			
	EPS cohort (n = 4)	LPS cohort (n = 3)	SD no tx (n = 14)	Normal (n = 7)
Heart abnormality[A]	3/4 (75) 11 ± 6.5	-	2/14 (14) 3.1 ± 1.5	-
GI dysfunction[B]	4/4 (100) 12 ± 5.6	-	1/14 (7.1) 1.8	-
Bladder dysfunction[C]	3/4 (75) 13 ± 2.0	-	-	-
Oral mass	1/4 (25) 6.0	-	-	-
Recurrent diarrhea	-	1/3 (33) 3.0	-	-
Respiratory infection	2/4 (50) 9.4 ± 9.8	-	1/14 (7.1) 1.8	-
Recurrent ocular/nasal discharge	1/4 (25) 2.5	-	6/14 (43) 1.3 ± 0.67	-

[A] Symptoms include heart enlargement diagnosed from radiographs or postmortem analysis; heart murmur upon auscultation; or abnormality associated with papillary muscle in the left ventricle.

[B] Refers to distended small intestines, distended abdomen, or esophageal dysmotility.

[C] Refers to distended bladder or small bladder upon palpation.

Abbreviations: LPS = late post-symptomatic; EPS = early postsymptomatic; GI = gastrointestinal; tx = treatment; dash = symptom was absent

Table S2. Vector copy number in nervous system, liver, muscle, and heart of post-symptomatic AAV-treated Sandhoff disease (SD) cats

Region	Block	Vector copy number per μg genomic DNA (mean, s,d.)	
		Post-symptomatic cohort	
		Early	Late
Cerebrum	A	**19,000** (16,000)	**20,000** (6,000)
	B	**5,300** (3,000)	**6,400** (330)
	C	**12,000** (11,000)	**6,900** (2,300)
	D	**30,000** (22,000)	**13,000** (11,000)
	E	**12,000** (5,000)	**18,000** (16,000)
Cerebellum	F	**38,000** (44,000)	**6,100** (5,800)
	G	**57,000** (73,000)	**4,100** (2,800)
	H	**32,000** (44,000)	**9,000** (6,200)
Spinal cord	I	**3,200** (2,400)	**1,700** (810)
	J	**4,500** (2,800)	**2,900** (850)
	K	**2,100** (150)	**1,900** (760)
	L	**5,000** (3,200)	**2,400** (5,600)
	M	**5,000** (900)	**1,900** (1,400)▼
	N	**5,800** (2,300)	**2,000** (680)▼
	O	**4,400** (1,100)	**1,600** (1,100)▼
Sciatic nerve	-	**0** (0)	**2,200** (3,400)
Liver	-	**20,000** (20,000)	**37,000** (26,000)
Muscle	-	**0** (0)	**2,200** (3,900)
Heart	-	**1,800** (2,800)	**180** (260)

▼, significantly lower than in the early post-symptomatic cohort, $P = 0.026$.

Block lettering corresponds to **Figure 4a.**

Abbreviations: CNS = central nervous system

Discussion

Lysosomal storage diseases (LSDs) comprise a group of over 50 disorders and have a collective frequency of 1 in 7700 live births[1]. Approximately 60% of LSDs are neuronopathic making them collectively a common cause of childhood neurodegeneration. Enzyme replacement therapy (ERT) and bone marrow transplantation (BMT) can effectively ablate many peripheral symptoms of non-neuronopathic LSDs. However, there is no effective treatment for the majority of neuronopathic LSDs. The gangliosidoses are progressively neurodegenerative and fatal. Several treatment approaches, including ERT, BMT, substrate reduction therapy (SRT) and combinations of the three, have demonstrated some degree of clinical benefit in gangliosidosis mouse models, but have proven ineffective at altering the course of the feline and human gangliosidoses (as discussed in the introduction). However, the disease stage at treatment must be considered when determining therapeutic efficacy in humans as studies in gangliosidosis cats (chapter 4) demonstrated that treatment benefit decreases with increasing age at treatment onset. Treatment benefit is often reported in animals treated pre-symptomatically as advanced knowledge of disease phenotype is possible by genotyping. Therapies are often tested in humans who are already in the symptomatic disease stage, when irreversible pathological changes may be refractory to therapy. However, BMT administered to two pre-symptomatic gangliosidosis patients failed to alter the disease course[96]

Gene therapy has proven to be unquestionably the most successful experimental treatment to date for gangliosidosis mice[135, 140, 142, 161]. Intracranial injections of adeno-associated

virus (AAV) vectors provided near global central nervous system (CNS) enzyme restoration resulting in substantial clearance of pathological storage material and normalization of neurodegeneration. While studies in AAV-treated GM1 gangliosidosis mice were not designed to determine long term survival beyond 1 year, near-normalization of lifespan was demonstrated in AAV-treated Sandhoff disease (SD) mice, which represents a >5-fold survival increase over untreated SD mice. The greatest clinical improvement that had previously been reported in SD mice was an ~2-fold survival increase over untreated following BMT[92] or neural stem cell transplantation combined with substrate reduction therapy[109]. Studies in mice are invaluable for the initial testing of therapeutic approaches, but treatments must be tested in large animal models with closer disease and size similarity to human patients.

This dissertation project described pre-clinical AAV gene therapy studies in feline gangliosidosis models. Prior to the initiation of these studies, the only reported treatment attempts in gangliosidosis cats were ERT in 1982 and BMT in 1994, neither of which altered the clinical disease course, although pathologic storage material was decreased in several peripheral tissues following ERT[86]. An unsuccessful attempt at BMT was also reported in a GM1 gangliosidosis Portuguese Water dog treated pre-symptomatically[93]. In the current project, intracranial injections of AAV vectors into only four brain locations of affected animals resulted in improved clinical outcome and significant increases in life span versus untreated animals. Survival of SD cats was increased up to 8.1-fold that of untreated, and survival of GM1 gangliosidosis cats is currently increased up to 6.6-fold that of untreated. However, a majority of GM1 gangliosidosis cats remain alive, so mean survival continues to increase. These studies are the first to demonstrate long term therapeutic benefit from AAV gene therapy in a large animal

LSD model, and represent a major advancement toward the development of an effective therapy for gangliosidosis patients as well as for other neuronopathic LSDs.

AAV vector delivery in both gangliosidosis models resulted in widespread nervous system distribution of therapeutic enzyme and vector. Similar distribution in two different disease models is encouraging for translation of approaches to other LSDs resulting from deficiencies of other proteins. Direct translation of a treatment approach from murine to feline gangliosidosis models is predictive of success in humans without the need to add many more additional injections. Although enzyme distribution was widespread, there was variation between cats in all groups. Also, activity was often not evenly distributed within blocks, resulting in some areas of supranormal activity, but other areas (such as the temporal lobe) lacking activity. It is unlikely that gene therapy will ever be able to restore enzyme activity to every enzyme deficient cell. The aim of gene therapy is therefore to maximize enzyme distribution to treat as many cells as possible and to be as reproducible as possible between patients. Additional or alternative injection sites could be tested to directly target areas that otherwise remain stubborn to enzyme correction, such as the temporal cortex. Also, procedures that reportedly increase enzyme distribution, such as provision of mannitol and sorbitol in the vehicle solution, could be tested in conjunction with the current protocol.

Results indicate that direct injection of AAV vectors into cerebrospinal fluid (CSF) (appendices 2 and 3) mediates superior enzyme delivery to the spinal cord versus deep cerebellar nuclei (DCN) injection of vectors (appendix 1). Furthermore, it is likely that CSF transport was an effective mode of enzyme dissemination following thalamus and DCN injections in cats as evidenced by high CSF enzyme activities. Anatomy of humans is different to cats and the ventricles may not be traversed in the same way during the injection procedure. Therefore, CSF

may not assist in enzyme dissemination to the same extent after thalamus and DCN injections in humans. Appendix 1 showed that DCN injection resulted in high level enzyme activity in the cerebellum, which alone provided clinical benefit, but that DCN injection was no more effective than thalamic injection at delivering enzyme to other CNS structures. As thalamus and ICV injection also resulted in substantial cerebellar enzyme correction (appendix 2), DCN injection may be dispensable for enzyme distribution to the cerebellum and spinal cord. Therefore, CSF injection routes are likely to be more effective at promoting widespread enzyme and vector distribution in human patients where ventricles may not be indirectly accessed during injection of other structures. These findings are important for informing future clinical trials as CSF injection would be preferred over DCN injections for safety reasons. Intracerebroventricular (ICV) delivery of therapeutics is commonly used in pediatric neurosurgery[141], but DCN injection would be more precarious due to the risk of hemorrhage in the posterior fossa. As much gangliosidosis disease progression is due to cerebellar involvement, it was initially thought that the cerebellum would have to be directly injected to accomplish adequate enzyme correction. However, these studies suggest otherwise.

Stabilization of CNS disease progression in treated SD cats allowed the emergence of numerous peripheral disease symptoms that were previously subclinical in untreated cats. Peripheral tissue dysfunction likely resulted from either tissue enzyme deficiency or dysfunction of the innervating nerves. Not all LSDs would suffer the same extent of peripheral problems as in Sandhoff disease. For example, Tay-Sachs disease (TSD) is characterized by enzyme deficiency that primarily affects the CNS. However, if further benefit is to be gained for LSDs with CNS and peripheral components then treatment of peripheral tissues must be addressed in conjunction with CNS treatment. Methods to restore enzyme activity in the periphery were

discussed in chapter 3 and include ERT and BMT as well as AAV gene therapy using newly characterized serotypes that reportedly mediate transduction of a range of peripheral tissues. It is highly unlikely that treatment of all peripheral tissues will ever be achieved, but methods must maximize treatment of as many tissues as possible. The emergence of peripheral problems in SD cats is testament in itself to the success of the CNS therapy described herein. Prior to pre-clinical trials it was unknown how much of a problem peripheral disease pathology would become as no gangliosidosis cats had ever lived long enough to know.

Gene therapy clinical trials for the gangliosidoses could be initiated in the near future as the two previous neuronopathic LSD clinical trials were initiated following far less impressive results in mouse models of Batten disease[224-226] and Canavan disease[227, 228]. However, prior to human trials, safety and toxicity studies must be carried out in non-human primates using the same vectors and therapeutic transgenes that will be injected into humans. This is especially important in light of the supranormal hexosaminidase levels demonstrated in treated SD cats. Although there was no evidence of any clinical sequelae from protein overexpression in gangliosidosis cats, toxicity may vary between species.

The finding that treatment was beneficial in SD cats treated in the early symptomatic disease stage (chapter 4) is a highly important finding as most gangliosidosis patients are diagnosed after symptoms become apparent. The average age of GM2 gangliosidosis patient diagnosis corresponds with the mean age of onset of elevated noise sensitivity and startle response to sounds, but before the mean age of onset of other symptoms[220]. Pre-symptomatic diagnosis is rare for infantile-onset patients as early disease onset makes parents aware of their carrier genotype before having more children. Later-onset patients are more likely to be diagnosed pre-symptomatically due to diagnosis of an older sibling. Apart from high risk

populations, screening for rare diseases such as the gangliosidoses is unlikely to become common practice, as it is not practical or cost-effective to screen every pregnancy for every rare disease. As disease progression is not reversed in gangliosidosis cats or mice it should be carefully considered whether the benefits of treatment are currently great enough to warrant intervention in aggressive infantile-onset LSD forms. The current 3.5-fold survival increase in early-onset gangliosidosis cats treated in the early post-symptomatic disease stage translates to a survival increase from about 3 to 5 years old to about 7 to 17 years old in gangliosidosis humans. However, the quality of the additional years must be considered. Knowing that gene therapy is not a cure for aggressive infantile-onset LSDs, delayed disease progression could result in an extended period of suffering, with patients experiencing relentless motor and mental regression throughout their childhood and teenage years, which would also prolong the emotional and financial drain on families. Therefore, each parent would have to carefully consider if they believe treatment to be in the best interests of the child.

The outcome of these pre-clinical gene therapy studies is particularly encouraging for the prospect of treating later-onset gangliosidosis disease forms, which have a small degree of residual enzyme activity and slower progression of clinical symptoms. Furthermore, disease pathology in late-onset disease forms is reported to affect specific structures more than others, which is in contrast to the infantile-onset disease form that affects the central nervous system diffusely[24]. Therefore, enzyme restoration in specific, highly affected structures may be enough to improve clinical outcome. Feline GM1 gangliosidosis is a replica of the human juvenile-onset disease. As described in chapter 1, current mean survival of GM1 gangliosidosis cats treated pre-symptomatically is >4.7 times that of untreated cats and continues to increase as the majority of the study group is still alive. Translation of outcome to human juvenile-onset patients represents

a survival increase from about 10 to 15 years old to about 47 to 70.5 years old. The endpoint of cats in the present protocol is earlier than the relative endpoint of human patients as cats are euthanized at a "humane" stage of disease progression. Therefore the actual survival increases of human juvenile-onset patients may be higher than those calculated by extrapolation from GM1 gangliosidosis cats. It is difficult to determine mental function in cats. However, MRI analysis showed that brain architecture is largely preserved up to 4 times longer than in untreated cats, so it is likely that mental as well as physical function would be well preserved in late-onset gangliosidosis patients. However, it must be noted that GM1 gangliosidosis cats treated pre-symptomatically are not representative of most later-onset patients who are diagnosed after symptom onset. In fact, two GM1 gangliosidosis cats treated in the early post-symptomatic disease stage had a mean survival of ~20 months old. Therefore, treatment benefit would likely not be as great as estimated above for post-symptomatic juvenile-onset patients. Nevertheless, these findings provide the first real indication that there may become effective treatments for later-onset gangliosidosis patients that could substantially restore neurological function well into adulthood. Results are also of relevance to other LSDs that have later-onset or slower progressing disease forms.

Although lysosomal enzyme deficiency also affects peripheral tissues, GM1 gangliosidosis cats did not develop clinical peripheral pathology throughout the duration of the current project. Symptoms such as hepatosplenomegaly and dysmorphism are less commonly reported in later-onset compared to early-onset GM1 gangliosidosis patients, but they do occur in some cases. Therefore, peripheral symptoms may remain subclinical following treatment of many later-onset gangliosidosis patients, but could become problematic in others. Protocols to

treat peripheral organs, such as those discussed in chapter 3, should also be developed for the eventuality of peripheral problems in GM1 gangliosidosis patients.

In summary, this dissertation research represents a significant advancement in the treatment of the feline gangliosidoses and supports the continued development and refinement of gene therapy approaches for application to human lysosomal storage diseases. Studies in large animal replicas of human disease are invaluable for informing the design and expectations of human clinical trials.

References

1. Meikle, PJ, Hopwood, JJ, Clague, AE, and Carey, WF (1999). Prevalence of lysosomal storage disorders. *The Journal of the American Medical Association* 281: 249-254.

2. Poorthuis, BJ, Wevers, RA, Kleijer, WJ, Groener, JE, de Jong, JG, van Weely, S, *et al.* (1999). The frequency of lysosomal storage diseases in The Netherlands. *Human Genetics* 105: 151-156.

3. Scriver, CR, Beaudet, AL, Sly, WS, and Valle, D (2001). *The metabolic and molecular bases of inherited disease*, 8th edn. McGraw-Hill, New York. Vol. 3.

4. Tay, W (1881). Symmetrical changes in the region of the yellow spot in each eye of an infant. *Transactions of the Ophthalmological Societies of the United Kingdom* 1: 155.

5. Hirsch, W (1898). The Pathological Anatomy of "A Fatal Disease of Infancy, With Symmetrical Changes in the Region of the Yellow Spot" (Warren Tay), "Amaurotic Family Idiocy" (Sachs), "Infantile Cerebral Degeneration" (Kingdon and Russell). *The Journal of Nervous and Mental Disease* 25: 538-549.

6. Sachs, B, and Strauss, I (1910). The cell changes in amaurotic family idiocy. *The Journal of Experimental Medicine* 12: 685-695.

7. Klenk, E (1935). Über die Natur der Phosphatide und anderer Lipoide des Gehirns und der Leber bei der Niemann-Pickschen Krankheit. *Hoppe-Seyler´s Zeitschrift für Physiologische Chemie* 235: 24-36.

8. Svennerholm, L (1962). The chemical structure of normal human brain and Tay-Sachs gangliosides. *Biochemical and Biophysical Research Communications* 9: 436-441.

9. Robinson, D, and Stirling, J (1968). N-Acetyl-β-glucosaminidases in human spleen. *Biochemical Journal* 107: 321-327.

10. Srivastava, S, and Beutler, E (1973). Hexosaminidase-A and Hexosaminidase-B: Studies in Tay-Sachs' and Sandhoff's Disease. *Nature* 241: 463.

11. Conzelmann, E, and Sandhoff, K (1978). AB variant of infantile GM2 gangliosidosis: deficiency of a factor necessary for stimulation of hexosaminidase A-catalyzed degradation of ganglioside GM2 and glycolipid GA2. *Proceedings of the National Academy of Sciences* 75: 3979-3983.

12. Norman, R, Urich, H, Tingey, A, and Goodbody, R (1959). Tay-Sachs' disease with visceral involvement and its relationship to Niemann-Pick's disease. *The Journal of Pathology and Bacteriology* 78: 409-421.

13. Jatzkewitz, H, and Sandhoff, K (1963). On a biochemically special form of infantile amaturotic idiocy. *Biochimica et Biophysica Acta* 70: 354-356.

14. O'Brien, JS, Stern, MB, Landing, BH, O'Brien, JK, and Donnell, GN (1965). Generalized gangliosidosis: Another inborn error of ganglioside metabolism? *Archives of Pediatricsand Adolescent Medicine* 109: 338-346.

15. Okada, S, and O'Brien, JS (1968). Generalized gangliosidosis: beta-galactosidase deficiency. *Science* 160: 1002-1004.

16. Kolter, T, Proia, RL, and Sandhoff, K (2002). Combinatorial ganglioside biosynthesis. *Journal of Biological Chemistry* 277: 25859-25862.

17. Kolter, T, and Sandhoff, K (1999). Sphingolipids—their metabolic pathways and the pathobiochemistry of neurodegenerative diseases. *Angewandte Chemie International Edition* 38: 1532-1568.

18. Rahmann, H, Probst, W, and Mühleisen, M (1982). Gangliosides and synaptic transmission. *The Japanese Journal of Experimental Medicine* 52: 275-286.

19. Zeller, CB, and Marchase, RB (1992). Gangliosides as modulators of cell function. *American Journal of Physiology* 262: C1341-C1355.

20. d'Azzo, A, Tessitore, A, and Sano, R (2006). Gangliosides as apoptotic signals in ER stress response. *Cell Death and Differentiation* 13: 404-414.

21. Schengrund, C-L (1990). The role (s) of gangliosides in neural differentiation and repair: a perspective. *Brain Research Bullitin* 24: 131-141.

22. Ledeen, R (2004). Biology of gangliosides: neuritogenic and neuronotrophic properties. *Journal of Neuroscience Research* 12: 147-159.

23. Walkley, SU (1998). Cellular pathology of lysosomal storage disorders. *Brain Pathology* 8: 175-193.

24. Suzuki, Y, Oshima, A, and Nanba, E (2001). Beta-galactosidase Deficiency (Beta-Galactosidosis): GM1 Gangliosidosis and Morquio B Disease. In: Scriver, CR, Beaudet, AL, Sly, WS, Valle, D (eds). *The Metabolic and Molecular Bases of Inherited Disease*, 8th edition. McGraw-Hill, New York, vol. 3, chapter 151.

25. Lenicker, HM, Vassallo Agius, P, Young, EP, and Attard Montalto, SP (1997). Infantile generalized GM1 gangliosidosis: high incidence in the Maltese Islands. *Journal of Inherited Metabolic Disease* 20: 723-724.

26. Sinigerska, I, Chandler, D, Vaghjiani, V, Hassanova, I, Gooding, R, Morrone, A, *et al.* (2006). Founder mutation causing infantile GM1-gangliosidosis in the Gypsy population. *Molecular Genetics and Metabolism* 88: 93-95.

27. Severini, MHA, Silva, C, Sopelsa, A, Coelho, J, and Giugliani, R (1999). High frequency of type 1 GM1 gangliosidosis in southern Brazil. *Clinical Genetics* 56: 168-169.

28. Baiotto, C, Sperb, F, Matte, U, da Silva, CD, Sano, R, Coelho, JC, *et al.* (2011). Population analysis of the GLB1 gene in South Brazil. *Genetics and Molecular Biology* 34: 45-48.

29. Yoshida, K, Oshima, A, Shimmoto, M, Fukuhara, Y, Sakuraba, H, Yanagisawa, N, *et al.* (1991). Human beta-galactosidase gene mutations in GM1-gangliosidosis: a common mutation among Japanese adult/chronic cases. *American Journal of Human Genetics* 49: 435-442.

30. Pshezhetsky, AV, and Ashmarina, M (2001). Lysosomal multienzyme complex: biochemistry, genetics, and molecular pathophysiology. *Progress in Nucleic Acid Research and Molecular Biology* 69: 81-114.

31. Wilkening, G, Linke, T, Uhlhorn-Dierks, G, and Sandhoff, K (2000). Degradation of membrane-bound ganglioside GM1. Stimulation by bis(monoacylglycero)phosphate and the activator proteins SAP-B and GM2-AP. *The Journal of Biological Chemistry* 275: 35814-35819.

32. Boustany, R, Qian, W, and Suzuki, K (1993). Mutations in acid beta-galactosidase cause GM1-gangliosidosis in American patients. *American Journal of Human Genetics* 53: 881-888.

33. Mahuran, DJ (1995). [beta]-Hexosaminidase: Biosynthesis and Processing of the Normal Enzyme, and Identification of Mutations Causing Jewish Tay-Sachs Disease. *Clinical Biochemistry* 28: 101-106.

34. Mahuran, DJ (1999). Biochemical consequences of mutations causing the GM2 gangliosidoses. *Biochimica et Biophysica Acta* 1455: 105-138.

35. Gravel, RA, Kaback, MM, Proia, RL, Sandhoff, K, Suzuki, K, Suzuki, K (2001). The GM2 Gangliosidoses. In: Scriver, CR, Beaudet, AL, Sly, WS, Valle, D (eds). *The Metabolic and Molecular Bases of Inherited Disease,* 8th edition. McGraw-Hill. New York, vol 3, chapter 153.

36. Myerowitz, R, and Costigan, FC (1988). The major defect in Ashkenazi Jews with Tay-Sachs disease is an insertion in the gene for the alpha-chain of beta-hexosaminidase. *Journal of Biological Chemistry* 263: 18587-18589.

37. Leinekugel, P, Michel, S, Conzelmann, E, and Sandhoff, K (1992). Quantitative correlation between the residual activity of b-hexosaminidase A and arylsulfatase A and the severity of the resulting lysosomal storage disease. *Human Genetics* 88: 513-523.

38. O'Brien, JS, Okada, S., Ho, M.W., Fillerup, D.L., Veath, M.L., Adams, K. (1971). Ganglioside Storage Diseases. *Federation Proceedings* 30: 956-967.

39. Brunetti-Pierri, N, and Scaglia, F (2008). GM1 gangliosidosis: review of clinical, molecular, and therapeutic aspects. *Molecular Genetics and Metabolism* 94: 391-396.

40. Salman, M, Clarke, J, Midroni, G, and Waxman, M (2001). Peripheral and autonomic nervous system involvement in chronic GM2-gangliosidosis. *Journal of Inherited Metabolic Disease* 24: 65-71.

41. Federico, A, Palmeri, S, Malandrini, A, Fabrizi, G, Mondelli, M, and Guazzi, G (1991). The clinical aspects of adult hexosaminidase deficiencies. *Developmental Neuroscience* 13: 280-287.

42. Modigliani, R, Lemann, M, Melancon, S, Mikol, J, Potier, M, Salmeron, M, *et al.* (1994). Diarrhea and autonomic dysfunction in a patient with hexosaminidase B deficiency (Sandhoff disease). *Gastroenterology* 106: 775-781.

43. Delnooz, CC, Lefeber, DJ, Langemeijer, SM, Hoffjan, S, Dekomien, G, Zwarts, MJ, *et al.* (2010). New cases of adult-onset Sandhoff disease with a cerebellar or lower motor neuron phenotype. *Journal of Neurology, Neurosurgery, and Psychiatry* 81: 968-972.

44. Navon, R, Argov, Z, Frisch, A, Opitz, JM, and Reynolds, JF (1986). Hexosaminidase A deficiency in adults. *American Journal of Medical Genetics* 24: 179-196.

45. Parnes, S, Karpati, G, Carpenter, S, Kin, N, Wolfe, LS, and Suranyi, L (1985). Hexosaminidase-A deficiency presenting as atypical juvenile-onset spinal muscular atrophy. *Archives of Neurology* 42: 1176-1180.

46. H.J.Baker, GDR, S.U. Walkley, N.R. Cox and G.H. Baker (1979). The Gangliosidoses: Comparitive Features and Research Applications. *Veterinary Pathology* 16: 635-649.

47. Walkley, SU, Baker, HJ, and Rattazzi, MC (1990). Initiation and growth of ectopic neurites and meganeurites during postnatal cortical development in ganglioside storage disease. *Developmental Brain Research* 52: 167-178.

48. Walkley, S (1987). Further studies on ectopic dendrite growth and other geometrical distortions of neurons in feline GMl gangliosidosis. *Neuroscience* 21: 313-331.

49. Walkley, S, Wurzelmann, S, Rattazzi, M, and Baker, H (1990). Distribution of ectopic neurite growth and other geometrical distortions of CNS neurons in feline GM2 gangliosidosis. *Brain Research* 510: 63-73.

50. Purpura, DP, Pappas, GD, and Baker, HJ (1978). Fine structure of meganeurites and secondary growth processes in feline GM1-gangliosidosis. *Brain Research* 143: 1-12.

51. Walkley, SU, and Wurzelmann, S (1995). Alterations in synaptic connectivity in cerebral cortex in neuronal storage disorders. *Mental Retardation and Developmental Disabilities Research Reviews* 1: 183-192.

52. Goodman, LA, Livingston, PO, and Walkley, SU (1991). Ectopic dendrites occur only on cortical pyramidal cells containing elevated GM2 ganglioside in alpha-mannosidosis. *Proceedings of the National Academy of Sciences* 88: 11330-11334.

53. Walkley, S, Wurzelmann, S, and Siegel, D (1987). Ectopic axon hillock-associated neurite growth is maintained in metabolically reversed swainsonine-induced neuronal storage disease. *Brain Research* 410: 89-96.

54. Walkley, SU, Baker, HJ, and Rattazzi, MC (1990). Initiation and growth of ectopic neurites and meganeurites during postnatal cortical development in ganglioside storage disease. *Developmental Brain Research* 51: 167-178.

55. Walkley, S, and Pierok, A (1986). Ferric ion-ferrocyanide staining in ganglioside storage disease establishes that meganeurites are of axon hillock origin and distinct from axonal spheroids. *Brain Research* 382: 379-386.

56. Walkley, SU, Baker, HJ, Rattazzi, MC, Haskins, ME, and Wu, JY (1991). Neuroaxonal dystrophy in neuronal storage disorders: evidence for major GABAergic neuron involvement. *Journal of Neurological Sciences* 104: 1-8.

57. van der Voorn, JP, Kamphorst, W, van der Knaap, MS, and Powers, JM (2004). The leukoencephalopathy of infantile GM1 gangliosidosis: oligodendrocytic loss and axonal dysfunction. *Acta Neuropathologica* 107: 539-545.

58. Huang, JQ, Trasler, JM, Igdoura, S, Michaud, J, Hanai, N, and Gravel, RA (1997). Apoptotic cell death in mouse models of GM2 gangliosidosis and observations on human Tay-Sachs and Sandhoff diseases. *Human Molecular Genetics* 6: 1879-1885.

59. Tessitore, A, and del P, M (2004). GM1-ganglioside-mediated activation of the unfolded protein response causes neuronal death in a neurodegenerative gangliosidosis. *Molecular Cell* 15: 753-766.

60. Pelled, D, Lloyd-Evans, E, Riebeling, C, Jeyakumar, M, Platt, FM, and Futerman, AH (2003). Inhibition of calcium uptake via the sarco/endoplasmic reticulum Ca2+-ATPase

in a mouse model of Sandhoff disease and prevention by treatment with N-butyldeoxynojirimycin. *Journal of Biological Chemistry* 278: 29496-29501.

61. Wada, R, Tifft, CJ, and Proia, RL (2000). Microglial activation precedes acute neurodegeneration in Sandhoff disease and is suppressed by bone marrow transplantation. *Proceedings of the National Academy of Sciences* 97: 10954-10959.

62. Jeyakumar, M, Thomas, R, Elliot Smith, E, Smith, D, Van Der Spoel, A, d'Azzo, A, *et al.* (2003). Central nervous system inflammation is a hallmark of pathogenesis in mouse models of GM1 and GM2 gangliosidosis. *Brain* 126: 974-987.

63. Takamura, A, Higaki, K, Kajimaki, K, Otsuka, S, Ninomiya, H, Matsuda, J, *et al.* (2008). Enhanced autophagy and mitochondrial aberrations in murine GM1-gangliosidosis. *Biochemical and Biophysical Research Communications* 367: 616-622.

64. Suzuki, K, Iseki, E, Katsuse, O, Yamaguchi, A, Katsuyama, K, Aoki, I, *et al.* (2003). Neuronal accumulation of [alpha]-and [beta]-synucleins in the brain of a GM2 gangliosidosis mouse model. *Neuroreport* 14: 551-554.

65. Itoh, M, Matsuda, J, Suzuki, O, Ogura, A, Oshima, A, Tai, T, *et al.* (2001). Development of lysosomal storage in mice with targeted disruption of the [beta]-galactosidase gene: a model of human GM1-gangliosidosis. *Brain and Development* 23: 379-384.

66. Matsuda, J, Suzuki, O, Oshima, A, Ogura, A, Noguchi, Y, Yamamoto, Y, *et al.* (1997). Beta-galactosidase-deficient mouse as an animal model for GM1-gangliosidosis. *Glycoconjugate Journal* 14: 729-736.

67. Hahn, CN, del Pilar Martin, M, Schröder, M, Vanier, MT, Suzuki, K, Hara, Y, *et al.* (1997). Generalized CNS disease and massive GM1-ganglioside accumulation in mice defective in lysosomal acid -galactosidase. *Human Molecular Genetics* 6: 205-211.

68. Phaneuf, D, Wakamatsu, N, Huang, J-Q, Borowski, A, Peterson, AC, Fortunato, SR, *et al.* (1996). Dramatically different phenotypes in mouse models of human Tay-Sachs and Sandhoff diseases. *Human Molecular Genetics* 5: 1-14.

69. Griflin, B, and Baker, HJ (2002). Domestic Cats as Laboratory Animals. *Laboratory Animal Medicine*: 459-482.

70. Baker, HJ, Lindsey, JR, McKhann, GM, and Farrell, DF (1971). Neuronal GM1 gangliosidosis in a Siamese cat with β-galactosidase deficiency. *Science* 174: 838-839.

71. Blakemore, W (1972). GM1 gangliosidosis in a cat. *Journal of Comparative Pathology* 82: 179-184.

72. Baker, H, and Lindsey, J (1974). Animal model: feline GM1 gangliosidosis. *The American Journal of Pathology* 74: 649-652.

73. Martin, DR, Rigat, BA, Foureman, P, Varadarajan, G, Hwang, M, Krum, BK, *et al.* (2008). Molecular consequences of the pathogenic mutation in feline GM1 gangliosidosis. *Molecular Genetics and Metabolism* 94: 212-221.

74. Cork, L, Munnell, JF, Lorenz, MD, Murphy, JV, Baker, HJ, and Rattazzi, MC (1977). GM2 ganglioside lysosomal storage disease in cats with beta-hexosaminidase deficiency. *Science* 196: 1014-1017.

75. Neuwelt, EA, Johnson, WG, Blank, NK, Pagel, MA, Maslen-McClure, C, McClure, MJ, *et al.* (1985). Characterization of a new model of GM2-gangliosidosis (Sandhoff's disease) in Korat cats. *The Journal of Clinical Investigation* 76: 482-490.

76. Kanae, Y, Endoh, D, Yamato, O, Hayashi, D, Matsunaga, S, Ogawa, H, *et al.* (2007). Nonsense mutation of feline beta-hexosaminidase beta-subunit (HEXB) gene causing Sandhoff disease in a family of Japanese domestic cats. *Research in Veterinary Science* 82: 54-60.

77. Bradbury, AM, Morrison, NE, Hwang, M, Cox, NR, Baker, HJ, and Martin, DR (2009). Neurodegenerative lysosomal storage disease in European Burmese cats with hexosaminidase [beta]-subunit deficiency. *Molecular Genetics and Metabolism* 97: 53-59.

78. Cork, LC, Munnell, JF, and Lorenz, MD (1978). The pathology of feline GM2 gangliosidosis. *The American Journal of Pathology* 90: 723-734.

79. Martin, DR, Krum, BK, Varadarajan, G, Hathcock, TL, Smith, BF, and Baker, HJ (2004). An inversion of 25 base pairs causes feline GM2 gangliosidosis variant 0. *Experimental Neurology* 187: 30-37.

80. Neufeld, EF, and Fratantoni, JC (1970). Inborn errors of mucopolysaccharide metabolism. *Science* 169: 141-146.

81. Hickman, S, and Neufeld, EF (1972). A hypothesis for I-cell disease: defective hydrolases that do not enter lysosomes. *Biochemical and Biophysical Research Communications* 49: 992-999.

82. Dahms, N, Lobel, P, and Kornfeld, S (1989). Mannose 6-phosphate receptors and lysosomal enzyme targeting. *Journal of Biological Chemistry* 264: 12115-12118.

83. Conzelmann, E, Kytzia, H, Navon, R, and Sandhoff, K (1983). Ganglioside GM2 N-acetyl-beta-D-galactosaminidase activity in cultured fibroblasts of late-infantile and adult GM2 gangliosidosis patients and of healthy probands with low hexosaminidase level. *American Journal of Human Genetics* 35: 900-914.

84. Hopwood, KMHaJJ (2011). Emerging therapies for neurodegenerative lysosomal storage disorders - from concept to reality. *Journal of Inherited Metabolic Disease* 34: 1003-1012.

85. Tsuji, D, Akeboshi, H, Matsuoka, K, Yasuoka, H, Miyasaki, E, Kasahara, Y, *et al.* (2011). Highly phosphomannosylated enzyme replacement therapy for GM2 gangliosidosis. *Annals of Neurology* 69: 691-701.

86. Rattazzi, M, Appel, A, and Baker, H (1982). Enzyme replacement in feline GM2 gangliosidosis: catabolic effects of human beta-hexosaminidase A. *Progress in Clinical and Biological Research* 94: 213-220.

87. Krivit, W, Peters, C, and Shapiro, EG (1999). Bone marrow transplantation as effective treatment of central nervous system disease in globoid cell leukodystrophy, metachromatic leukodystrophy, adrenoleukodystrophy, mannosidosis, fucosidosis, aspartylglucosaminuria, Hurler, Maroteaux-Lamy, and Sly syndromes, and Gaucher disease type III. *Current Opinion in Neurology* 12: 167-176.

88. Peters, C, and Steward, C (2003). Hematopoietic cell transplantation for inherited metabolic diseases: an overview of outcomes and practice guidelines. *Bone Marrow Transplantation* 31: 229-239.

89. Krivit, W (2004). Allogeneic stem cell transplantation for the treatment of lysosomal and peroxisomal metabolic diseases. *Springer Seminars in Immunopathology* 26: 119-132.

90. Sano, R, Tessitore, A, Ingrassia, A, and d'Azzo, A (2005). Chemokine-induced recruitment of genetically modified bone marrow cells into the CNS of GM1-gangliosidosis mice corrects neuronal pathology. *Blood* 106: 2259-2268.

91. Jeyakumar, M, Norflus, F, Tifft, CJ, Cortina-Borja, M, Butters, TD, Proia, RL, *et al.* (2001). Enhanced survival in Sandhoff disease mice receiving a combination of substrate deprivation therapy and bone marrow transplantation. *Blood* 97: 327-329.

92. Norflus, F, Tifft, CJ, McDonald, MP, Goldstein, G, Crawley, JN, Hoffmann, A, *et al.* (1998). Bone marrow transplantation prolongs life span and ameliorates neurologic manifestations in Sandhoff disease mice. *Journal of Clinical Investigation* 101: 1881-1888.

93. O'Brien, JS, Storb, R, Raff, RF, Harding, J, Appelbaum, F, Morimoto, S, *et al.* (1990). Bone marrow transplantation in canine GM1 gangliosidosis. *Clinical Genetics* 38: 274-280.

94. Walkley, S, and Dobrenis, K (1995). Bone marrow transplantation for lysosomal diseases. *The Lancet* 345: 1382-1383.

95. P. Shaw, KH-J, J. Hobbs, A. Cooper, G. Lealman (1986). GM1 gangliosidosis: failure to halt neurological regression by bone marrow transplantation. *Bone Marrow Transplantation* 1: 339.

96. Jacobs, J, Willemsen, M, Groot-Loonen, J, Wevers, R, and Hoogerbrugge, P (2005). Allogeneic BMT followed by substrate reduction therapy in a child with subacute Tay-Sachs disease. *Bone Marrow Transplantation* 36: 925-926.

97. Dobrenis, K, Wenger, D, and Walkley, S (1994). Extracellular release of lysosomal glycosidases in cultures of cat microglia. *Molecular Biology of the Cell* 5: 113a.

98. Biffi, A, Montini, E, Lorioli, L, Cesani, M, Fumagalli, F, Plati, T, *et al.* (2013). Lentiviral hematopoietic stem cell gene therapy benefits metachromatic leukodystrophy. *Science* 341: 1233158.

99. Platt, FM, Neises, GR, Reinkensmeier, G, Townsend, MJ, Perry, VH, Proia, RL, *et al.* (1997). Prevention of lysosomal storage in Tay-Sachs mice treated with N-butyldeoxynojirimycin. *Science* 276: 428-431.

100. Jeyakumar, M, Butters, TD, Cortina-Borja, M, Hunnam, V, Proia, RL, Perry, VH, *et al.* (1999). Delayed symptom onset and increased life expectancy in Sandhoff disease mice treated with N-butyldeoxynojirimycin. *Proceedings of the National Academy of Sciences* 96: 6388-6393.

101. Kasperzyk, JL, El-Abbadi, MM, Hauser, EC, d'Azzo, A, Platt, FM, and Seyfried, TN (2004). N-butyldeoxygalactonojirimycin reduces neonatal brain ganglioside content in a mouse model of GM1 gangliosidosis. *Journal of Neurochemistry* 89: 645-653.

102. Kasperzyk, J, d'Azzo, A, Platt, F, Alroy, J, and Seyfried, T (2005). Substrate reduction reduces gangliosides in postnatal cerebrum-brainstem and cerebellum in GM1 gangliosidosis mice. *Journal of Lipid Research* 46: 744-751.

103. Bembi, B, Marchetti, F, Guerci, V, Ciana, G, Addobbati, R, Grasso, D, *et al.* (2006). Substrate reduction therapy in the infantile form of Tay-Sachs disease. *Neurology* 66: 278-280.

104. Shapiro, BE, Pastores, GM, Gianutsos, J, Luzy, C, and Kolodny, EH (2009). Miglustat in late-onset Tay-Sachs disease: a 12-month, randomized, controlled clinical study with 24 months of extended treatment. *Genetics in Medicine* 11: 425-433.

105. Maegawa, GH, Banwell, BL, Blaser, S, Sorge, G, Toplak, M, Ackerley, C, *et al.* (2009). Substrate reduction therapy in juvenile GM2 gangliosidosis. *Molecular Genetics and Metabolism* 98: 215-224.

106. Tallaksen, C, and Berg, J (2009). Miglustat therapy in juvenile Sandhoff disease. *Journal of Inherited Metabolic Disease* 32: 289-293.

107. Wortmann, S, Lefeber, D, Dekomien, G, Willemsen, M, Wevers, R, and Morava, E (2009). Substrate deprivation therapy in juvenile Sandhoff disease. *Journal of Inherited Metabolic Disease* 32: 307-311.

108. Arthur, J, Lee, J, Snyder, E, and Seyfried, T (2012). Therapeutic Effects of Stem Cells and Substrate Reduction in Juvenile Sandhoff Mice. *Neurochemical Research* 37: 1335-1343.

109. Lee, JP, Jeyakumar, M, Gonzalez, R, Takahashi, H, Lee, PJ, Baek, RC, *et al.* (2007). Stem cells act through multiple mechanisms to benefit mice with neurodegenerative metabolic disease. *Nature Medicine* 13: 439-447.

110. Matsuda, J, Suzuki, O, Oshima, A, Yamamoto, Y, Noguchi, A, Takimoto, K, *et al.* (2003). Chemical chaperone therapy for brain pathology in GM1-gangliosidosis. *Proceedings of the National Academy of Sciences* 100: 15912-15917.

111. Suzuki, Y, Ichinomiya, S, Kurosawa, M, Ohkubo, M, Watanabe, H, Iwasaki, H, *et al.* (2007). Chemical chaperone therapy: clinical effect in murine GM1-gangliosidosis. *Annals of Neurology* 62: 671-675.

112. Suzuki, Y, Ichinomiya, S, Kurosawa, M, Matsuda, J, Ogawa, S, Iida, M, *et al.* (2012). Therapeutic chaperone effect of N-Octyl 4-Epi-β-valienamine on murine GM1-gangliosidosis. *Molecular Genetics and Metabolsm* 106: 92-98.

113. Rigat, BA, Tropak, MB, Buttner, J, Crushell, E, Benedict, D, Callahan, JW, *et al.* (2012). Evaluation of N-nonyl-deoxygalactonojirimycin as a pharmacological chaperone for human GM1 gangliosidosis leads to identification of a feline model suitable for testing enzyme enhancement therapy. *Molecular Genetics and Metabolism* 107: 203-212.

114. Maegawa, GH, Tropak, M, Buttner, J, Stockley, T, Kok, F, Clarke, JT, *et al.* (2007). Pyrimethamine as a potential pharmacological chaperone for late-onset forms of GM2 gangliosidosis. *Journal of Biological Chemistry* 282: 9150-9161.

115. Clarke, JTR, Mahuran, DJ, Sathe, S, Kolodny, EH, Rigat, BA, Raiman, JA, *et al.* (2011). An open-label Phase I/II clinical trial of pyrimethamine for the treatment of patients affected with chronic GM2 gangliosidosis (Tay–Sachs or Sandhoff variants). *Molecular Genetics and Metabolism* 102: 6-12.

116. Osher, E, Fattal-Valevski, A, Sagie, L, Urshanski, N, Amir-Levi, Y, Katzburg, S, *et al.* (2011). Pyrimethamine increases β-hexosaminidase A activity in patients with Late Onset Tay Sachs. *Molecular Genetics and Metabolism* 102: 356-363.

117. Vig, K, Herzog, R, Martin, D, Moore, E, Dennis, VA, Pillai, S, *et al.* (2006). Recombinant adeno-associated virus as vaccine delivery vehicles. *Gene Therapy and Molecular Biology* 12: 277-292.

118. Lowenstein, PR, Mandel, RJ, Xiong, W, Kroeger, K, and Castro, MG (2007). Immune responses to adenovirus and adeno-associated vectors used for gene therapy of brain diseases: the role of immunological synapses in understanding the cell biology of neuroimmune interactions. *Current Gene Therapy* 7: 347-360.

119. Ding, W, Zhang, L, Yan, Z, and Engelhardt, J (2005). Intracellular trafficking of adeno-associated viral vectors. *Gene Therapy* 12: 873-880.

120. Kotin, RM, Siniscalco, M, Samulski, RJ, Zhu, X, Hunter, L, Laughlin, CA, *et al.* (1990). Site-specific integration by adeno-associated virus. *Proceedings of the National Academy of Sciences* 87: 2211-2215.

121. Schnepp, BC, Clark, KR, Klemanski, DL, Pacak, CA, and Johnson, PR (2003). Genetic fate of recombinant adeno-associated virus vector genomes in muscle. *Journal of Virology* 77: 3495-3504.

122. Nakai, H, Montini, E, Fuess, S, Storm, TA, Grompe, M, and Kay, MA (2003). AAV serotype 2 vectors preferentially integrate into active genes in mice. *Nature Genetics* 34: 297-302.

123. Nakai, H, Yant, SR, Storm, TA, Fuess, S, Meuse, L, and Kay, MA (2001). Extrachromosomal recombinant adeno-associated virus vector genomes are primarily responsible for stable liver transduction in vivo. *Journal of Virology* 75: 6969-6976.

124. Atchison, RW, Casto, BC, and Hammon, WM (1965). Adenovirus-associated defective virus particles. *Science* 149: 754-755.

125. Samulski, RJ, Berns, KI, Tan, M, and Muzyczka, N (1982). Cloning of adeno-associated virus into pBR322: rescue of intact virus from the recombinant plasmid in human cells. *Proceedings of the National Academy of Sciences* 79: 2077-2081.

126. Asokan, A, Schaffer, DV, and Samulski, RJ (2012). The AAV vector toolkit: poised at the clinical crossroads. *Molecular Therapy* 20: 699-708.

127. Gao, G, Vandenberghe, LH, Alvira, MR, Lu, Y, Calcedo, R, Zhou, X, *et al.* (2004). Clades of adeno-associated viruses are widely disseminated in human tissues. *Journal of Virology* 78: 6381-6388.

128. Gao, G, Vandenberghe, LH, and Wilson, JM (2005). New recombinant serotypes of AAV vectors. *Current Gene Therapy* 5: 285-297.

129. Taylor, RM, and Wolfe, JH (1997). Decreased lysosomal storage in the adult MPS VII mouse brain in the vicinity of grafts of retroviral vector-corrected fibroblasts secreting high levels of beta-glucuronidase. *Nature Medicine* 3: 771-774.

130. Passini, MA, Lee, EB, Heuer, GG, and Wolfe, JH (2002). Distribution of a lysosomal enzyme in the adult brain by axonal transport and by cells of the rostral migratory stream. *Journal of Neuroscience* 22: 6437-6446.

131. Cearley, CN, and Wolfe, JH (2007). A single injection of an adeno-associated virus vector into nuclei with divergent connections results in widespread vector distribution in the brain and global correction of a neurogenetic disease. *Journal of Neuroscience* 27: 9928-9940.

132. Broekman, M, Tierney, L, Benn, C, Chawla, P, Cha, J, and Sena-Esteves, M (2008). Mechanisms of distribution of mouse β-galactosidase in the adult GM1-gangliosidosis brain. *Gene Therapy* 16: 303-308.

133. Lin, DS, Hsiao, CD, Liau, I, Lin, SP, Chiang, MF, Chuang, CK, *et al.* (2011). CNS-targeted AAV5 gene transfer results in global dispersal of vector and prevention of morphological and function deterioration in CNS of globoid cell leukodystrophy mouse model. *Molecular Genetics and Metabolism* 103: 367-377.

134. Elliger, S, Elliger, C, Aguilar, C, Raju, N, and Watson, G (1999). Elimination of lysosomal storage in brains of MPS VII mice treated by intrathecal administration of an adeno-associated virus vector. *Gene Therapy* 6: 1175-1178.

135. Baek, RC, Broekman, MLD, Leroy, SG, Tierney, LA, Sandberg, MA, d'Azzo, A, *et al.* (2010). AAV-mediated gene delivery in adult GM1-gangliosidosis mice corrects lysosomal storage in CNS and improves survival. *PloS one* 5: e13468.

136. Haurigot, V, Marco, S, Ribera, A, Garcia, M, Ruzo, A, Villacampa, P, *et al.* (2013). Whole body correction of mucopolysaccharidosis IIIA by intracerebrospinal fluid gene therapy. *The Journal of Clinical Investigation* 123: 3254-3271.

137. Sondhi, D, Hackett, NR, Peterson, DA, Stratton, J, Baad, M, Travis, KM, *et al.* (2006). Enhanced survival of the LINCL mouse following CLN2 gene transfer using the rh. 10 rhesus macaque-derived adeno-associated virus vector. *Molecular Therapy* 15: 481-491.

138. Dodge, JC, Haidet, AM, Yang, W, Passini, MA, Hester, M, Clarke, J, *et al.* (2008). Delivery of AAV-IGF-1 to the CNS extends survival in ALS mice through modification of aberrant glial cell activity. *Molecular Therapy* 16: 1056-1064.

139. Dodge, JC, Clarke, J, Song, A, Bu, J, Yang, W, Taksir, TV, *et al.* (2005). Gene transfer of human acid sphingomyelinase corrects neuropathology and motor deficits in a mouse model of Niemann-Pick type A disease. *Proceedings of the National Academy of Sciences* 102: 17822-17827.

140. Cachón-González, MB, Wang, SZ, McNair, R, Bradley, J, Lunn, D, Ziegler, R, *et al.* (2012). Gene Transfer Corrects Acute GM2 Gangliosidosis—Potential Therapeutic Contribution of Perivascular Enzyme Flow. *Molecular Therapy* 20: 1489-1500.

141. Virginia Haurigot, SM, Albert Ribera, Miguel Garcia, Albert Ruzo,, Pilar Villacampa, EA, Sònia Añor, Anna Andaluz, Mercedes Pineda,, Gemma García-Fructuoso, MM, Luca Maggioni, Sergio Muñoz, Sandra Motas,, and Jesús Ruberte, FM, Martí Pumarola, and Fatima Bosch (2013). Whole body correction of mucopolysaccharidosis IIIA by intracerebrospinal fluid gene therapy. *Journal of Clinical Investigation* 123: 3254-3271.

142. Cachón-González, MB, Wang, SZ, Lynch, A, Ziegler, R, Cheng, SH, and Cox, TM (2006). Effective gene therapy in an authentic model of Tay-Sachs-related diseases. *Proceedings of the National Academy of Sciences* 103: 10373-10378.

143. Cressant, A, Desmaris, N, Verot, L, Bréjot, T, Froissart, R, Vanier, MT, *et al.* (2004). Improved behavior and neuropathology in the mouse model of Sanfilippo type IIIB disease after adeno-associated virus-mediated gene transfer in the striatum. *The Journal of Neuroscience* 24: 10229-10239.

144. Desmaris, N, Verot, L, Puech, JP, Caillaud, C, Vanier, MT, and Heard, JM (2004). Prevention of neuropathology in the mouse model of Hurler syndrome. *Annals of Neurology* 56: 68-76.

145. Watson, G, Bastacky, J, Belichenko, P, Buddhikot, M, Jungles, S, Vellard, M, *et al.* (2006). Intrathecal administration of AAV vectors for the treatment of lysosomal storage in the brains of MPS I mice. *Gene Therapy* 13: 917-925.

146. Gray, SJ, Kalburgi, SN, McCown, TJ, and Samulski, RJ (2013). Global CNS gene delivery and evasion of anti-AAV-neutralizing antibodies by intrathecal AAV administration in non-human primates. *Gene Therapy* 20: 450-459.

147. Samaranch, L, Salegio, EA, San Sebastian, W, Kells, AP, Foust, KD, Bringas, JR, *et al.* (2012). Adeno-associated virus serotype 9 transduction in the central nervous system of nonhuman primates. *Hum Gene Therapy* 23: 382-389.

148. Vite, CH, Passini, MA, Haskins, ME, and Wolfe, JH (2003). Adeno-associated virus vector-mediated transduction in the cat brain. *Gene Therapy* 10: 1874-1881.

149. Broekman, M, Comer, L, Hyman, B, and Sena-Esteves, M (2006). Adeno-associated virus vectors serotyped with AAV8 capsid are more efficient than AAV-1 or-2 serotypes for widespread gene delivery to the neonatal mouse brain. *Neuroscience* 138: 501-510.

150. Cearley, CN, and Wolfe, JH (2006). Transduction characteristics of adeno-associated virus vectors expressing cap serotypes 7, 8, 9, and Rh10 in the mouse brain. *Molecular Therapy* 13: 528-537.

151. Salegio, E, Samaranch, L, Kells, A, Mittermeyer, G, San Sebastian, W, Zhou, S, *et al.* (2012). Axonal transport of adeno-associated viral vectors is serotype-dependent. *Gene Therapy* 20: 348-352.

152. Michael J. Castle, AG, Erika L. F. Holzbaur, John H. Wolfe (2013). AAV Serotypes 1, 8, aand 9 Share a Conserved Mechanism for Axonal Transport but Exhibit Differences in Gene Transfer In Vivo. *Molecular Therapy* 21: S48.

153. Klein, RL, Dayton, RD, Tatom, JB, Henderson, KM, and Henning, PP (2008). AAV8, 9, Rh10, Rh43 vector gene transfer in the rat brain: effects of serotype, promoter and purification method. *Molecular Therapy* 16: 89-96.

154. Klein, RL, Dayton, RD, Leidenheimer, NJ, Jansen, K, Golde, TE, and Zweig, RM (2006). Efficient neuronal gene transfer with AAV8 leads to neurotoxic levels of tau or green fluorescent proteins. *Molecular Therapy* 13: 517-527.

155. Peden, CS, Burger, C, Muzyczka, N, and Mandel, RJ (2004). Circulating anti-wild-type adeno-associated virus type 2 (AAV2) antibodies inhibit recombinant AAV2 (rAAV2)-mediated, but not rAAV5-mediated, gene transfer in the brain. *Journal of Virology* 78: 6344-6359.

156. Sanftner, LM, Sommer, JM, Suzuki, BM, Smith, PH, Vijay, S, Vargas, JA, *et al.* (2005). AAV2-mediated gene delivery to monkey putamen: evaluation of an infusion device and delivery parameters. *Experimental Neurology* 194: 476-483.

157. Bradbury, AM, Cochran, JN, McCurdy, VJ, Johnson, AK, Brunson, BL, Gray-Edwards, H, *et al.* (2013). Therapeutic Response in Feline Sandhoff Disease Despite Immunity to Intracranial Gene Therapy. *Molecular Therapy* 21: 1306-1315.

158. Ciron, C, Desmaris, N, Colle, MA, Raoul, S, Joussemet, B, Vérot, L, *et al.* (2006). Gene therapy of the brain in the dog model of Hurler's syndrome. *Annals of Neurology* 60: 204-213.

159. Ellinwood, NM, Ausseil, J, Desmaris, N, Bigou, S, Liu, S, Jens, JK, *et al.* (2010). Safe, efficient, and reproducible gene therapy of the brain in the dog models of Sanfilippo and Hurler syndromes. *Molecular Therapy* 19: 251-259.

160. Broekman, M, Baek, R, Comer, L, Fernandez, J, Seyfried, T, and Sena-Esteves, M (2007). Complete Correction of Enzymatic Deficiency and Neurochemistry in the GM1-gangliosidosis Mouse Brain by Neonatal Adeno-associated Virus–mediated Gene Delivery. *Molecular Therapy* 15: 30-37.

161. Cachon-Gonzalez, MB, Wang, SZ, Ziegler, R, Cheng, SH, and Cox, TM (2014). Reversibility of neuropathology in Tay-Sachs-related diseases. *Human Molecular Genetics* 23: 730-748.

162. Ahmed, SS, Li, H, Cao, C, Sikoglu, EM, Denninger, AR, Su, Q, *et al.* (2013). A single intravenous rAAV injection as late as P20 achieves efficacious and sustained CNS Gene therapy in canavan mice. *Molecular therapy* 21: 2136-2147.

163. Cabrera-Salazar, MA, Roskelley, EM, Bu, J, Hodges, BL, Yew, N, Dodge, JC, *et al.* (2007). Timing of therapeutic intervention determines functional and survival outcomes in a mouse model of late infantile batten disease. *Molecular Therapy* 15: 1782-1788.

164. Vite, CH, McGowan, JC, Niogi, SN, Passini, MA, Drobatz, KJ, Haskins, ME, *et al.* (2005). Effective gene therapy for an inherited CNS disease in a large animal model. *Annals of Neurology* 57: 355-364.

165. Ellinwood, NM, Ausseil, J, Desmaris, N, Bigou, S, Liu, S, Jens, JK, *et al.* (2011). Safe, efficient, and reproducible gene therapy of the brain in the dog models of Sanfilippo and Hurler syndromes. *Molecular therapy* 19: 251-259.

166. Marks, WJ, Ostrem, JL, Verhagen, L, Starr, PA, Larson, PS, Bakay, RA, *et al.* (2008). Safety and tolerability of intraputaminal delivery of CERE-120 (adeno-associated virus serotype 2–neurturin) to patients with idiopathic Parkinson's disease: an open-label, phase I trial. *The Lancet Neurology* 7: 400-408.

167. Kaplitt, MG, Feigin, A, Tang, C, Fitzsimons, HL, Mattis, P, Lawlor, PA, *et al.* (2007). Safety and tolerability of gene therapy with an adeno-associated virus (AAV) borne GAD gene for Parkinson's disease: an open label, phase I trial. *The Lancet* 369: 2097-2105.

168. Christine, C, Starr, P, Larson, P, Eberling, J, Jagust, W, Hawkins, R, *et al.* (2009). Safety and tolerability of putaminal AADC gene therapy for Parkinson disease. *Neurology* 73: 1662-1669.

169. McPhee, S, Janson, C, Li, C, Samulski, R, Camp, A, Francis, J, *et al.* (2006). Immune responses to AAV in a phase I study for Canavan disease. *The Journal of Gene Medicine* 8: 577-588.

170. Leone, P, Shera, D, McPhee, SW, Francis, JS, Kolodny, EH, Bilaniuk, LT, *et al.* (2012). Long-term follow-up after gene therapy for canavan disease. *Science Translational Medicine* 4: 163.

171. Worgall, S, Sondhi, D, Hackett, NR, Kosofsky, B, Kekatpure, MV, Neyzi, N, *et al.* (2008). Treatment of late infantile neuronal ceroid lipofuscinosis by CNS administration of a serotype 2 adeno-associated virus expressing CLN2 cDNA. *Human Gene Therapy* 19: 463-474.

172. Martin, DR, Cox, NR, Morrison, NE, Kennamer, DM, Peck, SL, Dodson, AN, *et al.* (2005). Mutation of the G M2 activator protein in a feline model of G M2 gangliosidosis. *Acta Neuropathologica* 110: 443-450.

173. Lacorazza, H, and Jendoubi, M (1995). In situ assessment of beta-hexosaminidase activity. *Biotechniques* 19: 434-440.

174. Svennerholm, L (1957). Quantitative estimation of sialic acids. II. A colorimetric resorcinol-hydrochloric acid method. *Biochimica et Biophysica Acta* 24: 604-611.

175. Miettinen, T, and Takki-Luukkainen, I (1959). Use of butyl acetate in determination of sialic acid. *Acta Chemica Scandinavica* 13: 856-858.

176. Farrell, DF, Baker, HJ, Herndon, RM, Lindsey, JR, and McKhann, G (1973). Feline GM1 gangliosidosis: biochemical and ultrastructural comparisons with the disease in man. *Journal of Neuropathology and Experimental Neurology* 32: 1-18.

177. Caciotti, A, Donati, MA, Boneh, A, d'Azzo, A, Federico, A, Parini, R, *et al.* (2005). Role of beta-galactosidase and elastin binding protein in lysosomal and nonlysosomal complexes of patients with GM1-gangliosidosis. *Human Mutation* 25: 285-292.

178. Georgiou, T, Stylianidou, G, Anastasiadou, V, Caciotti, A, Campos, Y, Zammarchi, E, *et al.* (2005). The Arg482His mutation in the beta-galactosidase gene is responsible for a high frequency of GM1 gangliosidosis carriers in a Cypriot village. *Genetic Testing* 9: 126-132.

179. Mosna, G, Fattore, S, Tubiello, G, Brocca, S, Trubia, M, Gianazza, E, *et al.* (1992). A homozygous missense arginine to histidine substitution at position 482 of the beta-galactosidase in an Italian infantile GM1-gangliosidosis patient. *Human Genetics* 90: 247-250.

180. Suzuki, Y, Crocker, AC, and Suzuki, K (1971). GM1-Gangliosidosis: Correlation of Clinical and Biochemical Data. *Archives of Neurology* 24: 58-64.

181. De Grandis, E, Di Rocco, M, Pessagno, A, Veneselli, E, and Rossi, A (2009). MR imaging findings in 2 cases of late infantile GM1 gangliosidosis. *American Journal of Neuroradiology* 30: 1325-1327.

182. Arruda, VR, Fields, PA, Milner, R, Wainwright, L, De Miguel, MP, Donovan, PJ, *et al.* (2001). Lack of germline transmission of vector sequences following systemic administration of recombinant AAV-2 vector in males. *Molecular Therapy* 4: 586-592.

183. Favaro, P, Downey, HD, Zhou, JS, Wright, JF, Hauck, B, Mingozzi, F, *et al.* (2009). Host and vector-dependent effects on the risk of germline transmission of AAV vectors. *Molecular Therapy* 17: 1022-1030.

184. Smith, BK, Collins, SW, Conlon, TJ, Mah, CS, Lawson, LA, Martin, AD, *et al.* (2013). Phase I/II trial of adeno-associated virus-mediated alpha-glucosidase gene therapy to the diaphragm for chronic respiratory failure in Pompe disease: initial safety and ventilatory outcomes. *Human Gene Therapy* 24: 630-640.

185. Flotte, TR, Trapnell, BC, Humphries, M, Carey, B, Calcedo, R, Rouhani, F, *et al.* (2011). Phase 2 clinical trial of a recombinant adeno-associated viral vector expressing alpha1-antitrypsin: interim results. *Hum Gene Therapy* 22: 1239-1247.

186. Jaski, BE, Jessup, ML, Mancini, DM, Cappola, TP, Pauly, DF, Greenberg, B, *et al.* (2009). Calcium upregulation by percutaneous administration of gene therapy in cardiac disease (CUPID Trial), a first-in-human phase 1/2 clinical trial. *Journal of Cardiac Failure* 15: 171-181.

187. Mendell, JR, Rodino-Klapac, LR, Rosales-Quintero, X, Kota, J, Coley, BD, Galloway, G, *et al.* (2009). Limb-girdle muscular dystrophy type 2D gene therapy restores alpha-sarcoglycan and associated proteins. *Annals of Neurology* 66: 290-297.

188. Gaudet, D, Methot, J, Dery, S, Brisson, D, Essiembre, C, Tremblay, G, *et al.* (2013). Efficacy and long-term safety of alipogene tiparvovec (AAV1-LPLS447X) gene therapy for lipoprotein lipase deficiency: an open-label trial. *Gene Therapy* 20: 361-369.

189. Wierzbicki, AS, and Viljoen, A (2013). Alipogene tiparvovec: gene therapy for lipoprotein lipase deficiency. *Expert Opinion on Biological Therapy* 13: 7-10.

190. Pike, LS, Tannous, BA, Deliolanis, NC, Hsich, G, Morse, D, Tung, CH, *et al.* (2011). Imaging gene delivery in a mouse model of congenital neuronal ceroid lipofuscinosis. *Gene Therapy* 18: 1173-1178.

191. Chen, CY, Zimmerman, RA, Lee, CC, Chen, FH, Yuh, YS, and Hsiao, HS (1998). Neuroimaging findings in late infantile GM1 gangliosidosis. *AmericanJjournal of Neuroradiology* 19: 1628-1630.

192. O'Brien, J, Ho, M, Veath, M, Wilson, J, Myers, G, Opitz, J, *et al.* (1972). Juvenile GM1 gangliosidosis: Clinical, pathological, chemical and enzymatic studies. *Clinical Genetics* 3: 411-434.

193. Jackson, GD, Briellmann, RS, Kuzniecky, RI (2005). Temporal lobe epilepsy. In: Kuzniecky, RI, Jackson, GD (eds). *Magnetic resonance in epilepsy: neuroimaging techniques,* Elsevier Academic Press, Burlington, pp. 99-176.

194. Blair, RDG (2012). Temporal lobe epilepsy seminology. *Epilepsy Research and Treatment* 2012:1-10.

195. Michelucci, R, Pasini, Nobile, C (2009). Lateral temporal lobe epilepsies: clinical and genetic features. *Epiplasia* 50:52-54.

196. Bell, WO (1995). Cerebrospinal fluid reabsorption. *Pediatric Neurosurgery* 23: 42-53.

197. Bu, J, Ashe, KM, Bringas, J, Marshall, J, Dodge, JC, Cabrera-Salazar, MA, *et al.* (2012). Merits of Combination Cortical, Subcortical, and Cerebellar Injections for the Treatment of Niemann-Pick Disease Type A. *Molecular Therapy* 20: 1893-1901.

198. McCurdy, VJ, Johnson, AK, Gray-Edwards, HL, Randle, AN, Brunson, BL, Morrison, NE, *et al.* (2014). Sustained normalization of neurological disease after intracranial gene therapy in a feline model. *Science Translational Medicine* 6: 231ra48.

199. Ciron, C, Cressant, A, Roux, F, Raoul, S, Cherel, Y, Hantraye, P, *et al.* (2009). Human alpha-iduronidase gene transfer mediated by adeno-associated virus types 1, 2, and 5 in the brain of nonhuman primates: vector diffusion and biodistribution. *Human Gene Therapy* 20: 350-360.

200. Baek, RC, Martin, DR, Cox, NR, and Seyfried, TN (2009). Comparative analysis of brain lipids in mice, cats, and humans with Sandhoff disease. *Lipids* 44: 197-205.

201. Kroll, RA, Pagel, MA, Roman-Goldstein, S, Barkovich, AJ, D'Agostino, AN, and Neuwelt, EA (1995). White matter changes associated with feline GM2 gangliosidosis (Sandhoff disease): correlation of MR findings with pathologic and ultrastructural abnormalities. *American Journal of Neuroradiology* 16: 1219-1226.

202. Matsuoka, K, Tamura, T, Tsuji, D, Dohzono, Y, Kitakaze, K, Ohno, K, *et al.* (2011). Therapeutic potential of intracerebroventricular replacement of modified human β-hexosaminidase B for GM2 gangliosidosis. *Molecular Therapy* 19: 1017-1024.

203. Kasperzyk, JL, El-Abbadi, MM, Hauser, EC, D'Azzo, A, Platt, FM, and Seyfried, TN (2004). N-butyldeoxygalactonojirimycin reduces neonatal brain ganglioside content in a mouse model of GM1 gangliosidosis. *Journal of Neurochemistry* 89: 645-653.

204. Dickson, PI, Hanson, S, McEntee, MF, Vite, CH, Vogler, CA, Mlikotic, A, *et al.* (2010). Early versus late treatment of spinal cord compression with long-term intrathecal enzyme replacement therapy in canine mucopolysaccharidosis type I. *Molecular Genetics and Metabolism* 101: 115-122.

205. Settembre, C, Zoncu, R, Medina, DL, Vetrini, F, Erdin, S, Huynh, T, *et al.* (2012). A lysosome-to-nucleus signalling mechanism senses and regulates the lysosome via mTOR and TFEB. *The EMBO Journal* 31: 1095-1108.

206. Hu, L, Sun, Y, Villasana, LE, Paylor, R, Klann, E, and Pautler, RG (2009). Early changes in the apparent diffusion coefficient (ADC) in a mouse model of Sandhoff's disease occur prior to disease symptoms and behavioral deficits. *Magnetic Resonance in Medicine* 62: 1175-1184.

207. Vogler, C, Galvin, N, Levy, B, Grubb, J, Jiang, J, Zhou, XY, *et al.* (2003). Transgene produces massive overexpression of human β-glucuronidase in mice, lysosomal storage

of enzyme, and strain-dependent tumors. *Proceedings of the National Academy of Sciences* 100: 2669-2673.

208. Itakura, T, Kuroki, A, Ishibashi, Y, Tsuji, D, Kawashita, E, Higashine, Y, *et al.* (2006). Inefficiency in GM2 ganglioside elimination by human lysosomal β-hexosaminidase β-subunit gene transfer to fibroblastic cell line derived from Sandhoff disease model mice. *Biological and Pharmaceutical Bulletin* 29: 1564-1569.

209. Arfi, A, Bourgoin, C, Basso, L, Emiliani, C, Tancini, B, Chigorno, V, *et al.* (2005). Bicistronic lentiviral vector corrects β-hexosaminidase deficiency in transduced and cross-corrected human Sandhoff fibroblasts. *Neurobiology of Disease* 20: 583-593.

210. Guidotti, J, Mignon, A, Haase, G, Caillaud, C, McDonell, N, Kahn, A, *et al.* (1999). Adenoviral gene therapy of the Tay-Sachs disease in hexosaminidase A-deficient knock-out mice. *Human Molecular Genetics* 8: 831-838.

211. Koelfen, W, Freund, M, Jaschke, W, Koenig, S, and Schultze, C (1994). GM-2 gangliosidosis (Sandhoff's disease): two year follow-up by MRI. *Neuroradiology* 36: 152-154.

212. Imamura, A, Miyajima, H, Ito, R, and Orii, KO (2008). Serial MR imaging and 1H-MR spectroscopy in monozygotic twins with Tay-Sachs disease. *Neuropediatrics* 39: 259-263.

213. Hadaczek, P, Eberling, JL, Pivirotto, P, Bringas, J, Forsayeth, J, and Bankiewicz, KS (2010). Eight years of clinical improvement in MPTP-lesioned primates after gene therapy with AAV2-hAADC. *Molecular Therapy* 18: 1458-1461.

214. Fu, H, Muenzer, J, Samulski, RJ, Breese, G, Sifford, J, Zeng, X, *et al.* (2003). Self-complementary adeno-associated virus serotype 2 vector: global distribution and broad dispersion of AAV-mediated transgene expression in mouse brain. *Molecular Therapy* 8: 911-917.

215. Gray, SJ, Matagne, V, Bachaboina, L, Yadav, S, Ojeda, SR, and Samulski, RJ (2011). Preclinical differences of intravascular AAV9 delivery to neurons and glia: a comparative study of adult mice and nonhuman primates. *Molecular Therapy* 19: 1058-1069.

216. Duque, S, Joussemet, B, Riviere, C, Marais, T, Dubreil, L, Douar, AM, *et al.* (2009). Intravenous administration of self-complementary AAV9 enables transgene delivery to adult motor neurons. *Molecular Therapy* 17: 1187-1196.

217. Foust, KD, Wang, X, McGovern, VL, Braun, L, Bevan, AK, Haidet, AM, *et al.* (2010). Rescue of the spinal muscular atrophy phenotype in a mouse model by early postnatal delivery of SMN. *Nature Biotechnology* 28: 271-274.

218. Bevan, AK, Duque, S, Foust, KD, Morales, PR, Braun, L, Schmelzer, L, *et al.* (2011). Systemic gene delivery in large species for targeting spinal cord, brain, and peripheral tissues for pediatric disorders. *Molecular Therapy* 19: 1971-1980.

219. Lachmann, R (2010). Treatments for lysosomal storage disorders. *Biochemical Society Transactions* 38: 1465-1468.

220. Bley, AE, Giannikopoulos, OA, Hayden, D, Kubilus, K, Tifft, CJ, and Eichler, FS (2011). Natural history of infantile GM2 gangliosidosis. *Pediatrics* 128: e1233-e1241.

221. Smith, NJ, Winstone, A, Stellitano, L, Cox, TM, and Verity, CM (2012). GM2 gangliosidosis in a UK study of children with progressive neurodegeneration: 73 cases reviewed. *Developmental Medicine and Child Neurology* 54: 176-182.

222. Lew, RM, Proos, AL, Burnett, L, Delatycki, M, Bankier, A, and Fietz, MJ (2012). Tay Sachs disease in Australia: reduced disease incidence despite stable carrier frequency in Australian Jews. *The Medical Journal of Australia* 197: 652-654.

223. Sun, B, Zhang, H, Bird, A, Li, S, Young, SP, and Koeberl, DD (2009). Impaired clearance of accumulated lysosomal glycogen in advanced Pompe disease despite high-level vector-mediated transgene expression. *The Journal of Gene Medicine* 11: 913-920.

224. Hackett, NR, Redmond, DE, Sondhi, D, Giannaris, EL, Vassallo, E, Stratton, J, *et al.* (2005). Safety of direct administration of AAV2CUhCLN2, a candidate treatment for the central nervous system manifestations of late infantile neuronal ceroid lipofuscinosis, to the brain of rats and nonhuman primates. *Human Gene Therapy* 16: 1484-1503.

225. Sondhi, D, Peterson, D, Giannaris, E, Sanders, C, Mendez, B, De, B, *et al.* (2005). AAV2-mediated CLN2 gene transfer to rodent and non-human primate brain results in long-term TPP-I expression compatible with therapy for LINCL. *Gene Therapy* 12: 1618-1632.

226. Passini, MA, Dodge, JC, Bu, J, Yang, W, Zhao, Q, Sondhi, D, *et al.* (2006). Intracranial delivery of CLN2 reduces brain pathology in a mouse model of classical late infantile neuronal ceroid lipofuscinosis. *The Journal of Neuroscience* 26: 1334-1342.

227. Matalon, R, Surendran, S, Rady, PL, Quast, MJ, Campbell, GA, Matalon, KM, *et al.* (2003). Adeno-associated virus-mediated aspartoacylase gene transfer to the brain of knockout mouse for canavan disease. *Molecular Therapy* 7: 580-587.

228. McPhee, S, Francis, J, Janson, C, Serikawa, T, Hyland, K, Ong, E, *et al.* (2005). Effects of AAV-2-mediated aspartoacylase gene transfer in the tremor rat model of Canavan disease. *Molecular Brain Research* 135: 112-121.

Appendix 1: Contribution of thalamus and deep cerebellar nuclei injection sites to overall therapeutic outcome following intracranial gene therapy

Study design

To test the contribution of the individual thalamus and deep cerebellar nuclei (DCN) injection sites, Sandhoff disease (SD) cats were treated with either bilateral thalamus (n = 3) or bilateral DCN (n = 3) injections of AAVrh8-*HEXA* + AAVrh8-*HEXB* in a 1:1 ratio (thalamus only group, 3.2 x 10^{12} vector genomes (vg) total; DCN only group, 1.1 x 10^{12} vg total) and were euthanized at humane endpoint. Controls were untreated SD cats (n = 5 for biochemical analysis; n = 14 for clinical follow-up) and age-matched normal cats (n = 4).

Results and discussion

Enzyme and vector distribution

Following thalamus only injections of AAV vectors, HexA activity against the α-subunit preferred substrate, MUGS, was present at near or above normal levels in the cerebrum, thoracolumbar spinal cord, and peripheral nervous system (PNS). HexA activity was also above normal in the rostral and middle cerebellum, but was only 0.33- to 0.55-fold normal in the caudal cerebellum and cervical spinal cord (**Figure 1** and **Table 1**). However, HexA activity in spinal cord blocks K-O was not significantly different than that of untreated SD cats due to negligible activity in one of three treated cats. After DCN injections of AAV vectors, cerebral Hex distribution was restricted to the meninges surrounding the brain. HexA activity was restored to

above normal levels in the middle and caudal cerebellum, thoracolumbar spinal cord, and PNS, but was only 0.33- to 0.42-fold normal in the rostral cerebellum and cervical spinal cord (**Figure 1** and **Table 1**). The cerebellar nuclei are reported to send input the to the cervical division of the spinal cord, and were shown to mediate efficient dissemination of enzyme and vector throughout the spinal cord of mice[133, 138]. Therefore, it is surprising that spinal cord activity was not higher following DCN injection in SD cats. Vector genomes were detected in all central nervous system (CNS) blocks and copy numbers generally corresponding to HexA activity (**Table 1**).

In cerebrospinal fluid (CSF), HexA activity was present at 0.69- and 7.6-fold normal in the thalamus only and DCN only groups, respectively. A portion of enzyme distribution to the spinal cord likely occurred through CSF, which pools in the lumbar region. However, it is unlikely that CSF transport alone determines spinal cord enzyme distribution, as both groups had comparable spinal cord Hex activity even though the DCN only group had higher CSF activity. HexA activity was not significantly different between groups in liver and muscle, which suggests that therapeutic enzyme reaches peripheral tissues after gaining direct access to blood vessels during the injection procedure. If reabsorption of CSF into circulation contributed to peripheral enzyme dissemination then we would expect to see higher peripheral activity in the DCN only group versus the thalamus only group.

Survival was comparable between both groups signifying that both injection sites contribute to clinical efficacy. Two cats in the thalamus only group progressed to neurological humane endpoint (score of 3 in Chapter 2, **Figure 7a**) and a third was euthanized due to substantial weight loss likely secondary to peripheral disease[157]. One cat in the DCN only group progressed to neurological humane endpoint following rapid weight loss, one cat died unexpectedly at 12.7 months old while at the stage of instability (score of 6.5 in Chapter 2,

Figure 7a), and a third was euthanized whilst also at the stage of instability (score of 6), due to blindness, consistent with enzyme deficiency in the cerebrum (the other two cats in the DCN only group also developed blindness). Therefore, thalamic injections mediated efficient enzyme distribution to the cerebrum and also to the rostral cerebellum, and lumbar spinal cord of most subjects. DCN injections mediated efficient enzyme distribution to the cerebellum and lumbar spinal cord, but not to the cerebrum. Both injection routes mediated efficient enzyme distribution to the PNS and contributed to the Hex activity in peripheral tissues.

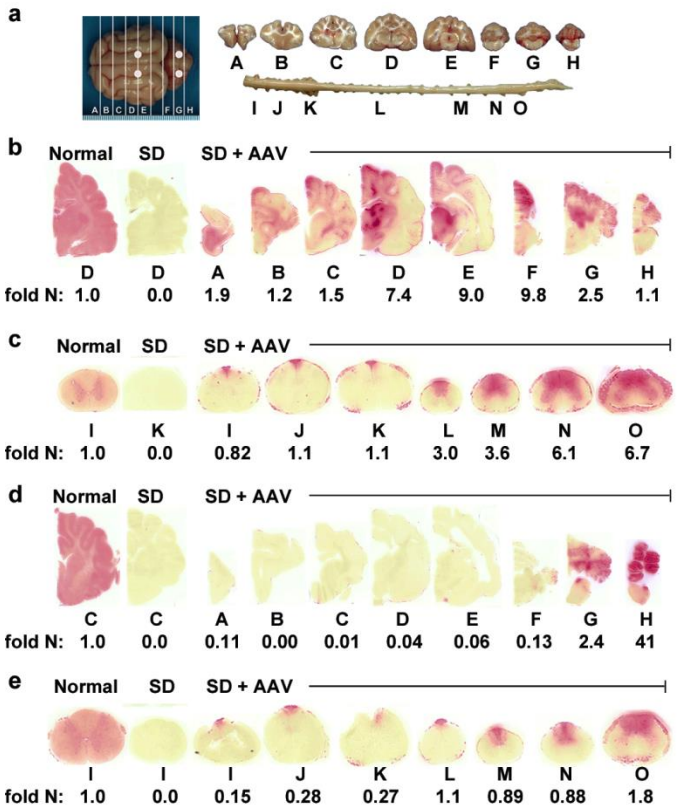

Figure 1. Therapeutic enzyme distribution in the CNS of Sandhoff disease (SD) cats treated with thalamus or DCN only injections of AAV vectors. Cats were treated with AAV-*fHEXA* + AAV-*fHEXB* and tissues were collected at endpoint. (**a**) Injection sites (white circles) and 0.6 cm coronal blocks of the brain (A-H) and spinal cord (I-O) collected at necropsy. Lysosomal Hex activity (red) detected with naphthol at acidic pH was visualized throughout the brain (**b**) and spinal cord (**c**) of the longest living thalamus only AAV-treated cat (SD + AAV) at 13.2 months old. Lysosomal Hex activity was visualized throughout the brain (**d**) and spinal cord (**e**) of the longest living DCN only AAV-treated cat (SD + AAV) at 12.7 months old. Corresponding HexA activity against MUGS substrate is shown below each block as fold normal level (fold N). Representative control sections are shown from normal cats along with untreated SD cats, which express ≤0.02-fold normal HexA activity in the brain and spinal cord. The ranges of specific

activities for normal control blocks were: brain, 27.8 (H) – 59.9 (D); spinal cord, 6.5 (L) – 17.6 (K) nmol 4MU/mg/hr.

Table 1. HexA and AAV vector distribution in the nervous system, liver, and muscle of Sandhoff disease (SD) cats treated with thalamus or DCN only injections of AAV vectors

		Fold normal Hex activity (mean, s.d.)		Vector copy number per μg genomic DNA	
Region	Block	Thalamus only[A]	DCN only[B]	Thalamus only	DCN only
CNS					
	A	**1.1** (0.72)▲	**0.13** (0.04)	**14,000** (4700)▲	**1,100** (750)
	B	**0.84** (0.33)▲	**0.09** (0.13)	**8,100** (1,300)▲	**350** (210)
Cerebrum	C	**0.83** (0.60)▲	**0.06** (0.10)	**9,900** (5,700)▲	**400** (300)
	D	**5.4** (4.3)▲	**0.11** (0.10)	**18,000** (13,000)▲	**400** (190)
	E	**5.5** (4.1)▲	**0.11** (0.11)	**27,000** (20,000)▲	**430** (380)
	F	**3.7** (1.1)	**0.42** (0.25)	**5,000** (4,900)	**1,400** (930)
Cerebellum	G	**1.1** (1.3)	**11** (11)	**1,700** (1,400)	**7,300** (10,000)
	H	**0.55** (0.52)▼	**46** (16)	**1,400** (550)▼	**2,000** (2140)
	I	**0.33** (0.43)	**0.34** (0.33)	**1,400** (1,100)	**1,200** (350)
	J	**0.47** (0.54)	**0.33** (0.11)	**2,200** (2,000)	**2,400** (2,000)
	K	**0.45** (0.59)	**0.40** (0.25)	**2,200** (2,000)	**850** (730)
Spinal cord	L	**1.2** (1.5)	**1.1** (0.13)	**1,800** (2,000)	**1,200** (600)
	M	**1.5** (1.9)	**1.2** (0.63)	**2,000** (2,200)	**1,600** (700)
	N	**2.4** (3.2)	**1.2** (0.62)	**1,900** (1,800)	**1,700** (750)
	O	**2.8** (3.4)	**2.1** (0.69)	**2,500** (1,700)	**3,500** (2,700)
CSF		**0.69** (0.36)	**7.6** (6.6)	nd	nd
PNS					
C DRG		**2.4** (2.0)	**5.6** (3.3)	nd	nd
L DRG		**20** (11)	**16** (12)	nd	nd
PN		**3.0** (3.5)	**2.0** (0.55)	nd	nd
Periphery				nd	nd
Liver		**0.23** (0.03)	**0.26** (0.08)	nd	nd
Muscle		**0.15** (0.09)	**0.19** (0.10)	nd	nd

[A] n = 3; HexA activity against the α-subunit preferred substrate (MUGS) was significantly higher than in untreated SD cats (n = 5) in **A-H** ($P \leq 0.013$ for each block), **I-J** ($P \leq 0.04$), **C DRG** ($P = 0.018$), **L DRG** ($P = 0.041$, only two of three samples were available for analysis), **PN** ($P = 0.018$), and **liver** ($P = 0.018$).

[B] n = 3; HexA activity against the α-subunit preferred substrate (MUGS) was significantly higher than in untreated SD cats (n = 5) in **A-H** ($P \leq 0.040$ for each block), **I-O** ($P \leq 0.016$ in each

block), **C DRG** (P = 0.018), **L DRG** (P = 0.018), **PN** (P = 0.018), **liver** (P = 0.018), and **muscle** (P = 0.018).

▲, HexA activity and vector copy number were significantly higher than in the DCN only cohort (P = 0.040); ▼, HexA activity and vector copy number were significantly lower than in the DCN only cohort (P = 0.040).

Abbreviations: CNS = central nervous system; PNS = peripheral nervous system; nd = not determined; CSF = cerebrospinal fluid; DCN = deep cerebellar nuclei; C DRG = cervical dorsal root ganglia; L DRG = lumbar dorsal root ganglia

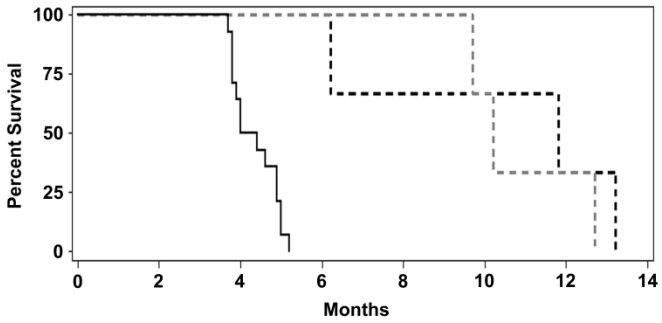

Figure 2. Survival of Sandhoff disease (SD) cats treated with thalamus only or DCN only injections of AAV vectors. Shown are Kaplan-Meier survival curves for untreated SD cats (solid black line, n = 14) and SD cats treated with thalamus only (dashed black line, n = 3) or DCN only (dashed gray line, n = 3) injections of AAV vectors. Both groups had significantly increased survival compared to untreated (P = 0.0035 for both groups), and survival of the thalamus only group was not significantly different to that of the DCN only group (P = 0.061).

Appendix 2: Widespread correction of central nervous system disease following thalamus and intracerebroventricular gene therapy in a feline model of Sandhoff disease

Study design

Studies in mice[160] and dogs[141], have shown that intracerebroventricular (ICV) injection of adeno-associated virus (AAV) vectors can mediate enzyme distribution to the spinal cord and or/brain. Because Hex restoration in the cervical spinal cord of Sandhoff disease (SD) cats is unpredictable following thalamus and DCN injections of AAV vectors, thalamus and ICV vector delivery was tested for its ability to restore spinal cord Hex activity. Also, alternative injection routes to the DCN are preferred in human patients due to the risk of hemorrhage in the posterior fossa. Four SD cats were treated with bilateral thalamus and left lateral ventricular injection of AAV-*fHEXA* + AAV-*fHEXB* in a 1:1 ratio (8×10^{12} vector genomes total) and were euthanized 16 weeks after injection for biochemical analysis of therapeutic effect. Six additional cats were treated in the same way for long term clinical follow-up and were euthanized at humane endpoint. Controls were age-matched untreated normal cats (n = 4 for short term cats; n = 6 for long term cats) and untreated SD cats (n = 5 for enzyme analysis, n = 6 for storage analysis, and n = 14 for clinical analysis).

Results and discussion

Widespread enzyme distribution

Sixteen weeks after injection Hex activity against the α-subunit preferred substrate, MUGS, was widely distributed throughout the brain and spinal cord (**Figure 1**). Brain HexA activity ranged from 4.3- to 72-fold normal, and average spinal cord activity ranged from 8.0- to 24-fold normal (**Table 1**). Values were significantly higher than in untreated SD cats and also significantly higher than in normal cats. Spinal cord HexA distribution was superior to that following thalamus and DCN injections of vectors. All short term cats demonstrated efficient transduction of gray matter in both the cervical and lumbar spinal cord, which was also evident at humane endpoint (up to 25.9 months old) in the three long term cats analyzed (**Figure 2**). The temporal lobe of most subjects remained Hex deficient (with the exception of cat 7-960 pictured in **Figure 1b**), which is another location that was not well corrected following thalamus and DCN vector delivery. Even though the cerebellum was not injected, cerebellar HexA activity was several fold that of normal. Vector copies were detected in all CNS blocks from representative short term and long term cats (**Table 2**).

Widespread clearance of storage material

Representative samples from cortex block C, thalamus block D, cerebellum block G, and cervical intumescence (CI, block K in **Figure 3a**) of AAV-treated SD cats and untreated controls were analyzed for gangliosides and other lipids by HPTLC (**Figure 3**). Total sialic acid in untreated SD cats accumulated significantly to 1.9- to 4.0-fold that of normal (**Table 2**). In AAV-treated SD cats, mean sialic acid concentration was decreased in all samples, but remained significantly higher than that of normal in the thalamus. GM2 ganglioside and its asialo derivative, GA2, were absent in samples from normal cats with the exception of sample K in which trace amounts were detected. In untreated SD cats, GM2 and GA2 concentrations were

significantly higher than in normal cats in all samples (**Table 2**). In AAV-treated SD cats, GM2 and GA2 concentrations were significantly decreased in the cortex (GM2, 94%; GA2, 97%), thalamus (GM2, 98%; GA2, 100%), and cerebellum (GM2, 98%; GA2, 98%). Residual GM2 storage only remained significantly higher than in normal cats in cortex C. In accordance with good enzyme distribution in the cervical spinal cord, GM2 and GA2 concentrations were significantly reduced in the CI (GM2, 98%; GA2, 100%) compared to untreated SD cats. Therefore, compared to thalamus and DCN vector delivery (chapter 2), thalamus and ICV vector delivery resulted in comparable reduction of storage material in the brain and greater reduction of storage material in the CI, which is in accordance with the superior Hex distribution to the CI.

Incomplete restoration of secondary lysosomal biomarker

In untreated SD cats, α-mannosidase activity was significantly elevated up to 8.4-fold normal in the brain and 11-fold normal in the spinal cord. Sixteen weeks after thalamus and ICV delivery of AAV-*fHEXA* and AAV-*fHEXB*, α-mannosidase activity was significantly reduced in all CNS blocks compared to untreated SD cats. However, activity remained significantly higher than in normal cats in brain blocks D, E, and G. As in thalamus and DCN treated cats, α-mannosidase activity also remained significantly higher than in normal cats in most spinal cord blocks, revealing incomplete restoration of this secondary lysosomal biomarker despite restoration of HexA activity to several fold that of normal. This finding was surprising as Hex activity appeared well restored throughout the spinal cord gray matter (**Figure 4**).

Delayed clinical disease progression

Clinical disease in untreated SD cats progressed according to the clinical rating scale in **Figure 5a** with attainment of humane endpoint at 4.4 ± 0.6 months old. Two SD cats in the short term study were treated with thalamus and ICV gene therapy before clinical disease onset and the other two cats were treated after clinical disease onset. At the pre-determined endpoint of 5 months old, the composite clinical rating score of the pre-symptomatic AAV-treated cats was 7.3 (similar to the thalamus and DCN group in chapter 2, score 7.7). Neither cat developed overt tremors, which are evident in untreated SD cats by 2.4 months old and become progressively debilitating. The cats treated post-symptomatically had an average score of 6.3 at the study endpoint, and both cats developed or continued to show overt whole body tremors (**Figure 5b**). Therefore, disease progression was delayed in all four cats up to the 16 weeks post-treatment experimental endpoint, but treatment was more effective when administered before disease onset. The six AAV-treated cats followed long term reached humane endpoint between 11.2 and 25.9 months old (**Figure 6**), and survival was not significantly different versus the long term thalamus and DCN treated group reported in chapter 3 ($P = 0.86$).

Summary

Compared to thalamus and DCN vector delivery, thalamus and ICV delivery resulted in similar brain Hex distribution, but superior spinal cord Hex distribution. However, there was no significant difference in long term survival between nine thalamus and DCN treated cats and six thalamus and ICV treated cats. Long term outcome based on gait defects is currently influenced by many variables other than CNS Hex activity, such as Hex deficiency in peripheral tissues. For example, bone abnormalities are apparent in SD cats at birth and have been documented to cause

soft tissue compression of the spinal cord[157], which could affect neurological function regardless of spinal cord Hex activity. Furthermore, progressive muscle weakness could affect ambulatory function. As ICV injection is routinely performed in human patients, but DCN injection is a precarious procedure, thalamus and ICV injection would be the preferred method to treat human patients based on current results.

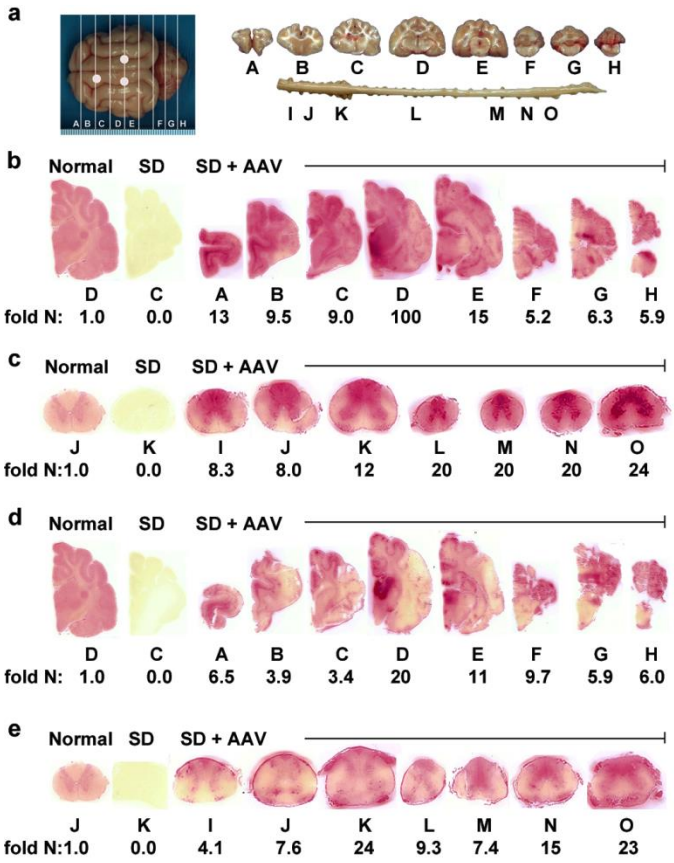

Figure 1. Therapeutic enzyme distribution in the CNS of Sandhoff disease (SD) cats after thalamus and ICV AAV treatment. SD cats were injected bilaterally in the thalamus and the left lateral ventricle with AAVrh8-*fHEXA* and AAVrh8-*fHEXB* (8.0×10^{12} vector genomes total). (**a**) Injection sites (white circles) and 0.6 cm coronal blocks of the brain (A-H) and spinal cord (I-O) collected at necropsy. Blocks were halved and analyzed for storage material (left) or for enzyme activity (right). Lysosomal Hex activity (red) detected with naphthol at acidic pH was visualized throughout the brain (**b**) and spinal cord **(c)** of a representative, short term treated SD cat (SD + AAV; 7-960) 16 weeks after treatment. Lysosomal Hex activity was detected throughout the brain (**d**) and spinal cord (**e**) of a long term treated SD cat (SD + AAV; 7-760) at 25.9 months old. Corresponding Hex activity against MUGS substrate is shown below each block as fold normal level (fold N). Representative control sections are shown from untreated normal cats

along with untreated SD cats, which express ≤0.02-fold normal βgal activity in the brain and spinal cord. The ranges of specific activities for normal control blocks were: short term (brain, 30 (F) – 51 (D); spinal cord, 8.3 (M) – 17.3 (K) nmol 4MU/mg/hr); long term (brain, 28 (H) – 57 (D); spinal cord, 6.7 (L) – 18 (K).

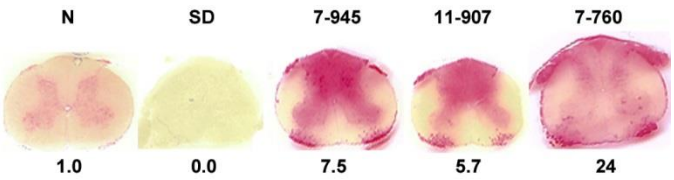

Figure 2. Therapeutic enzyme distribution in the cervical spinal cord of thalamus and ICV AAV-treated Sandhoff disease (SD) cats followed long term. Tissues were collected at humane endpoint. Lysosomal Hex activity (red) detected with naphthol is shown for the cervical intumescence (block K) of three AAV-treated SD cats (7-945, 11-907, and 7-760) at the humane endpoint of 16.8, 11.2, and 25.9 months old, respectively. Corresponding HexA activity against MUGS substrate is shown below each block as fold normal level. Representative control sections for block K are shown from untreated normal cats (N) and untreated SD cats (SD), which express 0.00 ± 0.01-fold normal HexA activity in block K. Specific activity for the normal control block was 17.6 ± 3.2 nmol 4MU/mg/hr.

Table 1. Hex activity in brain and spinal cord of thalamus and ICV AAV-treated Sandhoff disease (SD) cats and untreated controls

CNS Region	Block	Fold normal Hex activity						
		Short term SD + AAV					Long term SD + AAV	SD no tx
		11-792	7-957	7-960	7-981	Mean (s.d.)[A]	(Mean, s.d.)[B, C]	Mean (s.d.)
Cerebrum	A	**2.2**	**2.6**	**13**	**2.5**	**5.0** (5.1)	**3.9** (2.6)	**0.0** (0.0)
	B	**1.9**	**2.6**	**9.5**	**2.9**	**4.3** (3.5)	**2.3** (1.4)	**0.0** (0.0)
	C	**2.6**	**3.1**	**9.0**	**80**	**24**(38)	**1.8** (1.4)	**0.0** (0.0)
	D	**100**	**55**	**98**	**35**	**72** (32)	**16** (11)	**0.0** (0.0)
	E	**3.0**	**16**	**15**	**5.4**	**9.9** (6.7)	**8.3** (6.4)	**0.0** (0.0)
Cerebellum	F	**8.3**	**3.2**	**5.2**	**12**	**7.1** (3.8)	**5.5** (3.9)	**0.0** (0.0)
	G	**5.8**	**3.9**	**6.3**	**6.8**	**5.7** (1.3)	**3.7** (2.2)	**0.01** (0.01)
	H	**5.4**	**3.3**	**5.9**	**5.3**	**5.0** (1.2)	**3.2** (2.8)	**0.0** (0.0)
Spinal cord	I	**4.0**	**5.2**	**8.3**	**3.8**	**5.3** (2.1)	**4.5** (1.1)	**0.0** (0.0)
	J	**3.5**	**4.8**	**8.0**	**8.4**	**6.2** (2.4)	**6.6** (1.1)	**0.0** (0.0)
	K	**7.1**	**5.3**	**12**	**11**	**8.7** (3.0)	**12** (9.8)	**0.0** (0.01)
	L	**13**	**4.7**	**20**	**5.9**	**11** (7.1)	**5.4** (3.4)	**0.02** (0.03)
	M	**6.3**	**7.5**	**20**	**8.6**	**11** (6.3)	**5.1** (2.1)	**0.02** (0.04)
	N	**10**	**9.3**	**20**	**9.4**	**12** (5.4)	**9.4** (5.3)	**0.01** (0.02)
	O	**16**	**9.3**	**24**	**10**	**15** (6.6)	**13** (8.8)	**0.01** (0.01)

[A] n = 4; HexA activity against the α-subunit preferred substrate (MUGS) was significantly higher than in untreated SD cats in **A-H** ($P \leq 0.0075$ for each block) and **I-O** ($P \leq 0.0090$ for each block) and was significantly higher than in untreated normal cats (n = 4) in **A-H** and **I-O** ($P \leq 0.015$ for each block).

[B] n = 3; HexA activity against the α-subunit preferred substrate (MUGS) was significantly higher than in untreated SD cats in **A-H** ($P \leq 0.013$ for each block) and **I-O** ($P \leq 0.016$ for each block) and was significantly higher than in untreated normal cats in **A, B, D, F**, and **G** ($P = 0.026$), and in **I-O** ($P = 0.026$).

[C] HexA activity was significantly lower than in the short term cohort in block D ($P = 0.026$).

Abbreviations: tx = treatment; ICV = intracerebroventricular; CNS = central nervous system

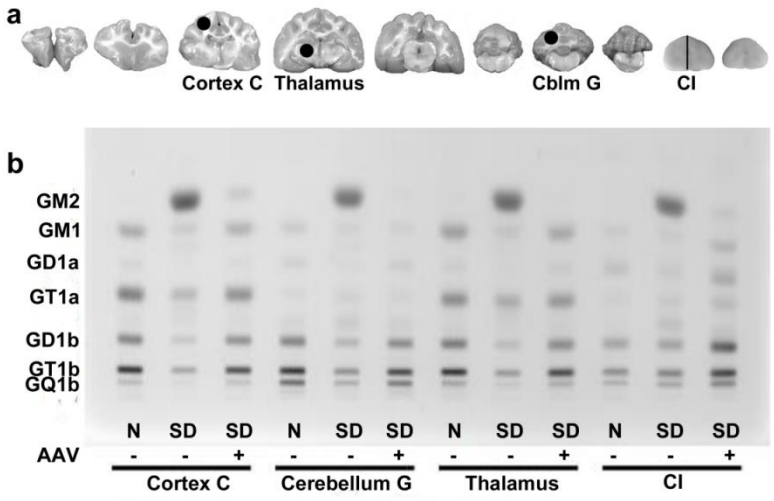

Figure 3. HPTLC of glycosphingolipids in the CNS of Sandhoff disease (SD) cats 16 weeks after thalamus and ICV AAV-treatment. AAV-treated SD cats were euthanized 16 weeks after treatment and ganglioside distribution was compared to normal cats (n = 4) and untreated SD cats (n = 5). (**a**) Locations of the 8 mm punch biopsy samples from representative CNS locations. (**b**) The qualitative distribution of gangliosides on chromatograms was visualized in the cortex block C, thalamus block D, cerebellum block G, and cervical intumescence (CI, block K in **Figure 1a**; half of the block was used). The amount of gangliosides spotted per lane was equivalent to 1.5 μg sialic acid. N, representative normal cat; SD, representative untreated SD cat or AAV-treated SD cat; AAV + or – indicates whether the cat received AAV-treatment. HPTLC plate was provided by Hannah E. Rockwell.

Table 2. Quantification of storage material in the CNS of Sandhoff disease (SD) cats 16 weeks after thalamus and ICV AAV-treatment

Sample[A]	Tx group	Total sialic acid	GM2	GA2
		(μg/100 mg dry weight, mean (s.d.))		
Cortex C	Normal no tx	**460** (35)	**0.0** (0.0)	**0.0** (0.0)
	SD no tx	**1,300** (460)	**630** (240)	**1,500** (800)
	SD + AAV	**510** (78)*	**37** (24)*▲	**120** (41)*
Thalamus	N no tx	**310** (48)	**0.0** (0.0)	**0.0** (0.0)
	SD no tx	**1,300** (330)	**450** (120)	**1,900** (470)
	SD + AAV	**470** (8.5)*▲	**9.3** (11)*	**0.0** (0.0)*
Cerebellum G	Normal no tx	**270** (63)	**0.0** (0.0)	**0.0** (0.0)
	SD no tx	**510** (170)	**240** (110)	**1,500** (830)
	SD + AAV	**330** (21)	**21** (22)*	**45** (79)*
CI	Normal no tx	**89** (6.2)	**1.4** (2.8)	**0.0** (0.0)
	SD no tx	**310** (100)	**130** (59)	**320** (150)
	SD + AAV	**100** (25)*	**2.0** (3.5)*	**0.0** (0.0)*

[A] Concentration of storage material was quantified in 8 mm punch biopsy samples shown in **Figure 3a** for comparison to normal cats (n = 4) and untreated SD cats (n = 6).

*, concentration was significantly lower than in untreated SD cats, $P \leq 0.026$; **, concentration was significantly lower than in untreated SD cats, $P = 0.040$; ▲, concentration was significantly higher than in normal cats.

Abbreviations: Tx = treatment; CI = cervical intumescence

HPTLC was performed by Hannah E. Rockwell and Julian R. Arthur

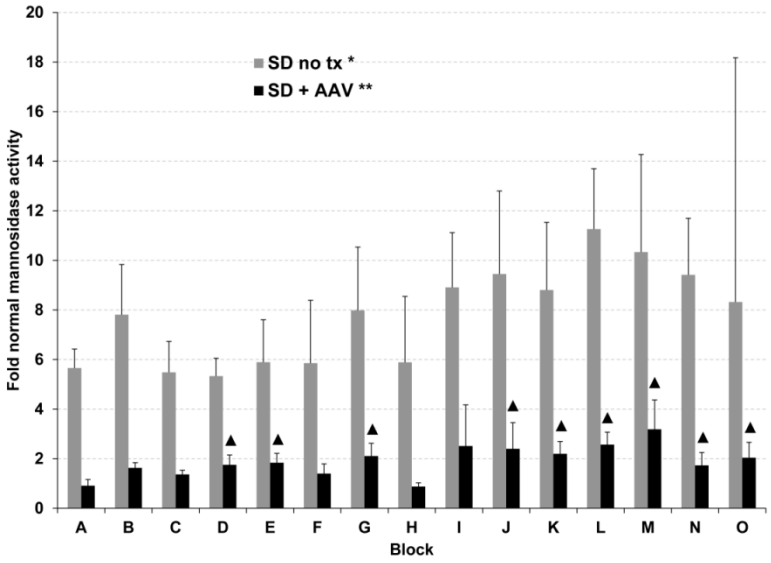

Figure 4. Lysosomal α-mannosidase activity in the CNS of Sandhoff disease (SD) cats 16 weeks after thalamus and ICV AAV-treatment. SD cats were injected bilaterally in the thalamus and in the left lateral ventricle with 8.0×10^{12} vg of AAV-*fHEXA* + AAV-*fHEXB* (n = 4). Tissues were collected 16 weeks after treatment and compared to untreated SD cats (n = 5) and normal cats (n = 4) in the brain (A-H) and spinal cord (I-O). Lettering of brain and spinal cord blocks correspond to **Figure 1a**. *, Activity in all samples from untreated SD cats was significantly higher than in normal cats ($P = 0.010$ for each block); **, activity in all samples from treated SD cats was significantly lower than in untreated SD cats ($P \leq 0.019$ for each brain block; $P \leq 0.037$ for each spinal cord block); ▲, samples from treated cats that had significantly higher activity compared to that of normal cats ($P \leq 0.030$).

a

Score	Clinical Status*	Age (Months)
10	Normal	< 1.3 ± 0.2
9	Hind limb muscle weakness	2.1 ± 0.0
8	Wide stance	2.2 ± 0.3
7	Ataxia	2.5 ± 0.1
6	Instability with occasional falling	2.9 ± 0.4
5	Limited walking	3.5 ± 0.5
4	Standing but not walking	3.9 ± 0.5
3	Cannot stand on 2 consecutive days	4.4 ± 0.6
2	Lateral recumbency	> 4.4
1	Uncontrollable neurological symptoms	> 4.4

*Onset of mild tremors begins at 1.3 ± 0.2 months old; Onset of overt whole body tremors begins at 2.4 ± 0.1 months old.

b

		Age (months)								
Cat	Tx age (mo.)[a]	1.0	2.0	2.5	3.0	3.5	4.0	4.5	5.0	Endpoint
7-957	1.1	10	10	10	10	9.5	9	7.5A		7.5A
7-960	1.6	10A	10A	10B	10B	9B	9B	7B	6.5B	6.5B
11-972	1.6	10A	9.5B	9.5B	9.5B	8B	7B	6.5B	6B	6B
7-981	1.2	10	10	10	10A	8.5A	7.5A	7.5A	7A	7A

Figure 5. Clinical progression of short term thalamus and ICV AAV-treated Sandhoff disease (SD) cats. AAV-treated SD cats were scored on a scale based on disease progression in untreated SD cats. (**a**) Age of symptom onset is shown for untreated SD cats (mean ± s.d., n = 14). The scale is based on gait defects, which ultimately define humane endpoint at 4.4 months old (score of 3). However, disease onset begins at 1.3 months old with subtle tremors of the head/tail that progress to overt whole-body tremors at 2.4 months old. (**b**) Shown are clinical rating scores for each individual AAV-treated SD. The letter designation A signifies mild tremors and the letter designation B signifies overt whole body tremors.

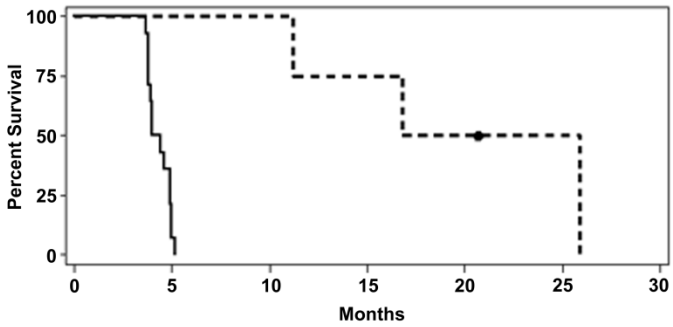

Figure 6. Survival of thalamus and ICV AAV-treated Sandhoff disease (SD) cats followed long term. Shown are Kaplan-Meier survival curves for untreated SD cats (solid black line, n = 14) and SD cats treated with thalamus and ICV injections of AAV vectors (dashed black line, n = 6), which had significantly increased survival versus untreated SD cats (P = 0.0010). The dot represents a living cat.

Appendix 3: Intracisternal gene therapy in GM1 gangliosidosis cats

Study design

Studies in mice[134], dogs[141] and non-human primates suggest that intracisternal (IC) injection of adeno-associated virus (AAV) vectors can mediate therapeutic enzyme distribution to the spinal cord. Because β-galactosidase (βgal) restoration in the feline GM1 gangliosidosis spinal cord is unpredictable following thalamus and deep cerebellar nuclei (DCN) injections of AAV vector (chapter 1), IC vector delivery was tested for its ability to restore βgal activity throughout the spinal cord. Also, alternative injection routes to the DCN may be required in human patients as DCN injection bears the risk of hemorrhage in the posterior fossa. Two GM1 gangliosidosis cats were treated with IC injection of AAVrh8-βgal (3.4×10^{12} vector genomes total) at 2.9 months old and were euthanized 6 weeks after injection. Enzyme and vector distribution were compared to three age-matched GM1 gangliosidosis cats treated with bilateral thalamus and DCN injections of the same vector (3.2×10^{12} vector genomes total). Controls were untreated GM1 gangliosidosis cats (n = 4) and age-matched normal cats (n = 4).

Results and discussion

βgal and AAV vector distribution in the central nervous system

Lysosomal βgal activity was detected by Xgal staining throughout the brain of both groups 6 weeks after treatment (**Figure 1**). In the thalamus and DCN group, brain activity was most intense in blocks corresponding to the thalamus and DCN injection sites (blocks D and G,

respectively, in **Figure 1b**) and decreased with increasing distance from those sites. Variability in βgal activity between cats in the same treatment group likely resulted from differences in the exact location of injection within the thalamus and DCN as well as differences in anatomy between cats. Following IC injection, gradients of staining were present in the brain, with most activity located near the brain surface (**Figure 1d**), consistent with transport of enzyme in cerebrospinal fluid (CSF). βgal activity was apparent in the dorsal spinal cord of both groups, but was more effectively distributed to the ventral spinal cord following IC injection.

In the IC group, mean βgal activity against a synthetic 4MU substrate was 0.09- to 2.4-fold lower in the brain, but 1.3- to 3.0-fold higher in the spinal cord versus the thalamus and DCN group. Significance could not be determined due low animal numbers. Vector copies were detected in every block, indicating widespread dissemination of vector from both injection procedures. In accordance with βgal activity, mean vector copies were higher in the spinal cord of the IC group versus the thalamus and DCN group.

Summary

At 6 weeks after treatment, IC vector delivery resulted in more effective βgal distribution in the spinal cord versus thalamus and DCN vector delivery. However, brain βgal activity was patchy following IC vector delivery and did not penetrate deeper structures. Therefore, IC injection could be tested in long term clinical studies in combination with thalamus and DCN injections for its ability to consistently restore βgal activity throughout the spinal cord.

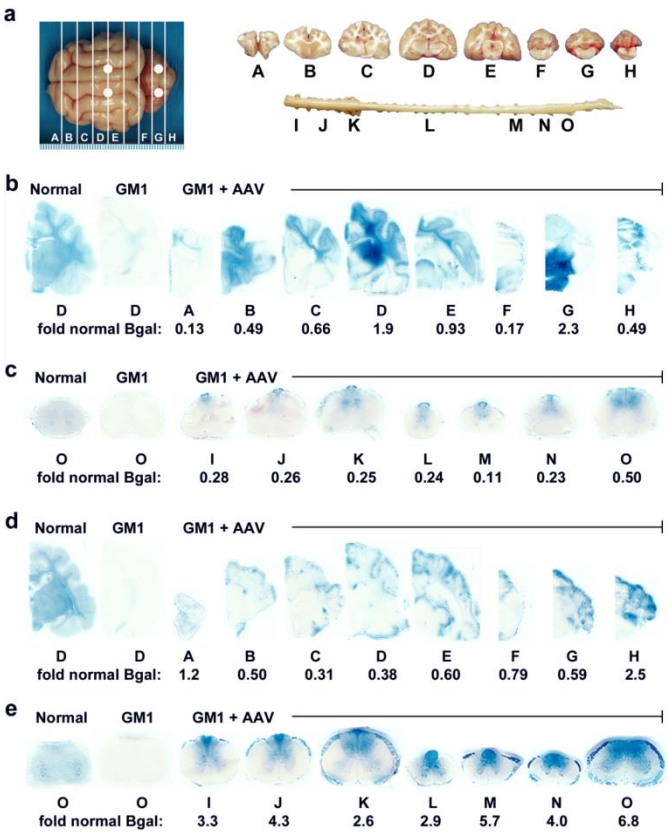

Figure 1. βgal distribution in the CNS of GM1 gangliosidosis cats 6 weeks after IC or thalamus and DCN injections of AAV vector. GM1 gangliosidosis cats received injection of AAVrh8-βgal in the thalamus and DCN or in the cisterna magna (IC), and tissues were collected 6 weeks later. (**a**) Injection sites (white circles) and 0.6 cm coronal blocks of the brain (A-H) and spinal cord (I-O) collected at necropsy. Lysosomal βgal activity (blue) detected with Xgal at acidic pH was visualized throughout the brain (**b**) and spinal cord (**c**) of a representative thalamus and DCN AAV-treated cat (GM1 + AAV). Lysosomal βgal activity was visualized throughout the brain (**d**) and spinal cord (**e**) of a representative IC AAV-treated cat (GM1 + AAV). Representative control sections are shown from untreated normal cats along with untreated GM1 gangliosidosis cats, which express ≤0.10-fold normal βgal activity in the brain and ≤0.04-fold normal βgal activity in the spinal cord. The ranges of specific activities for normal control blocks were: brain, 13 (A) - 45 (G); spinal cord, 4.6 (L) - 10 (K) nmol 4MU/mg/hr.

Table. 1. βgal activity and AAV vector copy number in the brain and spinal cord of GM1 gangliosidosis cats 6 weeks after IC or thalamus and DCN injections of AAV vector

CNS Region	Block	Fold normal β-gal activity, mean (s.d.)		Vector copies per μg genomic DNA	
		IC	T + DCN	IC	T + DCN
Cerebrum	A	**0.96** (0.33)	**1.3** (1.02)	**20,000** (3,500)	**12,000** (4,500)
	B	**0.37** (0.19)	**1.0** (0.33)	**13,000** (350)	**9,800** (6,300)
	C	**0.29** (0.04)	**1.0** (0.31)	**8,800** (450)	**7,300** (4,500)
	D	**0.37** (0.03)	**1.9** (0.58)	**12,000** (7,000)	**63,000** (45,000)
	E	**0.50** (0.14)	**1.2** (0.63)	**16,000** (10,000)	**35,000** (45,000)
Cerebellum	F	**0.82** (0.05)	**0.91** (1.0)	**16,000** (2,800)	**3000** (750)
	G	**0.66** (0.10)	**3.0** (1.1)	**4,800** (3,800)	**75,000** (50,000)
	H	**2.7** (0.29)	**3.1** (3.0)	**18,000** (1,300)	**35,000** (45,000)
Spinal Cord	I	**1.7** (2.2)	**0.33** (0.10)	**9,500** (2,300)	**2,100** (1,200)
	J	**2.7** (2.2)	**0.46** (0.14)	**9,000** (4,800)	**3,000** (1,400)
	K	**1.9** (0.97)	**0.59** (0.23)	**7,800** (3,500)	**2,400** (1,200)
	L	**2.3** (0.89)	**0.73** (0.51)	**16,000** (4,000)	**3,000** (450)
	M	**3.6** (3.0)	**0.59** (0.47)	**25,000** (6,500)	**2,800** (1,200)
	N	**2.7** (1.9)	**0.48** (0.20)	**9,500** (400)	**2,500** (2,100)
	O	**3.8** (4.2)	**0.72** (0.29)	**19,000** (21,000)	**4,300** (2,200)

Abbreviations: IC = intracisternal; T + DCN = thalamus and deep cerebellar nuclei; CNS = central nervous system